BIOMECHANICAL FACTORS INFLUENCING THE SUCCESSFUL NON-OPERATIVE TREATMENT OF ROTATOR CUFF TEARS

by

Robert Matthew Miller

BSE in Bioengineering, Case Western Reserve University, 2011

MS in Bioengineering, Case Western Reserve University, 2011

Submitted to the Graduate Faculty of

Swanson School of Engineering in partial fulfillment

of the requirements for the degree of

Doctor of Philosophy

University of Pittsburgh

2016

UNIVERSITY OF PITTSBURGH

SWANSON SCHOOL OF ENGINEERING

This dissertation was presented

by

Robert Matthew Miller

It was defended on

June 23, 2016

and approved by

Volker Musahl, MD, Associate Professor, Departments of Orthopaedic Surgery, Bioengineering, and Clinical Translational Science Institute

Spandan Maiti, PhD, Assistant Professor, Department of Bioengineering

Scott Tashman, PhD, Associate Professor, Departments of Orthopaedic Surgery and Bioengineering

James J. Irrgang, PT PhD ATC FAPTA, Professor and Chair, Department of Physical Therapy

Dissertation Director: Richard E. Debski, PhD, Associate Professor, Departments of Bioengineering and Orthopaedic Surgery

BIOMECHANICAL FACTORS INFLUENCING THE SUCCESSFUL NON-OPERATIVE TREATMENT OF ROTATOR CUFF TEARS

Robert Matthew Miller, PhD

University of Pittsburgh, 2016

The risk of developing a degenerative rotator cuff tear increases dramatically with age, reaching over 50% in the 7th decade of life. The severe pain and loss of function brought on by rotator cuff tears underscores the importance of swift and effective treatment. Unfortunately, failure rates for treating rotator cuff tears remain high. Unsuccessful treatment may relate to failure to restore joint kinematics or propagation of the rotator cuff tear. Furthermore, it is not clear which types of tears (i.e. geometry and amount of degeneration) will result in propagation. Therefore, the objective of this work was to investigate the effects of exercise therapy and initial tear characteristics on alteration of glenohumeral kinematics and tear propagation. Glenohumeral joint kinematics were measured in subjects with an isolated supraspinatus tear before and after 12 weeks of therapy. Although exercise therapy does not increase sub-acromial space, therapy decreases the overall joint contact path length by 36%, indicating a more stable joint. Cadaveric experiments measured tear propagation for increasing levels of loading using a novel cyclic loading protocol. Anterior supraspinatus tears propagate at lower loads than tears in the middle third (389 ± 237 N vs 714 ± 168 N). Mechanical testing also showed that tendons with pre-existing rotator cuff tears are not more likely to propagate than artificial tears representative of a "traumatic" rotator cuff tear (408 ± 86 N vs 580 ± 181). Histological analysis on cadavers (age 50-80) found no differences in degeneration between intact and torn supraspinatus tendons, indicating that age-related degeneration is a wide-spread phenomenon that can lead to the

initiation of rotator cuff tears. Using experimental data, finite element models of supraspinatus tendon were validated and used to predict effects of tear size, location, and degeneration on propagation. Overall, the model found that larger, more degenerative tears in the anterior third of the supraspinatus tendon are most at risk for propagation. These results provide valuable information to improve treatment of rotator cuff tears based on tear characteristics at diagnosis, by focusing on improving joint kinematics and advocating for early treatment of degenerative tears that interrupt the rotator cable structure.

TABLE OF CONTENTS

LIST OF TABLES

LIST OF FIGURES

PREFACE

I have grown a great deal over the past five years, and that is in no small part to all those listed below, without whom this dissertation would not have been possible. First, I must thank my PhD advisor, Dr. Richard Debski. I feel like I must have won some kind of PhD jackpot to have had him as my mentor through this whole process. Though the "Mother Goose & Grimm" cartoon posted in his office always reminds us that "there are only three letters between mentor and tormentor," he has been continually kind, patient, and supportive of me, even when I've made mistakes (especially when those mistakes include having to perform surgery with orthopaedic fellows on goat knees needed for an undergraduate lab after cutting too close to the joint line, and nearly cutting my little finger off with the meat saw). I have learned an incredible amount about research, mentorship, scholarship, teaching, time management, work-life balance, interpersonal relationships, and so much more through his tutelage. I am truly grateful for all he has done for me. I also can't thank Dr. Debski without also thanking his wife, Mandy, for always making me feel welcome in their home and reminding me that PhD advisors were also stressed out PhD students once upon a time.

I would also like to thank all the members of my dissertation committee for their abundance of knowledge and support: Dr. Volker Musahl, Dr. Scott Tashman, Dr. James Irrgang, and Dr. Spandan Maiti. You have all been with me from the beginning, providing thoughtful feedback and answering my questions when I would become stuck on some roadblock

or another. Dr. Musahl, thank you for all your much-needed clinical input, feedback, and good will throughout this process. Dr. Tashman, thank you for your insight and expertise in collecting and analyzing all of the in vivo data for this study, and for making what sometimes felt like an insurmountable problem manageable. Dr. Irrgang, thank you also for all of your clinical expertise and helping me to focus on the real-world impact of my work. Dr. Maiti, thank you for helping to teach me how to translate my experimental work to the world of computer modeling, and all the skills and concepts needed for me to complete this work.

Next, I would like to thank all my friends, whether listed here by name or not, who gave me support and temporary breaks from the assorted stresses of graduate school over the years. Special thanks to Neil and Marilyn, who provided a home away from home and a table that was always open for a game of Settlers of Catan. Hopefully I'll finally have time to visit a bit more often and meet Diana. Also thanks to Melissa, Bill, and Albert for participating in fun Pittsburgh activities with me, and for many (possibly too many) nights of pub trivia that somehow resulted in us winning a trip to Colorado, one of the best trips I've ever had the fortune to take. To Angela, thank you for the adventures with beer and baseball, and for emotional support during a particularly rough time. To Sara, Danny, and Matt, my staunch comrades in nerd esoterica, thank you for all the wonderful evenings, despite efforts to keep me up well past my bedtime.

I also need to thank everyone at the University of Pittsburgh who helped me through this process in one way or another. Thank you to all the other bioengineering and biomechanics students who made me feel welcome. Thanks in particular to Chelsea Marsh, whose friendliness and warmth helped me adjust to the life of a PhD student, and who provided countless instances of advice and mentorship while working on my in vivo experiments, and to James Thunes, whose computational expertise guided me through the perils of finite element modeling to

somehow finally complete my work (and who was also patient with my incessant questions and frustration when something inevitably went wrong). I must also thank the Pitt administrative staff who assisted me over my 5 years completing my thesis. Thanks in particular to Nick Mance for always answering my nagging questions about the administrative minutiae of being a grad student, and to Shoshana Matusak for helping me in procuring hard-to-find shoulders with existing rotator cuff tears for my thesis. Unfortunately, the statistic of 30% of people having rotator cuff tears does not seem to extend to cadavers for research. Thank you also to Dr. Besterfield-Sacre, CIRTL, and the EERC for helping me find and develop my passion for teaching. Lastly, I need to thank Linda Burke, Sue Harter, and everyone at the ARCS Foundation in Pittsburgh for the financial support that allowed me to present my research at many conferences over the years. Your support and belief in me means more than I can say.

When mentioning all those at the University of Pittsburgh who helped me through my graduate work, I would be remiss if I did not also thank my extended family in the Orthopaedic Robotics Laboratory. It definitely would not have been possible to finish this work without their advice and support. I would like to thank in particular the other PhD students in the lab, Adam Gustafson and Gerald Ferrer. Thanks to Adam for always making the lab a friendlier place and providing lots of advice on building geometry for computational models. Thanks to Gerald for all his assistance working with me since he joined the lab as an undergrad, and then sticking around for his PhD. Thank you also to Dr. Kevin Bell, who provided lots of much-needed advice and perspective on completing my dissertation work. Much thanks also to all the Orthopaedic Fellows who helped me with my many rotator cuff experiments over the years: Daisuke Araki, Yoshimasa Fujimaki, Masahito Yoshida, and Ata Azar. You all taught me not only a lot about orthopaedic medicine, but also about what lies outside of Pittsburgh. Hopefully someday I can

adventure out to your parts of the world and appreciate your cultures first-hand. I greatly appreciate all of your help. Last but not least, thanks to the many undergraduate students over the years who assisted me in completing various aspects of this work.

I want to thank my family for all their support. Mom, thank you for putting up with me being stressed out throughout this whole process and giving me the love and support I needed to get through. I hope Dad would be proud of what I've been able to accomplish, and I will always be grateful to him for providing the means and support to lead me down this path. To my sister Megan, I'm so proud of everything you've done since I started working on this dissertation, and I hope Hamish and Sherlock are being good "nephews." I love all of you dearly.

To Britt, my best friend of over a decade and loving girlfriend of the last two and a half years, you mean the world to me. Thank you for putting up with the long-distance difficulties and the days when I would be too tired or frustrated to act like a normal person. I'm so thankful to have you in my life to always inject some joy and absurdity into my day. I look forward to when we can spend a weekend together without worrying about one of us needing to get to the airport on time. I like you and I love you.

1.0 INTRODUCTION AND BACKGROUND

The shoulder is unique in that it is the most mobile "joint" in the body, but as a consequence of this, it is also one of the most unstable (1, 2). Therefore, significant contributions from both active and passive stabilizers are required to ensure stable joint function over a wide range of shoulder motions (3-8). Many studies have investigated the active and passive stabilizers of the shoulder, focusing on contributions from the glenohumeral ligaments, glenohumeral capsule, scapular stabilizers, and rotator cuff muscles. The rotator cuff muscles in particular provide active stabilization of the shoulder via a force couple around the glenohumeral joint that compresses the head of the humerus into the glenoid cavity on the scapula (9-17). As an extremely important shoulder stabilizer, injury to the rotator cuff can result in severe dysfunction (18-23). Therefore, it is of the utmost importance to understand both how rotator cuff injury occurs and how to optimize its treatment.

1.1 ANATOMY OF THE SHOULDER AND ROTATOR CUFF

Although the shoulder complex is commonly referred to as a single joint, it is in fact an assortment of four separate joints, which all contribute to the shoulder's large range of motion. These joints include the sternoclavicular joint between the sternum of the rib cage and the clavicle; the acromioclavicular joint between the acromion of the scapula and the clavicle; the scapulothoracic "joint", which is not a true joint, but is an articulation between the thorax and the scapula; and the glenohumeral joint between the glenoid of the scapula and the head of the humerus. This combination of joints allows for a range of approximately 0° to 180° of ab/adduction and 150° of internal/external rotation, with most of this motion being contributed by the scapulothoracic and glenohumeral joints (24-27). The glenohumeral joint in particular allows for a wide range of motion with relatively minimal joint translation of less than 1.5 mm in normal subjects (28). This high stability is achieved through a variety of passive and active joint stabilizers that assist in maintaining congruence between the articular surfaces of the humerus and scapula, despite the small amount of contact on the surface of the humeral head relative to the glenoid cavity at any given time (29, 30).

One of the most important active stabilizers of the glenohumeral joint is the rotator cuff (31-34). The rotator cuff consists of a group of muscles forming a sheath around the glenohumeral joint, including the subscapularis, supraspinatus, infraspinatus, and teres minor muscles (Figure 1.1 and Figure 1.2). These four muscles originate as distinct entities from the scapula, but the fibers of their tendons blend together at their insertions on the greater and lesser tuberosity of the humeral head (35). Together, the tendons of these muscles pass under the

"coracoacromial arch" of the scapula, which consists of the coracoid process, acromion, and coracoacromial ligament. The boundary of the coracoacromial arch serves as a passive restraint to superior migration of the humeral head, but its presence also results in contact with the rotator cuff tendons, potentially leading to wear (36-38). The joint bursa fills the space between the rotator cuff tendons and the coracoacromial arch to reduce friction and minimize potential wear of the tendons. Lastly, beneath the rotator cuff tendons is the glenohumeral joint capsule, another passive stabilizer of the shoulder that has been extensively studied. Together, the muscles of the rotator cuff serve as active stabilizers of the shoulder during elevation and internal/external rotation of the humerus with respect to the scapula (18, 39). When functioning properly, the rotator cuff serves to balance the force couples around the glenohumeral joint, compressing the humerus into the glenoid cavity and maintaining stability for normal glenohumeral motion (19).

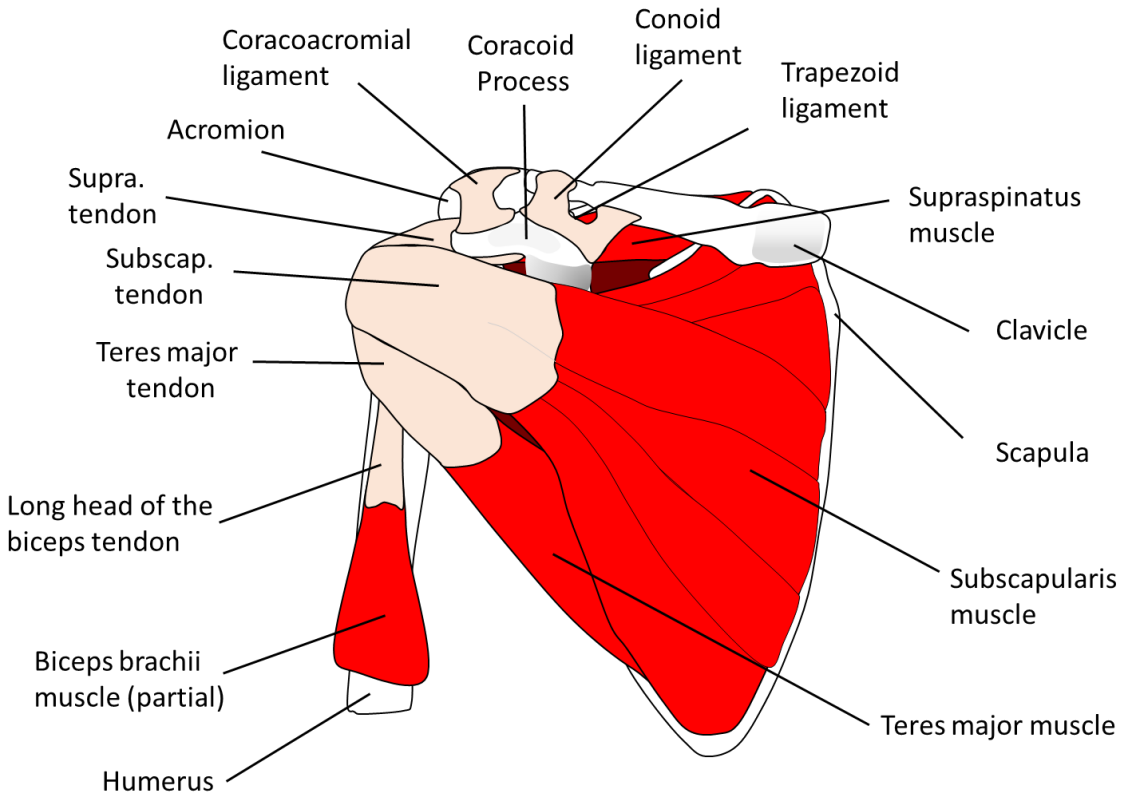

Figure 1.1. Anterior view of right shoulder

The subscapularis muscle originates from the subscapular fossa on the anterior face of the scapula and inserts on the lesser tuberosity of the humerus, attaching on the anterior aspect of the bicipital groove (35, 40). From this position, the subscapularis forms the anterior half of the glenohumeral force couple, and is primarily responsible for internal rotation of the shoulder (41). On the posterior side of the scapula, the infraspinatus and teres minor muscles originate from the infraspinous fossa and lateral border of the scapula, and insert over the majority of the surface of the greater tuberosity of the humerus (40, 42). While both the infraspinatus and teres minor muscles contribute to external rotation of the humerus, the infraspinatus provides the majority of the force (41), and is the posterior half of the glenohumeral force couple formed with the subscapularis. Not only does this force couple compress the head of the humerus into the glenoid to improve stability, it actively resists superior translation of the humeral head due to forces exerted by the deltoid during arm abduction (43). If this force couple is injured, such as by the presence of a rotator cuff tear, glenohumeral kinematics can be severely altered, leading to joint dysfunction and potential further injury (9, 16, 44-47).

The supraspinatus muscle originates from the supraspinous fossa at the superior and posterior aspect of the scapula, and inserts on the greater tuberosity of the humeral head. The supraspinatus muscle is primarily involved in abduction of the arm, providing an initial force to begin elevation of the arm at lower abduction angles. At angles greater than 30° of abduction, forces produced by the deltoid surpass those produced by the supraspinatus, and the deltoid becomes the primary arm abductor (48). Unlike the subscapularis and infraspinatus muscles, which do not border one another, the fibers of the supraspinatus tendon intermingle with the fibers of the subscapularis and infraspinatus tendons on their insertions to the humerus (35, 42). Though there is minimal interaction between the fibers of the supraspinatus and subscapularis,

together their fibers form a sheath over the long head of the biceps tendon (35). However, there is a much greater amount of fiber intermingling between the infraspinatus and supraspinatus due to their shared insertions on the greater tuberosity of the humerus (35, 49), resulting in significant load sharing between the two tendons (50, 51).

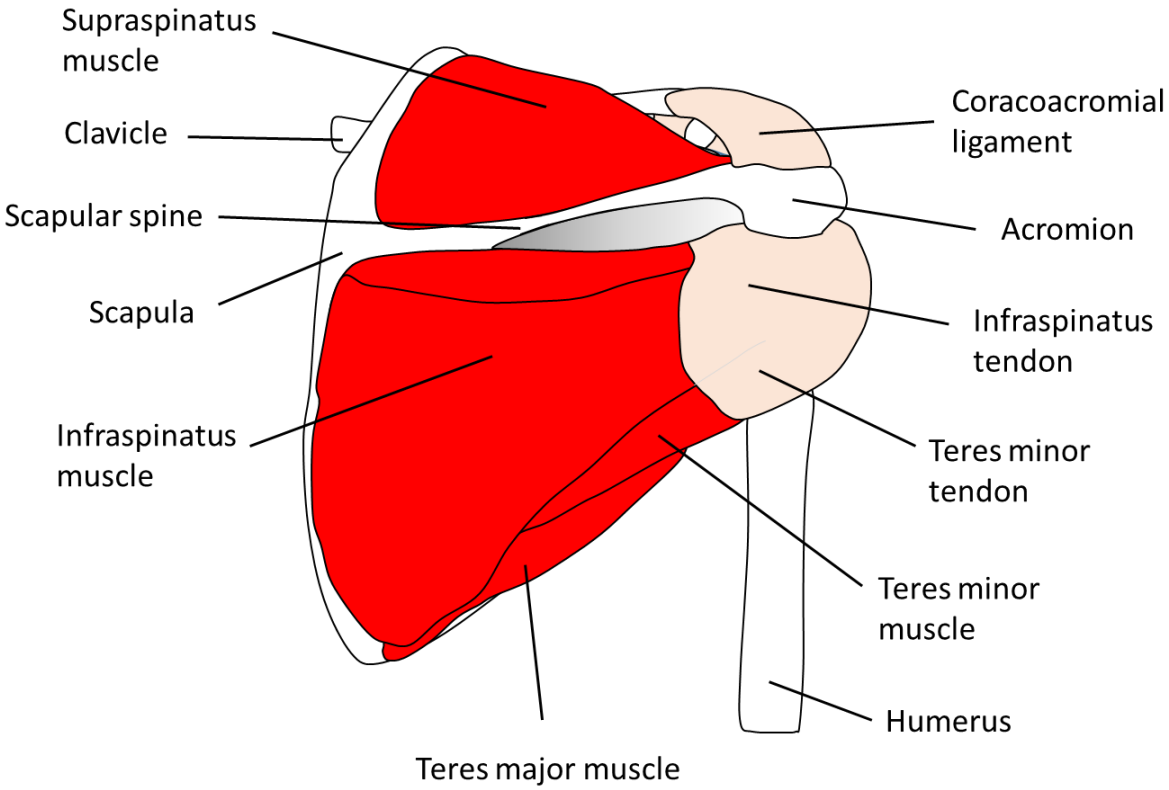

Figure 1.2. Posterior view of right shoulder

Investigations of the macrostructure of the rotator cuff tendons have shown the presence of a thick, cable-like structure running through the supraspinatus and infraspinatus from the posterior border of the bicipital groove to the inferior border of the infraspinatus tendon (19, 52). This structure, referred to as the "rotator cable," has been proposed to act as a stress transfer system that shields the "rotator crescent" region of the tendon bordered by the cable and the

tendon insertion on the humerus, and therefore may have a significant role in the biomechanical stability of tendons with rotator cuff tears. At the microstructural level, histology has revealed five distinct layers within rotator cuff tendon (35) (Figure 1.3). At the bursal surface of the tendon is a thin (1 mm thick) layer of fibers of the coracohumeral ligament and tissue from the bursa. The second layer is a 3-5 mm thick superficial layer of tendon fibers that are densely packed and well-organized. The third layer consists of the deep fibers of the tendon and is slightly thinner and less organized than the second layer, due to this being the layer at which interweaving of fibers from separate tendons occurs. The fourth layer is composed of connective tissue at the boundary between the tendon and the joint capsule, while the fifth layer closest to the articular surface consists entirely of joint capsule tissue.

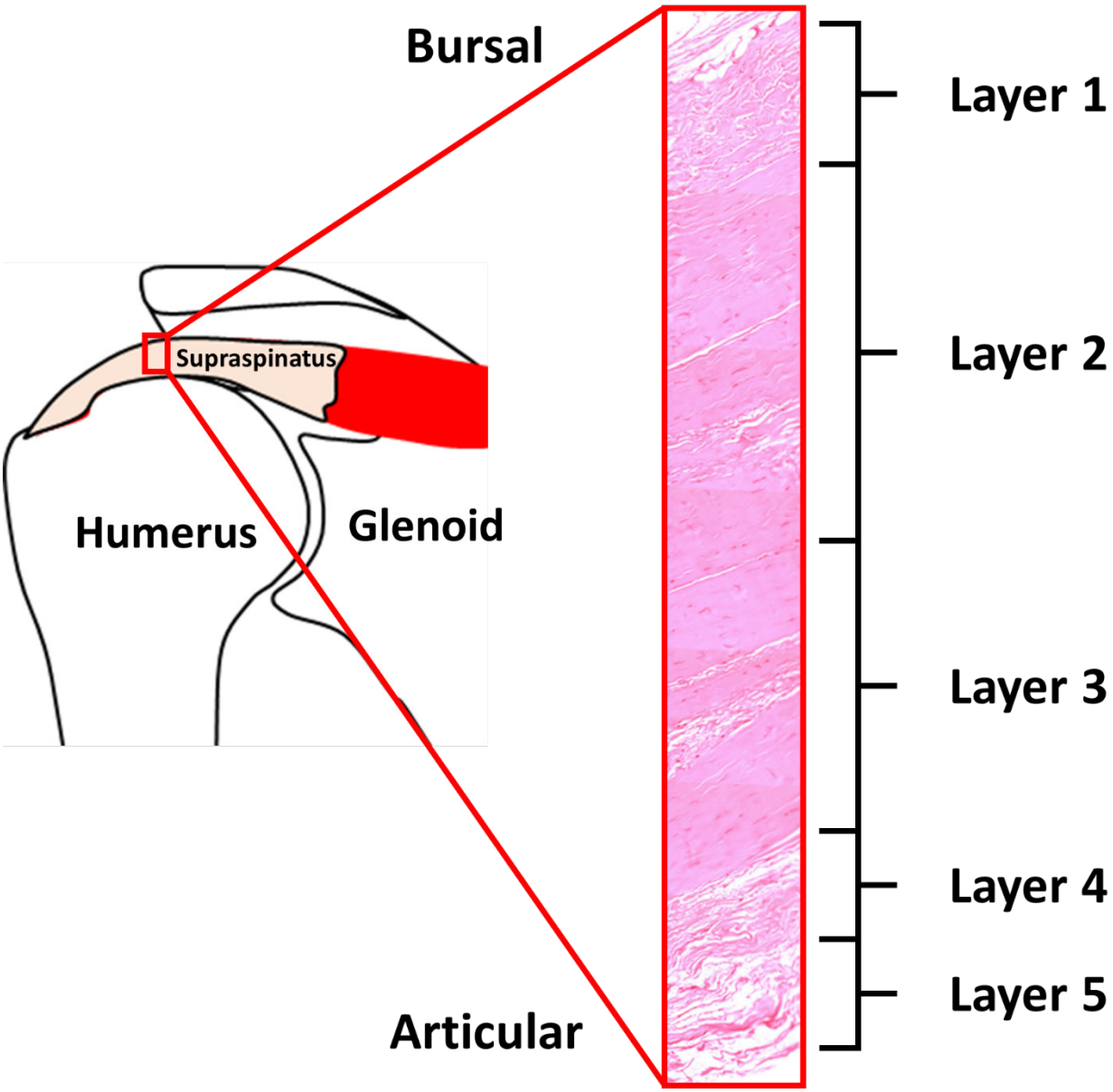

Figure 1.3. Supraspinatus tendon layers. The tendon can be separated into 5 distinct layers through the bursal-articular tendon thickness. Layer 1 includes fibers of the coracohumeral ligament and tendon bursa, layers 2 and 3 include the superficial and deep layers of the tendon fibers, and layers 4 and 5 include connective tissue and fibers from the glenohumeral capsule.

1.2 IMPACT OF ROTATOR CUFF TEARS

Shoulder pain is one of the most common orthopaedic complaints, with approximately 4.5 million patients visiting their doctors due to this issue annually in the United States (53). Chronic shoulder pain and loss of range of motion and shoulder strength can frequently be attributed to injury to the rotator cuff, and in particular due to tears of the rotator cuff tendons (54-58). Patients that are of working age account for two-thirds of all patients treated for rotator cuff tears, and therefore this injury can have a significant impact on the labor force that can be a large burden on society and the economy (59). Over 200,000 rotator cuff repairs are performed yearly in the United States (60, 61), resulting in treatment costs of over $3 billion (62). Therefore, improving treatment of rotator cuff tears has been a topic of considerable interest to orthopaedic researchers and clinicians.

1.2.1 DEMOGRAPHICS AND SOCIETAL IMPACT

Previous studies have investigated a variety of risk factors related to the development of degenerative rotator cuff tears. One of the most important of these factors is patient age. There is a 20% prevalence of rotator cuff tears in the general population (63), with an increasing incidence of degenerative rotator cuff tears with age that can reach upwards of 50% in the seventh decade of life (64-67). Smoking (68-70), hypercholesterolemia (70-72), and genetic predisposition (70, 73, 74) have also all been linked to increased risk of developing a degenerative rotator cuff tear. In addition, studies have shown that patients are more likely to develop a rotator cuff tear if they have poor posture (75) or history of prior trauma (63). The

likelihood of a patient developing an asymptomatic tear in their contralateral shoulder is also higher if they are already suffering from a symptomatic, degenerative rotator cuff tear (76, 77).

The presence of a rotator cuff tear can result in severe pain and limited range of motion with the potential for altered glenohumeral kinematics, decreased shoulder strength, and long-term dysfunction (18-23). The high incidence of rotator cuff tears in a growing middle-to-late aged population in the United States combined with their capacity to severely impact quality of life and productivity, make rotator cuff tears a significant clinical problem. Furthermore, there is currently a lack of clear evidence on the optimal method of initial treatment for rotator cuff tears. Approximately 30% of all visits to orthopaedic surgeons occur due to rotator cuff pathology (78), putting a significant burden on the health care system. Together, the personal, societal, and economic impacts of rotator cuff tears underscore the importance of timely and effective treatment before an initial tear can substantially propagate into a large or massive tear, which is considerably more difficult to treat and is associated with worse clinical outcomes (20, 79-81).

1.2.2 CURRENT TREATMENT

Current management of degenerative rotator cuff tears generally consists of prescription of non-operative management, which has been shown to be effective for many patients as an initial therapy (82). Non-operative management of rotator cuff tears can include nonsteroidal anti-inflammatory drugs and cortisone injections for pain management and physical therapy exercises to restore normal range of motion, reduce pain, strengthen the remaining uninjured rotator cuff muscles and scapular motors, and return patients back into normal activities of daily living (83-88). Though there are variations in rotator cuff tear rehabilitation protocols that can consist of supervised physical therapy or home exercise programs, these protocols typically involve range

of motion, stretching and flexibility, and strengthening exercises (86). Additionally, these exercises can serve to reestablish the force balances necessary for stabilization of the glenohumeral joint (89), potentially helping to restore normal joint kinematics. In the case that non-operative management fails, it is followed by surgical repair of the tendon. Surgical repair can be performed using either open or arthroscopic techniques, though modern surgeries are more often performed arthroscopically. The torn edge of the tendon is mobilized and pulled back to the insertion on the humeral head in order to approximate the tendon footprint on the humerus and maximize surface area to promote tendon-bone healing (90-95). Sutures are used to reestablish the tendon-bone interface using a variety of different configurations that can include one (single-row) or two (double-row) rows of sutures (96-99). Sutures are typically connected to the bone using a transosseous repair technique for open surgeries, whereas arthroscopic repairs use either suture anchors or a transosseous-equivalent method (100).

The established treatments for rotator cuff tears currently show high failure rates: non-operative treatment fails in 25-50% of cases (83, 85, 101-104), while surgical repair procedures for rotator cuff tears fail in 10-50% of cases (92, 105-113). Larger tears have even higher failure rates that can approach 90% for massive tears with poor-quality tissue (80, 81, 105, 114-117). Although the reasons behind these relatively high failure rates are not entirely known, various intrinsic and extrinsic factors have been proposed to be associated with success or failure of surgical repair and physical therapy. Factors influencing the failure of surgical repair due to re-tearing have been extensively investigated. Previous studies have found fatty infiltration, larger tear size, advanced age, and double-row repairs to be associated with greater risk of repair failure (19, 106, 109, 110, 113, 118, 119). Failure of the repair most often occurs at the tendon-suture

interface due to the suture pulling through the tendon tissue (120-129), indicating that poor tissue quality is a significant factor affecting the outcomes of surgical repair.

Although failure of surgical repair has been studied by many investigators, the reasons for failure of physical therapy or exercise therapy are much less understood. Success or failure of exercise therapy may relate to early anterior-posterior tear propagation based on tear geometry and tendon quality, or to what extent exercise therapy restores normal glenohumeral joint kinematics. Previous studies have found that 50% of patients show clinically significant increases in rotator cuff tear size due to tear propagation within 2 years after completion of exercise therapy (85, 87, 130-133). Additionally, larger increases in size of full-thickness rotator cuff tears have been shown to be associated with asymptomatic tears becoming symptomatic, indicating an association between patient outcomes and tear propagation (130, 134).

Proposed factors influencing in vivo propagation of rotator cuff tears include intra-tendinous strain (50, 135, 136) and tendon quality (81, 137, 138). In particular, regions of increased tendon strain at the edges of tears have been shown to be a significant factor contributing to initiation and propagation of rotator cuff tears (50, 135, 136, 139-142). Numerous studies have also found relationships between rotator cuff tears and changes in glenohumeral kinematics (9, 16, 23, 28, 47, 143-147), though not in the context of failure of exercise therapy. Though many factors have been proposed as reasons for the failure of rotator cuff tear treatments, the relationship between these factors to the outcome of exercise therapy has not been sufficiently researched. These factors must be better established to provide clinicians with improved guidelines for which patients should be treated with physical therapy versus immediate surgical repair.

1.3 DEVELOPMENT OF ROTATOR CUFF TEARS

Due to the significant clinical and social impact of rotator cuff tears, many studies have been performed to investigate their initiation and progression. Tears typically originate as partial thickness tears on the articular side of the supraspinatus tendon, and over time progress through the thickness of the tendon to the bursal side and create full-thickness tears (56, 148). Since full-thickness rotator cuff tears do not heal spontaneously (58, 149), these tears can propagate and extend into additional tendons if not treated and given sufficient time. In order to optimize the treatment of rotator cuff tears, it is therefore important to understand which tear characteristics and conditions will result in a greater risk of tear propagation.

1.3.1 Mechanics of Tear Initiation and Tear Propagation

Rotator cuff tendon tears typically initiate as partial thickness tears on the articular surface of the supraspinatus tendon, which can propagate over time through the full thickness of the tendon and extend into multiple tendons (56). Although rotator cuff tears can occur in the infraspinatus and subscapularis tendons, tears are most commonly located in the supraspinatus tendon, approximately 1.5 cm posterior to the long head of the biceps tendon (150). This location is approximately in the anterior-posterior center of the supraspinatus tendon. In the medial-lateral direction, tears are usually located just proximal to the supraspinatus tendon insertion to the greater tuberosity of the humerus (Figure 1.4).

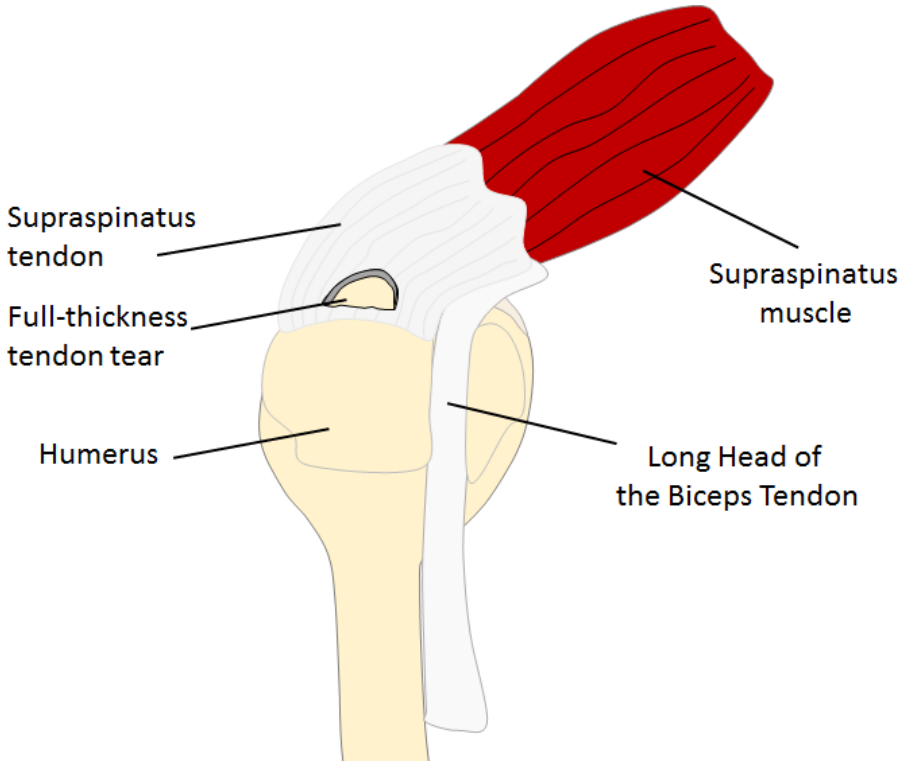

Figure 1.4. Supraspinatus tendon tear

Studies have shown that this most common location for rotator cuff tears to occur in is related to tendon strain, a significant mechanical factor contributing to initiation and propagation of rotator cuff tears (50, 135, 136, 139-141). In particular, the articular surface of the tendon is generally under greater strain than the bursal side of the tendon, providing a rationale for tears initiating on the articular side of the tendon and propagating through the thickness from a high-strain to low-strain region to create full-thickness tears over time (136). Additionally, tendon strain increases with glenohumeral abduction angle for both sides of the tendon (136, 141, 151), which suggests a possible reason for the increased occurrence of rotator cuff tears in overhead athletes.

Although the mechanical factors related to quantifying the initiation of rotator cuff tears have been investigated, the factors responsible for propagation of rotator cuff tears are not as

well understood. Tear shape (152, 153), size (135, 139), and location (150, 154, 155) (i.e. tear geometry) have all been proposed as factors that may affect the risk of tear propagation. The effects of tear geometry on tear propagation are supported by the previously established relationship between elevated strains at tendon tear edges and tear size (135, 139). However, clinicians are not currently able to determine which types of tears will be at the highest risk for propagation based on their geometric factors at presentation. Additionally, multiple in vivo studies have demonstrated propagation of rotator cuff tears of varying sizes after physical therapy at follow-up periods ranging from 2 to 4 years (130-132) that may indicate a risk of tear propagation during certain types of treatments. In one study, 50% of patients showed a clinically significant increase in tear size at 2-year follow-up, with most of these tears being symptomatic (130). Therefore, there is a need to understand if different types of tears respond differently to different types of treatment.

1.3.2 Tendon Degeneration and Tear Chronicity

In addition to extrinsic factors such as mechanical environment that contribute to the development and treatment of rotator cuff tears, intrinsic factors such as tissue quality are also important. For example, it has been shown that tendons with degenerative rotator cuff tears exhibit less ability to heal (149, 156, 157) and reduced blood flow (158, 159) compared to healthy, intact rotator cuff tendons, and are therefore more difficult to treat. This is reflected in the high failure rates for rotator cuff repairs that cite poor tissue quality and suture pull-out as the primary reason for tendon re-tear after surgery (120-129, 160).

Age-related degeneration of rotator cuff tendons has been quantified histologically to demonstrate the relationship between age and tissue degeneration. Signs of histological

degeneration include changes in tenocyte nuclei morphology, hypercellularity, loss of collagen fiber organization, and break-down of the tendon extracellular matrix (161, 162). The greatest amounts of tendon degeneration are typically found in the regions closest to degenerative rotator cuff tears (163-166), indicating poorer tissue quality associated with un-treated rotator cuff tears. Unfortunately, since the chronicity of rotator cuff tears in patients is often unknown (150), it is difficult to quantify "chronicity," or predict tissue quality based on how long a patient has had a degenerative rotator cuff tear. Furthermore, while poor tissue quality has been shown to be an important contribution to failure rates of rotator cuff repair surgery, the effect of tissue quality on the propagation and initiation of rotator cuff tears is not as well understood.

2.0 MOTIVATION

Due to the significant clinical burden of rotator cuff tears on society, there is a clear need to optimize their treatment. The high failure rates of exercise therapy (83, 85, 101-104) and rotator cuff repair (92, 105-113) indicate that there are many unknown factors related to the failure of treatment that must be better understood. Previous studies have found significant pathologic changes in glenohumeral kinematics due to rotator cuff tears (9, 23, 28, 145-147, 167-169). These persistent changes in glenohumeral kinematics have the potential to severely injure the structures of the glenohumeral joint over time (9, 16, 44-47), ultimately leading to increased pain, loss of function, and the need for shoulder arthroplasty in extreme cases. If treatment of rotator cuff tears does not restore glenohumeral kinematics to normal, there is potential for this persistency in abnormal kinematics to lead to further shoulder problems long after treatment. Therefore, a potential reason for the failure of exercise therapy may be due to failure to restore normal glenohumeral joint kinematics.

Propagation of rotator cuff tears after exercise therapy has been shown to be a common occurrence (130-132), suggesting that propagation of a rotator cuff tear during therapy may contribute to failure of this treatment. The initiation and propagation of rotator cuff tears is a complex process that is still not fully understood. Research suggests that a combination of mechanical (50, 135, 136, 139-141) and biological factors (149, 156, 157) contribute to the etiology of rotator cuff tears. However, the relationship of these factors to tear propagation has

been insufficiently quantified, and so success or failure of different rotator cuff tear treatments cannot be predicted. Optimally, by being able to predict the risk of tear propagation based on initial tear characteristics, patients can be more effectively treated by being assigned at the time of diagnosis to the type of treatment that is most likely to be successful for that type of tear. If certain types of tears are more likely to propagate earlier than other tears, early surgical intervention may be more effective than non-operative management such as exercise therapy.

In order to begin to quantify the effects of initial tear characteristics on tear propagation, it is important to understand both the material properties of the tendon and its mechanical environment within the body. The inherent biomechanical behavior and properties of the rotator cuff relate to its ability to resist initiation or propagation of a tear. Meanwhile, stresses and strains acting on the tendons during normal activities of daily living, or even when performing exercise therapy, can potentially lead to propagation of a tear. A combination of poorer tissue properties, for example due to age-related tendon degeneration, and increased stresses and strains acting on the tissue can potentially result in a greater risk of tear propagation.

Factors affecting tendon strain can either result from loading of the tendon from muscle activation, or, in the case of a rotator cuff tear, the tear itself can affect the strain field directly around the tear (50, 135, 139, 170). Strains around a tear can be affected by the tear size and shape, or even by the tear's location in the tendon. The supraspinatus tendon exhibits an anterior-posterior gradient in structural and material properties that is a consequence of the inhomogeneous properties of the rotator cuff (171). Therefore, a difference in tear location can considerably change the measured strains. Additionally, tendon degeneration associated with rotator cuff tears will affect the tendon material properties. As collagen fibers within the tendon become more disorganized and the extracellular matrix begins to break down, the tissue becomes

less able to resist strains acting upon it. Ultimately, risk of tear propagation can be predicted by quantifying the effects of combinations of different tear characteristics.

Therefore, in order to better understand the biomechanical factors influencing treatment of rotator cuff tears, the objective of this dissertation is to use combined in vivo imaging techniques, in vitro cadaveric experiments, and computational approaches to better characterize the effects of tear propagation and glenohumeral kinematics that can affect the success of exercise therapy. By understanding the various biomechanical factors that contribute to failure of exercise therapy, treatment of rotator cuff tears can be improved by maximizing patient outcomes and minimizing time and cost of treatment. In order to investigate the effect of exercise therapy on in vivo glenohumeral kinematics, dynamic stereoradiography combined with a previously-developed model-based tracking method will be used. By measuring patient kinematics before and after a standard exercise therapy program for the treatment of rotator cuff tears, changes in glenohumeral kinematics due to exercise therapy can be quantified and related to patient outcomes. In vitro cadaveric experiments will be used to study the effects of tear location and tendon degeneration on tear propagation in order to better characterize their effects on risk of tear propagation. Additionally, cadaveric testing will be used to gather subject-specific geometry and inhomogeneous, anisotropic material properties to develop and validate computational models. These models will then be used to predict tear propagation based on tear size, location, and tendon degeneration through application of finite element methods and fracture mechanics theory.

Ultimately, this work will provide important information on the mechanical factors behind tear propagation and potential reasons for the failure of exercise therapy based on glenohumeral joint kinematics and tear propagation. The results of this study can assist in the

development of new treatment decision protocols for effective treatment of rotator cuff tears. Eventually, a "rotator cuff tear index" can be developed to apply personalized treatments to patients based on initial tear characteristics such as tear size, shape, location, and tendon degeneration.

2.1 SPECIFIC AIMS AND HYPOTHESES

In order to meet the objectives of the study, the following specific aims were implemented:

2.1.1 Aim 1

Determine changes in *in vivo* glenohumeral joint kinematics in patients with rotator cuff tears after exercise therapy.

Hypothesis 1: Exercise therapy will result in improved glenohumeral kinematics in terms of reduced glenohumeral translations and increased acromiohumeral distance.

2.1.2 Aim 2

Develop a subject-specific finite element model of rotator cuff tear propagation validated by uniaxial tensile cyclic loading experiments on cadaveric supraspinatus tendon to assess the effects of tear location and geometry on tear propagation.

Hypothesis 2a: Anteriorly located tears will exhibit lower loading magnitudes required to reach critical amounts of tendon retraction compared to middle tears.

Hypothesis 2b: Increased tear size will correlate with lower loads required to reach critical amounts of tendon retraction.

2.1.3 Aim 3

Assess the effects of tendon degeneration on load required to cause tear propagation using histology and computational modeling.

Hypothesis 3: Increased tissue degeneration will be correlated with greater risk of tear propagation in terms of lower stress and strain required to propagate a tear.

3.0 AIM 1: EFFECT OF EXERCISE THERAPY ON JOINT KINEMATICS

There is currently no clear protocol for deciding which patients with rotator cuff tears should undergo which treatments (172). This is due to a clear lack of evidence on which types of treatments provide the optimal outcomes for patients. Currently, most patients with degenerative rotator cuff tears are prescribed exercise therapy with a physical therapist to reduce pain and restore shoulder function. However, the high failure rates of exercise therapy indicate that not all patients will respond well to this treatment type, and may require surgery at a later time. In order to improve the success rate of exercise therapy, it is important to understand which specific factors contribute to its success or failure. It is presently unknown to what extent exercise therapy alters or restores the glenohumeral joint kinematics of patients with rotator cuff tears, which may be a significant factor related to the outcome of exercise therapy. Therefore, the first aim of this dissertation was to assess the effects of exercise therapy on glenohumeral joint kinematics, specifically as it relates to the successful treatment of rotator cuff tears.

3.1 EFFECTS OF EXERCISE THERAPY FOR TREATMENT OF SYMPTOMATIC ROTATOR CUFF TEARS ON IN VIVO GLENOHUMERAL KINEMATICS

3.1.1 Introduction

Rotator cuff disease is a serious clinical issue, with a high incidence of degenerative rotator cuff tears in persons greater than 50 years old (63, 67). Despite the high incidence of rotator cuff tears, controversy remains on the optimum method for management of rotator cuff injury (172). Surgical repair of rotator cuff tears is becoming increasingly common (60), but can lead to re-tearing or other complications with varying failure rates ranging from 17% to 69%, depending upon initial tear characteristics (105, 173). Non-operative management of rotator cuff tears remains the recommendation for initial management of patients with a degenerative rotator cuff tear (83-88), but is also associated with failure rates of up to 50% (83, 85, 86, 101), resulting in greater costs of late surgical treatment in terms of both time and money.

Presently, it is unclear which factors are most important for choosing non-operative versus surgical treatment (138, 174) of rotator cuff tears. Previous clinical studies have investigated both initial tear size and change in tear size during exercise therapy as potential factors for defining which types of patients are likely to respond better to non-operative management (85, 87, 130, 133). However, these studies do not assess changes in glenohumeral kinematics, which may relate to long term changes in joint instability, rotator cuff impingement, and osteoarthritis. Studies investigating changes in glenohumeral joint kinematics after a rotator cuff tear in a rat model have indicated that cuff tears lead to changes in joint kinematics and pathology (16, 47). Therefore, there is a need to better understand the impact of glenohumeral joint kinematics as a measure for determining the successful outcome of non-operative

management of rotator cuff tears. Changes in glenohumeral kinematics due to rotator cuff disease have been reported for both cadaveric (9, 23, 28, 145, 147) and in vivo (146, 167-169) experimental conditions. In particular, previous in vivo studies have observed changes in glenohumeral contact position and sub-acromial space after rotator cuff surgical repair (144) and relationships between changes in kinematics and shoulder strength measured post-rehabilitation (143).

Although rotator cuff surgery has been shown to improve the in vivo kinematics of the glenohumeral joint, the effect of exercise therapy on the restoration of glenohumeral kinematics remains unclear. Therefore, the objective of this study was to assess the effects of a 12-week exercise therapy program on glenohumeral kinematics for patients with a small, symptomatic full-thickness supraspinatus tear. It was hypothesized that: 1) successful exercise therapy would result in improved glenohumeral kinematics in terms of decreased joint translation and greater sub-acromial space, and 2) smaller translations and larger acromiohumeral distance after exercise therapy would correlate with improvements in shoulder strength and patient-reported measures of symptoms, activity, and participation.

3.1.2 Materials and Methods

3.1.2.1 Subject Recruitment

Five subjects (3 women and 2 men, mean BMI 32.0 ± 7.8, mean age 60.2 ± 7.6 years,) were recruited for the study after providing Institutional Review Board-approved written informed consent. Subjects were included into the study if aged between 45 and 70 years with a symptomatic small, degenerative full-thickness rotator cuff tear isolated to the supraspinatus

tendon. Subjects with previous shoulder surgeries, injections within 3 months prior to study participation, or exercise therapy within 2 years prior to the study were excluded. MRI confirmation of a supraspinatus tear with a greater percentage of muscle than fat (Goutallier Grade 2 or less) was also required for study eligibility. Subjects who were smokers, had diabetes mellitus, severe capsular tightness (defined as internal/external rotation less than 30°), or work-related or traumatic injury were excluded from participation in the study.

3.1.2.2 Exercise Therapy Protocol and Assessments

All five patients participated in a standard 12-week exercise therapy program for non-operative management of rotator cuff tears, with a focus on restoring range of motion (ROM) and strengthening the rotator cuff and scapular muscles. Patients were treated with oral nonsteroidal anti-inflammatories as needed, but no additional use was made of corticosteroid injections to the sub-acromial space. This program consisted of 6 weeks of supervised exercise with a single physical therapist for two 45-60 minute sessions a week. This was followed by 6 weeks of a home exercise program while completing a daily home exercise log to ensure patient compliance. An additional session at the 12-week time point was included for data collection purposes and to assess patient status after the completion of the home exercise sessions (Figure 3.1).

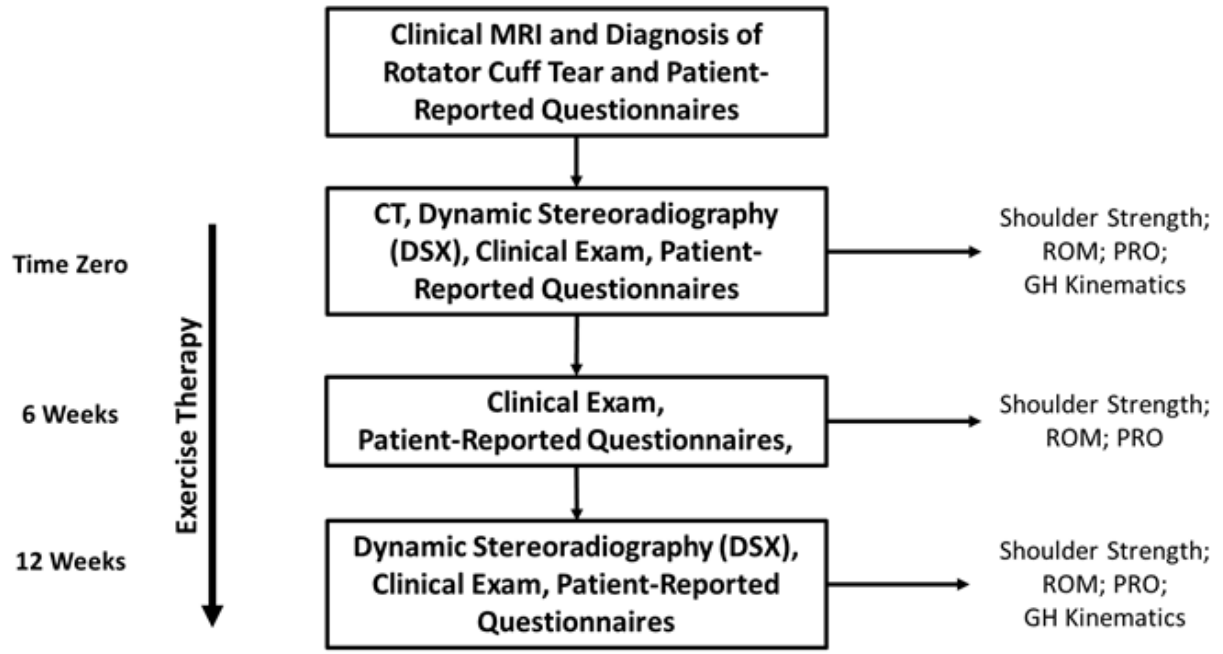

Figure 3.1. Flow chart of in vivo experimental testing.

Initially, isometric and active ROM exercises were used to strengthen the rotator cuff and scapular muscles. Progressive resistance exercises (PREs) were introduced once the patient could actively move the shoulder through a full ROM without a lag or increased pain. Exercise resistance and number of repetitions were determined based on a modification of the daily adjustable progressive resistance exercise (DAPRE) program (175) (Table 3.1). The specific exercises to target each of the rotator cuff muscles (supraspinatus, infraspinatus, teres minor and subscapularis), as well as the serratus anterior and middle and lower trapezius, were selected based upon electromyographic (EMG) evidence of maximal activity for each muscle (176-178). At the conclusion of each exercise session, cold therapy was applied to minimize shoulder pain as needed based on response to exercise, pain level, and patient preference. Patient pain during each session was measured with a 0 to 10 numerical pain rating scale and was used by the physical therapist to adjust the exercise program on an individual basis.

During the exercise therapy sessions at 0 and 12 weeks, isometric shoulder strength and patient-reported symptoms, activity, and participation were assessed for each patient. Isometric strength measurements were taken with a handheld dynamometer (Lafayette Manual Muscle Testing System, Lafayette Instrument Company, Lafayette, IN) for four shoulder positions. The dynamometer was placed distally on the forearm, just proximal to the wrist joint, along the dorsal radius and ulna when taking the measurement. Maximal isometric strength was assessed for external rotation at 0° of coronal plane abduction (biases infraspinatus), external rotation at 90° of abduction (biases teres minor), scapular plane abduction (biases supraspinatus), and internal rotation at 90° of abduction (involves subscapularis and pectoralis muscles).

Patients performed three trials of each task, and the average value was taken as a measure of isometric strength. At the same time points, patients filled out three patient-reported outcome measures including Disabilities of the Arm, Shoulder and Hand (DASH) Outcome Measure (179), the American Shoulder and Elbow Surgeons (ASES) Shoulder Rating Scale (180), and the Western Ontario Rotator Cuff (WORC) Index (181) The DASH, ASES, and WORC are commonly used to assess patient-reported outcomes for a variety of shoulder conditions, including rotator cuff tears. The reliability and validity of DASH (182), ASES (183), and WORC (184) scores for rotator cuff disease have been previously demonstrated. Changes in the DASH, ASES, and WORC scores were compared to minimal clinically important differences (MCID) (185) for each outcome measure to determine if improvements could be considered clinically relevant (186, 187).

Table 3.1. Exercise Therapy Program Exercises

Week #1. Acute Phase	Weeks # 2, 3. Transitional Phase	Weeks # 4, 5, 6. Advanced Phase
PROM cane external rotation	Horizontal adduction stretch	Continued progression of flexibility and strengthening from transitional phase
PROM cane internal rotation	Internal Rotation towel stretch	Proprioceptive neuromuscular facilitation patterns (PNF)
PROM supine flexion	Sleeper Stretch	Lat pull down
	ER at 0° with elastic resistance	Rhomboids (retractions)
PROM standing extension	IR at 0° with elastic resistance	Pecs (press, flies)
AAROM supine cane external rotation	ER at 90° with elastic resistance	Deltoids (raises)
AAROM standing cane flexion	Subscapularis hug with elastic resistance	Closed kinetic chain protraction with rhythmic stabilization
AAROM standing cane abduction	Scapular Plane Abduction	ADL or sport specific activities
AAROM wall climb / wall walk	Prone Row into external rotation	
AAROM standing cane extension	Prone T's (horizontal abduction at 90°)	
Isometric ER at 0 degrees	Prone Y's (horizontal abduction at 120°)	
Isometric IR at 0 degrees	Serratus protraction with forward flexion	
Side-lying ER in pain-free ROM	Wall push up with plus	
Prone GH extension with ER	Lat pull down	
Scapular Plane Abduction	Rhythmic stabilization with manual resistance	
Scapular Retraction	Biceps curl	
Manually resisted scapular movements	Triceps push down	
PROM: Passive Range of Motion; AAROM: Active Assistive Range of Motion; ADL: Activities of Daily Living; IR: Internal Rotation; ER: External Rotation		

3.1.2.3 Glenohumeral Kinematics Protocol and Assessments

A previously established model-based tracking technique using dynamic stereoradiography (DSX) (188) was used to measure glenohumeral kinematics during coronal-plane abduction before and after the exercise therapy program. Prior to beginning exercise therapy, subjects underwent computed tomography (0.625 × 0.625 × 1.25 mm voxels) of the affected shoulder. These computed tomography images were segmented using the MIMICS 14 software package (Materialise, Leuven, Belgium) to generate three-dimensional, subject-specific models of the

humerus and scapula. For collection of x-ray images using the DSX system, subjects were seated with their affected glenohumeral joint positioned at the center of the system (Figure 3.2). Subjects performed 3 arm abduction trials starting in a resting positon with their affected arm at their side, and then raising the arm in the coronal plane to their maximum attainable elevation over a period of 2 seconds. A metronome was used to assist in timing of the motion, and subjects were allowed a maximum of two practice trials before collecting data to minimize pain and fatigue. For each arm abduction trial, subjects performed 3 abduction/adduction cycles, with data collected on the second cycle. Position in the coronal plane throughout the path of motion was maintained using a laser pointer strapped to the hand on the affected arm, and asking subjects to keep the laser dot within a properly aligned vertical stripe of tape. Subjects were instructed to keep their backs straight and not lean to compensate for loss of humerothoracic elevation due to their rotator cuff tear.

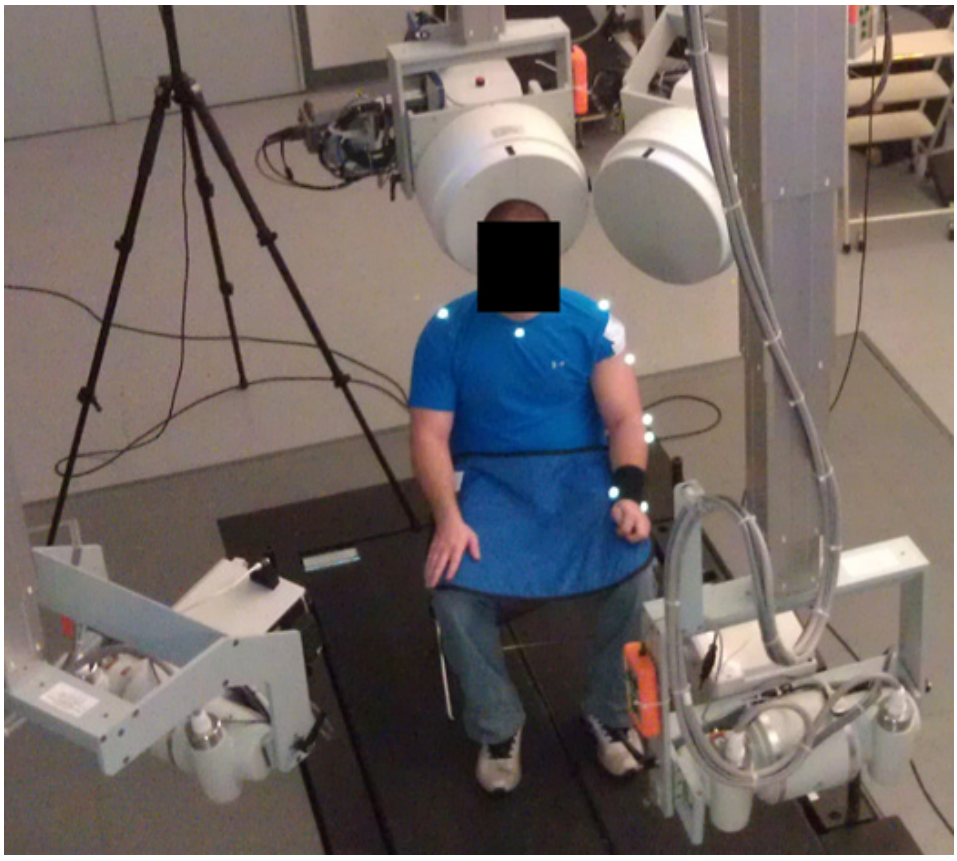

Figure 3.2. Dynamic Stereoradiography (DSX) system setup.

High-speed dynamic stereo x-ray images (75 kVp, 125 mA, 2 ms pulse width) of the glenohumeral joint were collected at 50 Hz during a 2-second period starting just prior to the subject raising their arm and continuing until the point at which the arm was maximally elevated. Two subjects had severe shoulder pain at their first DSX session, and thus the required motion was performed more slowly (same number of images captured over a 4 second period at 25 Hz) to help minimize pain. For these subjects, the post-therapy trial was also captured at 25 Hz. Three-dimensional kinematics of the glenohumeral joint were obtained using a well-established technique that has been previously validated for the glenohumeral joint (188). Briefly, volumetric models for the humerus and scapula were generated from the 3D CT scan by segmenting each bone from surrounding tissues using commercial software (Mimics,

Materialize, Inc.). Digitally reconstructed radiographs (DRRs) of the 3D bone models were simulated using the known projection geometry of the biplane imaging system. The six degree-of-freedom pose of each bone model was manipulated using custom image correlation tracking software until the DRRs matched the DSX images simultaneously in both views for every frame. The resulting dynamic, three-dimensional positions of each bone were combined to generate glenohumeral kinematics.

The 3D reconstructed model for the humerus was assigned a local coordinate system based on International Society of Biomechanics standards (189). The local coordinate system of the scapula was modified from ISB standards to create a glenoid-based coordinate system with origin at the midpoint between the most anterior-posterior points of the glenoid rim. Axes were aligned with the most superior-inferior and anterior-posterior points along the rim of the glenoid (190), with positive directions pointing superior and anterior. Translations and rotations of the humerus with respect to the scapula were then calculated using an Euler rotation sequence (Y-X-Y) (189) and expressed in the glenoid coordinate system, with an accuracy of ±0.4 mm and ±0.5° (188). The glenohumeral contact center location was estimated for each motion frame using the centroid determined from the 3D distance between the two bone surfaces, as previously described (191). Minimum acromiohumeral distance was calculated as the absolute smallest distance between points on the surface of the humeral head (including greater and lesser tuberosities) and the undersurface of the acromion within a 200 mm^2 area defined by a specific region of interest on each bone (191, 192).

Kinematic variables of interest included the average contact center of the humeral head on the glenoid surface (190) and the minimum acromiohumeral distance (AHD) (144, 167, 168). From the glenohumeral contact data, the contact path length (i.e. translation of the humerus on

the glenoid surface through the range of abduction) was calculated as the change in frame-by-frame position of the joint contact center and was normalized to glenoid height (144). Normalized ranges of AP and SI translation of the joint were calculated as the largest difference in anterior-posterior and superior-inferior position of the joint contact center over the entire contact path length. The absolute minimum AHD and average minimum AHD across the full ROM were determined for each subject. Similarly, the absolute and average minimum AHD were also determined for the abduction range of 40-60°. This subset of the full ROM was chosen as an additional parameter to measure AHD at lower joint angles, and provided a measure of the minimum AHD just as the greater tuberosity begins to roll underneath the acromion during abduction (as determined during the tracking process). For each subject, the average values of the above kinematic variables across the three abduction trials were calculated and used for subsequent statistical analysis.

Due to the large variation in ROM between subjects resulting from shoulder pain and loss of rotator cuff function, comparisons between pre- and post-therapy were made on an individual basis using the largest shared ROM between data collection sessions. For example, for a subject with a pre-therapy ROM of 20-60° and a post-therapy ROM of 20-80°, the shared ROM over which kinematic variables were calculated was 20-60°. The 3-trial average values for each kinematic variable were averaged across all subjects both pre- and post-therapy and were used for statistical analysis. Paired t-tests were performed to compare the contact center path length, path range, and minimum AHD variables before and after completion of exercise therapy (0 and 12 week time points). Paired t-tests were also used to compare the four strength measurements and shoulder questionnaire scores, with the exception of the ASES survey, which used a Wilcoxon Signed Rank test due to the data being non-parametric. Due to the small sample size,

Spearman's rho correlation coefficients were calculated to determine relationships between changes in the patient-reported outcome scores, changes in shoulder strength, and changes in kinematic variables from pre- to post-therapy. The significance level for all tests was $p < 0.05$.

3.1.3 Results

All five subjects successfully completed the 12 weeks of therapy and none had sought surgical treatment at 24 months follow up. One subject showed poor compliance with the home exercise protocol and did not give maximal effort during supervised exercise therapy sessions as determined by the supervising physical therapist (i.e. did not complete all exercises during scheduled sessions and did not follow the DAPRE program as the other four subjects did). However, this subject was satisfied with their clinical outcomes and did not elect to undergo surgical repair after completing the study. The maximum elevation attained during testing varied substantially between subjects, resulting in different ranges of glenohumeral elevation for comparison between subjects (Table 3.2). Subjects 1 and 3 had significant shoulder pain and were unable to achieve much greater than 50° of elevation at the pre-therapy time point. Subject 2 had minimal shoulder pain and near-normal range of motion, and thus was able to achieve maximum elevation greater than 90° pre-therapy. Subjects 4 and 5 had shoulder pain during testing at the pre-therapy session, but were able to attain elevations of at least 70° pre-therapy.

Table 3.2. Individual Differences in Kinematics after 12 Weeks of Exercise Therapy

	Patient 1		Patient 2		Patient 3		Patient 4		Patient 5	
	Pre	Post	Pre	Post	Pre	Post	Pre	Post	Pre	Post
Elevation Range Shared Between Trials	21-56°		34-92°		31-51°		44-73°		52-77°	
Minimum AHD over full ROM (mm)	0.1	0.3	0.8	1.4	0.3	0.1	0.3	0.8	1.4	0.3
Minimum AHD from 40-60° abduction (mm)	0.1	0.3	0.7	1.4	0.3	0.0	0.8	1.6	1.6	2.0
Average AHD over full ROM (mm)	0.3	0.9	2.5	3.0	1.1	0.4	1.2	1.1	2.2	2.2
Average AHD from 40-60° abduction (mm)	0.2	0.5	1.1	1.7	0.5	0.3	0.8	1.5	1.8	2.2
SI contact center range (% glenoid SI height)	13.6	15.0	23.8	20.8	7.8	7.0	32.4	35.8	8.4	7.3
AP contact center range (% glenoid AP width)	5.7	4.6	4.7	4.5	1.1	0.9	3.4	4.5	1.2	1.3
Contact Path Length (% glenoid height)	53.2	23.9	104.8	81.4	26.0	28.3	107.5	61.2	43.2	20.5

All five subjects showed improvements in isometric shoulder strength and patient-reported outcomes after 12 weeks of exercise therapy (Table 3.3). Strength measures showed significant increases of 54%, 31%, 74%, and 54% for external rotation at 0° abduction ($p = 0.005$), internal rotation at 0° abduction ($p = 0.036$), external rotation at 90° abduction ($p = 0.009$), and scaption at 90° abduction ($p = 0.024$), respectively. Average improvements in the DASH ($p = 0.047$), ASES ($p = 0.043$), and WORC ($p = 0.02$) scores were all greater than the MCID for DASH (10.2) (187), ASES (6.4) (187), and WORC (245.26) (186) outcomes. At the individual patient level, all subjects showed improvements in the ASES, and four of five showed improvements in the DASH and the WORC greater than the MCID for each. The subject that did not show improvements in the DASH or WORC greater than the MCID exhibited a ceiling effect, already having very good scores pre-therapy (DASH: 9.2 vs. 4.2; WORC: 613 vs 388).

Table 3.3. Average Differences in Clinical Outcomes After 12 Weeks of Exercise Therapy

Clinical Measure	Pre	Post	p-value
Strength for ER @ 0° abduction (N)	54.2 ± 31.3	83.9 ± 22.3	*0.005*
Strength for IR @ 0° abduction (N)	93 ± 45.2	121.8 ± 36.9	*0.036*
Strength for ER @ 90° abduction (N)	46.7 ± 34.1	81.2 ± 20.3	*0.009*
Strength for Scaption @ 90° abduction (N)	40.1 ± 27.4	61.9 ± 20.2	*0.024*
DASH Score	35 ± 18.2	5.6 ± 3.4	*0.047*
ASES Score*	50.7 ± 19.3	88.1 ± 16.3	*0.043*
WORC Score	1198.8 ± 347.6	344.8 ± 393.2	*0.02*
*Data was non-parametric and used Wilcoxon Signed Rank for comparisons			

Overall, four out of five subjects showed individual decreases of at least 20% in glenohumeral contact path length post-therapy. Path length decreased by an average of 36% after 12 weeks of exercise therapy (pre-therapy: 67.2 ± 36.9 % of glenoid height, post-therapy: 43.1 ± 26.9 % of glenoid height, $p = 0.036$, Figure 3.3). However, while the overall distance traveled by the humerus on the glenoid surface was shorter after exercise therapy, the overall SI and AP range of translation was similar ($p = 0.88$ and $p = 0.89$, respectively) to baseline values. Prior to therapy, the SI range was 17.1 ± 10.0 % glenoid height and the AP range was 3.5 ± 2.3 % glenoid AP width. Post-therapy, the SI and AP ranges were 17.2 ± 12.0 % glenoid height and 3.2 ± 1.9 % glenoid AP width, respectively.

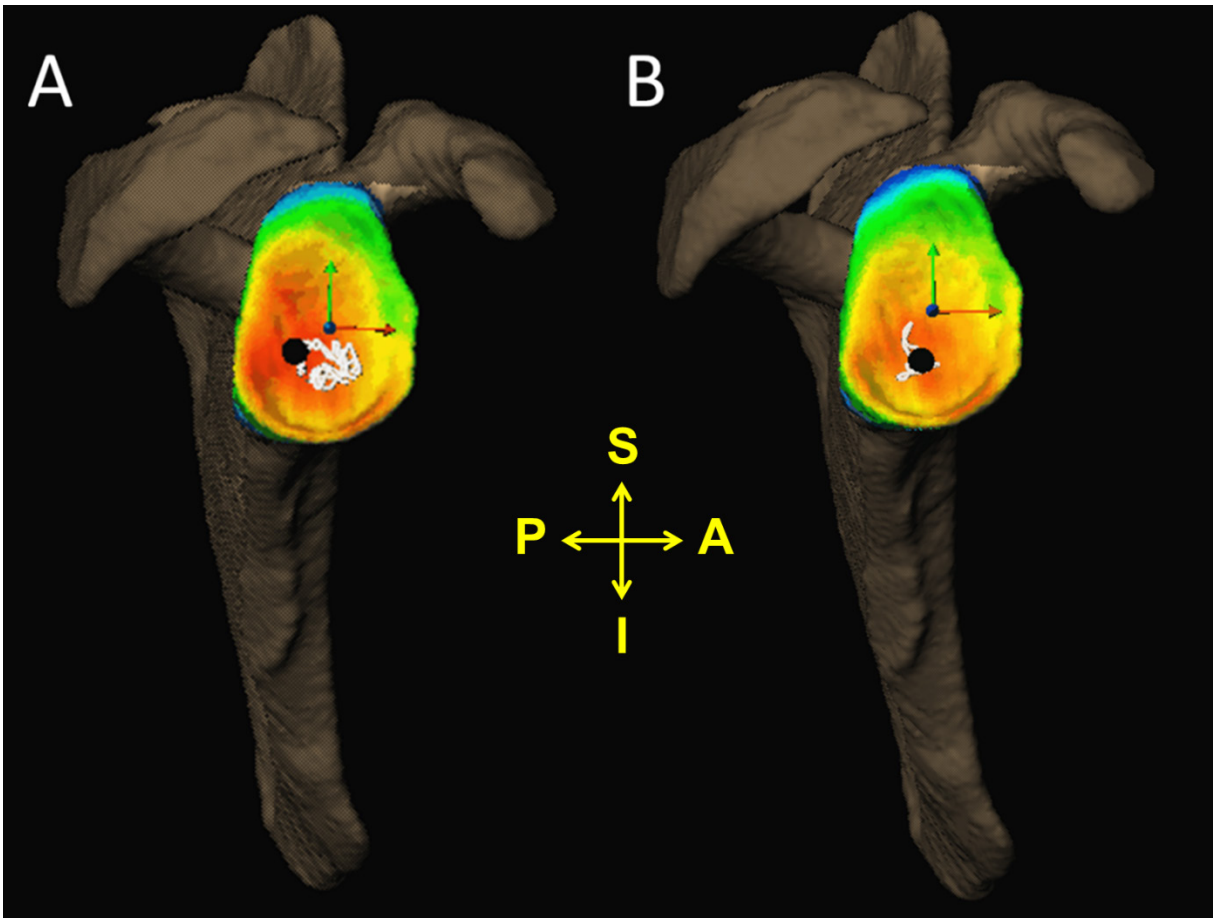

Figure 3.3. Representative contact path kinematics for the right shoulder of a single patient at A) pre-therapy and B) post-therapy. The contact center of the head of the humerus on the surface of the glenoid is represented by a black circle, and the path followed by the contact center throughout the range of abduction is represented by the white line drawn on the glenoid surface. Qualitatively, there is a significant reduction in contact path length post-therapy.

Three of five subjects showed increases of at least 0.4 mm in absolute and average minimum AHD after exercise therapy compared to pre-therapy, though these changes were not statistically significant in any of the subjects. The largest individual increase in sub-acromial space observed over the full range of motion was approximately 0.7 mm (Table 3.2, Patient 2). Over the full range of glenohumeral elevation, the absolute minimum AHD was 0.6 ± 0.6 mm pre-therapy and 0.7 ± 0.8 mm post-therapy ($p = 0.31$). The average minimum AHD over the full

ROM for pre- and post-therapy were 1.5 ± 0.9 mm and 1.5 ± 1.1 mm, respectively (p = 0.81) (Figure 3.4). When considering only the range between 40-60°, the absolute minimum AHD pre-therapy was 0.7 ± 0.6 mm, which increased to 1.1 ± 0.9 mm post-therapy (p = 0.099). Similarly, there was an increase from 0.9 ± 0.6 mm to 1.3 ± 0.8 mm for the average minimum AHD between 40-60° (p = 0.079).

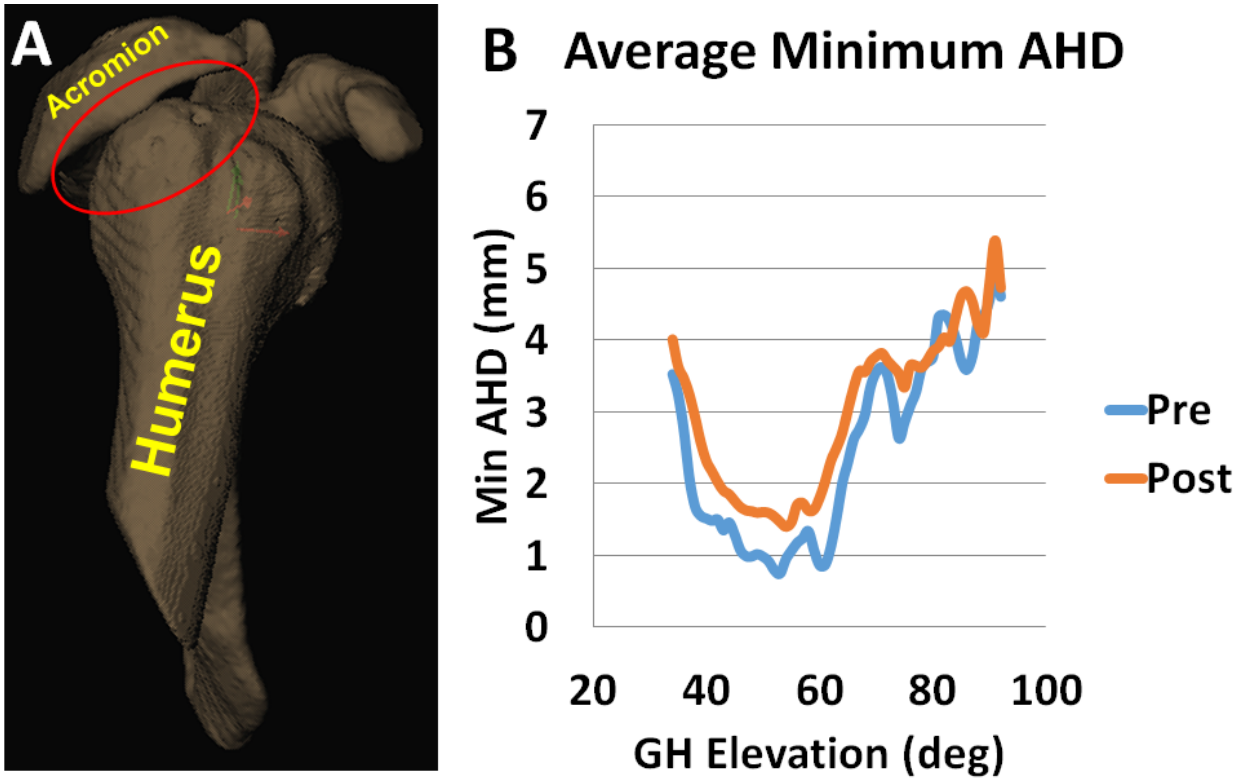

Figure 3.4. Minimum acromiohumeral distances for a representative subject. A) 3D kinematic models of the humerus and scapula showed a small space between the greater tuberosity of the humeral head and the undersurface of the acromion (red oval). B) Minimum AHD remained less than 2 mm even after completion of exercise therapy.

When comparing magnitude of changes in kinematics parameters with the percent strength increase between 0 and 12 week time points, the change in path length showed non-significant negative correlations with strength measures for scaption at 90° abduction (ρ = -0.10, p = 0.87), internal rotation at 0° abduction (ρ = -0.10, p = 0.87), external rotation at 0° abduction (ρ = -0.50, p = 0.39), or external rotation at 90° abduction (ρ = -0.70, p = 0.19). The change in minimum AHD for the elevation range of 40-60° was negatively correlated with strength measures for external rotation at 0° abduction (ρ = -0.90, p = 0.037), but was not significantly correlated with internal rotation at 0° abduction (ρ = -0.60, p = 0.28), scaption at 90° abduction (ρ = -0.60, p = 0.28), or external rotation at 90° abduction (ρ = -0.80, p = 0.10). No correlations were observed between changes in any kinematics variables with the change in DASH, ASES, or WORC scores.

3.1.4 Discussion

The primary findings of this study were that 1) patients showed improvements in patient-reported outcomes and shoulder strength and 2) an overall decrease in the translation of the glenohumeral joint occurred after a 12 week exercise therapy program for treatment of a full-thickness supraspinatus tear. There was a substantial decrease in contact path length that indicates greater joint stability during coronal plane arm abduction and supports the hypothesis that exercise therapy improves joint kinematics. This improvement in stability likely resulted from compensatory increases in rotator cuff and scapular stabilizer muscle strength brought on by the 12 weeks of exercise therapy. The finding that isometric shoulder strength increased for all test positions indicates that exercise therapy was successful in improving muscle strength to compensate for loss of rotator cuff function, one of the primary goals of exercise therapy (89).

Additionally, though the contact path length was found to decrease after exercise therapy, the SI and AP range of the contact path showed no differences post-therapy. This shows that the excursion of the humerus on the glenoid surface remained within the same SI/AP area, but traveled a shorter distance after exercise therapy. Therefore, glenohumeral joint translation is not more restricted after exercise therapy, but translates less within a given space. This may indicate that if left untreated, joint instability could lead to greater wear on joint cartilage, possibly inducing pain and leading to a higher risk of osteoarthritis.

The contact path length results of this study differ from those of a previous study comparing changes in kinematics following rotator cuff repair to contralateral and healthy shoulders using biplane x-ray (144). No differences were found in contact path length or SI contact range between repaired and contralateral shoulders or between repaired shoulders and shoulders from healthy individuals, suggesting that rotator cuff repair restores the glenohumeral joint kinematics to near normal. However, the overall contact path length measured by Bey et al. was only 20-25% of the glenoid SI height, which was 1/2 of the contact path length measured post-therapy in this study (and approximately 1/3 of the path length measured pre-therapy). This may indicate that while exercise therapy improves joint stability and reduces translation of the glenohumeral joint compared to pre-therapy, it does not restore kinematics to the levels of an intact or repaired tendon.

In this study any increases observed in sub-acromial space post-therapy were all sub-millimeter in magnitude, and in a range that was similar to the accuracy of the system (±0.4 mm). Therefore, any changes in sub-acromial space due to exercise therapy would likely not be clinically relevant, indicating that in this small sample of subjects exercise therapy does not appreciably increase the minimum AHD in the glenohumeral joint. The absolute minimum

AHDs measured in this study were found to be 2-3 mm smaller than those of healthy controls (167) or individuals after rotator cuff repair (144), which may indicate that sub-acromial impingement can still occur in patients after completing exercise therapy, potentially leading to later shoulder pain.

The finding that increases in minimum AHD were not correlated with improvements in shoulder strength suggests that while exercise therapy for treating impingement syndrome often leads to improvements in patient-reported outcomes and reduction of pain (86), these improvements may not be due to increased sub-acromial space for the affected rotator cuff tendons. However, additional studies with larger patient groups are required to better assess relationships between glenohumeral joint kinematics and changes in patient-reported outcomes after exercise therapy. No correlations were observed between kinematic parameters and patient-reported outcome scores, which is consistent with what has been previously reported (144).

A limitation of this study is the small sample size. Although only five patients were tested, all patients completed the exercise therapy program without electing to undergo surgery and fit specific recruitment critiera representing the general population of individuals with a degenerative rotator cuff tear that are treated with exercise therapy. Overall, the group chosen was sufficient to determine statistically significant differences in important kinematic parameters. Post-hoc power analysis indicated that a sample size of 12 subjects would be required to achieve statistical significance in the minimum AHD parameter, and 9 subjects would be required to achieve statistical significance in correlations between the strength parameters and path length. Additionally, tear size was not measured, and so it was not possible to compare the results to previous studies that found changes in tear size during exercise therapy. Future studies will require expert ultrasound operators to track tear propagation over time to make comparisons

with changes in joint kinematics as a potential factor for determining the success or failure of exercise therapy. The effect of soft-tissue passive stabilizers of the shoulder, such as the glenohumeral capsule, was also not accounted for in this study. Patients with varying amounts of capsular tightness or laxity may show variations in measured glenohumeral kinematics. However, none of the patients in this study exhibited severe capsular tightness (less than 30° of internal/external rotation), and therefore it is expected that most of the changes in kinematics were due to differences in active stabilization due to increased muscle strength, rather than differences in joint capsule laxity. Lastly, the model tracking technique used does not account for cartilage on the humerus or glenoid surface, which can lead to overestimations of contact path length and range (193). However, since the current study was designed to test differences in joint contact from pre- to post-exercise therapy, a lack of cartilage in the model should not have affected the main findings.

3.1.5 Conclusion

Despite exercise therapy not improving glenohumeral joint kinematics to the level of healthy individuals or to individuals following rotator cuff tear repair, this study shows that exercise therapy leads to satisfactory improvements in patient-reported outcomes, strength, and glenohumeral contact path length. These changes are generally sufficient to restore function and minimize shoulder pain to satisfactory levels for patients. However, it is unknown if patient-reported outcomes remain improved over the long term or revert back to pre-therapy levels. Therefore, a future direction of this work is to determine the long-term effects of exercise therapy on glenohumeral joint kinematics for tasks that mimic common activities of daily living. Additional individuals with a rotator cuff tear, including those that fail to improve with exercise

therapy, must be studied to evaluate specific factors associated with success or failure of exercise therapy. The ultimate goal is to develop an algorithm to identify those individuals with a rotator cuff tear who will best respond to non-operative treatment that includes exercise therapy. This study provides preliminary data on the use of in vivo glenohumeral kinematics as a factor for predicting the successful outcome of exercise therapy for the treatment of rotator cuff tears.

4.0 AIM 2: EFFECT OF TEAR GEOMETRY ON PROPAGATION

In order to improve treatments of rotator cuff tears, it is important to understand their etiology. Propagation of rotator cuff tears after completion of exercise therapy protocols for the treatment of rotator cuff tears has previously been observed (85, 87, 130-133), and therefore this may be another potential contributor to the failure of exercise therapy. However, there is a lack of information on which specific tear characteristics lead to propagation of a rotator cuff tear. Previous research has shown that the geometry of a rotator cuff tear can drastically alter the strain environment at the edges of the tear. Large increases in strain due to the geometry of the tear could therefore result in a greater likelihood of tear propagation. Although tear size has been shown to relate to tear propagation (135), the effects of tear location on tendon strain and tear propagation are less understood. Therefore, the second aim of this dissertation was to quantify the effects of tear geometry on tear propagation. By determining how the size and location of a tear relate to its propensity to propagate, treatment protocols can be optimized based on which patients are at greater risk to develop larger tears.

4.1 EFFECT OF TEAR LOCATION ON SUPRASPINATUS TEAR PROPAGATION

4.1.1 Introduction

Rotator cuff tears are the most common cause of disability related to the shoulder. More than 30% of asymptomatic persons over the age of 60 years have a partial or full thickness rotator cuff tear (66, 70). Non-operative treatment is the first option for management of rotator cuff disorders and has been shown to be effective for many patients (131). However, it has been shown that non-operative treatments such as exercise therapy fail in 25 - 50% of cases (101). Early detection and intervention, including surgical treatment, has been shown to improve the outcome of patients with rotator cuff tears (164, 194, 195). It is currently unknown which factors, such as patient or tear characteristics, are most related to successful early intervention for rotator cuff tears, but potential for tear propagation may be an important factor. Several studies have examined potential risk factors for tear propagation (130, 132, 152), including patient demographics such as age, gender, and smoking, and tear characteristics such as size and fatty infiltration. Previously, no correlations have been found to exist between increases in tear size and age or gender, occurrence of a prior trauma, initial size of the tear, or tear laterality (130). On the other hand, full-thickness tears and fatty infiltration of the rotator cuff muscles in patients greater than 60 years old are associated with progression of a rotator cuff tear (132). A correlation between habitual smoking and rotator cuff tear propagation has also been documented (69, 196). However, little is known about the influence of tear location on tear propagation.

It has been proposed that most rotator cuff tears start at the anterior insertion of the supraspinatus on the humeral head and extend posteriorly into the supraspinatus tendon (136, 139, 148, 151, 197). However, degenerative rotator cuff tears typically initiate 1.3 to 1.7 cm posterior to the biceps tendon and extend anteriorly and posteriorly from that point (150). This region corresponds to the center of the rotator crescent (198) which has been suggested to be the area of poorest vascularity in the rotator cuff tendons (159). From anatomical examination of the rotator cuff cable and crescent complex, the rotator cuff cable was determined to be the primary load-bearing structure in the tendon, whereas the crescent was stress shielded (52, 199).

The clinical significance of tear location on the choice of timely clinical treatment is unclear. Due to differences in tendon structure and material properties throughout the rotator cuff footprint (171), there is a discrete possibility of rotator cuff tears propagating differently based on their location of initiation. Therefore, the purpose of this study was to determine the effects of initial tear location on rotator cuff tear propagation in a cadaveric model under increasing levels of cyclic loading. It was hypothesized that tears initiating in the anterior third of the supraspinatus tendon would propagate more easily and would require lower loads to reach critical amounts of tear propagation than tears initiating in the middle third of the tendon.

4.1.2 Materials and Methods

Twenty-three fresh frozen human cadaveric shoulders with a mean age of 60 years (range 42 to 83 years; five females and eighteen males) were used in this study. No specimens had prior rotator cuff injury or osteoarthritis of the shoulder joint. Shoulders were stored at -20°C and allowed to thaw overnight at room temperature prior to dissection and testing. All soft tissue except for the supraspinatus, infraspinatus, and subscapularis tendons was removed from the

humerus, and the individual rotator cuff tendons were isolated. The specimens were kept moistened with physiologic saline solution to prevent dehydration throughout testing. Each humerus was potted in epoxy putty and secured in a custom clamp to a materials testing machine (Model 4502; Instron Corp., Norwood, MA, USA). In order to prevent slippage of the tendon from the clamps, suture loops (#2 Ethibond sutures, Ethicon Inc, Somerville, NJ, USA) were made using Krackow loop stitches (200) in the supraspinatus tendon at the site where it was clamped. The supraspinatus tendon was then attached to the crosshead for tensile loading to simulate 90° of coronal-plane abduction. In addition, a 22 N load was applied to the infraspinatus via a cable-pulley system (Figure 4.1).

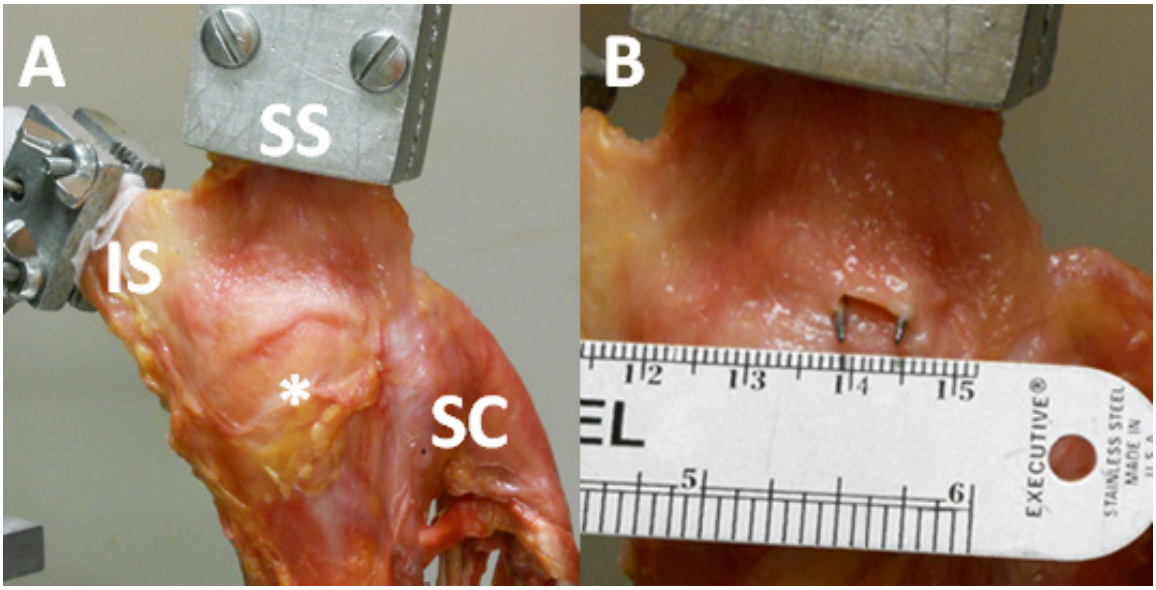

Figure 4.1. Mechanical testing setup for cyclic loading. Pictured is a left shoulder with supraspinatus tendon (SS) clamped to the crosshead of a materials testing machine. Also shown are the humerus (*), subscapularis tendon (SC), and clamped infraspinatus tendon (IS). A 22-N weight (not shown) is applied to the infraspinatus by pulley. A: Intact tendon prior to tear creation. B: Tendon bursal surface after creation of 1 cm anterior tear.

Prior to testing, a preload of 50 N and preconditioning from 50 to 100 N for 100 cycles were applied to the supraspinatus tendon in order to minimize soft tissue viscoelasticity. The preload of 50 N sufficed to ensure that all tendon fibers were adequately loaded prior to tear creation and to allow clear visualization of tear geometry. A 1 cm long incision in the anterior-to- posterior direction was then created with a scalpel blade in the anterior third of the supraspinatus tendon of 10 specimens, cutting through all but the most anterior edge of the rotator cable (52, 201), leaving the remainder of the cable attached to the greater tuberosity of the humerus (Group A, Figure 4.2-A) (mean age, 64.1 years; range, 51 to 83 years; 1 female and 9 male specimens). In the remaining 13 shoulders, a tear was created in the middle-third of the supraspinatus tendon (Group M, Figure 4.2-B) (mean age, 58.0 years; range, 42 to 78 years; 4 female and 9 male specimens). To create these tears, the center of the tendon in the AP direction was located using a ruler, from which point an incision was created that extended 0.5 cm in the anterior and posterior directions, thus modeling a 1 cm long tear. There was no statistically significant difference in age between the two groups ($p = 0.15$). The choice of location for tears was based on previous studies showing that the anterior portion of the supraspinatus tendon is stronger than the other portions (171). In addition, rotator cuff tears typically begin 13 to 17 mm posterior to the biceps tendon and extend anteriorly and posteriorly from that point (198).

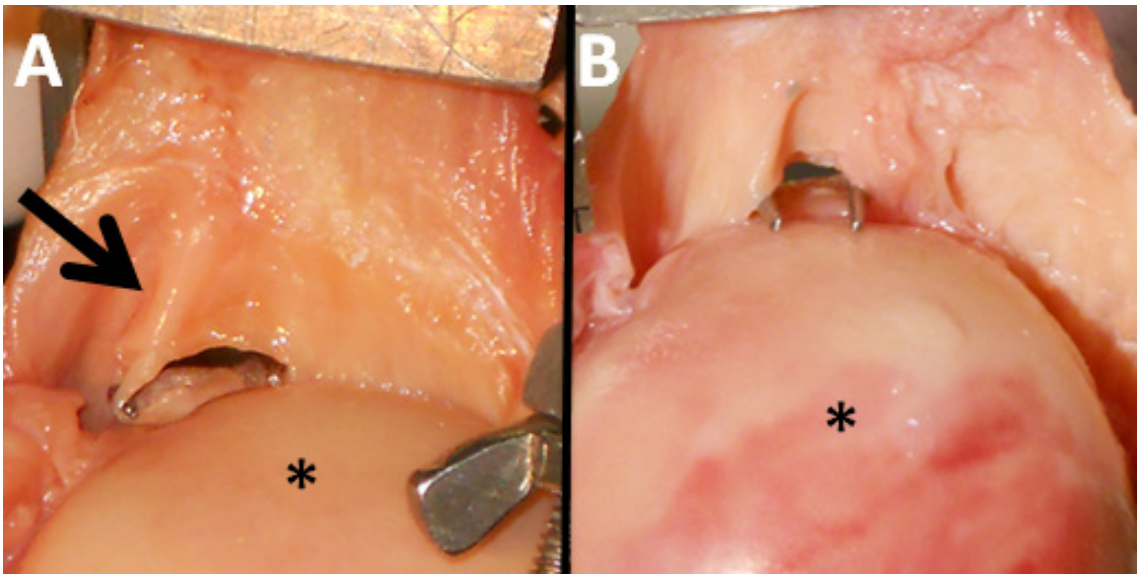

Figure 4.2. Articular-side views of artificially created tears. A) Anterior tear. B) Middle-third tear. Note the presence of the rotator cable (arrow), which is interrupted by the tear. The humerus is denoted by an asterisk (*).

After creating the tear, specimens were loaded for 100 cycles from 50 - 100 N at a rate of 20 mm/min. This loading was followed by additional sets of 100 cycles, increasing the maximum load by 100 N for each set until a critical tendon retraction of 2 cm in the medial to lateral direction was reached (Figure 4.3). The choice of 2 cm was made based on this being a transition point from “minor” to “medium” retraction (92). At this stage, tears begin to take on a “U-shape” that is more complex to repair (202), thus representing a transition point from good to potentially poor clinical repair outcomes. Additionally, the maximum increase of 100 N for each set of 100 cycles was chosen to investigate the loading level required to induce tear propagation, with the first loading set of 100 N being the approximate peak load experienced by the supraspinatus tendon at 90° abduction during normal activity (41). The use of 100-cycle sets was chosen to approximate longer-term, repetitive rotator cuff use during daily activities that can lead to tissue fatigue damage and tear propagation. To determine if a tear had reached the critical tendon retraction, a ruler was used to measure the tear at the end of each set of 100 cycles. Testing was

terminated if the retraction reached 2 cm between cycle sets, or if tissue failure occurred during a given set of cycles.

To measure changes in tear length and area over time, digital images (4320 x 3240 pixels) were taken at the conclusion of each loading set and were processed with NIH ImageJ software (National Institute of Health, Bethesda, MD, USA). Tear area was measured using the "polygon selection" tool to carefully outline the edges of the tear (Figure 4.2) in each image. All measurements of tear dimensions were performed at the 50 N preloaded state between cycle sets, allowing for comparisons of tear dimension to be made at a consistent load. This is conceptually similar to the conventional clinical practice of measuring rotator cuff tendon retraction on MRI or ultrasound images under conditions of minimal tendon loading.

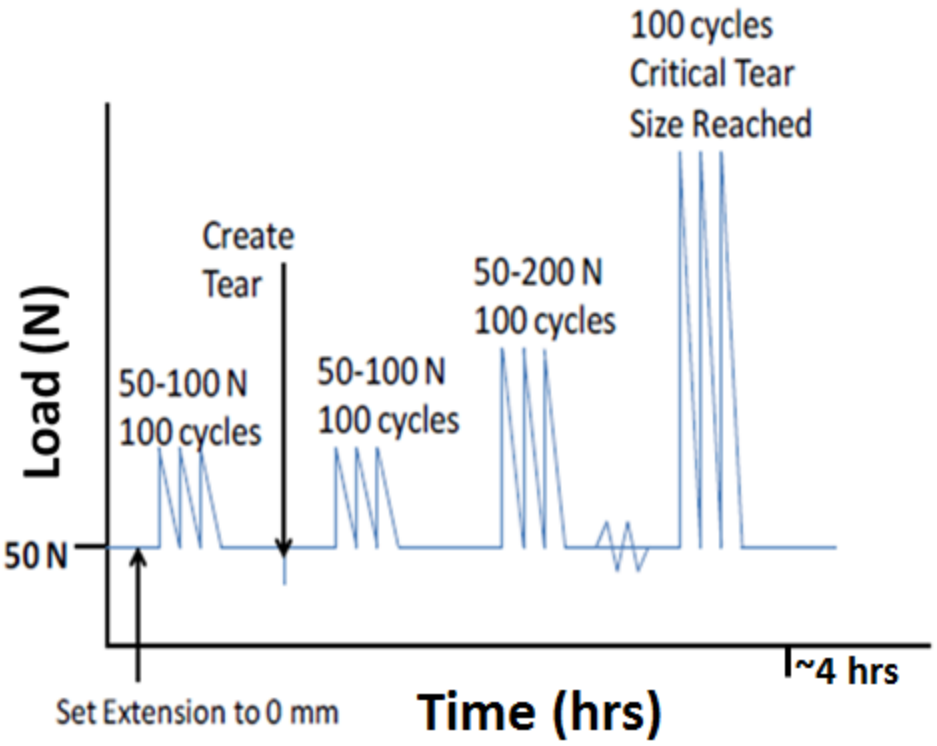

Figure 4.3. Loading protocol as a function of time.

The peak cyclic load at which the critical tendon retraction was reached, and the tear area for the cycle set prior to the final loading cycle (i.e. the set of cycles immediately prior to the set where the 2 cm tendon retraction was reached) were compared between Groups A and M, using unpaired t-tests to determine the effect of tear location on the extent of tear propagation. An unpaired t-test was also used to compare the lowest cycle-maximum load at which at least a 100% increase in tear area was observed between groups, as a measure of when tear progression initiated. This choice of a 100% increase in tear area between cycle sets represents a sudden doubling in tear size, and serves as a plausible benchmark of change from an asymptomatic to a symptomatic tear (130).

Additionally, correlation analysis was performed for age versus maximum load and for age versus the lowest load to cause a 100% increase in tear area for each group in order to assess the effects of age on tear propagation. Pearson's r value was calculated for Group M. The data for Group A were found to be non-parametric with a large number of tied ranks. Therefore, for Group A, Kendall's Tau-b was used as the correlation coefficient. R^2 was also calculated for each group to determine goodness of fit. Effect sizes were set at 0.1 for small, 0.3 for moderate, and 0.5 for strong correlation values (203). Significance was set at $p < 0.05$ for all tests.

4.1.3 Results

In Group A, the maximum load at which the critical tendon retraction was reached averaged 587 ± 188 N (range 400 - 900 N). The maximum load at which the critical tendon retraction was reached in Group M was similar: 736 ± 220 N (range 400 - 1100 N) (p = 0.09) (Figure 4.4-A). The tear area at the conclusion of the cycle set prior to failure for Group A was 0.52 ± 0.41 cm^2, whereas for Group M it was 0.41 ± 0.34 cm^2 (p = 0.6; Figure 4.4-B). Tendons in Group A

generally showed larger increases in tear area for earlier loading sets compared to Group M. This phase was followed by large increases for both groups in tear area prior to reaching the critical tear size (Figure 4.5). The lowest load at which at least a 100% increase in tear area occurred was 389 ± 237 N in Group A, a value that was significantly ($p = 0.03$) lower than the corresponding value (714 ± 168 N) in Group M (Figure 4.6).

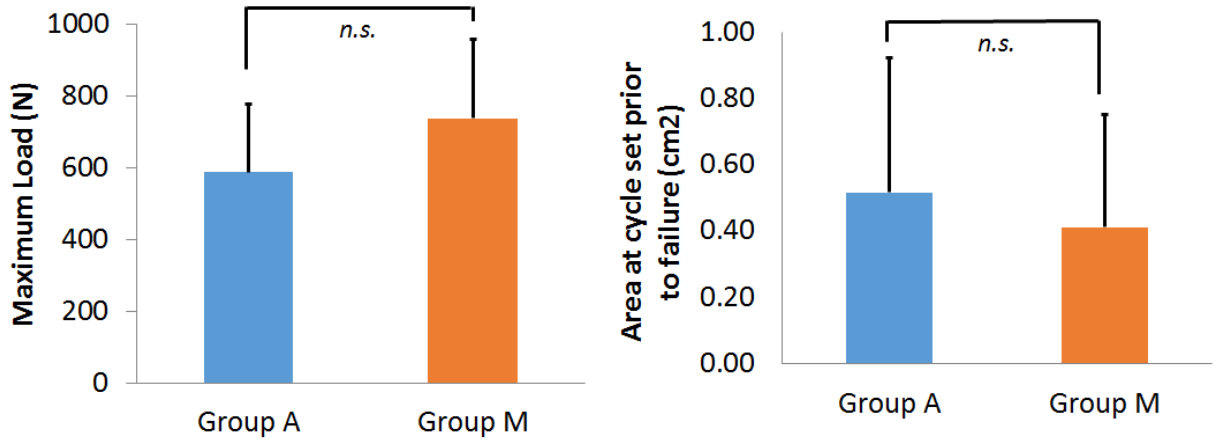

Figure 4.4. Tear propagation results between locations. A) Maximum tensile load. B) Tear area at the end of the cycle set prior to the final loading cycle (before reaching the 2 cm retraction or failure occurred).

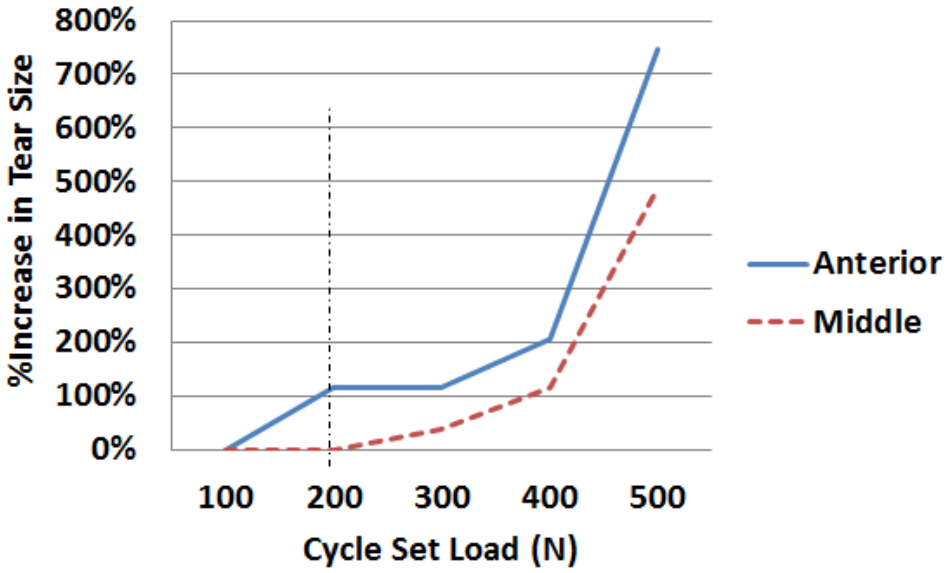

Figure 4.5. Representative plots of the cumulative increase in tear area between cycle sets. Note that the tear in the Group A specimen reaches a 100% increase in tear area (200 N) much earlier than the specimen in Group M (400 N).

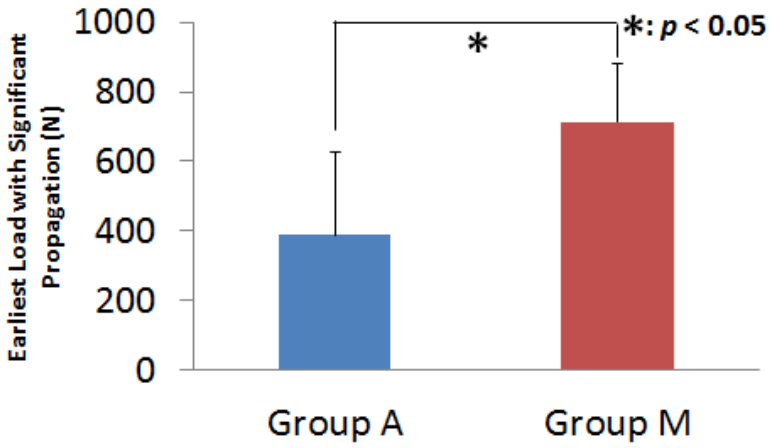

Figure 4.6. Earliest loading cycle set at which at least a 100% increase in tear area is seen. Group A showed a significantly lower load was required than for Group M ($p < 0.05$).

Age correlated negatively with maximum cyclic load to the supraspinatus tendon. Strong negative correlations were detected for both Group M (r = -0.63, p = 0.04; Figure 4.7-A) and Group A (τ = -0.82, p = 0.01; Figure 4.7-B). Correlations between age and the load required to cause a 100% increase in tear area between cycle sets showed a strong negative correlation in Group A (τ = -0.64, p = 0.02), but there was no statistically significant correlation in Group M (r = -0.23, p = 0.55). Of the 10 shoulders tested in the anterior tear group, two tendons failed in the mid-substance during the final loading set before reaching the critical tendon retraction and were excluded from the analysis. In the middle-third tear group, 2 out of 13 shoulders had mid-substance failures and were similarly excluded. All other tendons reached the critical tendon retraction of 2 cm. Tears showed significant medial-lateral and anterior-posterior propagation in both groups. All tears remained isolated to the supraspinatus tendon.

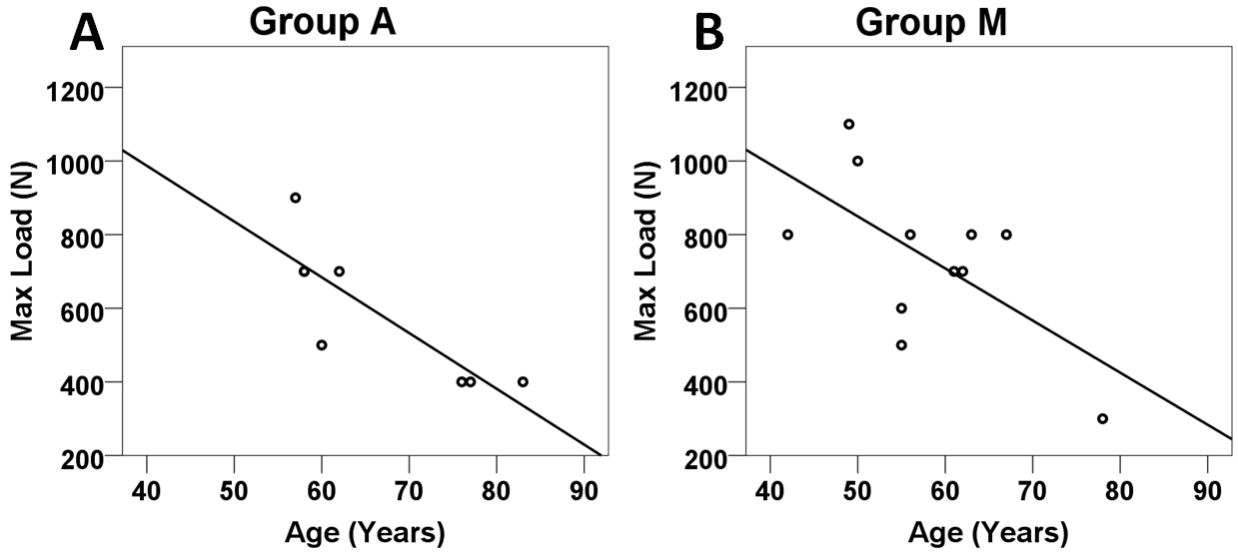

Figure 4.7. Correlations between age and cycle-maximum tensile load. Correlations were significant for both A) Group A (τ = -0.82) and for B) Group M (r = -0.63).

4.1.4 Discussion

The current study demonstrates the effect of tear location on tear propagation for small, full-thickness tears of the supraspinatus tendon during increasing levels of extended cyclic loading. Under the conditions of this study, tear location did not have a significant effect on the propagation of the tear in terms of the maximum load at which the critical tendon retraction was reached, or on the tear area at the end of the cycle set prior to failure, thus partially refuting the hypothesis of this study. However, with respect to the earliest loading cycle set at which at least a 100% increase in tear area was seen, Group A showed significantly earlier tear propagation than Group M. According to Burkhart et al. (52), the region from the biceps tendon to the inferior border of the infraspinatus tendon spans the rotator crescent, the margin of which is outlined by the arch-shaped thick bundles of fibers called the ‘‘rotator cable.’’ Those authors theorized that the rotator cable shields the rotator crescent from stress through a ‘‘suspension bridge’’ configuration. In the present study, the tear in Group A involved cutting through all but the most anterior edge of the rotator cable. Other studies which have used similar surgically-created tear models to investigate the effects of rotator cuff tendon tears on tendon strain (139, 148) and tear propagation (45, 135) have shown that the rotator cuff cable is the primary structure within the supraspinatus responsible for force transmission to the proximal part of the humerus (154). Recently, anterior tears of the supraspinatus tendon have been associated with greater tear gapping, decreased tendon stiffness, and increased regional tendon strain under physiologic loading conditions compared to equivalently sized tears located in the rotator cuff crescent (154). Those earlier findings support the results of this study, which suggest that tears in the anterior part of the supraspinatus tendon that interrupt the rotator cable tend to propagate more readily than tears in the middle third. Motions or exercises that put increased tensile stress

on the anterior supraspinatus tendon (e.g. external rotation) should therefore be avoided in patients with anteriorly located rotator cuff tears.

The location of a rotator cuff tear is crucial for prognosis. Detection of early propagation may be beneficial for establishing a treatment strategy for rotator cuff tears. The results of this study suggest that tears in the anterior part of the supraspinatus tendon tend to propagate more readily than tears in the middle third. Therefore, if the location of the rotator cuff tear can be identified, the results of the current study may help predict the likelihood of tear propagation and thus constitute an indication for early surgical treatment. Previous work has shown that 51% of asymptomatic tears become symptomatic after an average of 2.8 years (76). In a separate study, 49% of patients were found to have an increase in anterior-posterior tear size of 5 mm or more at a mean follow-up of 29 months, and a significant correlation was found between the existence of pain and an increase in tear size (130). Therefore, early examinations and treatments for rotator cuff tears are considered to be crucial to prevent the progression of tears.

A strong negative correlation was observed between age and maximum tensile load (Figure 4.7). In a previous study investigating progression of tear size over time, 52% of patients with full-thickness symptomatic rotator cuff tears showed an increase in tear size at an average of 24 month follow-up (132). An age of more than 60 years and initial rotator cuff fatty infiltration were found to correlate with tear propagation. Additionally, while a strong negative correlation was found between age and the load required to cause a 100% increase in tear area between cycles in Group A, no such statistically significant correlation was found for Group M. This may indicate that older patients may be more at risk for early propagation of anterior rotator cuff tears than of centrally located tears. The results from the current study and from clinical experience suggest that age could be an important risk factor for tear propagation.

Limitations of this study include that the physical size of the cadavers used was not uniform. However, all specimens were free of degenerative joint disease, and a consistent 1-cm tear was made in each specimen. In addition, other factors such as tendon quality or metabolic status were not controlled, and may have had an effect on the maximum load and/or tear areas observed. This study investigated only small, full-thickness tears of the supraspinatus tendon surgically created in normal tendons. Pre-existing tears in tendons may behave differently due to tendon degeneration and tissue quality. Tears of different size and shape, or tears in tendons of different tissue quality, may behave differently in terms of propensity for propagation of the tear.

While there was a disparity in donor gender, previous studies have found no gender-related differences in soft tissue material properties (204, 205) or in the prevalence (66) or propagation (130) of rotator cuff tears. There was no statistically significant difference in specimen age between Groups A and M. Therefore, it is believed that the statistical comparisons made between groups are valid. A post-hoc power analysis to determine sample size required to achieve statistical significance in maximum load between groups showed that at least 60 specimens would have been required.

Although no histology or measures of fiber alignment were performed to investigate differences in collagen fiber alignment by location, previous studies have found collagen fibers to be primarily aligned with the long axis of the tendon, with intermingling of the infraspinatus and subscapularis tendon fibers at the insertion on the humerus (35). These fibers increasingly align along the tendon long axis during loading (206). Therefore, it is likely that tear propagation was primarily due to collagen fiber rupture perpendicular to the direction of tear propagation. However, the patterns of tear propagation observed in this study may differ for other types of loading scenarios that can unevenly load the tendon and result in transverse shear, such as

internal/external rotation of the shoulder. Future studies should consider the effects of other glenohumeral joint motions on the potential for tear propagation.

4.1.5 Conclusion

Based on the results of this study, early examination and treatment for rotator cuff tears appears to be beneficial for preventing the progression of tears located in the anterior supraspinatus tendon that interrupt the rotator cable. The results from this study may improve assessment of risks for tear propagation, especially for tears that interrupt the rotator cable structure. Potential areas for future work include performing mechanical testing of specimens with pre-existing degenerative rotator cuff tears, and developing an experimentally-validated finite element model to investigate other factors (such as tear shape) that may affect rotator cuff tear propagation.

4.2 EFFECT OF ANTERIOR SUPRASPINATUS TEARS ON TENDON STRAIN

4.2.1 Introduction

Tears of the rotator cuff tendons are a significant clinical problem that affects the middle-to-late aged population, with a 50% likelihood of having a bilateral tear in people over the age of 66 years (67). As patients continue to age, the likelihood of a degenerative full-thickness rotator cuff tear further increases (64, 207). Rotator cuff tears have the potential to cause severe pain and limit shoulder strength and mobility, leading to long-term dysfunction of the glenohumeral joint (18-22). Therefore, it is important to treat smaller rotator cuff tears early (208) before they can propagate into large or massive tears that have much higher re-tear rates (80). Massive tears are significantly more difficult to repair and are associated with worse clinical outcomes (20, 80, 81).

Previous studies have investigated tendon surface strains as a factor contributing to the initiation and propagation of rotator cuff tears (135, 139-141, 148). These studies showed relationships between regions of high strain and common regions of tear initiation (136, 141, 151), between direction of propagation and strain magnitude (135), and between tear size and tendon strain (135). Increases in strain at the edges of tears have been found for central supraspinatus tears in a cadaveric, static loading model (148) and in a sheep infraspinatus cyclic loading model (135). Therefore, elevated strains at tear edges lead to increased tendon retraction and anterior-posterior propagation of a small tear into a large, multi-tendon tear. Although these studies investigated a variety of factors that have an effect on tendon strain, the tears created in

the studies were all located in the central third of the supraspinatus tendon. However, tear location might be a clinically significant factor for tendon strain and tear propagation.

The most common location for rotator cuff tears is in the central third of the supraspinatus tendon (150). The anterior supraspinatus tendon incorporates the rotator cable complex, believed to provide structural support and load distribution function to the rotator cuff (52). If the rotator cable structure is interrupted by an anterior tear, then any reinforcement to the tissue by this structure is lost, potentially leading to greater risk of tear propagation. In addition, due to the higher structural and mechanical properties of the anterior supraspinatus tendon (171), anterior tears may be more likely to propagate posteriorly into the structurally weaker portions of the tendon. Therefore, anterior tears may propagate more easily or in an unexpected manner compared to centrally located tears. It is not currently understood how tears that are more anteriorly located will propagate or if they will exhibit altered strain distributions compared to supraspinatus tendons with more centrally located tears. Investigation of the strain distribution in supraspinatus tendons with anteriorly located tears can provide information on how these types of tears propagate during loading. Ultimately, this information can assist in development of better treatment options for rotator cuff tears by improving knowledge of tear propagation risk for anteriorly located tears. Therefore, the objective of this study was to determine the strain distribution for tears in the anterior third of the supraspinatus tendon and the relationship to tear propagation during a cyclic loading protocol. It was hypothesized that the highest maximum principal strain would correspond with the direction of tear propagation and is located posteriorly to anterior supraspinatus tears.

4.2.2 Materials and Methods

4.2.2.1 Mechanical Testing

Eight fresh-frozen cadaveric shoulders (age 65.5 ± 11.5 years) with no visible injury to the rotator cuff tendons or signs of osteoarthritis were dissected. All tissues were stored at -20°C and allowed to thaw overnight at room temperature before testing. All soft tissue except for the supraspinatus, infraspinatus, and subscapularis tendons was removed from the humerus. Each humerus was potted in epoxy putty and secured in a custom clamp to the base of a materials testing machine (Model 4502; Instron Corp., Norwood, MA, USA). The supraspinatus tendon was clamped to the crosshead for tensile loading to simulate 90° of glenohumeral abduction in the scapular plane, and a 22 N load (41) was placed on the infraspinatus via a pulley system. Only the supraspinatus tendon was dynamically loaded. The infraspinatus tendon was loaded statically to approximate the load-sharing interaction between the fibers of the infraspinatus and supraspinatus tendons inserting on the humeral head. The subscapularis was not loaded due to minimal interaction between its fibers and the supraspinatus tendon. Similar loading configurations have been utilized previously (50, 51, 209, 210).

A 5 by 4 array of strain markers was attached using cyanoacrylate glue to the bursal surface of the tendon (Figure 4.8-A). The top row was placed directly below the edge of the supraspinatus tendon clamp to visually detect any clamp slippage, and the bottom row was placed just below the tendon insertion to the greater tuberosity. The middle rows were placed on the tendon mid-substance. A custom digital motion tracking system (Spica Technology, Kihei, Maui, HI; 0.01 mm accuracy) (211), was used to track the 2D displacements of the strain markers using a single video camera aligned perpendicular to the plane of the bursal surface of

the tendon. The surface of the tendon was representatively broken into twelve “elements” based on the placement of the strain markers to allow for comparisons of strain based on location on the bursal surface. A preload of 50 N was applied to the supraspinatus tendon to sufficiently load the tendon for visualizing the tear, and preconditioning from 50-100 N for 100 cycles at 20 mm/min was performed. The preload was then reapplied and the location of the strain markers was recorded as the reference configuration.

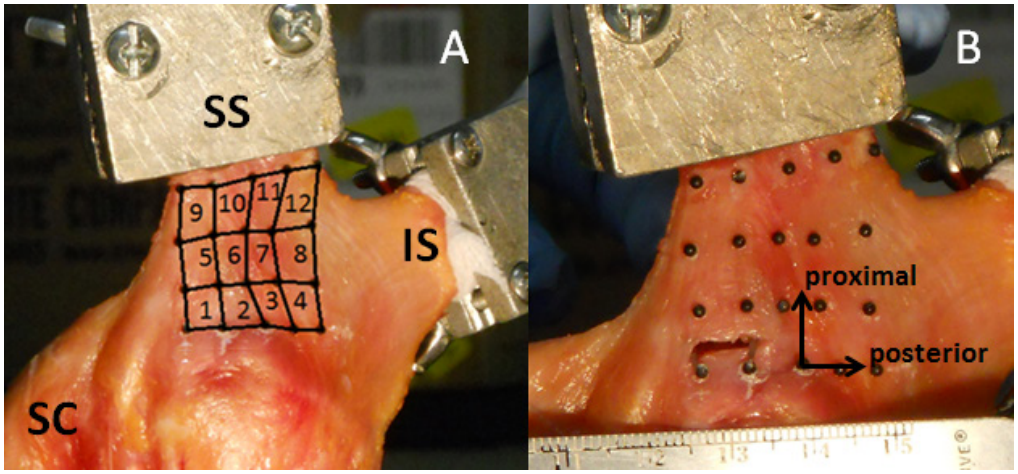

Figure 4.8. Tendon surface markers for strain calculations. Lateral view of a left shoulder showing subscapularis tendon (SC), clamped infraspinatus tendon (IS) with 22N weight attached by pulley, and supraspinatus tendon (SS) clamped to the materials testing machine crosshead. A) Strain markers are connected to show elements. B) Tendon surface after creation of 1 cm tear in the anterior third of the supraspinatus tendon. Each element has a coordinate system defined for calculation of strain direction.

After recording the reference configuration of the strain markers, a 1 cm tear in the anterior-posterior direction was created in the anterior third of the supraspinatus tendon between the bottom and second row of strain markers. The anterior border of the rotator cable was identified in each specimen visually and by palpating the specimen to find the characteristic

thickening of the cable (52). The anterior edge of the tear was created just posterior to the anterior edge of the rotator cable using a scalpel, cutting through all but 1 mm of the anterior cable width (Figure 4.8-B). Tendons were then loaded for 100 cycles from 50-100 N at a rate of 20 mm/min, followed by additional sets of 100 cycles increasing the maximum load by 100 N for each set until a critical tendon retraction of 2 cm was achieved (Figure 4.3). The maximum increase of 100N for each set of 100 cycles was chosen to investigate the loading level required to induce tear propagation, with the first loading set of 100N being the approximate peak load experienced by the supraspinatus tendon at 90° abduction during normal activity (41). The use of 100 cycle sets was chosen to approximate longer-term rotator cuff use leading to tear propagation. Tear size was measured using a ruler at the end of each set of 100 cycles, i.e. loading set, to determine when the critical tendon retraction was reached. Saline solution was sprayed on the tendons throughout the experimental protocol to maintain tissue hydration.

After tear creation and prior to the first set of loading, the location of the strain markers was again recorded at 50N of load. Once the cyclic loading protocol was started, strain maker location data was recorded at the beginning and end of each set of 100 cycles at 50N of load to observe changes in the strain state with increasing load. In addition to calculating the strain magnitude at the final load set before the tear reached the critical tendon retraction, the load required to reach 5% and 10% strain with respect to the reference configuration in each tendon was determined. These strain states represent approximate lower and upper bounds of the linear region of the stress-strain curves for the intact tendon. 5% is a sub-failure strain marking the point at which permanent deformation begins to occur, while 10% strain represents the point at which tissue failure begins to occur (141).

4.2.2.2 Strain Calculation

The location of the strain markers for each loading set was input into ABAQUS (ABAQUS/CAE Student Version 6.4; Simulia, Providence, RI) as a set of 20 nodes comprising 12 elements to calculate the magnitude and direction of the maximum principal strain. Calculations were performed for each element at the end of each loading set as the difference in marker location between the reference configuration and the current strained configuration (211-213). Green-Lagrange strain was calculated in 2D assuming large deformations and non-linear geometry. Magnitude of maximum principal strain was output for the centroid of each element, and direction was output at each of the four element integration points and averaged to give a single value for each element.

In order to test the first hypothesis that regions of highest maximum principal strain magnitude would be located adjacent to the tear, a one-way repeated measures ANOVA was performed for each tendon ($n = 8$) to compare the magnitude of maximum principal strain based on location on the tendon bursal surface. Strain magnitude was compared element-by-element in each tendon using strain data from each loading set, i.e. 100 N, 200 N, 300 N, etc. Significance was set at $p < 0.05$. Contour plots of the tendon surface strain were then used to determine which element exhibited the largest value of strain for each tendon, noting the location of the element relative to the tear site. Elements that included the tear were excluded from this portion of the analysis.

The direction of maximum principal strain was determined for the end of the first loading set and for the last loading set prior to the tear reaching the critical tendon retraction. A coordinate system was established for each element in the tendons where the x-axis was directed

positively in the posterior direction and the y-axis in the medial direction (Figure 4.8). The strain direction was defined by the angle between the x-axis and the vector representing the maximum principal strain (orange arrows in fringe plots). The strain direction was then compared to the direction of tear propagation recorded on video for each tendon during loading. Tendons were grouped based on whether the strain direction shifted between first and final loading sets in a posterior or anterior direction. A paired t-test was then performed to compare the strain direction between first and last loading sets in each group (significance set at $p < 0.05$).

4.2.3 Results

During the loading protocol, three of the supraspinatus tendons showed unequal amounts of tear propagation on the articular and bursal sides. In these tendons, the tear visibly propagated on the articular side of the tendon and remained small on the bursal side (Figure 4.9). Once the tears reached the critical tendon retraction, catastrophic propagation was visible on both sides in all tendons. In a single tendon, pulling apart of the tendon fibers from the humerus without an increase in tear size was observed for the first two sets of 100 cycles during loading.

The tendons reached the critical tendon retraction at 580 ± 181 N. Five of the tendons showed similar failure patterns (Figure 4.10), demonstrating large amounts of tear propagation in addition to tendon retraction. At the end of the final loading cycle a mostly intact posterior third of the tendon was observed with the anterior third of the tendon attached to the humerus by a small strand of fibers. These five tendons shared similar strain distributions at the load set prior to reaching critical tendon retraction. Regions of highest strain were located in the lateral-anterior edge of the tendon, showing regions of decreasing strain radiating out from the tear

(Figure 4.11). The remaining three tendons either failed mid-substance prior to reaching the critical tendon retraction or did not show anterior-posterior tear propagation (Table 4.1).

Six of the eight tendons showed a statistically significant difference in maximum principal strain magnitude by element location on the bursal surface ($p < 0.001$). The region of highest strain in each of these tendons was located in the elements medially and posteriorly adjacent to the element containing the tear (Figure 4.11). The maximum principal strain magnitude in the elements adjacent to the tear for the load set prior to the tear reaching the critical tendon retraction was 26.1 ± 9.4% (Table 4.2). Two tendons (tendon 1 and tendon 7) showed much larger amounts of tear propagation at lower loads, resulting in larger strain magnitudes around the tear edges compared to tendons that showed smaller amounts of propagation prior to reaching the critical tendon retraction. The load at which the elements directly adjacent to the tear reached a minimum of 5% strain was 112 ± 35 N, and the average load at which at least 10% strain was reached in these elements was 275 ± 183 N. In six of the tendons, the region of highest strain was posterior to the tear, while in the remaining two tendons the region of highest strain was located medially to the tear. In these two tendons, no anterior-posterior tear propagation was observed (Table 4.1).

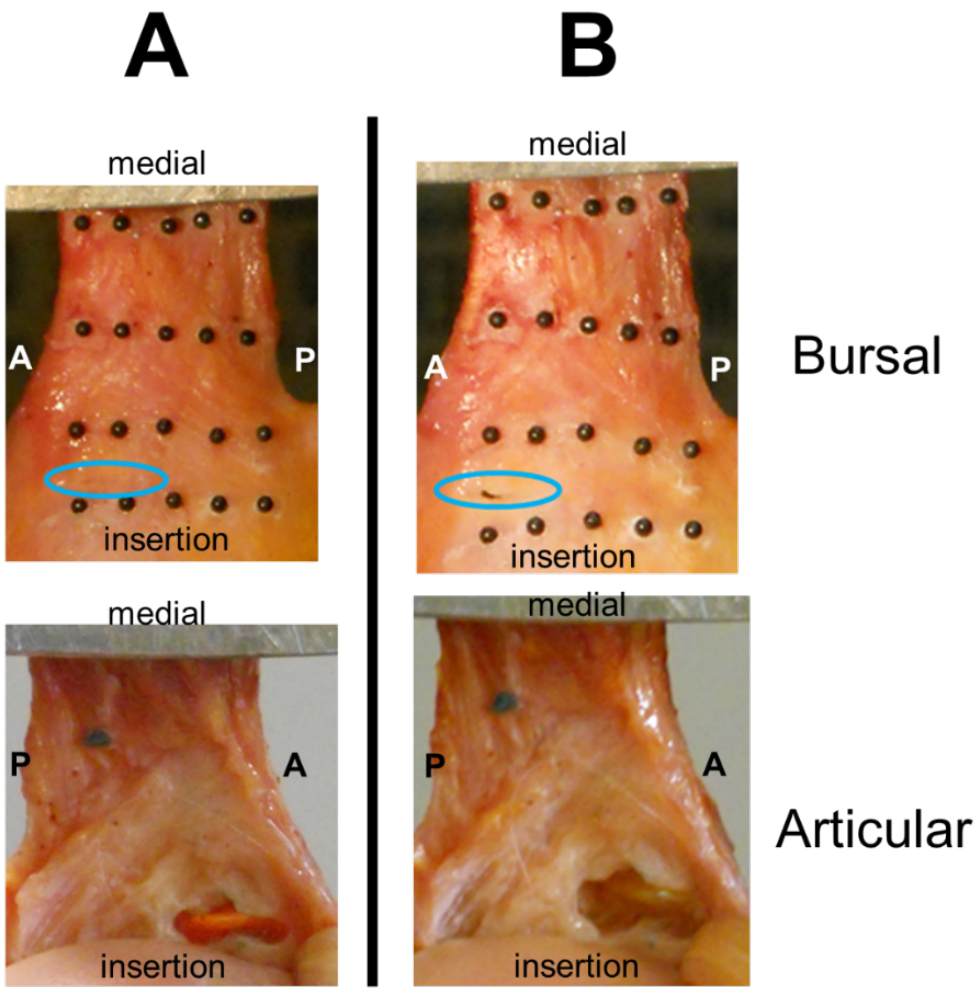

Figure 4.9. Bursal and articular images of artificial supraspinatus tears before and after testing. A) The first load set after tear creation and B) the final load set prior to the critical tendon retraction. Although the tear did not propagate on the bursal side of the tendon (blue oval) until the final cycle set in some specimens, appreciable propagation was observed on the articular surface.

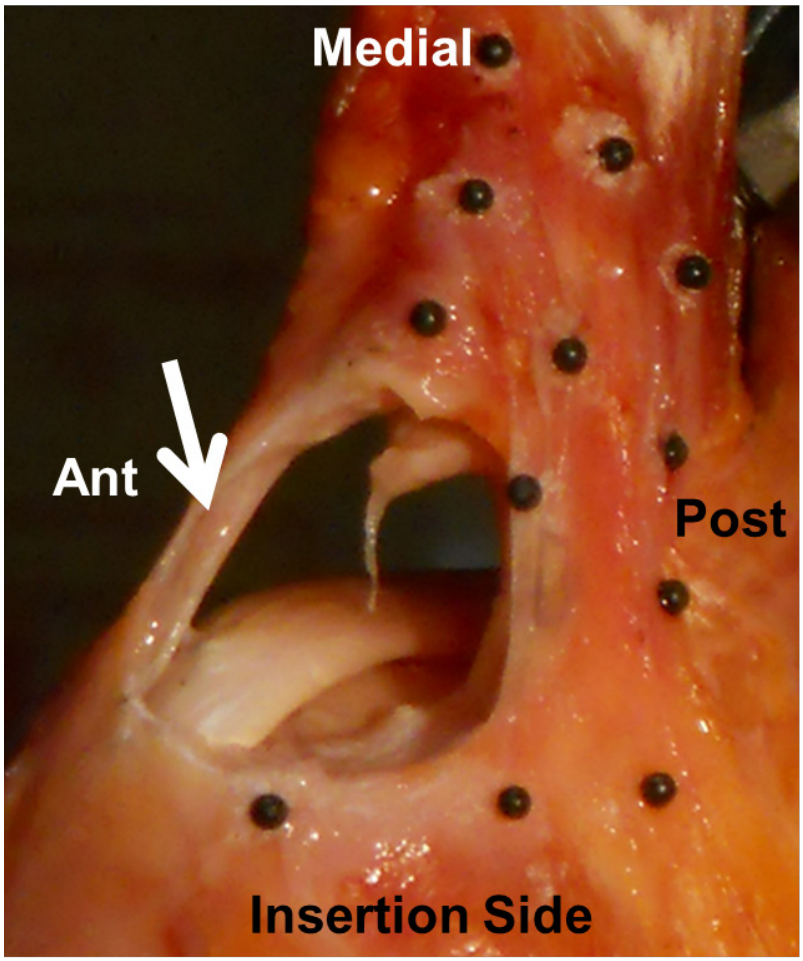

Figure 4.10. Failure pattern of the tendon after reaching critical tendon retraction of 2 cm. AP propagation of the tear occurred in addition to retraction. Though the posterior third of the tendon remained mostly intact, the anterior third was attached to its insertion to the humeral head by a thin piece of tissue after catastrophic propagation of the tear (white arrow).

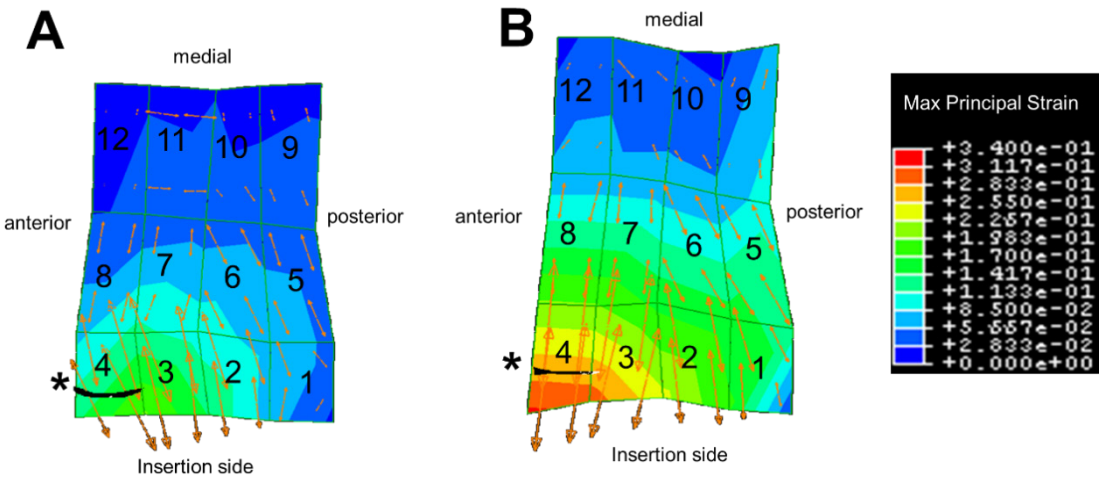

Figure 4.11. Representative fringe plots of maximum principal strain for a single tendon. Strain magnitude is represented as a color map and strain direction is represented by vectors (orange lines). The tear location on the bursal surface is denoted by "*". A) The first load set after tear creation and B) the final load set prior to critical tendon retraction. Color scale is for maximum principal strain, ranging from 0% to 34% strain.

Table 4.1. Summary of relevant data for each tendon at end-of-test

	Tendon 1	**Tendon 2**	**Tendon 3**	**Tendon 4**	**Tendon 5**	**Tendon 6**	**Tendon 7**	**Tendon 8**
End-of-test Condition	Critical tendon retraction	Posterior edge Failure	Critical tendon retraction	Critical tendon retraction	Critical tendon retraction	Mid-substance Failure	Critical tendon retraction	Critical tendon retraction
Direction of Propagation	Posterior and Ant	Posterior and Ant	Posterior	None	Posterior	None	Posterior	Posterior
Location of Max Strain	Posterior to tear	Posterior to tear	Posterior to tear	Medial to tear	Posterior to tear	Medial to tear	Posterior to tear	Posterior to tear
Direction of Max Strain	Posterior	Anterior	Posterior	Anterior	Posterior	Anterior	Posterior	Posterior
Load at end-of-test (N)	500	700	400	900	700	700	400	400

In the group that showed a posterior shift in strain direction (5 tendons), the direction at the end of the initial load set was 114 ± 28° and was 86 ± 20° at the end of the final load set ($p < 0.01$). In these tendons, significant posterior tear propagation was observed in all cases, corresponding to the direction of strain (Figure 4.10 and Figure 4.11). As shown in element 3 in Figure 4.11, the vectors representing strain direction shift from an anterior orientation to a posterior orientation after cyclic loading. In the group that showed an anterior shift in strain direction (3 tendons), the strain direction was 59 ± 62° for the first load set and 78 ± 62° in the last load set ($p > 0.05$). In two of these tendons, no significant anterior-posterior tear propagation was found, with the increase in tear size resulting due to tendon retraction. In the remaining tendon, the tear propagated anteriorly but failure occurred in the posterior third of the tendon mid-substance.

Table 4.2. Maximum principal strain in element adjacent to tear

Load Set	Tendon 1 (Elem 2)	Tendon 2 (Elem 2)	Tendon 3 (Elem 1)	Tendon 4 (Elem 6)	Tendon 5 (Elem 3)	Tendon 6 (Elem 8)	Tendon 7 (Elem 2)	Tendon 8 (Elem 6)
100N	5.8%	5.4%	2.5%	8.2%	18.9%	30.6%	2.1%	3.3%
200N	25.8%	6.1%	6.4%	8.4%	23.2%	28.0%	20.5%	16.0%
300N	30.1%	21.4%	14.9%	8.0%	26.3%	34.0%	43.0%	18.8%
400N	29.0%	20.5%	15.6%	7.8%	27.4%	32.3%	43.0%	18.8%
500N	30.4%	20.6%	-	7.9%	28.3%	31.4%	-	-
600N	-	23.7%	-	9.9%	28.0%	29.4%	-	-
700N	-	31.3%	-	13.5%	26.7%	31.3%	-	-
800N	-	-	-	15.3%	-	-	-	-
900N	-	-	-	15.3%	-	-	-	-

4.2.4 Discussion

This study investigated small, full-thickness tears in the anterior third of the supraspinatus tendon and found two patterns of strain. In five tendons, the direction and location of maximum principal strain corresponded to the observed posterior tear propagation. In the remaining three tendons, the tears either did not propagate or failed mid-substance. Since tear propagation could not be assessed in these tendons, no relationship between direction of tear propagation and maximum principal strain was observed. The time zero experimental tear severed most of the rotator cable, eliminating the greater part of its structural reinforcement to the tendon. Highest maximum principal strain was observed in the elements directly adjacent to the tears, located posteriorly and medially. Furthermore, the direction of tear propagation during cyclic loading was primarily observed to be in the posterior direction, toward the center of the supraspinatus tendon. This corresponded to the direction of maximum principal strain.

The results of this study can inform treatment decisions for management of rotator cuff tears. This study observed the highest maximum principal strain to be posterior to the supraspinatus tear, and a posterior direction of tear propagation toward the infraspinatus tendon. Due to the high loads (greater than 400 N) required to cause significant increases in tear size, tears similar to those investigated in this study will likely remain isolated to the supraspinatus tendon during activities of daily living. Therefore, for tendon tear propagation to occur at loads in the supraspinatus associated with normal activities of daily living (less than 200 N) (41, 214, 215), changes to tendon quality due to biologic factors such as tendon degeneration are likely necessary. Other factors such as pain, functional deficit, and age can also affect risk of tear propagation and choice of treatment.

Additionally, nearly all of the tendons tested reached a strain of at least 5% in the elements directly adjacent to the tear within the first 100N loading set. These loads are within the normal range of supraspinatus activity (41), but still result in large strains (compared to intact tendon) that do not lead to macroscopic tear propagation. Nearly all tendons showed a minimum of at least 10% strain in the elements directly adjacent to the tear at 300 N, the upper range of loading expected during physical therapy (89), and tear propagation was observed in many of the tendons. Overuse (cyclic loading through repeated arm abduction) or traumatic loading to the rotator cuff may result in initiation of tear propagation that will lead to tear propagation if the tear is not properly managed. There are implications that the large number of patients with asymptomatic rotator cuff tears (67) still experience strains at the edges of the tear well above normal levels of strain in the tendon (5-10%), but these strains are not enough to result in propagation and potential shoulder pain. Increases in loading on the tendon that result in increased magnitudes of strain may contribute to tear propagation that leads to these tears becoming symptomatic (134).

The findings that the regions of highest strain are located directly around the tear and that tear propagation follows this direction are similar to the results of previous studies that examined different tear locations and sizes. Adarawis-Puri et al. (135) created circular-shaped tears in a sheep infraspinatus rotator cuff injury model using an incremental loading protocol. Their study found that regions of highest maximum principal strain were directly medial to the tear, corresponding to the direction of tear propagation. The maximum principal strain was approximately 10% for a maximum load of 240N, which is comparable to strains observed at similar loads in the current study. Reilly et al. (148) found increases in strain for a static 150 N load through a range of abduction angles at both the anterior and posterior edges of 6-mm full-

thickness, centrally located supraspinatus tears, but no observations of tear propagation were made. Mesiha et al. (154) investigated anterior rotator cuff tears that interrupt the rotator cable and found increased regional strains across the tendon bursal surface after cyclic loading. However, their study used a short-term cyclic loading protocol and did not investigate tear propagation.

Compared to intact supraspinatus tendon, the maximum principal strain observed in the area adjacent to the tear in the current study was over twice as large (136, 139, 141). The large values of strain observed near the tear likely result from the combined effects of tendon retraction and permanent deformation to the surrounding tissue. Additionally, some tendons showed tear propagation only on one surface (bursal versus articular). Since marker displacement data was collected for only the bursal surface of each tendon, tears that propagated on the articular side may have shown reduced strain on the bursal surface when compared to tears that opened primarily on the bursal surface, or opened equally through the full tendon thickness.

The limitations of this study include measuring only the bursal surface strain in 2D. Therefore, strains on the articular surface were not measured and the 2D nature of the measurements does not take into account the curvature of the tendon. However, the small curvature compared to the tendon surface area makes the 2D assumption reasonable. Additionally, the resolution of the marker placement used to calculate surface strains did not allow for strains to be determined at the edge of the tears in high resolution. However, the strain at the centroid of the element that contained the edge of the tear was utilized and allowed for sufficient visualization of strain distributions. This model collects strain data for only a single joint position (90° of glenohumeral abduction) and ignores the effects of the tendon wrapping

over the humeral head. Therefore, the results of this experiment are applicable only to 90° of glenohumeral abduction. The extent of degenerative tissue changes in the tendons tested was also unknown, since no histology was performed. Finally, the infraspinatus tendon was loaded statically to approximate the load-sharing interaction between tendon fibers inserting on the humeral head. This does not account for dynamic changes in load in the infraspinatus tendon during activities of daily living. Additionally, the subscapularis remained unloaded during the experimental protocol, which may have affected the observed strains and limited evaluation of anterior tear propagation.

4.2.5 Conclusion

The results from this study indicate that anterior tears of the supraspinatus tendon are likely to remain isolated to the tendon without other pathologic changes, based on the observed strain patterns and loads required for propagation. By better understanding the biomechanical factors contributing to the propagation of rotator cuff tears, clinical decisions for rotator cuff tear treatment can be improved by choosing treatments for tears based on their risk of propagation. In the future, a finite element model will be developed to assess the effects of degenerative tissue and tear shape on tear propagation. Additional studies investigating tear propagation and glenohumeral joint kinematics during physical therapy are also planned. Ultimately, the goal of this study is to better understand the mechanical factors related to rotator cuff tear propagation and develop patient-specific treatment algorithms to improve clinical outcome.

4.3 VALIDATION OF A SUBJECT-SPECIFIC FINITE ELEMENT MODEL FOR PREDICTIONS OF ROTATOR CUFF TEAR PROPAGATION

4.3.1 Introduction

The initiation and propagation of rotator cuff tears are poorly understood phenomena, despite the high clinical burden of rotator cuff tears and an incidence of over 30% in the general population (63-67). Various studies have shown the importance of tendon surface strains on the initiation and propagation of rotator cuff tears (50, 135, 136, 139-142, 148, 151). These studies used in vivo or cadaveric experiments to assess the effects of tear size and location for both partial and full-thickness tears, finding an increase in strain with an increase in tear size, and that highest strains were located at the edges of the tear. Additionally, some of these studies quantified the strains in the regions where tears are most commonly located and determined that the highest strains were generally co-localized with the regions in which tears most commonly initiate (136, 141, 151).

Although experiments provide valuable information on the behavior of biological tissues, it is not feasible to test all possible conditions that may have an effect on tendon strain. Thus, numerous computational models have been developed to further elucidate the role of mechanical factors, such as tendon strain, on rotator cuff tear propagation and repair (152, 170, 216-224). Computational models provide powerful tools to investigate the effects of tear geometry on potential risk factors for tear propagation. However, these previous models also assume simplified geometry or isotropic elastic material properties, which are not representative of the

true properties of tendon tissue and can have a significant effect on the predicted strains. Furthermore, few of these studies performed experimental validation to confirm the accuracy of the model predictions. Consequently, there is a need for an experimentally validated computational model of rotator cuff tendon that can be used to predict realistic tendon strains for the purposes of investigating rotator cuff injury and tear propagation.

Therefore, the objective of this study was to develop and experimentally validate a three-dimensional finite element model of supraspinatus tendon using subject-specific geometry and anisotropic material properties to predict strains in intact supraspinatus tendon at multiple joint angles. The model was considered valid if the difference between experimental and predicted strains was less than the experimental repeatability of 3% strain, and if the strain distributions predicted by the model were similar to experimental measures of strain in terms of anterior-posterior, medial-lateral, and articular-bursal strain magnitude gradients.

4.3.2 Materials and Methods

The computational model of the rotator cuff tendons was developed by obtaining subject-specific geometry, material properties, and loading conditions from a cadaveric specimen. An appropriate reference configuration for strain calculations was determined, and experimental strains during cyclic loading were calculated. Model predictions of tendon surface strains were compared to the experimentally measured strains in order to validate the model for use in simulations of tear propagation (Figure 4.12).

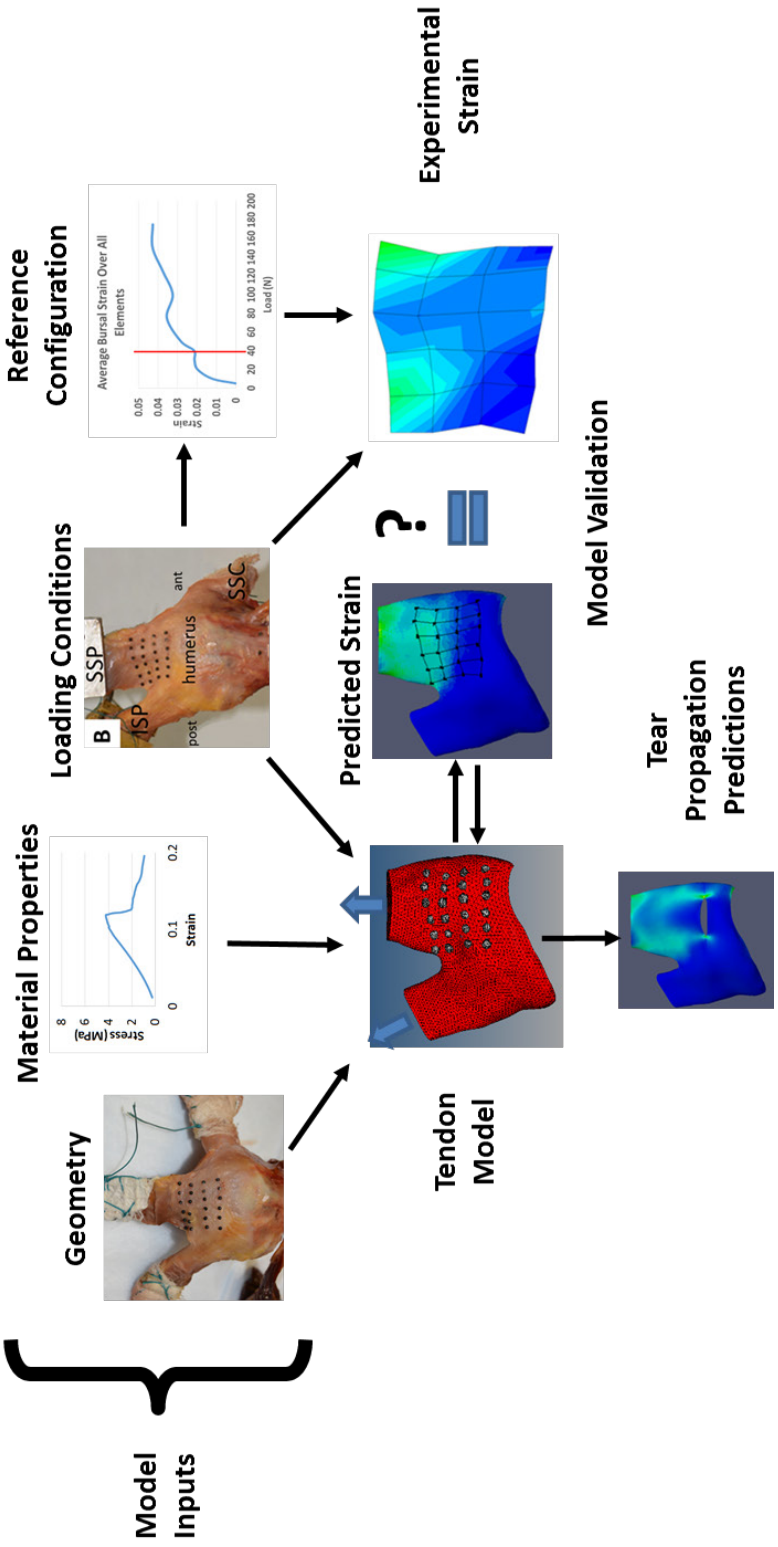

Figure 4.12. Flow chart for finite element model development and validation.

4.3.2.1 Model Geometry

One intact, fresh-frozen cadaveric shoulder (male, 70 years old, right limb) was procured with permission from the University of Pittsburgh ethical oversight board (CORID Protocol #131). The shoulder was stored at -20°C and allowed to thaw overnight at room temperature before dissection. During dissection, all soft tissue was removed except for the supraspinatus, infraspinatus, and subscapularis tendons of the rotator cuff, which were left attached to their insertions on the humerus. Additionally, the long head of the biceps tendon was left in place in the bicipital groove between the greater and lesser tuberosity of the humerus. The presence of any tendon thickenings (such as the rotator cable) was noted and their dimensions were recorded.

After dissection, a 6 x 4 array of black delrin plastic markers was affixed to the bursal and articular surfaces of the tendon using cyanoacrylate (Figure 4.13) for calculation of tendon surface strains during experimental testing. This resulted in 30 surface elements (15 on each side) constructed from sets of four surface markers (Figure 4.14). The 2 mm-diameter markers were placed approximately 5 mm apart, with the bottom row located just medial to the tendon insertion on the greater tuberosity for the bursal side. On the articular side, the bottom row of markers was placed approximately 1 cm medial to the tendon insertion to improve marker visibility at lower abduction angles due to the presence of the humeral head.

The humerus was potted in epoxy putty and loaded into a custom Plexiglas jig that allowed for the rotator cuff tendons to be oriented freely with respect to the fixed humerus and aligned along their normal lines of action. The three-dimensional geometries of the humerus, tendons, and affixed plastic markers were obtained using a computed tomography (CT) scanner (GE Lightspeed 16, Milwaukee, WI) (225-227). A soft-tissue scanning protocol (300 mA, 120

kV, 0.625 mm slice thickness) was used to better visualize the tendon geometry, with the scanning direction running parallel to the long axis of the humerus (from the tendon insertion to the myotendinous junction of the supraspinatus). Two image sets were captured: the first at 70° of glenohumeral abduction, and the second at 20° in order to obtain geometry at joint positions near the beginning and end of the range of glenohumeral abduction.

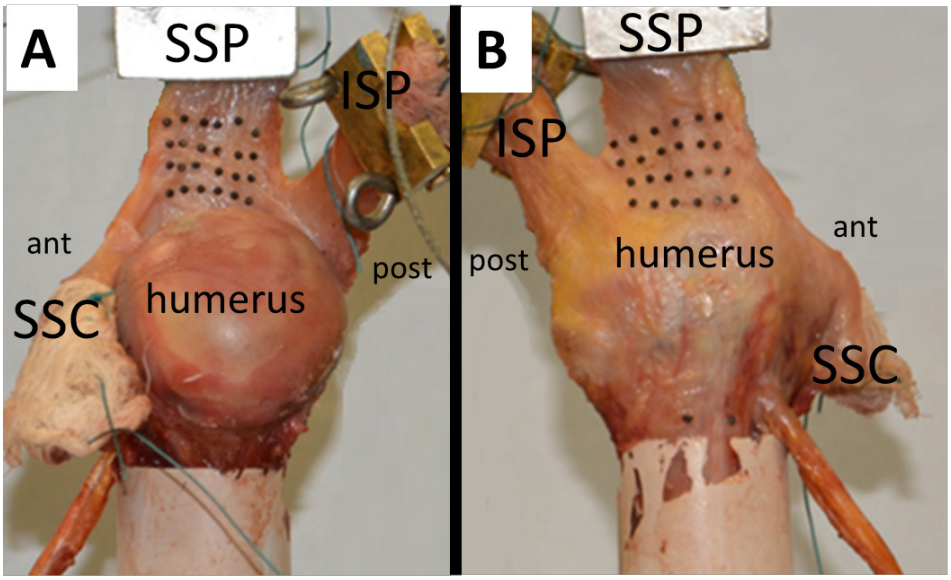

Figure 4.13. Mechanical testing and geometry of supraspinatus tendon. Experimental setup for the A) articular and B) bursal surfaces of the supraspinatus tendon. A 6 x 4 array of markers is affixed to both surfaces for tracking marker displacement for strain calculations during the experiment. SSP: Supraspinatus tendon; ISP: Infraspinatus tendon; SSC: Subscapularis tendon.

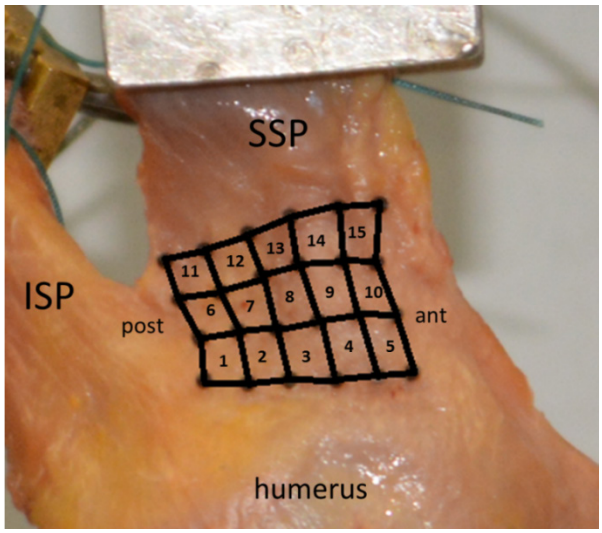

Figure 4.14. Strain marker placement for the bursal surface. A 6 X 4 array of markers was affixed to the bursal and articular surfaces of the supraspinatus tendon to create 15 elements on each surface for strain calculations.

4.3.2.2 Experimental Validation and Model Boundary Conditions

Mechanical testing of the intact tendon was performed to obtain experimental data to validate the model and determine appropriate loading and boundary conditions. The humerus was secured in a set of custom clamps to a materials testing machine with a 5 kN load cell (Model 5965, Instron Corp, Norwood, MA), and the supraspinatus tendon was then clamped to the crosshead for cyclic tensile loading at 90° of glenohumeral abduction (Figure 4.13). A physiologic 22 N load was placed on the infraspinatus via a pulley system to simulate load sharing between the supraspinatus and infraspinatus tendons (142, 228). A four-camera optical tracking system was used for tracking marker positions on the articular and bursal sides of the tendon (DMAS7 software, Spica Technology, Kihei, Maui HI) throughout testing (227, 229). This system allows for calculation of three-dimensional surface strains on both tendon surfaces simultaneously,

providing greater fidelity for model validation and allowing for strain calculations through the full tendon thickness.

A 5 N preload was first applied to the supraspinatus tendon, and then the tendon was preconditioned between 5 and 50 N for 10 cycles. Next, uniaxial tensile cyclic loading from 5 to 200 N was performed for 50 cycles at 20 mm/min, covering the normal range of loads expected for the supraspinatus tendon during activities of daily living and physical therapy exercises (41, 178). The location of the strain markers was recorded at the peak of the final load cycle (200 N) to obtain the strained configuration. This process was then repeated for 70, 60, 30, and 20° of glenohumeral abduction by rotating the clamp holding the humerus. These joint angles were chosen in order to obtain strain data to validate the model at discrete positions throughout the normal range of shoulder motion. No abduction angles less than 20° were tested due to limits in clamp range of motion. For each experimental test condition, the maximum principal Green-Lagrange strain was calculated at the centroid of each surface element created from the surface markers on the articular and bursal sides of the tendon. All calculations of experimental strains were performed by inputting the reference and strained configurations of the surface markers into ABAQUS (ABAQUS/CAE Student Version 6.4; Simulia, Providence RI) (142, 227). The reference configuration for strain calculations was defined as the tendon under a 40 N preload clamped at a joint position of 70° of glenohumeral abduction.

4.3.2.3 Determination of Reference Configuration

Accurate calculations of tissue strains are dependent upon the reference configuration used (206, 230-232). For investigation of musculoskeletal connective tissues, the reference configuration is typically found by determining the joint position and preload at which all collagen fibers in the

tissue start to be loaded (i.e. all "slack" within the tissue is removed). Failure to adequately define an appropriate reference configuration can lead to over- or under-estimation of tissue strains. The reference configuration therefore must be rigorously defined to ensure that all experimental measures and computational predictions accurately represent the mechanical behavior of the tendon. The rotator cuff tendons inherently experience uneven loading due to their inhomogeneous structural and mechanical properties, complex insertion site geometry, and natural tendon curvature. Preliminary experiments to measure supraspinatus tendon surface strains using a preload of 5 N as the reference configuration resulted in inaccurate calculations of strain for model validation. Therefore, in order to account for the inhomogeneous mechanical behavior of the supraspinatus tendon, rigorous analysis of experimentally measured tendon surface strains for various loading conditions was performed to establish an appropriate reference configuration.

To determine the reference configuration, strains were calculated on articular and bursal surfaces of the supraspinatus tendon during cyclic loading experiments. Strain calculations were made using different loaded configurations of varied magnitudes of load with the joint positioned at 70° of glenohumeral abduction, which was the same joint position captured using CT imaging for subject-specific model geometry, and is close to the extreme of maximum glenohumeral abduction. The joint position of 20° of glenohumeral abduction was also considered as a potential position for the reference configuration. However, since the tendon is in contact with the humerus at lower abduction angles, this joint position was excluded due to the likelihood of contact affecting calculations of strain.

Using the experimental marker location data obtained during cyclic loading between 5 N and 200 N, bursal and articular surface strains were calculated at applied loads ranging from

10 N to 200 N in increments of 10 N (i.e. 10 N, 20 N, 30 N, …, 200N). At each loaded configuration, strain was calculated as the change in deformation relative to the 5 N preload state for each of the 15 elements on both sides of the tendon (Figure 4.14). The strain for all elements on both articular and bursal surfaces was averaged to provide a measure of the average deformation across the tendon surface during loading throughout the experiment, since strains within individual elements can vary substantially across the tendon.

In addition to average surface strains, the difference in strain between loaded configurations was calculated for each load increment (i.e. strain at 20 N minus strain at 10 N, strain at 30 N minus strain at 20 N, etc.). The calculated difference in strain was plotted versus applied load, representing the first derivative of the strain versus applied load relationship. From examination of the plot of the first derivative, the preloaded state was defined as the load at which the minimum inflection point was located (Point 3 in Figure 4.15 B,D). The minimum inflection point represents a point at which the collagen fibers in the tissue begin to be loaded. The load at the inflection point for 70° of glenohumeral abduction was then used as the reference configuration to calculate strains at 200 N for each experimental joint position.

Plots of average surface strains versus load at 70° of glenohumeral abduction showed similar strain distributions for bursal and articular surfaces (Figure 4.15). Between 5 N and 20 N, strain increased non-linearly with load as collagen fibers in the tendon began to take up load and wrinkles were removed from the tissue (Point 1 to Point 2 in Figure 4.15-A,C). At ~20 N of load, the curve reached a plateau for which load increased but the average strain over the surface of the tendon did not change (Point 2 to Point 3 in Figure 4.15-A,C). At 40 N on the bursal side and at approximately 30 N on the articular side, strain again began to increase with load. The end of the plateau region corresponded with the minimum point of inflection on the plot of difference in

strain versus load (Point 3 in Figure 4.15-B,D). After the plateau region, average surface strain continued to increase with load on the bursal side of the tendon. However, on the articular side, although average surface strains increased with load overall, the strains fluctuated considerably more than on the bursal side. Multiple inflection points existed at loads higher than the preload, indicating non-uniform strains measured across the tendon surface (Point 4 in Figure 4.15-B,D). By examining the strain versus applied load relationship for the individual elements on the bursal and articular surfaces, it was observed that elements closest to the infraspinatus tendon and those bounded by the rotator cable structure showed the largest fluctuations in strain, whereas elements furthest from the infraspinatus and medial to the rotator cable showed relatively uniform increases in strain with load.

As further validation of the chosen reference configuration, fringe plots of surface strain were generated for the 200 N loaded configuration at 20°, 30°, 60°, 70°, and 90° of glenohumeral abduction using a reference configuration of a 40 N preload at 70° of glenohumeral abduction (Figure 4.16). The largest strains were observed at the lowest joint abduction angles and generally decreased as joint angle increased. At joint abduction angles without contact between the tendon and humeral head, strains increased from lateral to medial, whereas at joint angles with contact (20° to 30°), strains decreased, likely due to the tendon tissue being in contact with the humeral head near the insertion. The largest strains ranged from approximately 30% strain at 20° of glenohumeral abduction to 15% strain at 90° of abduction.

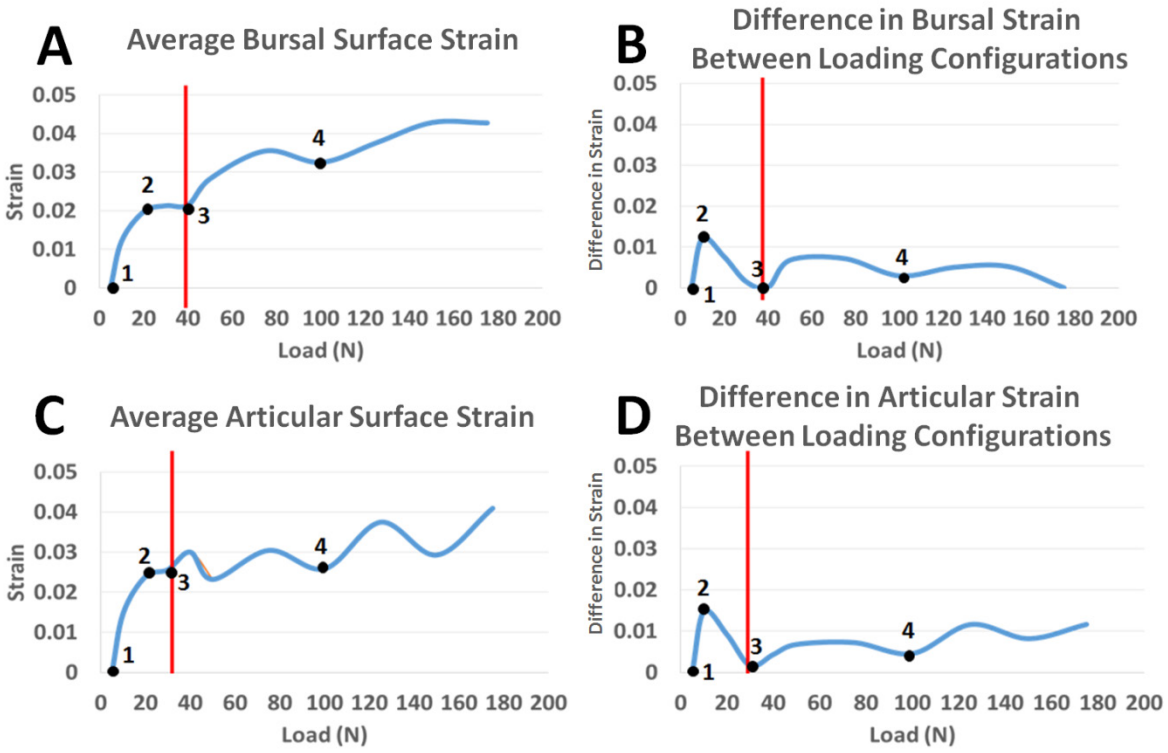

Figure 4.15. Plots of average strain and average difference in strain versus load for bursal and articular tendon surfaces at 70° of glenohumeral abduction. From 0 to 20 N, measures of strain increased quickly due to "unfolding" of the tendon tissue as collagen fibers began to be loaded (points 1 to 2). The minimum inflection point on the bursal side was at 40 N, while on the articular side it was at 30 N (marked by red lines, point 3). This inflection point denotes the end of a plateau in the curve of strain versus load that is indicative of rigid body motion and the tissue taking up load without deforming uniformly (points 2 to 3). Additional inflection points after the minimum point indicate non-uniform deformations across the tendon surface with increasing load (point 4).

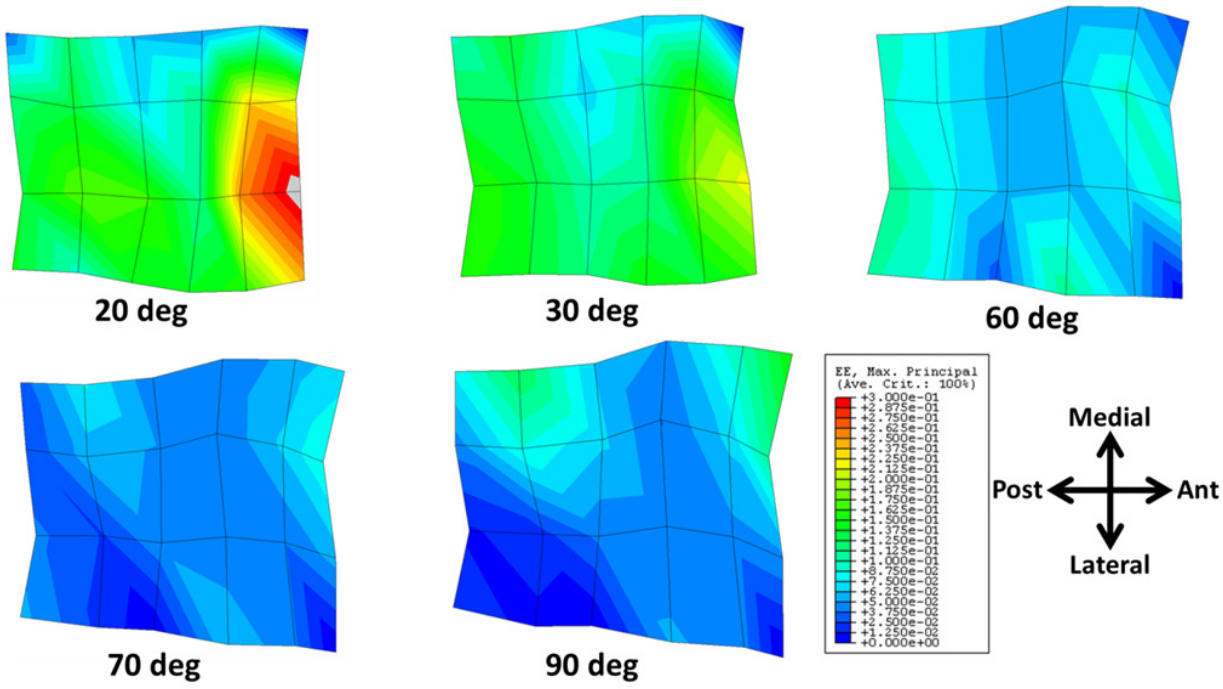

Figure 4.16. Fringe plots of supraspinatus tendon bursal surface strains at 200 N at 20°, 30°, 60°, 70°, and 90° of glenohumeral abduction using a reference configuration of a 40 N preload at 70° of glenohumeral abduction. The largest strains were observed at 20° of glenohumeral abduction, with strain decreasing as joint angle increased.

The plots of surface strain versus applied load showed a region of rapidly increasing strain at loads less than 20 N, followed by a plateau region from 20-40 N, and lastly a region of more slowly increasing strain. Below 20 N, large increases in experimental strain were likely due to removal of "slack" and wrinkles from the tissue before the tendon itself began to take up load. From 20-40 N, average surface strain remained relatively constant with increasing load. In this phase, the wrinkles have been removed from the tissue, collagen fibers begin to be recruited as they are loaded, and rigid body motion of the tendon occurs as it rotates into the preloaded position. Lastly, at around 40 N, all slack was removed from the tissue and all collagen fibers

began to be loaded throughout the tendon. This point marks the state at which the tendon is considered to be "preloaded."

Although both the articular and bursal sides of the tendon showed similar plots of surface strain versus applied load, the minimum inflection point for the articular surface was located closer to 30 N whereas the minimum inflection point for the bursal surface was located at 40 N at 70° of glenohumeral abduction. The difference in position of the minimum inflection point indicates that there is uneven loading between the bursal and articular surfaces of the tendon, and the articular surface becomes preloaded earlier than the bursal surface. This is potentially due to the presence of the rotator cable and the natural curvature of the tendon, especially near its insertion to the greater tuberosity on the humerus. It is therefore important to consider the uneven loading between the bursal and articular surfaces of the tendon when determining a reference configuration and when making comparisons in strain between the two surfaces. This observation is supported by previous studies that have found the articular surface to have higher strains than the bursal surface (136, 141), and that the articular surface is the most common location for partial-sided rotator cuff tears (233-235). Additionally, the presence of multiple points of inflection after the preload indicates non-uniformity in strains across the surfaces of the tendon, with larger fluctuations in strain occurring in regions closest to the infraspinatus tendon. Therefore, it is also important to consider loading of the infraspinatus tendon and its effect on the supraspinatus tendon when establishing the reference configuration for the supraspinatus tendon.

Overall, the most appropriate reference configuration for the supraspinatus tendon was a 40 N preload at 70° of glenohumeral abduction. At 40 N, slack is fully removed from both articular and bursal sides of the tendon. Moreover, the 70° of abduction reference configuration showed substantial changes in calculated surface strains due to differences in joint abduction

angle, which has been observed by previous studies. Lastly, experimental strain data is available for both articular and bursal sides of the tendon for model validation when using 70° of abduction as the reference configuration. It is important to consider that this reference position is specific to the chosen loading conditions, experimental protocol, and model to be validated.

4.3.2.4 Subject Specific Material Properties

After completion of cyclic loading for all joint angles, the tendon was split into thirds of approximately equal anterior-posterior width to determine material properties. First, a laser scanning device with 2% accuracy (NextEngine 3D Scanner HD, Santa Monica, CA) was used to measure the cross-sectional area at the mid-substance of each tendon third. After applying a 5 N preload and preconditioning between 5 N and 50 N for 10 cycles, each third was loaded to failure at a rate of 20 mm/min. The optical tracking system recorded marker positions continuously throughout load-to-failure testing to calculate strain. Stress was calculated by dividing the load recorded during testing by the cross-sectional area at the tendon mid-substance, and this was plotted versus the strain measurements calculated from elongation data collected during testing. In order to obtain material parameters for inputs to the model, a transversely isotropic, fiber reinforced Neo-Hookean model was chosen to represent the behavior of the tendon (216, 236, 237). Assuming that the tendon is incompressible, the strain energy function was represented by:

$$\Psi = \Psi_M + \Psi_F$$

where

$$\Psi_M(I_1) = c_1(\bar{I}_1 - 3)$$

$$\Psi_F = \begin{cases} \frac{k_1}{2k_2}[\exp(k_2(\bar{I}_4 - 1)^2) - 1] & \bar{I}_4 > 0 \\ 0 & \bar{I}_4 \leq 0 \end{cases}$$

Here, $\bar{I}_1 = \mathrm{tr}\mathbf{C}$ and $\bar{I}_4 = a_0\bar{\mathbf{C}}{a_0}^{\mathrm{T}}$. **C** is the right Cauchy-Green tensor, which is a function of the deformation gradient **F**, and a_0 is the direction of the collagen fibers in the reference configuration, which was chosen to be oriented along the axis of loading. A set of three material parameters (c_1, representing the soft matrix in which the collagen fibers are embedded, and k_1 and k_2 representing the collagen fiber strength and stiffness) were fit to the experimental stress-strain data for each tendon third using a least squares approach (MATLAB, MathWorks, Natick, MA) and the equation for Cauchy stress:

$$\boldsymbol{\sigma} = 2\mathbf{F}\frac{\partial\Psi}{\partial\mathbf{C}}\mathbf{F}^{\mathbf{T}}$$

Due to the stiffness of the tendon being orders of magnitude less than that of bone, and any deformations in the cartilage being sufficiently small as to likely not effect strains in the tendon, the humerus and cartilage were considered to be fixed rigid bodies (238).

4.3.2.5 Model Development

In order to build the finite element model, the humerus and rotator cuff tendon surface geometry were manually segmented from the CT dataset using Mimics 17 (Materialize, Leuven, Belgium) and converted to a solid model. The dimensions of any visible tendon thickenings in the model geometry were measured using the Mimics software suite for comparisons with the measurements made after dissection. The mesh generated for finite element modeling using Hypermesh (Altair Engineering, Troy, MI, USA) consisted of 18544 nodes and 93869 tetrahedral elements. This mesh was chosen after testing convergence by decreasing the element size from 4 mm (approximately 2000 elements) to 0.5 mm (approximately 66,000 elements) based on the criterion of an average difference in strain of less than 0.002 strain (0.2% strain) between meshes. Temporal convergence tests were also performed to determine the minimum number of load steps required to reach convergence between 50 and 400 steps with the criteria that change should not change more than 5%, and determined that 100 steps were sufficient.

Using the displacements recorded at 200 N during cyclic loading, displacement-driven quasi-static finite element analyses were performed for each joint angle greater than 30° of abduction using custom non-linear code (216). The joint positions for 30° and 20° were not modeled to avoid overcomplicating simulations by incorporating contact between the tendon and humeral head. Starting with the reference configuration captured at 70° of glenohumeral abduction, the model of the tendon was first preloaded by applying the displacement recorded at 40 N to the supraspinatus tendon. Nodal displacements for the given preload were recorded, and then all nodes in the model were displaced using these values such that the model was in the "preloaded state" for use in model simulations. Next, the difference in displacement between the

preloaded state and at 200 N (approximately 3.5 mm) was applied to the clamped edge of the tendon in the direction of loading (Figure 4.17). This process was repeated for 90° and 60° of glenohumeral abduction. For all loading cases, a 22 N load was applied to the infraspinatus along the tendon line of action to mimic experimental conditions using a traction boundary condition. Inhomogeneous material properties were assigned to the supraspinatus by varying material parameters in the anterior-posterior direction based on experimental data (216), i.e. parameters for the anterior third were assigned to the anterior third, etc., with a linear gradient between regions to minimize stress concentrations due to changes in material properties (Figure 4.18).

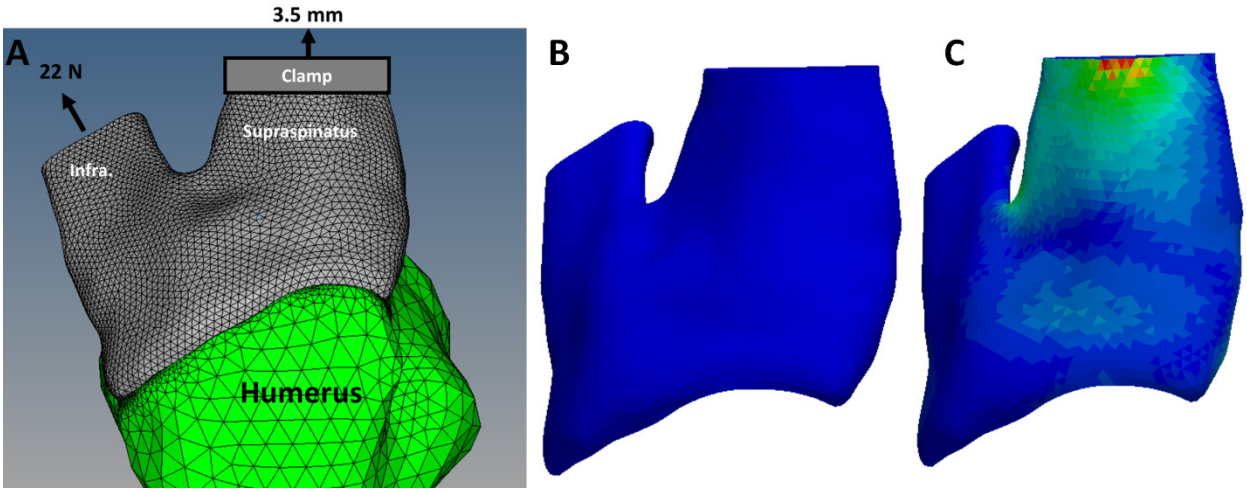

Figure 4.17. Finite element mesh of rotator cuff tendon. A) Displacement for a 200 N load (relative to the 40 N preload reference configuration) was applied to the clamped tendon edge and a 22 N load was applied to the infraspinatus tendon along its line of action to simulate experimental loading conditions. B) Tendon model in reference configuration geometry (40 N preload at 70° glenohumeral abduction). C) The displacement at 200 N was applied to the preloaded reference configuration geometry to obtain the deformed (loaded) configuration of the tendon.

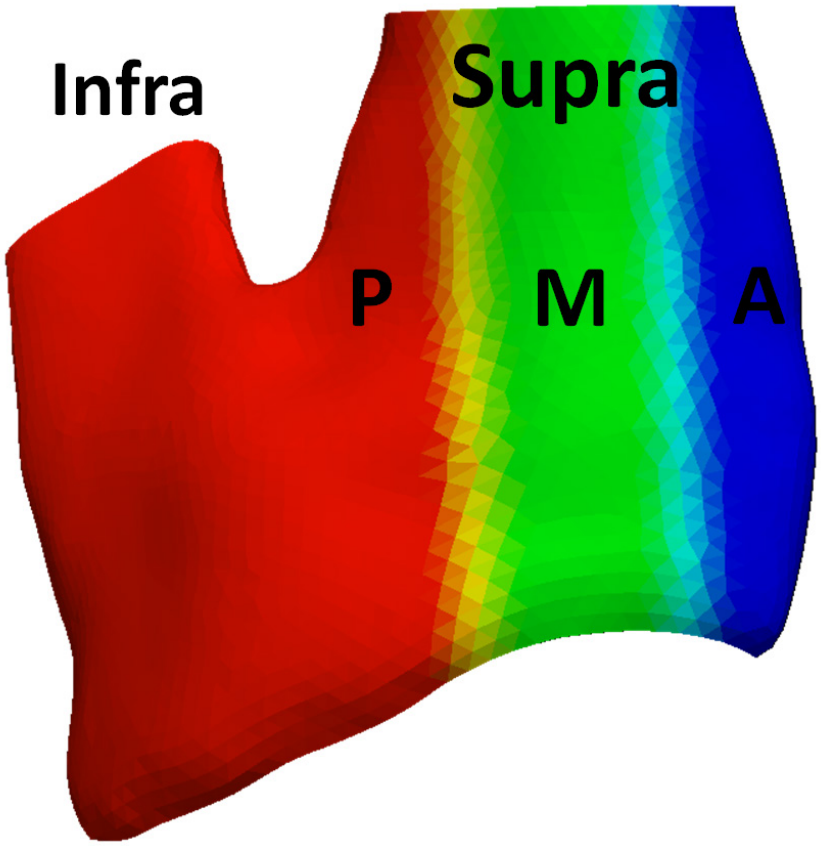

Figure 4.18. Material property assignment for the supraspinatus tendon. Subject-specific anisotropic material properties determined from fitting experimental data to a fiber-reinforced Neo-Hookean model were assigned to the posterior (P, red), middle (M, green), and anterior (A, blue) regions of the tendon. Linear interpolation was performed to assign properties in a transition region between each third to minimize stress concentrations.

4.3.2.6 Model Validation

Maximum principal Green-Lagrange strains for each tetrahedral element were computed for the model and output for comparison with experimental data at each joint position. The nodes nearest to the center of each marker segmented from CT image data were recorded in order to make comparisons within the same regions of interest for the model and experimental conditions

(Figure 4.19). The strains of all tetrahedral elements bounded within each experimental strain element were recorded and averaged to determine an average strain for each region in the model (15 regions for bursal and articular sides, 30 regions total for each loading condition). This value was compared to the strains for each experimental surface element to determine the ability of the model to predict regional strains compared to experimental testing (227). The primary validation criterion was that the average absolute difference in strain between the model and experimental conditions should be less than the experimental repeatability of 3% strain. In order to validate the ability of the model to predict the experimental strain distributions, plots of average surface strains by joint abduction angle were made to compare average maximum principal strain between articular and bursal surfaces, across the anterior-posterior tendon width, and along the medial-lateral axial length of the tendon.

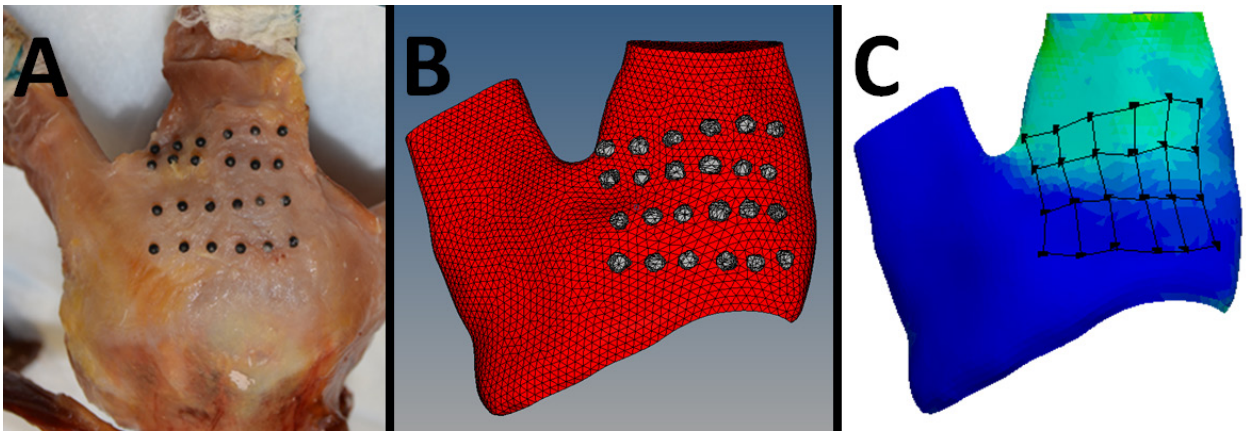

Figure 4.19. Strain marker location for comparisons between experimental strain model predictions. A) Marker positions on cadaveric specimen are captured to obtain marker geometry and location. B) Marker geometry is segmented to obtain locations relative to tendon surface. C) The node closest to the center of each marker is used to partition the surface of the tendon mode for one-to-one comparisons of model strain predictions with experiment.

4.3.3 Results

From material testing, it was determined that the middle third of the tendon had the highest modulus and ultimate stress, with the properties of the anterior third being closer to those of the middle third than the posterior third (Table 4.3). This relationship was captured by the parameters k_1 and k_2, representing the behavior of the collagen fibers in the tendon. From inspecting the tendon geometry, it was determined that the middle third of the tendon also showed the presence of a thickening on the bursal surface approximately 9 mm wide (Figure 4.20A). On the articular side, a tendon thickening approximately 3 mm wide was found, running in an arc from the anterior to the posterior borders of the supraspinatus tendon. Based on the location and dimensions, this thickening was likely the rotator cable structure (52). All thickenings found during dissection were also visible on the model surface geometry and were measured to have dimensions within a millimeter of experimental dimensions (Figure 4.20-B).

Table 4.3. Material Properties of Supraspinatus Tendon Thirds

Location	Cross Sectional Area (mm^2)	Ultimate Stress (MPa)	Ultimate Strain	Modulus (MPa)	k_1 (MPa)	k_2
Anterior	44	5.8	0.12	65.4	10.0	1.09e-7
Middle	42	5.8	0.07	97.1	14.4	5.02
Posterior	42	4.3	0.12	47.0	7.9	0.63

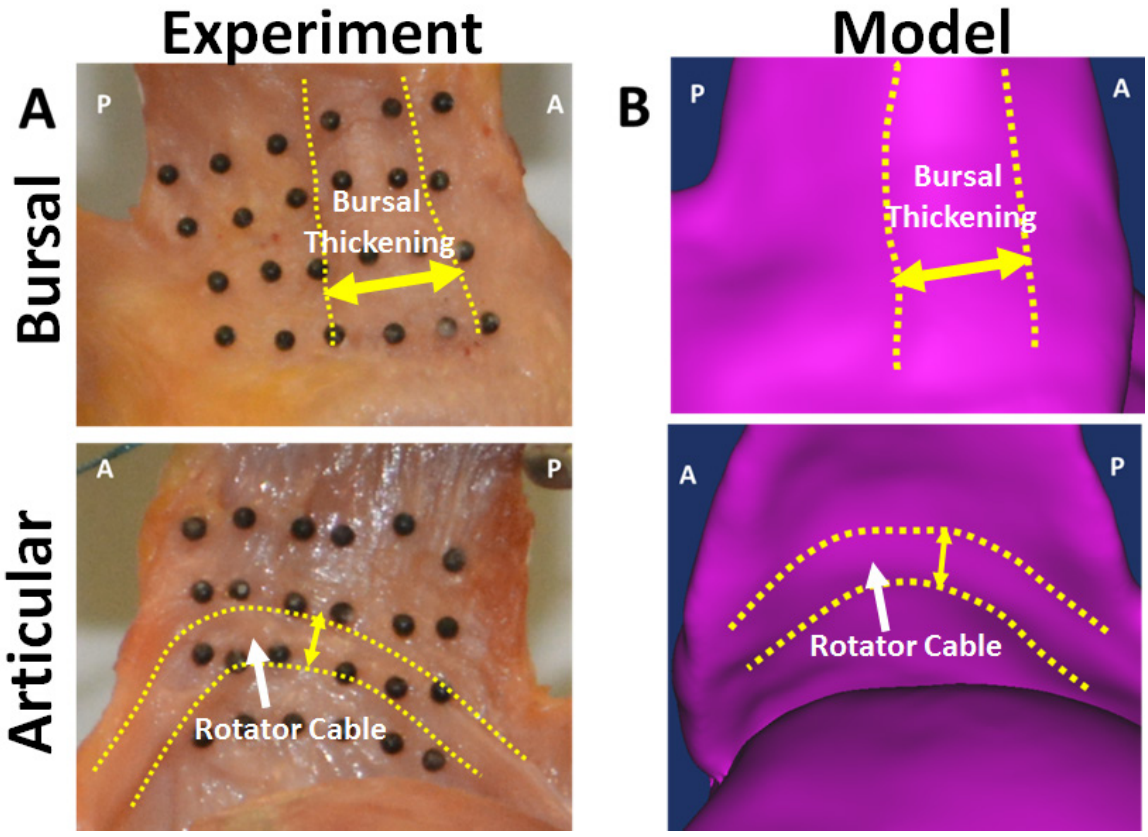

Figure 4.20. Tendon thickenings visible on the supraspinatus tendon. These thickenings were visible both A) during dissection and B) on the model surface geometry segmented from CT images of the tendon. On the bursal side, a thickening was observed in the middle third of the tendon (bordered by dotted yellow lines). On the articular side, a thickening corresponding to the presence of the rotator cable was found (bordered by yellow dotted lines).

Experimentally, at joint positions where the tendon was not in contact with the humeral head (90°, 70°, 60°) the largest maximum principal strains were found on the articular side of the tendon. On the articular side, the largest strain observed was 16.1% at 90° of abduction (Table 4.4, Figure 4.21). This element was located in the middle row of elements near the center of the marker array, coinciding with the top of the arc of the rotator cable. For the same joint positions, the largest strain on the bursal side was 12.5%, also at 90° of abduction. This element was located more anteriorly and closer to where the load was applied to the tendon (Figure 4.14).

Strains could not be calculated in the bottom row of markers closest to the insertion at 60°, due to the humerus blocking the view of the cameras. For joint positions with contact between the humerus and the articular surface of the tendon, strains on the articular surface could not be measured. However, strains on the bursal surface for 20° and 30° were much larger than strains for joint positions 60° and above. At 20° of abduction, the highest strain was 33.6%, located in the middle row of markers near the anterior edge of the tendon. In general, strains increased in magnitude from the bursal to the articular side, and from the lateral to the medial edge of the tendon. The largest strains also tended to be located closer to the mid-anterior portion of the tendon.

Table 4.4. Experimental Surface Strains by Surface Element (% Strain)

	20°		**30°**		**60°**		**70°**		**90°**	
	Bursal	**Art**	**Bursal**	**Art**	**Bursal**	**Art**	**Bursal**	**Art**	**Bursal**	**Art**
E1	10.4	-	12.2	-	7.3	-	2.9	6.7	0.6	7.1
E2	16.2	-	12.6	-	4.3	-	0.8	3.1	0.0	0.0
E3	8.8	-	7.9	-	3.7	-	2.6	0.0	1.1	1.2
E4	8.8	-	10.7	-	5.3	-	1.8	0.0	4.1	4.4
E5	25.3	-	17.4	-	0.0	-	0.0	0.0	0.0	7.1
E6	13.8	-	13.0	-	8.5	5.8	1.2	2.0	0.6	6.7
E7	15.1	-	9.8	-	5.2	6.7	3.2	6.8	1.9	11.8
E8	8.5	-	7.3	-	5.5	10.2	5.2	11.3	5.4	16.1
E9	8.5	-	7.5	-	3.6	5.8	2.1	6.1	0.3	2.6
E10	33.6	-	21.7	-	11.1	8.3	7.2	7.2	4.4	5.2
E11	8.8	-	11.8	-	8.4	2.2	5.1	8.1	7.7	11.3
E12	8.6	-	10.5	-	6.3	2.8	5.6	2.5	8.7	3.5
E13	5.4	-	6.4	-	6.0	9.2	4.2	8.4	5.6	13.0
E14	1.3	-	3.6	-	3.9	6.4	3.6	6.8	5.2	3.3
E15	4.9	-	3.1	-	3.2	3.0	6.3	3.8	12.5	6.8

Quantitatively, the model was able to predict strains within 3% strain of the experimental measures for most joint positions (Table 4.5). For all joint positions 60° of abduction or greater, the average difference in strain between experiment and model was always less than 3% strain on the bursal side. However, differences in strain were larger for the articular side for all joint positions, and were above 3% strain at 70° and 90° of abduction. When considering the presence of the rotator cable and removing those elements (E1, E2, E7, E8) from the calculation of average difference in percent strain, the average differences are 2.5% strain and 2.8% strain for 70° and 90°, respectively, which are both below the 3% strain threshold. In general, differences between experiment and model predictions of strains were largest in regions that included the visible tendon thickenings or on the medial tendon edge where load was applied.

Qualitatively, the model predicted similar patterns of strain as the experiment. When comparing strains in the bursal and articular surfaces of the tendon, both the experimental and predicted strains showed that strains were larger on the articular surface (Figure 4.22). However, the model predicted smaller differences in strains between bursal and articular surfaces than the experiment. Across the anterior-posterior tendon width, the model was able to predict similar patterns of strain as the experiment, with the largest strains being located between the middle and the anterior edge of the tendon (Figure 4.23). Additionally, the model predicted that the largest strains were at 60° of glenohumeral abduction and decreased with increasing joint angle, similar to the average strains measured from the experiment. Along the axial length of the tendon, both the experiment and model indicated that strains were lowest near the insertion and increased along the length, with the largest strains located closest to where the load was applied to the tendon medial edge (Figure 4.24). Additionally, model predictions of strains appeared to be most

different from the experimental measurements closest to where the load was applied to the tendon.

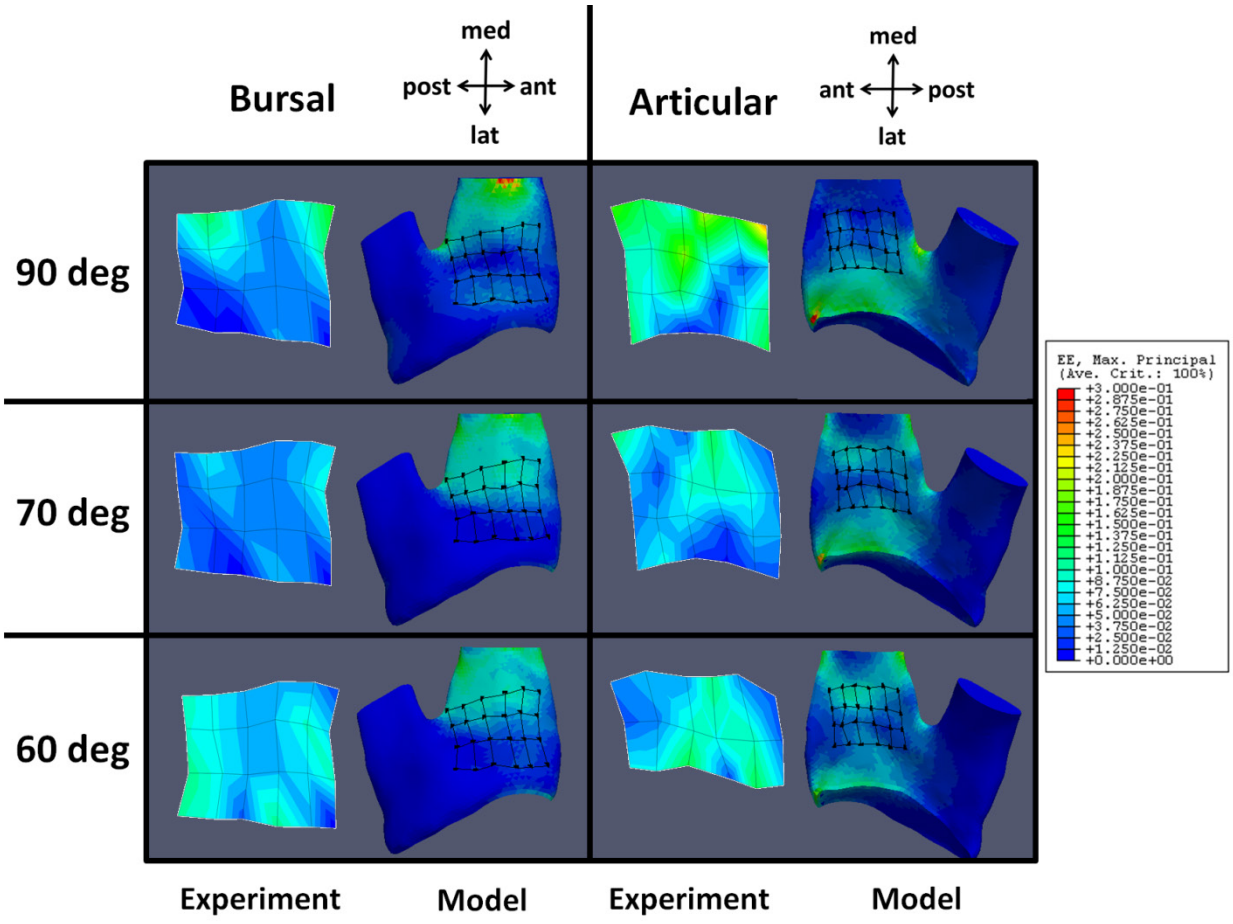

Figure 4.21. Experimental and predicted fringe plots of strain for the bursal and articular tendon surfaces at 90°, 70°, and 60° of glenohumeral abduction. Strains were generally higher on the articular side of the tendon, and the largest strains were typically located more anteriorly. Only the top two rows of markers on the articular side were visible at 60° during the experiment due to the bottom row being blocked by the head of the humerus.

Table 4.5. Difference in % Strain between Experimental Measures and Model Predictions

	60°		70°		90°	
Element ID	**Bursal**	**Articular**	**Bursal**	**Articular**	**Bursal**	**Articular**
E1	6.4	-	2.0	2.7	2.8	1.6
E2	2.7	-	0.2	1.3	4.0	5.7
E3	0.7	-	1.3	5.2	2.9	4.3
E4	1.8	-	0.3	4.9	0.4	0.9
E5	3.1	-	1.6	4.6	3.2	1.2
E6	5.8	0.2	1.7	1.3	1.6	2.7
E7	0.5	0.1	1.2	3.2	0.0	7.5
E8	0.4	3.5	0.0	7.8	3.9	13
E9	0.6	0.9	2.7	2.4	1.6	1.1
E10	6.5	4.1	1.9	2.3	1.9	0.1
E11	1.5	6.8	2.4	1.8	1.8	7.7
E12	1.8	7.9	2.7	4.7	3.9	0.2
E13	1.9	1.0	4.7	2.2	1.5	11
E14	4.2	1.5	5.4	1.4	0.9	0.6
E15	4.4	2.9	1.7	1.6	7.4	3.5
Average	2.8	2.9	2.0	3.2	2.5	4.1

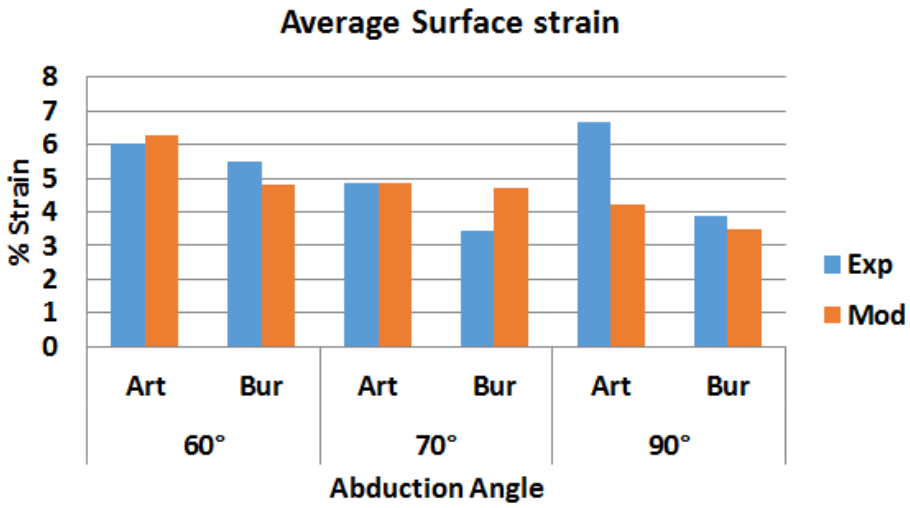

Figure 4.22. Average strains for the articular and bursal surfaces. Magnitude of strain was similar between the experimental measures and the strains predicted by the model. Additionally, the model predicted larger articular strains than bursal strains at all joint positions, and a decrease in strain with increased abduction angle, as was measured during experiments.

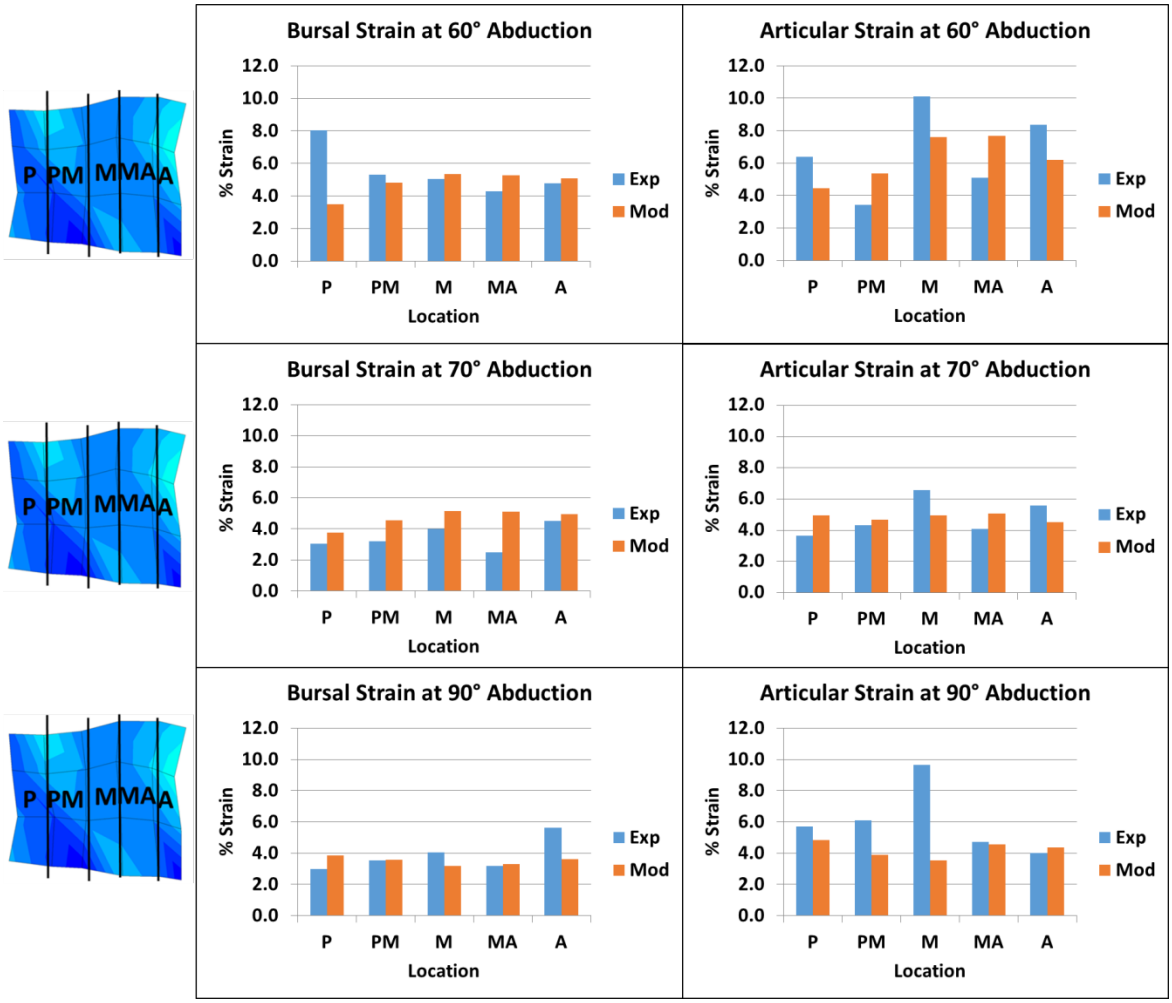

Figure 4.23. Average strains for the articular and bursal surfaces across the anterior-posterior tendon width at 60°, 70°, and 90° of abduction. On average, both the experimental strains and model predictions showed the largest strains to be located between the middle (M) and anterior edge (A) of the tendon on both surfaces. The largest strains in both the experiment and model were generally at 60° of abduction. P: Posterior; PM: Posterior-Middle; M: Middle; MA: Middle-Anterior; A: Anterior.

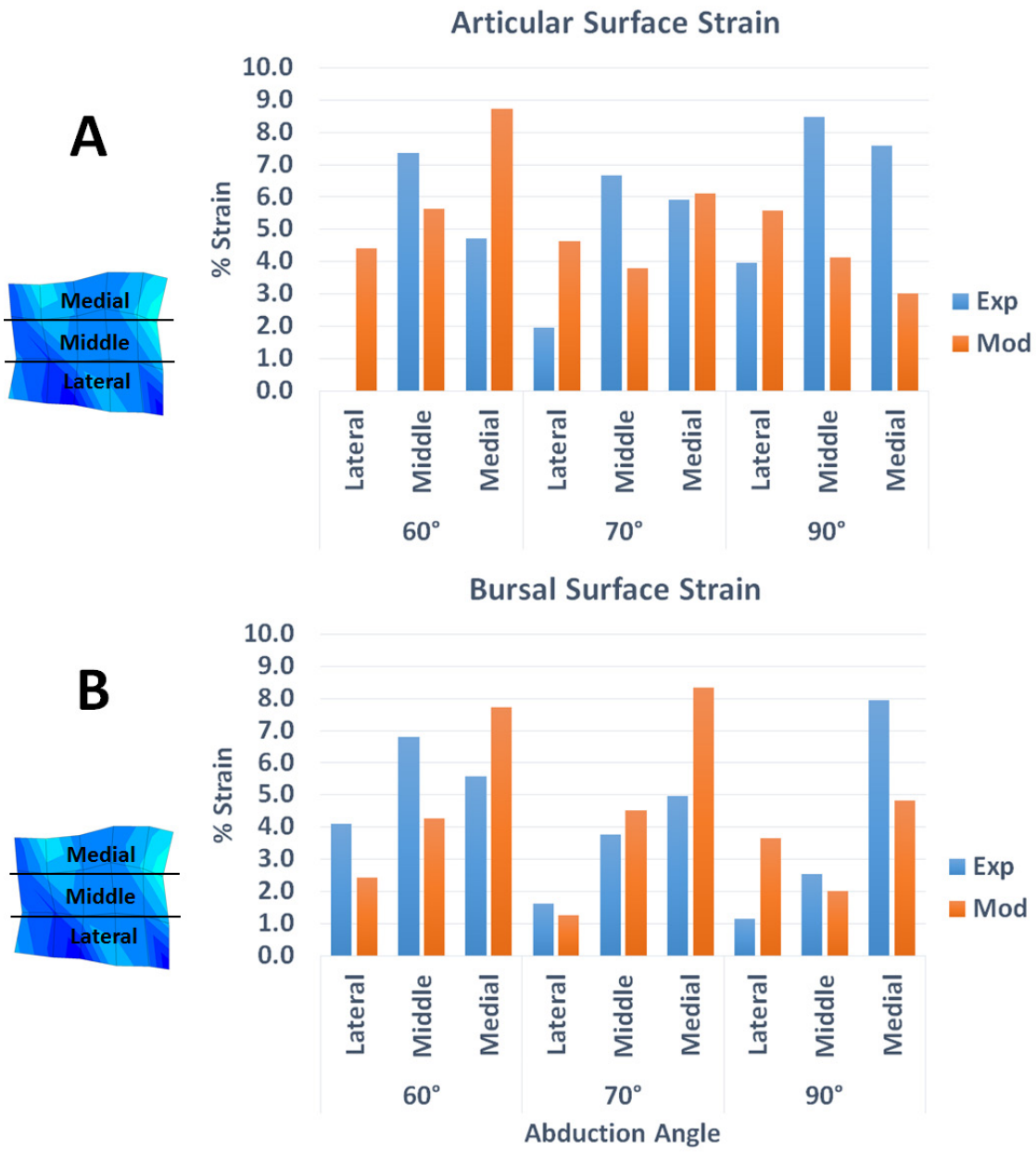

Figure 4.24. Average strains for the articular and bursal surfaces along the tendon axial length at 60°, 70°, and 90° of abduction. Both the experimental strains and model predictions generally showed the largest strains to be located at the medial edge of the tendon, where the load was applied. Although the model predicted similar relationships between joint angle and strain as the experiment, these predictions were most different from the experiment closest to where the load was applied at the medial edge of the tendon. On the articular side of the tendon, large differences in experimental and predicted strains were also observed for the middle row, which included the rotator cable structure.

4.3.4 Discussion

This study developed and validated a subject-specific, three-dimensional finite element model of rotator cuff tendons for prediction of strains at multiple glenohumeral joint angles. On average, bursal and articular surface strains predicted by the model were within the experimental repeatability of 3% strain of the experimentally determined values, though predictions on the bursal surface were typically closer to the experimental measures of strain than predictions on the articular surface. The larger differences in strain between experimental measures and predictions on the articular surface are likely due to the presence of the rotator cable. Although the rotator cable geometry was included in the model, it was not assigned separate fiber orientations and material properties from the rest of the tendon, which likely affected predictions of strain. Additionally, the model was able to predict similar distributions of strain as the experiment for articular versus bursal sides, along the anterior-posterior tendon width, and along the axial length of the tendon. Overall, this model can be used to reliably predict the mechanical behavior of the supraspinatus tendon for various loading conditions that do not involve contact with the humeral head, including propagation of supraspinatus tears.

The material properties measured for the tendons used in this study fell within the range of expected values for the anterior, middle, and posterior thirds of the supraspinatus tendon (171). However, it should be noted that in most human supraspinatus tendons, the anterior third has been shown to have the highest mechanical properties in terms of ultimate stress and modulus. In this study, the anterior and middle thirds of the tendon had similar ultimate stresses, and the elastic modulus of the middle third was approximately 30 MPa greater than that of the anterior third. This difference in properties may be due to the presence of a thickening found in the middle third of the tendon, whereas most tendons show the anterior third to be thickest (171).

Therefore, the results of this study are specific to the tendon tested, and the model predictions are not generalizable to human supraspinatus tendons as a whole. Therefore, additional subject-specific models are required in order to provide a library of geometries and material properties to allow for prediction of tendon behavior at a larger scale.

The experimental measures and model predictions of tendon strain in this study were of similar magnitudes to those determined in previous studies that have experimentally investigated tendon strain in intact supraspinatus tendons (136, 141, 151). Although the magnitudes of strain were similar, there were differences in the distribution of strain as reported by this and previous studies. The differences in strain distribution among studies may relate to different methods of quantifying strain (strain gauges versus image analysis), analysis of different regions of interest, or use of different reference configurations for calculations of strain. Although these studies reported different distributions of strain, the general consensus is that the articular surface shows larger strains than the bursal surface, and that joint position has a significant effect on tendon surface strains.

Similar to experimental studies, previous models of intact rotator cuff tendon using simplified geometry and isotropic elastic material properties found highest stresses to be located more anteriorly along the tendon width on the articular side of the tendon (221, 223), similar to the present study. However, these models also showed that the magnitude of stress increased with joint angle, which was not observed during experiments or predicted by the model. This discrepancy may be due to different reference configurations used between different studies. Previous experimental and modeling studies have not reported the reference configuration used to compute tendon surface strains, and therefore direct comparisons cannot be made. Since the reference configuration used can drastically affect the results of strain calculations, it is

imperative that future experiments and models investigating rotator cuff tendon strains clearly establish and thoroughly report the reference configuration used in order to correctly interpret results and model predictions.

Unlike previous models of the rotator cuff, this model uses experimental validation with subject-specific geometry and anisotropic, inhomogeneous material properties that better represent the behavior of the tendon. Overall, the model developed in this study establishes a framework to predict the effect of loading on tendon strain, providing a useful tool to better evaluate the mechanical environment of the supraspinatus tendon as it relates to rotator cuff injury. Based on the validation data, future iterations of the model will be improved by varying material parameters at the tendon insertion, and where fibers from the infraspinatus merge with the supraspinatus to better account for local differences in material properties. It may also be necessary to account for the fiber direction and material properties of tendon thickenings, such as the rotator cable, to better predict strains and regions of stress shielding in those regions.

This model has only been validated for the region medial to the tendon insertion for the joint positions tested. However, the goal of this model is to predict tear propagation within the region most common to rotator cuff tears, and therefore it can serve as a basis for further studies. The next iteration of this model will incorporate contact between the rotator cuff tendon and the humeral head to allow for strain predictions for the lower bounds of normal glenohumeral range of motion. Ultimately, by introducing “tears” of different geometry, location, and tendon degeneration into the intact tendon geometry, this model can be used to predict tendon strains for investigating risk factors related to rotator cuff tear initiation and propagation. This information will provide surgeons with updated guidelines for proper management of rotator cuff tears to minimize the time and costs associated with rotator cuff tear treatment.

4.3.5 Conclusion

This study successfully developed and validated a subject specific, three-dimensional finite element model of the supraspinatus tendon to predict rotator cuff tendon strain. Magnitude and distribution of strains predicted by the model were also similar to previous studies investigating strain in the rotator cuff tendons. The validated model can be used to perform analyses of tear propagation for tears of varying geometry and tendon degeneration to improve knowledge about rotator cuff tear propagation. Large differences were found in calculated strains when using different joint positions and preloads for the reference configuration. Therefore, future models need to clearly define the reference configuration and boundary conditions used when calculating or predicting tissue strains in order to assist in interpreting results.

4.4 EFFECTS OF TEAR SIZE AND LOCATION ON PREDICTIONS OF SUPRASPINATUS TEAR PROPAGATION

4.4.1 Introduction

Degenerative rotator cuff tears remain a significant clinical problem due to their very high incidence rate (over 30%) and no clear consensus among clinicians on the most effective form of treatment (63-67, 172). Studies investigating changes in tear size after treatment with exercise therapy have found that over 50% of patients show an increase during follow-up (85, 87, 130-133). Furthermore, those patients showing larger increases in tear size are most likely to have previously asymptomatic tears become symptomatic (130, 134). Therefore, changes in rotator cuff tear size are likely related to outcomes of treatment. The importance of tear size on patient outcomes is further demonstrated by the findings that larger tears are typically more difficult to repair surgically and are associated with worse clinical outcomes (20, 79-81).

In recent years, various studies have investigated the effects of rotator cuff tear geometry on tear propagation by focusing on tear size (135, 139), and location (150, 154, 155, 228). The general findings of these studies were primarily that larger tears are at greater risk for tear propagation, and that tears in the anterior third of the supraspinatus tendon that interrupt the rotator cable are at higher risk for propagating than tears in the middle of the supraspinatus tendon. In addition, numerous studies have developed finite element models of the rotator cuff to test different combinations of tear geometry and assess the risk of tear propagation (152, 170, 216, 219, 239). While finite element models can provide valuable information to predict the

behavior of rotator cuff tears, previous models share similar limitations. First, most of these models assume simplified material properties that do not account for the inhomogeneity and anisotropy of tendon tissue. Second, many models lack experimental validation of the results, and so the behavior of the model cannot be confirmed. Last, these models are not capable of predicting damage to the tendon, and therefore the tear is unable to change in size over the course of the simulation. In order to more accurately predict the effects of rotator cuff tear size and location on tear propagation, it is important to use subject-specific material properties that represent the actual behavior of the tendon, to use a model that can be directly compared to experimental results, and to be able to visualize changes in tear dimensions over time.

Therefore, the objective of this study was to use an experimentally validated three-dimensional finite element model of supraspinatus tendon using subject-specific geometry and anisotropic material properties to predict tear propagation for various combinations of tear size and location. Based on previous experimental testing, and since the anterior supraspinatus tendon is known to have higher structural and mechanical properties than the posterior supraspinatus (171), it was hypothesized that 1) larger rotator cuff tears will propagate at lower loads than smaller tears, and 2) tears in the posterior third of the supraspinatus tendon will require higher loads to propagate than anterior tears.

4.4.2 Materials and Methods

As described in Section 4.3, an experimentally validated finite element model of the supraspinatus and infraspinatus tendons was developed using subject-specific geometry and material properties taken from a single cadaveric shoulder specimen (male, 70 years old, right limb). Briefly, material testing was performed to determine subject-specific material properties for the anterior, middle, and posterior thirds of the supraspinatus tendon. The tendon material behavior was represented using a transversely-isotropic fiber-reinforced Neo-Hookean material model (216, 236, 237). The properties of each tendon third were assigned to that region of the model, with a linear gradient of material properties separating each third (Figure 4.18). Validation of the model was performed by applying the same boundary conditions used during mechanical testing of the intact tendon to the model and predicting strains on the articular and bursal surfaces of the tendon. Overall, the model successfully predicted strains within 3% strain of the experiment, and also predicted similar distributions of strain on both tendon surfaces.

Using the validated model, tears were introduced to the geometry in varying combinations of size and location. All tears were located approximately 5 mm medial to the tendon insertion on the humerus on the articular side. This position was chosen such that the model predictions could be compared with the results of previous experiments investigating supraspinatus tendon tear propagation (142, 228). In the anterior-posterior direction, tears were either located in the center of the tendon anterior-posterior width, at the posterior edge of the tendon, or at the anterior edge of the tendon. Tear size was 0.5 cm, 1 cm, or 1.5 cm in each location, for a total of 9 combinations of tear size and location simulated. The tear sizes chosen represent a range of small to medium sized tears that would initially remain isolated to the supraspinatus tendon (240). Tears modeled in the posterior third originated at the posterior point

and extended into the anterior direction, while tears in the anterior third originated at the anterior point and extended into the posterior direction. Tears in the middle of the tendon originated at the center point and extended for half the length of the tear in both the anterior and posterior directions (Figure 4.25). The tear was modeled in the mesh by creating duplicate nodes for the elements along the tear surface using the "detach" function in Hypermesh (Altair Engineering, Troy, MI, USA), such that the medial and lateral tear surfaces were allowed to separate during loading. The models consisted of approximately 35,000 nodes and 160,000 solid tetrahedral elements. The surfaces along which the tear was able to propagate consisted of approximately 3,000 2D cohesive elements that were roughly 0.5 mm in size in order to ensure mesh convergence (Table 4.6). The number of elements varied between models in order to provide a sufficient resolution to predict stress and strain at the tear tips, depending on tear size and location. In general, a greater number of cohesive elements were needed to model smaller tears, due to a greater tendon surface area that did not include a tear.

To model tear propagation, cohesive elements were created on the surface of any elements that could conceivably separate to allow for the tear to propagate, starting at the anterior and posterior edges of the tear. Cohesive elements are special surface elements that have been previously used to model crack propagation in metals, brittle materials, and, more recently, hyperelastic materials. In the past few years, cohesive elements have been used in biological tissues to model a peel test in aortic tissue (241) and investigate failure of cartilage implants (242). By putting cohesive elements on the connected surfaces of adjacent elements, failure can be modeled by allowing the overlapping cohesive elements to separate at some critical failure point.

Table 4.6. Number of Nodes and Elements for Each Tear Model

Location	Tear size (mm)	Nodes	Elements	Cohesive
Anterior	0.5	34665	160611	2979
	1	38165	177656	2618
	1.5	30755	140656	2283
Middle	0.5	36080	165877	2999
	1	31982	148306	2587
	1.5	30192	137397	2343
Posterior	0.5	33935	158077	2972
	1	33536	155985	2671
	1.5	35127	161981	2337

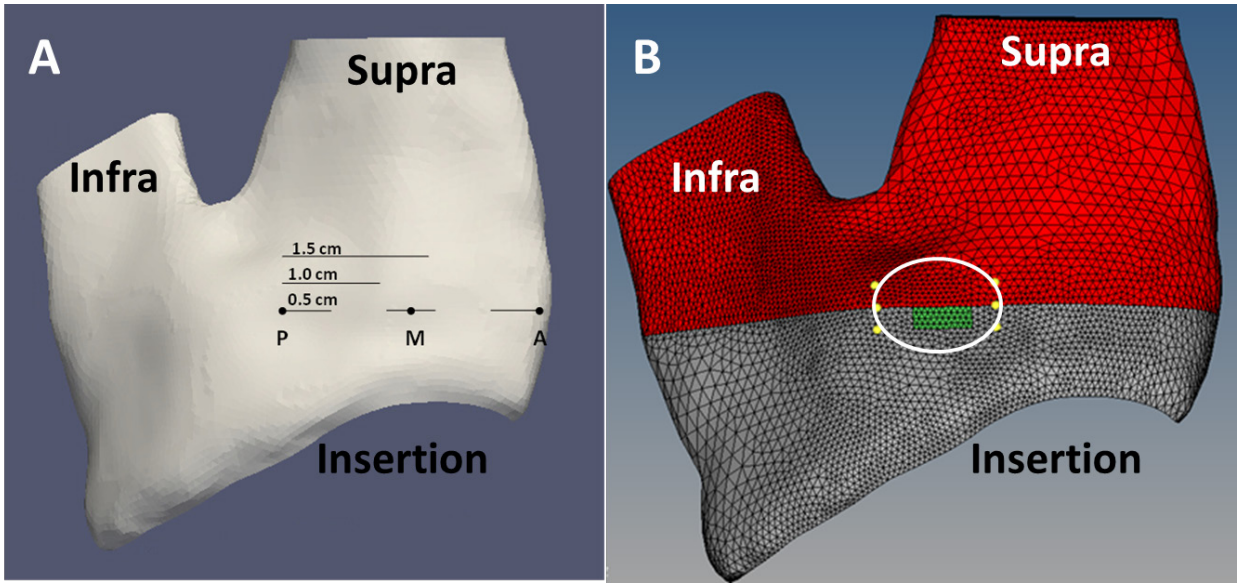

Figure 4.25. Tear locations for propagation simulations. A) Nine combinations of tear size and location were tested. Tears originated either in the posterior (P), middle (M), or anterior (A) thirds of the tendon, and were 0.5 cm, 1.0 cm, or 1.5 cm long. The lines for 1.0 cm and 1.5 cm tears are offset from their initiation point for comparison with the 0.5 cm tear. B) Example mesh for a 0.5 cm posterior tear (tear location is circled in white).

The behavior of the cohesive elements is defined based on a cohesive traction-separation law (243, 244). Assuming a bi-linear relationship between traction and separation, the overall traction-separation relationship can be defined by the parameters σ_{max}, the maximum stress, and δ_{max}, the maximum separation (or critical displacement) (Figure 4.26). Assuming failure occurs primarily in the mode I (tensile) case, the area under the traction-separation curve is the fracture toughness of the material (G_c). In this case, the traction-separation law can be written as

$$\sigma = k_c \delta,$$

where the stiffness of the cohesive elements, k_c, is defined by the failure properties of the material:

$$k_c = \frac{S}{1-S} \frac{\sigma_{max}}{S_{init}} \frac{1}{\delta_{max}}.$$

Here, S is a parameter representing damage to the material, which monotonically decreases from 1 to 0, depending on how close the separation between elements is to the maximum separation. S_{init} is the initial damage to the material (in this case equal to 0.98) that defines the starting point along the traction-separation curve. Damage to the material does not occur until the maximum stress is reached. Failure can be defined as the point on the traction-separation curve at which the connection between cohesive surface elements with a shared surface is broken upon reaching the maximum separation.

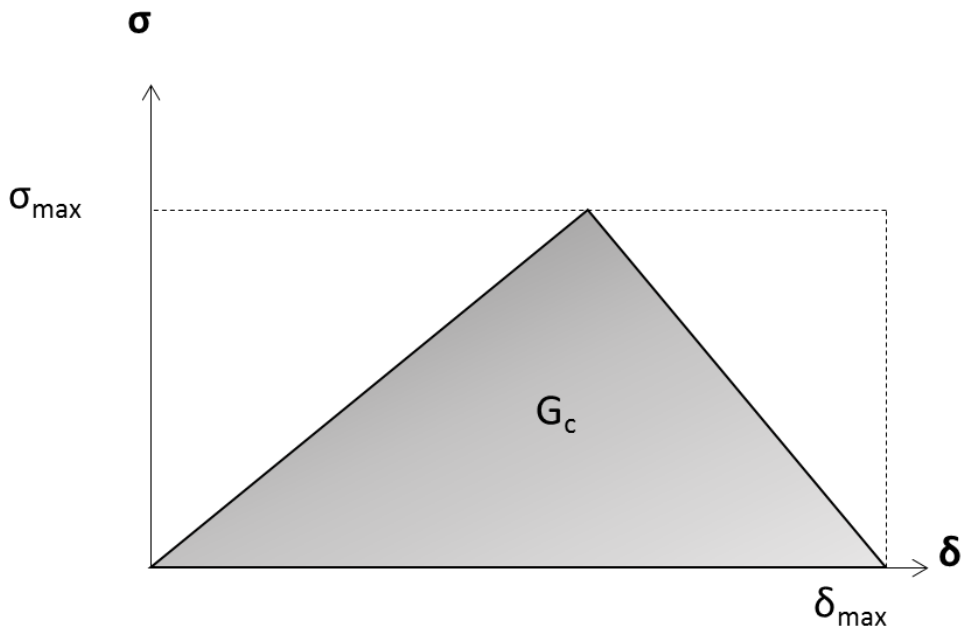

Figure 4.26. Cohesive traction-separation law for cohesive elements. Fracture toughness (G_C) is represented as the area under the curve and depends on both the maximum stress (σ_{max}) and maximum separation (δ_{max}) for a given material.

In order to determine fracture toughness parameters for simulations, the fracture toughness of supraspinatus tendon at the macroscopic scale was first estimated based on the change in work required to increase tear area (245, 246) using previously collected data from experimental testing of tear propagation (228). During the experiment, cadaveric supraspinatus tendons with an artificial rotator cuff tear were cyclically loaded for 100 cycles between two load limits, and measures of tear area were made at the beginning and end of cyclic loading. Energy absorbed by the tendon was calculated as the area under the loading curve of the force-displacement plot for two cycles of the protocol: one cycle at the beginning of the test prior to tear propagation, and one cycle at the end of the test after tear propagation. To calculate the fracture toughness, it is assumed that any energy lost between cycles goes into increasing the

surface area of the tear. Based on these simplifying assumptions, fracture toughness can be calculated as the change in energy divided by the change in tear area between cycles (Figure 4.27). Using the calculated value of fracture toughness and the known value of ultimate stress, maximum separation can be calculated from the traction-separation curve and used as a model input.

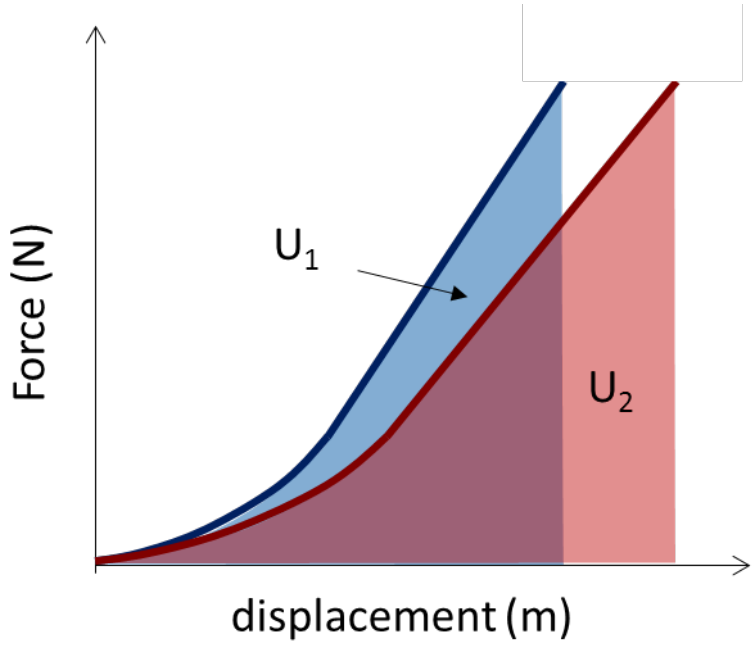

Figure 4.27. Estimation of fracture toughness (G_C) from experimental tear propagation data. Fracture toughness can be approximated at the macroscopic scale as the work done to increase the surface area of a tear. In this case, the energy absorbed by the tendon is divided by the difference in tear area between time points at the start and end of cyclic loading.

Material failure properties were assigned to the cohesive elements using the same method as for the Neo-Hookean model parameters. Specifically, the ultimate stress and estimated fracture toughness were varied along the anterior-posterior width of the tendon, with the anterior third having the highest ultimate stress and fracture toughness and the posterior third having the lowest ultimate stress and fracture toughness (Table 4.7). The medial edge of the supraspinatus tendon was displaced 5 mm (~15% bone-to-clamp strain) at a 70° angle (representing 70° of glenohumeral abduction) over 100 load steps. This loading condition was based on the reference configuration used to validate the model and the approximate strain required to cause tissue failure in intact tendon. Stress and strain values were averaged for elements within a 2mm-diameter sphere at the anterior and posterior tear tips for the time step in which the critical load was reached, indicating the point of critical failure. Model outputs included critical load and displacement required to propagate the tear, and principal stress magnitude and maximum principal strain at the critical load for the anterior and posterior tear tips. Correlation analyses (Pearson's r) were performed to investigate the relationship between these parameters and tear size and location (distance of anterior tear tip from anterior edge). The significance level was set at $p < 0.05$.

Table 4.7. Failure Properties of Supraspinatus Tendon Thirds for Cohesive Elements

Location	Ultimate Stress (MPa)	G_c (J)	Maximum Separation (mm)
Anterior	5.8	1854.6	0.64
Middle	5.8	1545.5	0.53
Posterior	4.3	1221.3	0.57

4.4.3 Results

In all simulations, tear propagation began at approximately 2.7-3.6 mm (approximately 7% bone-to-clamp strain) of displacement applied to the medial end of the tendon (Table 4.8). For all tear sizes, tears located in the posterior third of the supraspinatus tendon required the highest loads to propagate, ranging from 247 N for 1.5 cm tears to 567 N for 0.5 cm tears (Figure 4.28). The tear location that required the lowest load to propagate depended on the size of the tear. For small tears, the middle location required the least amount of load to propagate (373 N), whereas for the largest tears the anterior location required the lowest load (171 N). For the 1 cm size tear, approximately the same loading magnitude was required to propagate the tear for both middle and anterior locations (280 N). In addition to the critical load being dependent on tear location and size, the size of the tear also affected the magnitude of the difference in critical load between tear locations. For the smallest tear size, the critical load for the posterior tear was approximately 1.2 times higher than for anterior tears, and 1.5 times higher than for middle tears. For the medium tear size, the posterior tear critical load was approximately 1.75 times higher than for both anterior and middle tears. Lastly, for the largest tear size, the critical load for the posterior tear was 1.4 times larger than the load for the anterior tear, but was 1.2 times larger compared to the middle tear.

Table 4.8. Critical Failure Values at Point of Tear Propagation

	Size	Crit Load	Crit Disp	Stress at Critical Load (MPa)				Strain at Critical Load (% Strain)			
				Bursal		Articular		Bursal		Articular	
Location	(mm)	(N)	(mm)	Ant Tip	Post Tip	Ant Tip	Post Tip	Ant Tip	Post Tip	Ant Tip	Post Tip
Anterior	0.5	465	3.4	3.8	4.1	4.2	8.3	20.1	17.5	20.7	20.5
	1	284	2.9	4.5	4.6	4.0	8.5	23.0	19.6	22.7	24.1
	1.5	171	2.7	4.7	3.4	3.9	5.6	22.5	15.4	18.7	21.4
Middle	0.5	373	3.2	5.4	4.0	7.7	6.2	21.8	20.1	28.1	21.4
	1	280	3.1	5.7	3.4	6.7	5.2	24.9	18.4	32.6	22.1
	1.5	213	3.2	5.4	2.7	7.3	5.1	26.1	16.2	29.1	20.1
Posterior	0.5	567	3.6	1.2	0.8	7.9	3.1	6.8	5.9	24.0	15.5
	1	488	3.4	3.0	1.3	7.7	2.2	14.7	8.9	18.9	12.1
	1.5	247	3.2	6.2	1.9	7.7	3.6	27.8	12.0	33.9	18.1

Among all simulations, stresses and strains for the anterior tear tip ranged from 1.2 to 6.2 MPa and 6.8 to 27.8 % strain on the bursal side, and from 3.9 to 7.9 MPa and 18.7 to 33.9 % strain on the articular side. For the posterior tip, stresses and strains ranged from 0.8 to 4.6 MPa and 5.9 to 20.1 % strain on the bursal side and from 2.2 to 8.5 MPa and 12.1 to 24.1 % strain on the articular side. Largest stresses and strains were generally located on the articular side of the tendon and at the anterior tip of the tear. For tears located in the anterior third of the tendon, although the anterior tear tip showed higher stress and strain than the posterior tip on the bursal side of the tendon, this trend was reversed for the articular side, where the posterior tip showed higher stress and strain.

All simulations of tear propagation showed stress concentrations located at the anterior and posterior tips of the tear (Figure 4.29). The stress concentrations took on an oval pattern that was approximately perpendicular to the plane of the tear. When comparing the model predictions of tear shape and propagation to experimental observations, the model was able to capture a

similar elliptical shape of the tear (Figure 4.30-A). The model also predicted "opening" of the tear on the articular surface of the tendon before propagating through to the bursal side, which was also observed experimentally (Figure 4.30-B,C). However, the model was not able to predict tear "blunting" (i.e. less sharp angle between tear surfaces at the tear tips) as was observed during experiments.

Tear size was only significantly correlated with critical load, but showed a strong negative correlation ($r = -0.816$, $p = 0.007$) (Figure 4.31). Tear location (distance of the anterior edge of the tear to the anterior edge of the tendon) was significantly correlated with stress at the posterior tear tip for both bursal ($r = -0.878$, $p = 0.002$) and articular ($r = -0.899$, $p = 0.001$) sides, stress at the anterior tear tip on the articular side ($r = 0.928$, $p < 0.001$), and strain at the posterior tear tip for both bursal ($r = -0.738$, $p = 0.023$) and articular ($r = -0.783$, $p = 0.013$) sides.

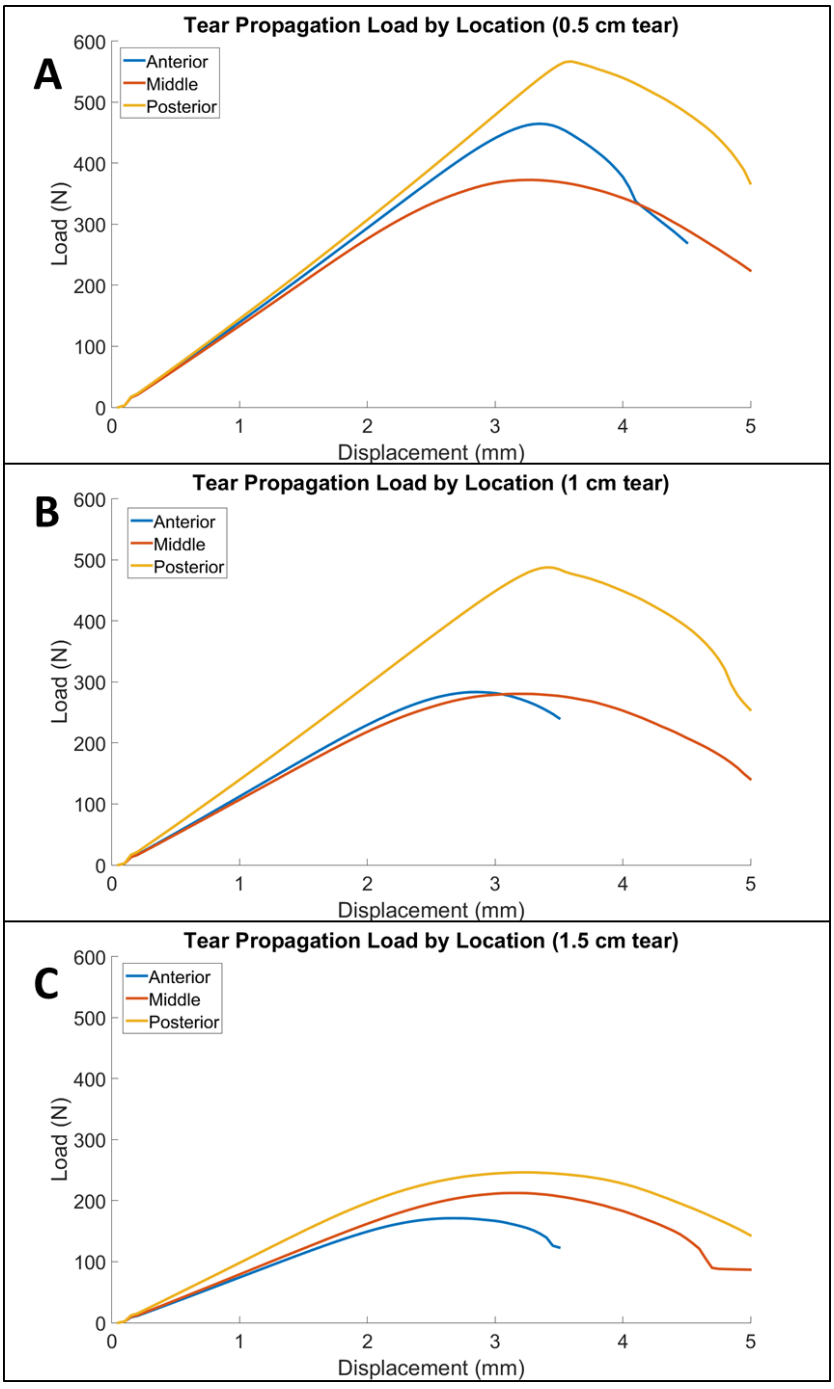

Figure 4.28. Load-displacement curves for tear propagation simulations. A) 0.5 cm tear size. B) 1 cm tear size. C) 1.5 cm tear size. Posterior tears required the greatest loads in order to propagate regardless of tear size, and the smallest tears required the largest loads to propagate regardless of tear location.

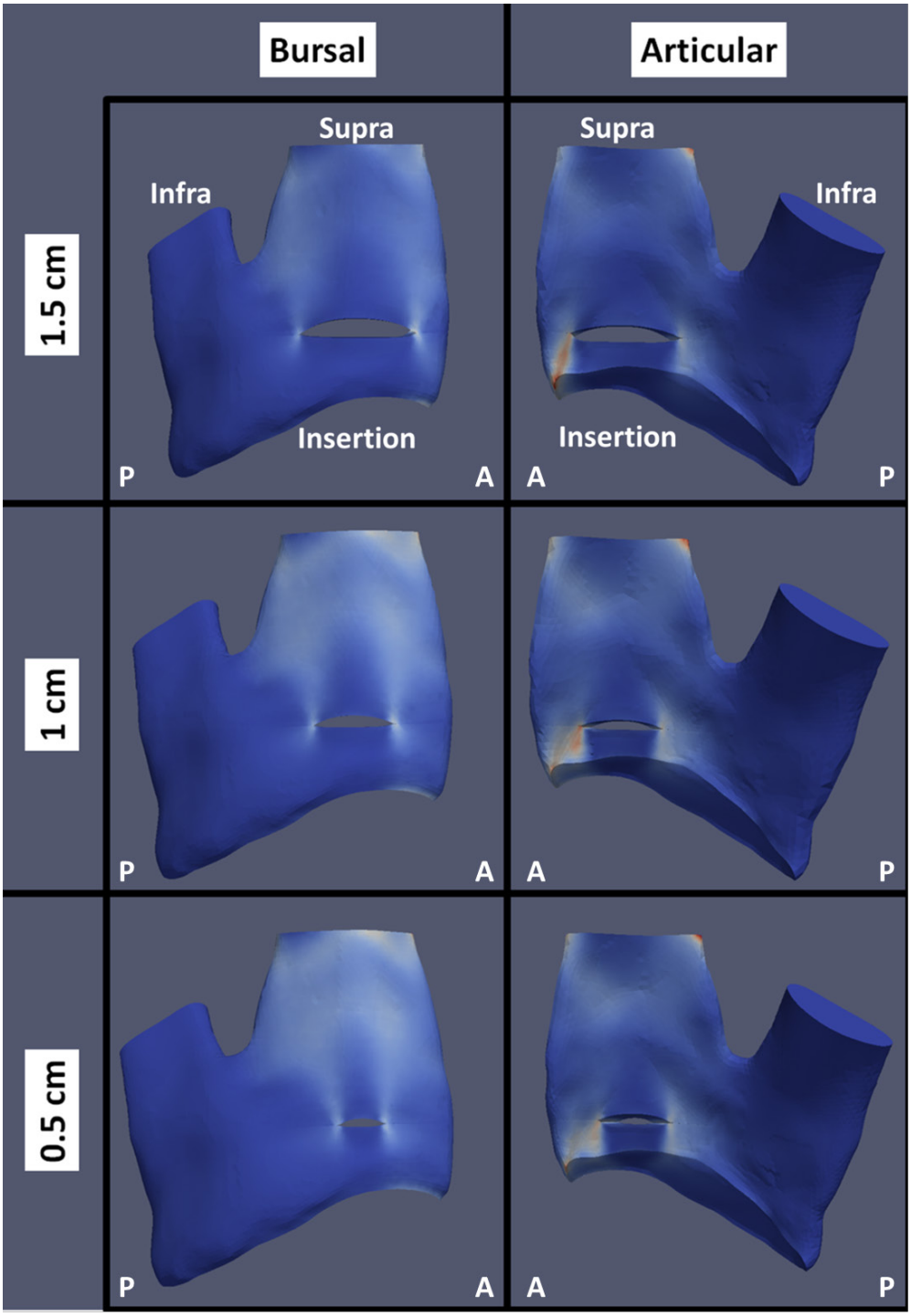

Figure 4.29. Representative images of tendon with a middle third tear. Stress concentrations were located at the edges of the tear. Tears generally increased in size on the articular side before the bursal side, and tended to propagate in the anterior direction.

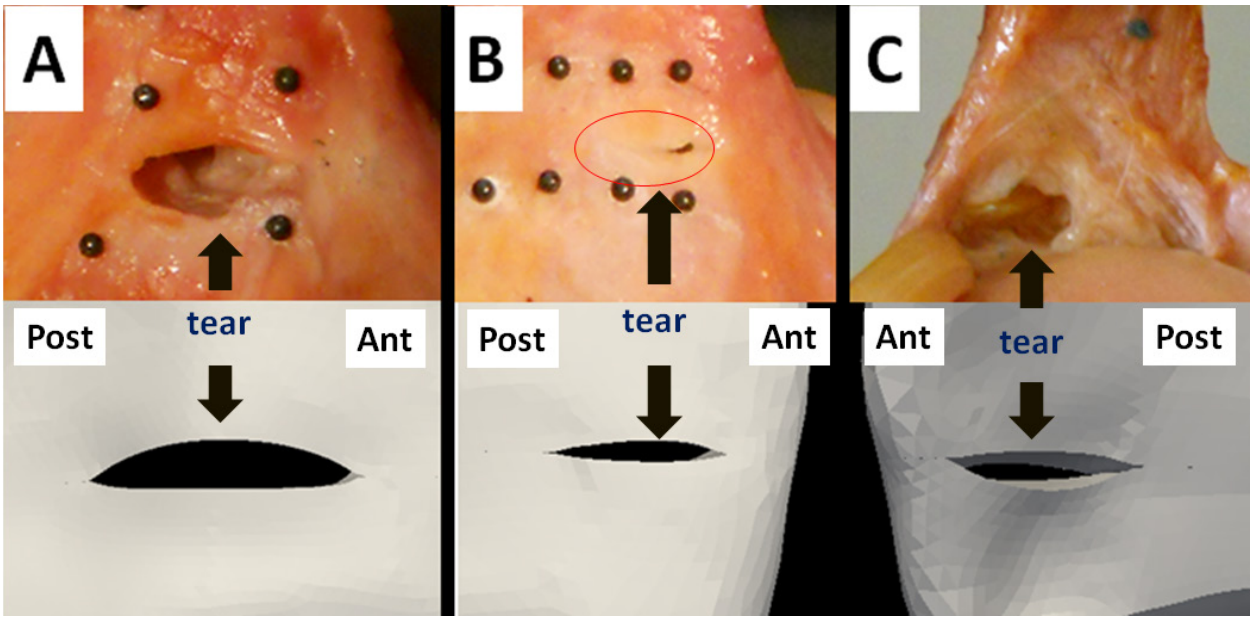

Figure 4.30. Comparison of experimental supraspinatus tendon tear shapes to predicted tear shapes during tear propagation. A) The model predicted a similar elliptical shape as was observed during tear propagation experiments. B) In some experimental cases, full-thickness tears in the anterior third of the tendon did not show substantial propagation on the bursal side (red oval). C) However, the tear was much more visible on the articular side of the same tendon, which was also observed for the tear propagation simulations of tears in the anterior third. A larger tear size on the articular side versus the bursal side for a given point in time indicates propagation of the tear on the articular side prior to propagating on the bursal side.

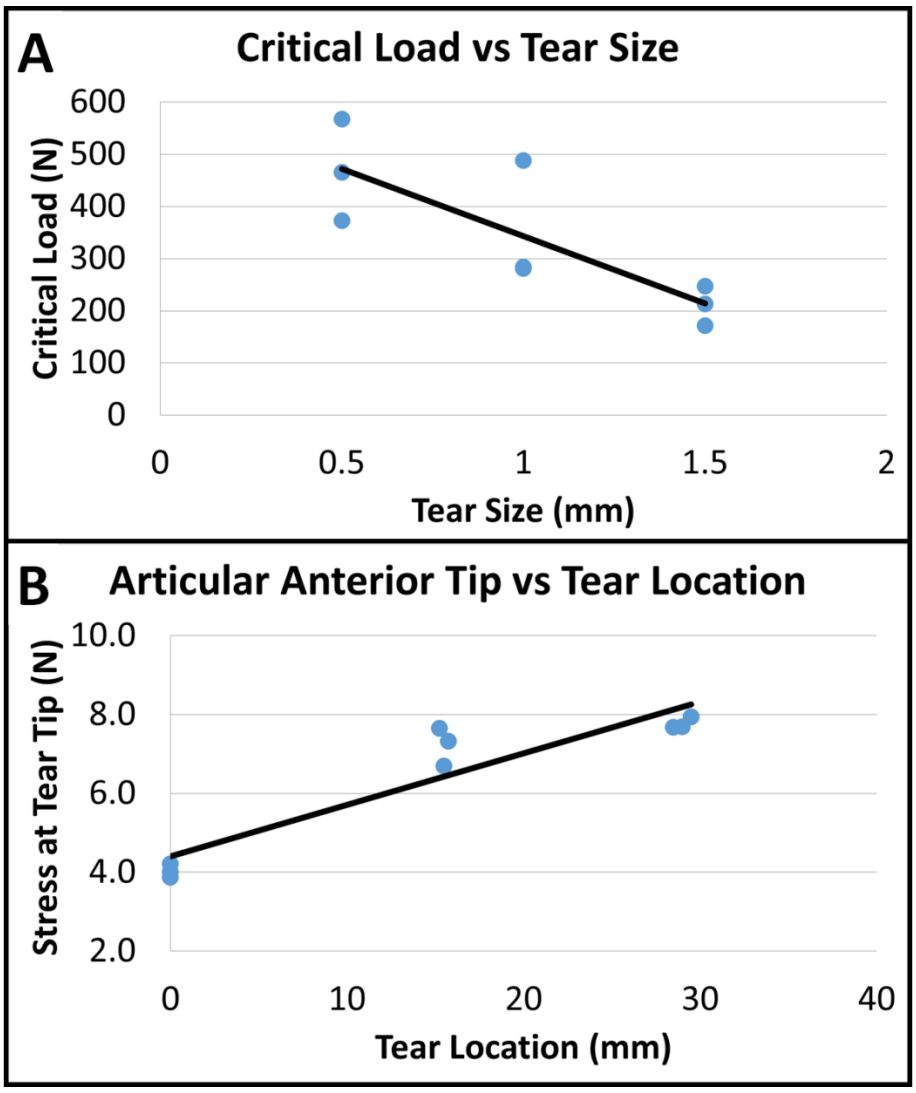

Figure 4.31. Significant correlations for tear size and location. A) Critical load showed a strong negative correlation with tear size ($R^2 = 0.66$). B) Tear location showed a strong positive correlation for stress at the anterior tear tip on the articular side of the tendon ($R^2 = 0.86$).

4.4.4 Discussion

This study used finite element models developed using subject-specific geometry and material properties from a single specimen to investigate the effects of tear size and location on tear propagation. For the specific tendon geometry and material properties tested, it was found that tears 1 cm wide or larger in the anterior third of the rotator cuff are most at risk for propagation. Additionally, it was determined that larger rotator cuff tears require lower loads to propagate, supporting one of the study hypotheses. This finding indicates that as tears propagate, they require less and less load to do so. Therefore, tears in the anterior third of the rotator cuff that require lower loads to propagate than tears in other regions should be treated earlier, before they can develop into massive tears. While the least amount of load was required to propagate tears in the anterior third, posterior tears required the highest magnitude of loads to propagate, as was hypothesized. This result is likely due to the greater thickness and higher mechanical properties of the middle and anterior thirds of the tendon, making it more difficult for tears in the posterior third of the tendon to disrupt collagen fibers and propagate. However, posteriorly located tears that were 1.5 cm long required drastically lower loads to propagate than smaller tears, likely since the anterior edge of the tear was already located within the stronger middle third of the tendon.

The magnitude of load required to propagate a 1 cm wide tear predicted by the model ranged from 280 N for tears in the middle third to 488 N for tears in the posterior third. Experimentally, the average load at which at least a 100% increase in tear size occurred was 389 ± 237 N for 1 cm wide anterior tears and 714 ± 168 N for middle tears of the same size (228). The critical load values predicted by the model generally fell within the experimental range for anterior tears, but the loads predicted for middle tears were lower. The discrepancy in results

may be due to the middle third having similar failure properties as the anterior third for this specific tendon. Another possible explanation is that the model did not separately account for the properties and fiber orientation of the rotator cable structure, which is believed to reinforce the supraspinatus tendon (52). Although anterior tears interrupt the rotator cable, potentially causing the tendon to lose this reinforcement, tears in the middle third of the tendon generally do not break the cable unless they propagate to a much larger size. Future models that incorporate the properties of the rotator cable might therefore show higher loads required to propagate tears in the middle third of the supraspinatus tendon. Regardless, the simulations predicted the experimental result of a 2:1 ratio of critical load required to propagate anterior tears versus tears in other locations.

Largest magnitudes of stresses and strains at the anterior and posterior edges of the tears generally corresponded with the direction of tear propagation. For most cases, the largest strains were observed at the anterior tear tip, and for these cases the tear tended to propagate anteriorly more than posteriorly. For anterior tears, highest stresses and strains were located at the posterior, but only on the articular side of the tendon. In these cases the articular tear propagated posteriorly; therefore, the direction of propagation was still predicted by the tear edge with the highest stress and strain. When comparing the maximum principal strains predicted by the model to those determined experimentally, the strains fell within the range of expected values at the tear tips (26.1 ± 9.4 % strain), further validating the results of the model (142). It is important to consider how the variations in stress and strain at the tear tips for different tear locations and sizes affect tear propagation. Tears with higher strains at the tear tips (i.e. larger tears, tears located in the anterior third) are likely at higher risk for propagation, and therefore these types of tears should be monitored closely for propagation. Additionally, variations in strain across the

tear width have implications for rotator cuff repair. Even when loading being distributed across the tendon-suture interface, local variations in tendon geometry and material properties can result in a gradient of strains across the interface that may increase risk of failure.

Additionally, stresses and strains were higher on the articular side of the tendon than for the bursal side for all tear cases. This observation corresponded to most tears visibly increasing in size on the articular side of the tendon before the tear on the bursal side grew in size. The model predictions of non-uniform tear propagation throughout the tendon thickness are supported by experimental testing that also showed that tears "opened" more on the articular side before propagating on the bursal side (228). Therefore, when monitoring tears for propagation or considering treatment for isolated supraspinatus tendon tears, it is important to consider both bursal and articular sides of the tendon, even when a tear is full-thickness.

This study also found strong, statistically significant correlations between tear size and location for various model outputs. A strong negative correlation between tear size and critical load indicates that larger tears begin to propagate at lower loads, which can be predicted by fracture mechanics theory. However, there was no effect of tear location on critical load. Tear location showed strong negative correlations with stress and strain at the posterior tip of the tear, suggesting that tears further from the anterior edge of the tendon are less likely to propagate posteriorly. Meanwhile, the strong positive correlation between location and stress at the anterior tip indicates that posteriorly located tears are more likely to propagate anteriorly.

A main limitation of this study is that the results are specific to a single tendon with its own geometry and material properties, and so the results cannot be generalized to describe tear propagation for all supraspinatus tendons. However, the model successfully predicted similar tear behaviors, loading magnitudes, and maximum principal strains at the tear tips that were

comparable to previous experimental testing, and therefore it is reasonable that the model predictions are applicable to a variety of tear conditions. Furthermore, the simulations performed use a single static loading condition, rather than cyclic loading conditions that are more representative of activities of daily living. Although the model did not model failure due to fatigue, the predicted loads, stresses, and strains provide a good estimate of failure conditions for different tear locations and sizes. Additional subject-specific models must be developed and validated in order to confirm the results of this study, and also provide a library of varied tendon geometries and material properties to make generalizations about the behavior of rotator cuff tears. An established library of subject-specific geometry, material properties, and loading conditions can allow for creation of a simulation workbench to allow for prediction of tear propagation for a variety of patient types and treatments.

Other limitations that will be addressed in future models include that the model does not account for the rotator cable structure, only applies loads for a single joint position, assumes tear propagation along a single plane, and only assumes failure due to tension (i.e. mode I failure). By including additional cohesive elements throughout the solid model or varying failure properties for both tensile and shear failure conditions, different tear propagation behavior may occur. Lastly, the computational model does not account for biological remodeling of the tendon over time, which has the potential to retard or otherwise affect tear propagation at longer time scales.

4.4.5 Conclusion

This study identified rotator cuff tear characteristics in terms of tear size and location that indicate a greater risk for tear propagation. Specifically, tears located in the anterior third of the tendon and tears of larger size may be at higher risk for propagation at loading magnitudes encountered during regular activities of daily living. Therefore, these types of tears should be a priority for early treatment and close follow-up observation when considering options for a patient. Future iterations of this model can allow for predictions of tear propagation for a variety of tear sizes, locations, and shapes. Ultimately, these results will contribute to the development of a "rotator cuff index" that will assist physicians in determining appropriate treatment protocols for their patients with rotator cuff tears based on their tear characteristics at initial diagnosis.

5.0 AIM 3: EFFECT OF DEGENERATION ON PROPAGATION

In addition to the effects of tear geometry on tear propagation, the intrinsic properties of the tendon can also have a significant effect on the behavior of a rotator cuff tear. Whereas the geometry of the tear can affect the magnitude of strains around the edges of the tear, the quality of the tissue can affect its ability to resist tear propagation. If the tendon integrity is severely compromised by tissue degeneration, this may have a significant impact on the outcome of treatments for rotator cuff tears. Although previous studies have investigated the effects of degenerative rotator cuff tears on tendon tissue quality, especially with regard to surgical repair outcomes, the relationship between tendon degeneration and tear propagation is not well understood. Furthermore, the relationships between rotator cuff tendon degeneration and the mechanical behavior of the tendon have not been quantified. Therefore, the third aim of this dissertation was to elucidate the role of rotator cuff tendon degeneration on the mechanical behavior of rotator cuff tendons. By understanding how tissue degeneration associated with rotator cuff tears changes the structure and mechanical behavior of rotator cuff tendons, estimates of tendon degeneration as a risk factor for tear propagation can be used to tailor treatment options for patients with degenerative rotator cuff tears.

5.1 LOCALIZED DIFFERENCES IN DEGENERATION BETWEEN TORN AND INTACT SUPRASPINATUS TENDONS

5.1.1 Introduction

Rotator cuff tears are a significant clinical problem with an incidence greater than 30% in the general population (63). Despite the high number of patients requiring treatment for rotator cuff injury, the biological and mechanical factors that lead to rotator cuff tears remain poorly understood. Age-related degeneration has been proposed as a significant intrinsic factor likely related to the development of rotator cuff tears (247-249). Previous studies have shown an increased prevalence of rotator cuff tears with age (64-67, 250), as well as an association between increased age and worse outcomes and rotator cuff healing after surgical repair of rotator cuff tears (113, 251-255). Furthermore, it has been shown that in the case of re-tears of surgically repaired degenerative rotator cuff tears, failure typically occurs at the tendon-suture interface (120-129), potentially indicating poor tissue quality due to tendon degeneration.

In order to characterize the extent of degeneration in rotator cuff tendon tissue, numerous studies have performed histological analysis of both intact and torn rotator cuff tendon (161-166, 256-258). These studies found a strong relationship between increased age and increased degeneration, as measured by degenerative changes in tenocytes and tendon extracellular matrix (161, 162). Sano et al. further supported the relationship between tendon mechanical behavior and tissue degeneration by linking a decrease in tendon mechanical properties to increased degeneration at the insertion of supraspinatus tendon specimens (256). Importantly, it was also confirmed that regions of greater tendon degeneration were localized to areas adjacent to

degenerative rotator cuff tears (163-166), providing a potential link to the high failure rates of surgical repairs at the tendon-suture interface.

However, these studies typically take tissue samples only from a single region of the tendon, for example at the medial edge of degenerative tears. Therefore, they do not account for localized degeneration that may exist elsewhere in the tendon. Recent modeling of supraspinatus tears has shown that localized differences in strain exist throughout the tendon and around the edges of a tear, indicating that cells in different regions of the tendon experience different mechanical stimuli based on the presence of a tear. Specifically, tendons show elevated strains at the anterior and posterior tear edges and a stress-shielded region of low strains compared to the rest of the tendon at the medial tear edge (216). Due to the mechano-sensitivity of tendon cells and their effects on the tendon extracellular matrix (259-261), spatial gradients of strain and mechanical stimuli have the potential to lead to local differences in the extent of degeneration throughout the tendon in the case of degenerative rotator cuff tears. These differences in degeneration may relate to the ability of tendon tissue to resist tear propagation or suture pull-out during mobilization or after repair. By providing quantitative information to surgeons about which regions of tendon are of the poorest quality, surgical techniques can be improved to reduce suture pull-out rates. Therefore, the objective of this study was to investigate histological differences in localized rotator cuff tendon degeneration in tendons with and without degenerative rotator cuff tears. It was hypothesized that 1) degeneration would be worst at the insertion of the supraspinatus tendon to the humerus, the most common location for tears, and 2) degeneration around the tear will be worst in the stress-shielded region medial to the tear.

5.1.2 Materials and Methods

Four intact fresh-frozen cadaveric shoulders (55 ± 12 years, 3 female, 1 male) and four shoulders with small rotator cuff tears isolated to the supraspinatus tendon (70 ± 9 years, 3 female, 1 male) were procured with permission from the University of Pittsburgh ethical oversight board. All tissues were stored at -20°C and allowed to thaw overnight at room temperature before dissection. All shoulders were dissected to isolate the supraspinatus and infraspinatus tendons to obtain tissue biopsies for histology. In the shoulders in which a tear was present, the anterior-posterior and medial-lateral dimensions of the tear were measured using a pair of digital calipers. Both tendons were split into anterior and posterior halves of approximately equal width using a No. 11 scalpel blade. Tendon biopsies (dimensions of ~2 x 4 mm) were then taken near the myotendinous junction, tendon mid-substance, and the insertion for each tendon half. For tendons with an existing tear, three samples were taken from around the tear: one sample from the medial edge of the tear, one from the anterior edge of the tear, and one from the posterior edge of the tear (Figure 5.1). The bursal side of each biopsy sample was marked with a line of India ink to allow for easy identification of bursal versus articular sides during histological analysis.

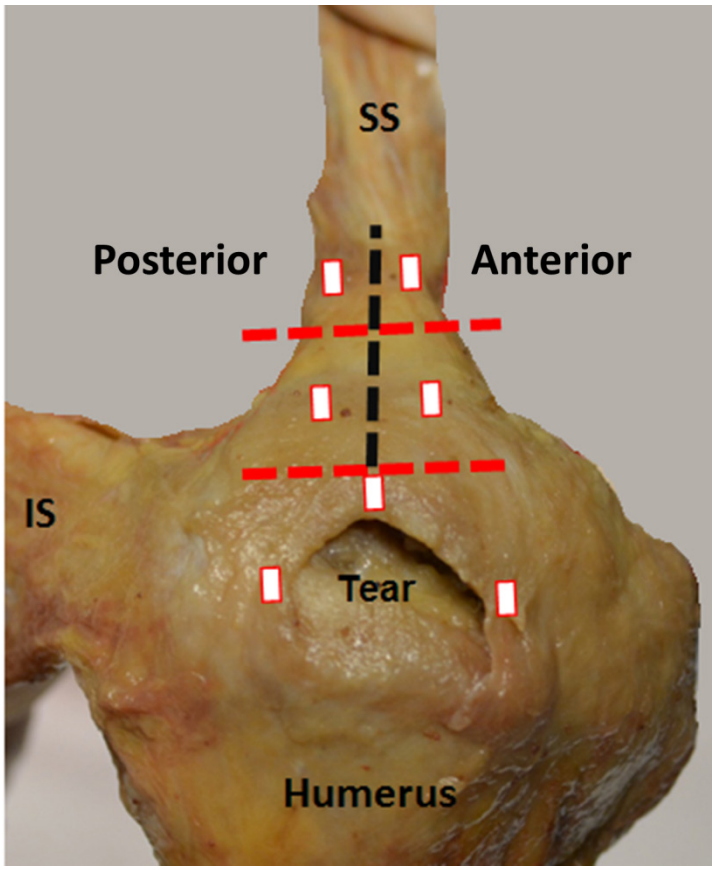

Figure 5.1. Schematic of biopsy locations for histological analysis of torn supraspinatus tendon. Biopsy locations are represented by white boxes. Biopsies are taken from the anterior and posterior halves of the tendon from locations at the tendon insertion, mid-substance, and myotendinous junction. For tendons with a tear, biopsies are taken at the anterior and posterior tear edges, as well as from the medial border of the tear. SS: Supraspinatus tendon. IS: Infraspinatus tendon.

All samples were fixed in 10% buffered formalin solution for at least three days. After fixation and paraffin embedding, samples were sectioned at a thickness of 5 μm and cut longitudinally such that three slices were obtained throughout the anterior-posterior width of each biopsy. All slides were stained with hematoxylin and eosin (H&E) to visualize tendon morphology, and then imaged using a light microscope with a 20x objective lens across the full tendon thickness. Since each tendon slice includes layers of the bursa and glenohumeral capsule

(35), these layers were removed from the images to ensure that only degeneration in the tendon proper was analyzed. Based on measurements of the thicknesses of these layers in the literature, a set percentage of the total image articular-bursal thickness was removed to isolate the superficial and deep layers of the tendon. The remaining tendon in the image was then split into equal halves to compare degeneration between bursal and articular layers of the tendon (161).

All histological images were graded by three independent observers for tendon degeneration using a semi-quantitative scale. Four main parameters were chosen to evaluate tendon degeneration: collagen fiber organization, tenocyte nuclei shape, tenocyte cell number, and lipoid degeneration (161-164, 262). The chosen grading scale was modified from Sano et al. to create a 4-point scale of degeneration (0 = no change, 1 = slight localized change <25% of tendon area, 2 = multifocal change 25-50% of tendon area, 3 = diffuse or global change >50% of tendon area) (165). The articular and bursal halves of each histological image were graded by each observer using this 4-point scale for each degeneration parameter, and the scores of the four degeneration parameters were summed to generate an "overall" degeneration score ranging from 0 (no degeneration) to 12 (completely degenerated). The scores of the three observers were then averaged to determine an overall degeneration score for each degeneration parameter for each image. The scores of the three images from each biopsy sample were combined to determine a representative degeneration score for each biopsy sample to be used for statistical analysis.

To test for differences between anterior and posterior samples and between bursal and articular surfaces, Wilcoxon signed-rank tests were performed. Three-way ANOVA was used to make comparisons in degeneration based on location, and to investigate interaction effects between tendon state (intact vs torn) and tendon (supraspinatus versus infraspinatus). One-way ANOVA was used to make comparisons by location around the rotator cuff tear. Post-hoc tests

for location were performed using a Games-Howell test, and independent samples Mann-Whitney U tests were used to make comparisons for the main effects of the presence of a tear and tendon, due to the data being non-parametric. Lastly, degeneration scores for each category from each biopsy specimen were averaged over all locations. For example, scores from all biopsy samples taken from the myotendinous junction of a given supraspinatus tendon were averaged together into a single score for each degeneration parameter. Spearman correlation was performed between grades from each category with specimen age. Significance was set at $p < 0.05$ for all tests.

5.1.3 Results

There was no statistically significant difference in cadaveric specimen age between tear groups ($p = 0.09$). In tendons with a tear, the average AP tear width was 14.8 ± 11.8 mm, and the average ML tendon retraction was 11.0 ± 7.0 mm. All tears showed a "crescent" shape, and all tendons showed various stages of tissue degeneration, with the worst degeneration qualitatively located around the supraspinatus tear (Figure 5.2-C). Grading among the three examiners showed good inter-rater reliability for total degeneration (ICC = 0.89). Intraclass correlation coefficients for grades of fiber organization, nuclei shape, increased cellularity, and lipoid degeneration also showed high reliability (0.76, 0.81, 0.77, and 0.94, respectively).

No statistically significant differences were found in any degeneration parameter between anterior and posterior samples or between articular and bursal sides of the tendons, indicating that it was acceptable to combine these samples together for analysis. Additionally, no statistically significant differences were found in total degeneration, fiber organization, nuclei shape, or cellularity by location. However, the myotendinous junction showed a significantly

greater amount of lipoid degeneration compared to the tendon mid-substance or insertion ($p < 0.001$) (Table 5.1, Figure 5.2B). Similarly, lipoid degeneration was the only parameter to show a statistically significant difference between tendons with and without rotator cuff tears ($p = 0.03$) (Table 5.1). Small but statistically significant differences in fiber organization ($p = 0.01$), nuclei shape ($p = 0.003$), and total degeneration ($p = 0.008$) were found between the supraspinatus and infraspinatus tendons, with the supraspinatus showing greater amounts of degeneration (Table 5.1).

No statistically significant interaction effects were found between location (insertion versus mid-substance versus myotendinous junction) and tendon state, between location and tendon, or between combinations of all three independent variables (Table 5.1). However, significant interaction effects were found between tendon state and tendon in fiber organization ($p = 0.01$), nuclei shape ($p = 0.01$), and total degeneration ($p = 0.001$) parameters. When comparing degeneration around tendon tears, the medial edge of the tear showed slightly greater amounts of degeneration for all parameters compared to the anterior and posterior edges of the tear. However, these differences were not statistically significant (Table 5.2). No correlations were found between specimen age versus any degeneration score, or between the majority of degeneration categories ($p > 0.05$). However, a very strong negative correlation was found between the degeneration score for fiber organization versus lipoid degeneration ($\rho = -0.922$, $p = 0.001$, Figure 5.3).

Table 5.1. Degeneration Parameter Values (Mean ± SD)

	Fiber Organization	Nuclei Shape	Increased Cellularity	Lipoid Degeneration	Sum
Insertion	2.5 ± 0.3	2.5 ± 0.3	0.6 ± 0.3	0.2 ± 0.2	5.9 ± 0.7
Mid-substance	2.4 ± 0.4	2.4 ± 0.4	0.6 ± 0.2	0.3 ± 0.3	5.6 ± 0.9
Junction	2.4 ± 0.3	2.4 ± 0.3	0.8 ± 0.4	0.9 ± 0.6	6.4 ± 1.1
p	0.349	0.168	0.616	**< 0.001**	0.051
Intact	2.5 ± 0.2	2.5 ± 0.3	0.6 ± 0.2	0.3 ± 0.3	5.9 ± 0.7
Torn	2.3 ± 0.4	2.4 ± 0.4	0.8 ± 0.3	0.6 ± 0.6	6.1 ± 1.2
p	0.328	0.546	0.163	**0.033**	0.476
Supraspinatus	2.5 ± 0.3	2.6 ± 0.1	0.7 ± 0.1	0.5 ± 0.6	6.3 ± 1.0
Infraspinatus	2.3 ± 0.3	2.3 ± 0.3	0.6 ± 0.2	0.4 ± 0.4	5.6 ± 0.7
p	**0.010**	**0.003**	0.239	0.806	**0.008**
Interaction Effects (*p* value)					
*Location*Tear*	0.971	0.544	0.992	0.122	0.607
*Location*Tendon*	0.949	0.825	0.695	0.971	0.834
*Tear*Tendon*	**0.010**	**0.010**	0.098	0.056	**0.001**
*Location*Tear*Tendon*	0.888	0.761	0.933	0.647	0.806

Table 5.2. Degeneration Parameter Values around Supraspinatus Tear (Mean ± SD)

	Fiber Organization	Nuclei Shape	Increased Cellularity	Lipoid Degeneration	Sum
Anterior	2.6 ± 0.4	2.7 ± 0.4	0.9 ± 0.4	0.2 ± 0.3	6.3 ± 1.0
Posterior	2.6 ± 0.2	2.1 ± 0.6	0.4 ± 0.3	0.3 ± 0.5	5.4 ± 1.3
Medial	2.8 ± 0.2	2.9 ± 0.1	1.1 ± 0.6	0.5 ± 0.4	7.3 ± 0.8
p	0.575	0.096	0.159	0.583	0.096

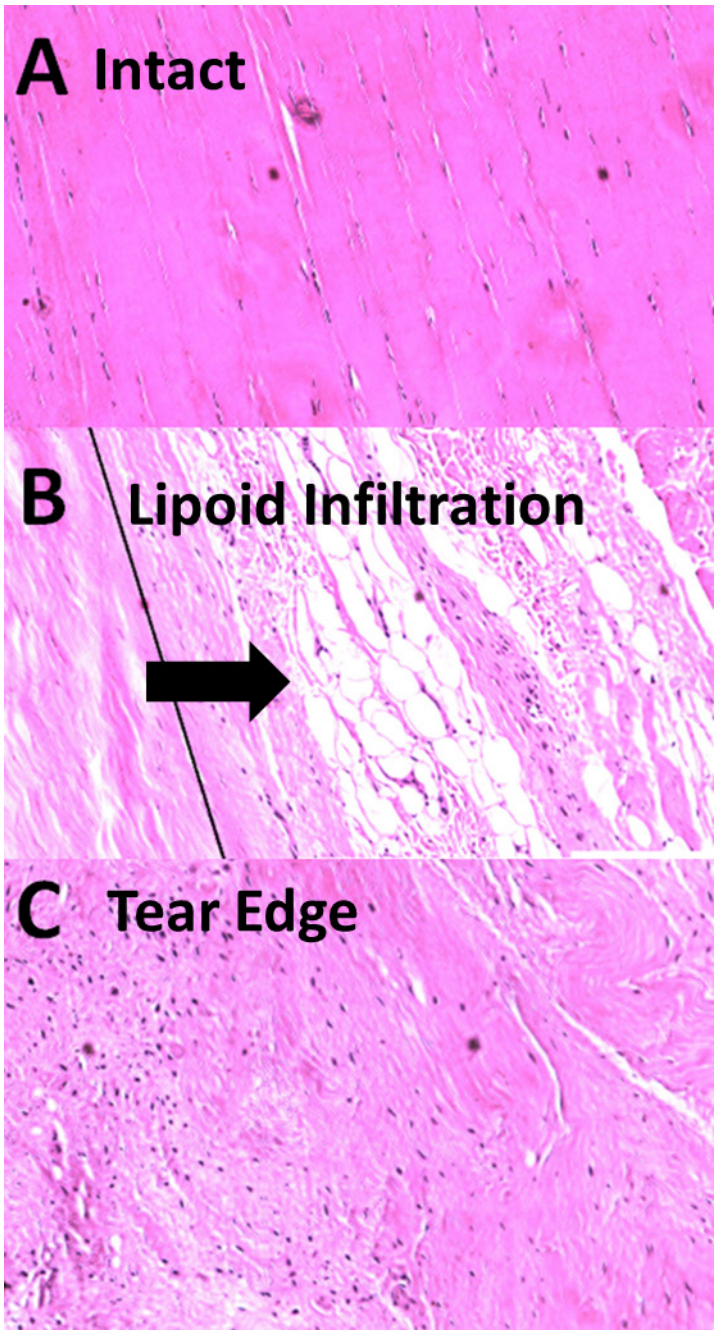

Figure 5.2. Histological images of rotator cuff tendons at 20X magnification. A) Intact infraspinatus tendon mid-substance with well-aligned collagen fibers and healthy cells. B) Intact supraspinatus tendon near the myotendinous junction showing fatty infiltration (black arrow). C) Medial edge of supraspinatus tendon tear showing hypercellularity and complete loss of fiber organization and tenocyte nuclear shape.

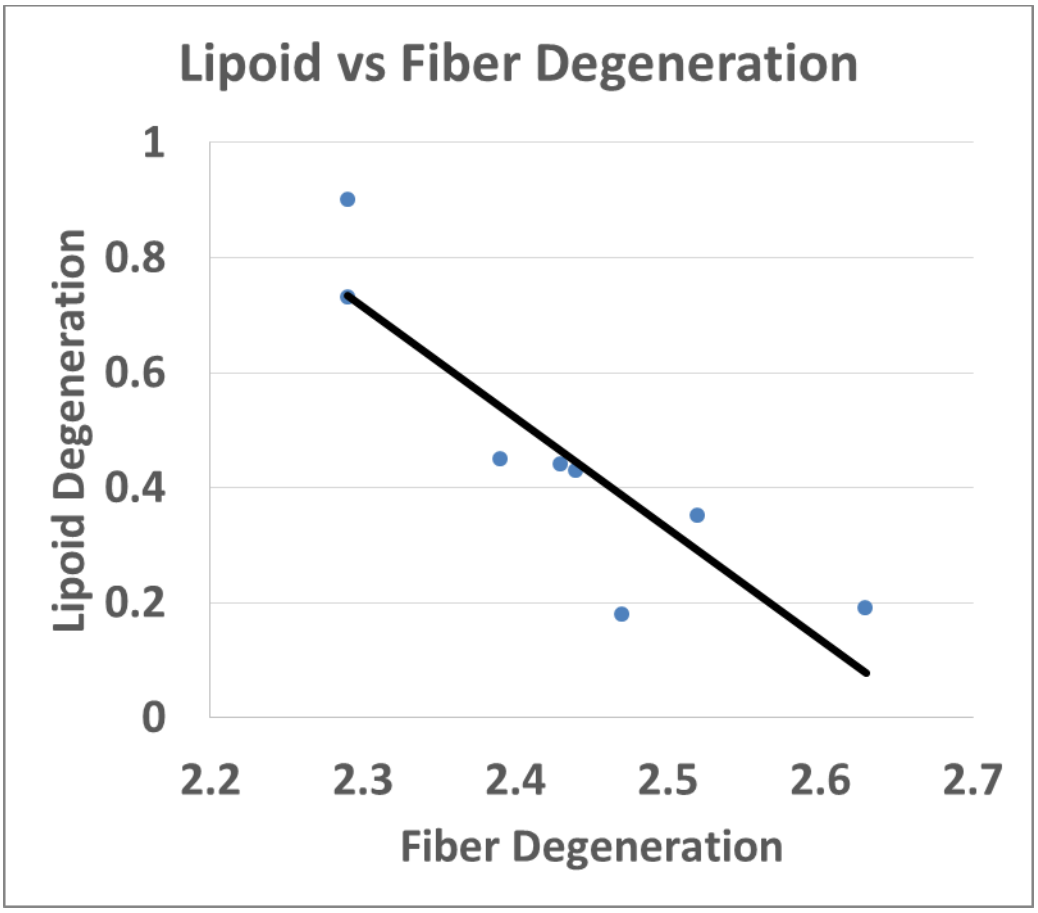

Figure 5.3. Correlation between the degeneration scores for lipoid degeneration and fiber organization. A very strong negative correlation was found ($\rho = -0.922$), indicating tendons with less fiber organization also had less lipoid degeneration.

5.1.4 Discussion

The results of this study indicate that age-related degeneration is a wide-spread phenomenon for not only tendons with small rotator cuff tears, but also for intact tendons from older individuals. Additionally, this study shows that tendon degeneration is not localized to the tendon insertion, where rotator cuff tears most commonly originate. Other factors such as biological processes or

local strain distributions may more likely influence the location of tear initiation and propagation. Although the insertion did not show greater degeneration, lipoid degeneration in the tendon was found to be much greater near the myotendinous junction. This finding may indicate that muscle fatty infiltration can also lead to tendon lipoid degeneration. Therefore, due to the increased degeneration in this region, there is potentially a greater risk of suture pull-out when this portion of the tendon is mobilized for rotator cuff repair.

Between intact and torn tendons, lipoid degeneration was the only parameter that showed a statistically significant difference. This result supports the notion that age-related tendon degeneration likely occurs prior to the development of a rotator cuff tear, and is similar to findings from previous histological studies (161, 256). Conversely, when the material properties of the tissue are reduced due to degeneration, tissue strains in the region become sufficient to initiate a tear that can propagate and result in further degeneration (141, 151). The greater amount of lipoid degeneration in tendons with tears may be related to the increases in muscle fatty infiltration observed in patients with rotator cuff tears (263, 264). Therefore, surgeons may consider checking for tendon fatty infiltration on MRI scans in addition to muscle when planning treatments. Additional histology of both the tendon and muscle sides of the myotendinous junction and muscle belly is necessary in order to determine relationships between muscle and tendon fatty infiltration for patients with and without degenerative rotator cuff tears.

When comparing degeneration between supraspinatus and infraspinatus tendons, supraspinatus tendons showed greater amounts of tendon degeneration, and especially less fiber organization. Since all infraspinatus tendons in this study were intact and half of the supraspinatus tendons had rotator cuff tears, it is reasonable to conclude that the supraspinatus tendons showed greater amounts of tendon degeneration due to the presence of rotator cuff tears.

This is further supported by the statistically significant interaction affect between tendons having a tear and from which tendon the biopsy sample was taken.

Considering only the samples with a rotator cuff tear, no statistically significant differences were found between the medial and anterior/posterior edges of the tear. Previous cadaveric and computational studies have shown that the medial edge of a rotator cuff tear becomes unloaded as the anterior and posterior edges of the tear experience increased strain (142, 216). Differences in the local stress environment for tenocytes in these regions have the potential to result in different tissue remodeling scenarios, depending on if the cells are under increased strain or are in the stress-shielded medial edge. Although it was hypothesized that the medial edge would show greater degeneration as a result of the cells in that region experiencing much lower stress, it does not appear that the medial edge becomes significantly more degenerated than the rest of the tissue surrounding the tear. However, due to the substantial degeneration observed throughout the tendon, there may still be a significant risk of suture pull-out at the tendon-suture interface due to poor tissue quality, even if the medial edge of the tear is trimmed prior to surgical repair.

Considering the average scores of degeneration for each shoulder specimen, there were generally no noticeable relationships between different categories of degeneration, or between specimen age and categories of degeneration. Although age has been shown to be related to increased tendon degeneration, the severity of degeneration does not seem to scale with age. This finding is consistent with a previous study that found no correlations between specimen age and amount of degeneration (165). Interestingly, the only significant correlation found was a negative correlation between amount of lipoid degeneration and fiber organization. Therefore, shoulder specimens with less fiber organization on average showed less amounts of lipoid degeneration. A

possible reason for this finding is that lipoid degeneration occurs late in the disease process whereas fiber organization deteriorates more quickly, but this must be confirmed in future work.

A limitation of this study was that only H&E staining was performed to assess degeneration based on changes in tendon morphology. Unlike previous studies that found significant differences in degeneration between bursal and articular layers of the supraspinatus tendon (161, 163, 165), this study was unable to find statistically different differences between layers of the tendon. While H&E staining was sufficient to find significant differences in key degenerative parameters, use of more rigorous biochemical procedures, including stains specific to collagen, fat, and proteoglycans in the extracellular matrix, in future work may assist in confirming additional local differences in degeneration through the tendon thickness. The use of different stains, combined with more quantitative measures of collagen fiber organization, cell density, cell shape, and area of lipoid infiltration, can confirm the more qualitative measures used for this study. Additionally, the results of this study only apply for tendons within the age range of specimens tested, and only for small, crescent-shaped supraspinatus tendon tears. Larger, multi-tendon tears or tears of a different shape may show different amounts of degeneration.

5.1.5 Conclusion

This study provides insight on age-related degeneration in intact and torn rotator cuff tendons. Such tendon degeneration is not always macroscopically visible to surgeons, which can potentially lead to overestimation of the quality of rotator cuff tissue during repair. Future directions for this study include performing quantitative ultrasound analysis and mechanical testing on specimens with known histological degeneration in order to correlate histological degeneration to mechanical properties for prediction of tissue quality. The long-term goal of this work is to better quantify the etiology of rotator cuff tear progression and provide a guide for orthopaedic surgeons by defining a "danger zone" of poor tissue around a rotator cuff tear. By understanding local differences in tendon degeneration, surgical and biological treatment protocols can be improved to account for regions of the tendon that are less degenerative for repair and healing.

5.2 DIFFERENCES IN TEAR PROPAGATION BETWEEN ARTIFICIALLY-CREATED AND PRE-EXISTING ROTATOR CUFF TEARS

5.2.1 Introduction

The high frequency of rotator cuff tears in an aging population (64-67) and the capacity of rotator cuff injury to inflict severe limitations on normal activity have led to a significant clinical and societal burden for treating this injury. Previous studies investigating biological factors related to rotator cuff tears have found intrinsic, age-related degeneration to be a significant contributor to the development of rotator cuff tears (247-249). Additionally, more advanced age has been shown to lead to worse surgical outcomes after rotator cuff repair and increased fatty muscle degeneration (113, 251-255). Furthermore, tendons with chronic rotator cuff tears exhibit less ability to heal (149, 156, 157) and increased degeneration in the regions of the tendon adjacent to the tear (163-166). Therefore, age-related degeneration is an important factor that must be considered when evaluating the etiology and treatment of rotator cuff tears.

In order to better understand the initiation and propagation of rotator cuff tears, various studies have performed experiments on cadaveric rotator cuff tendons using surgically-created acute tear models (45, 51, 135, 139, 148). However, a limitation of using surgically-created tears is that they are unable to model the complex patterns of tissue degeneration and remodeling that occur due to the presence of a rotator cuff tear. Since previous studies investigating propagation of rotator cuff tears in human cadaveric models almost exclusively model tears as “traumatic,” it is not currently understood how degenerative rotator cuff tears propagate versus traumatic tears.

Whereas acute tears resulting from a traumatic event are generally repaired as soon after the event as possible (265, 266), there is substantial debate over the proper treatment methods for degenerative rotator cuff tears (172). In order to improve treatment of degenerative rotator cuff tears, it is important to understand the contribution of tissue degeneration to tendon mechanics and how degenerative rotator cuff tears propagate versus acute tears. Therefore, the objective of this study was to characterize tear propagation in cadaveric shoulders with pre-existing, untreated supraspinatus tears during a tensile cyclic loading protocol. It was hypothesized that degenerative tears would propagate at lower loads compared to artificially-created tears.

5.2.2 Materials and Methods

Six fresh frozen cadaveric shoulder specimens (age 61 ± 10 years; range 49 to 75 years old, 3 male, 3 female) with pre-existing rotator cuff tears were obtained with University ethics approval (CORID ID #131) and stored at -20°C. Prior to dissection, shoulders were thawed at room temperature for 24 hours and ultrasonography was performed on each shoulder to determine if a rotator cuff tear was present. Shoulders were then dissected to remove all soft tissue except for the supraspinatus, infraspinatus, and subscapularis tendons, and the presence of the tear was confirmed. After dissection, the anterior-posterior tear width was measured at the widest anterior-posterior margins of the tear, and then the medial-lateral tendon retraction was measured as the furthest distance from the medial boarder of the tear to the tendon insertion on the humerus (Figure 5.4-B).

Tears were grouped based on the anterior-posterior tear size based on the DeOrio and Cofield classification of tear size (Small/Medium: < 3 cm, Large: 3 – 5 cm, Massive: > 5 cm) (240) (Figure 5.4). The distance of the anterior border of the tear to the posterior border of the

long head of the biceps tendon was also recorded. All measurements were made three times using a pair of digital calipers (Model 147, General Tools & Instruments, accuracy ±0.02 mm, repeatability 0.01 mm) and averaged to obtain a single measure of anterior-posterior size, medial-lateral retraction, and distance from the long head of the biceps tendon for each tear. All measurements were made with the tendon at positions corresponding to 0° of glenohumeral abduction and to 90° of glenohumeral abduction.

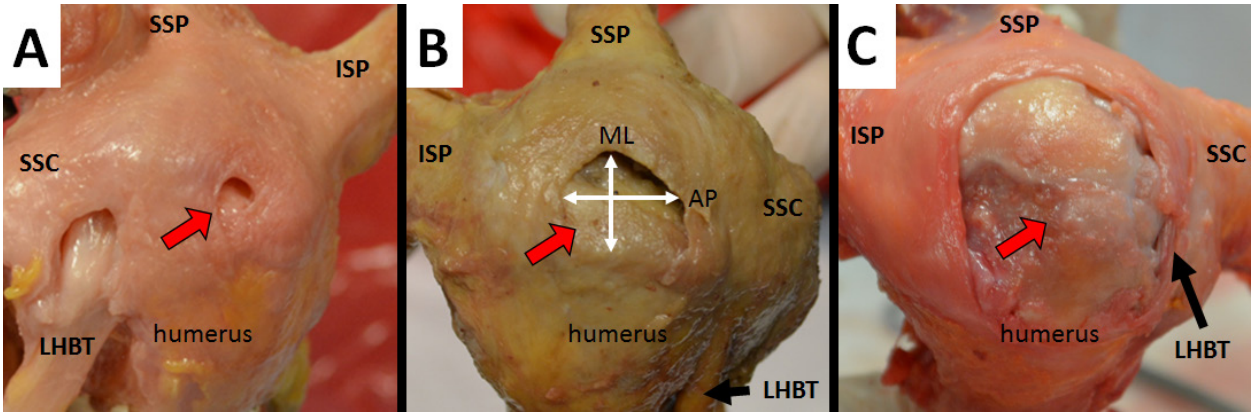

Figure 5.4. Example supraspinatus tendon tears. Tear sizes ranged from A) small to B) medium to C) large. Anterior-posterior and medial-lateral tear dimensions (white arrows) were measured for each tear. Here, the tear is denoted with a red arrow. In the specimens with a large or massive tear, the tear spanned multiple tendons. SSP: Supraspinatus tendon; ISP: Infraspinatus tendon; SSC: Subscapularis tendon; LHBT: Long head of the biceps tendon.

The diaphysis of each humerus was potted in epoxy putty and secured to the base of a materials testing machine (Model 5965, Instron) using a set of custom clamps. The supraspinatus tendon was secured to the crosshead for uniaxial tensile loading corresponding to 90° of glenohumeral abduction in the scapular plane. A static 22 N load was placed on the infraspinatus

tendon via a pulley system to mimic in vivo load interaction between the infraspinatus and supraspinatus tendons (Figure 5.5). A 10 N preload was first applied to the supraspinatus tendon, followed by preconditioning between 10 and 25 N at a rate of 20 mm/min for 100 cycles. After preconditioning, the maximum load was increased to 50 N for 100 cycles. This was followed by additional loading sets of 100 cycles each, increasing the maximum load by 50 N each time a set of cycles was completed (228). Cyclic loading was continued until a critical amount of tendon retraction was reached. The definition of "critical tendon retraction" changed depending on tear size: 100% increase in medial-lateral retraction for small/medium sized tears, 50% increase for large tears, and 25% increase for massive tears. The tendon retraction was measured at the end of each loading set to determine if the tear reached the critical tendon retraction. If the tendon failed during cyclic loading prior to reaching the critical tear size, testing was also terminated. If the tear reached the critical tendon retraction without the tendon failing, a load-to-failure test was performed on the tendon at 20 mm/min to measure the ultimate load of the construct.

Parameters recorded during cyclic loading included the peak cyclic load at which the tear reached the critical tendon retraction (or for which the tendon failed during cyclic loading), as well as the peak number of cycles before reaching the critical tendon retraction/failure. The ultimate load at failure and the failure mode for each specimen were also recorded. Stiffness of the torn tendon complex was calculated for each specimen at 300N, the highest peak cyclic load shared between all specimens. To calculate stiffness, the linear region of the second cycle from the load-elongation curve was fit with a best-fit line equation, and the R^2 measure of fit was recorded. Points used to fit the line were removed in an iterative process and the data was fit with a new line until the R^2 value was at least 0.999. Peak cyclic load at failure and stiffness at the

300N cyclic loading set were also recorded for ten previously tested tendons with surgically-created artificial supraspinatus tears (age 64 ± 11 years; range 51 to 83 years old) (228).

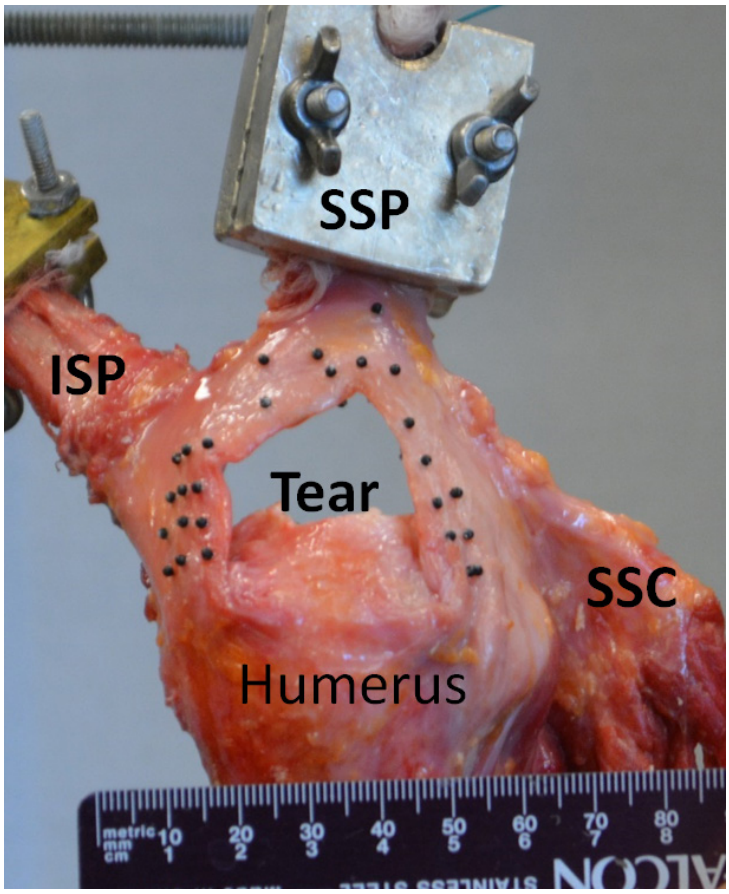

Figure 5.5. Experimental testing set up for cyclic loading of pre-existing rotator cuff tears. The supraspinatus tendon is clamped to the cross-head of the materials testing machine, and the infraspinatus tendon is clamped and weighted with a 22 N load via a pulley system (not pictured). SSP: Supraspinatus tendon; ISP: Infraspinatus tendon; SSC: Subscapularis tendon.

In order to investigate the effect of age and degeneration on the mechanical behavior of tendons with pre-existing tears, correlation analysis was performed between specimen age, AP tear size, ML tendon retraction, peak cyclic load, stiffness at 300 N, and peak number of cycles.

Pearson correlations were performed for all parameters except for comparisons made with peak cyclic load, due to the non-parametric data and large number of tied ranks. Therefore, Kendall's Tau-b was used for comparisons with peak cyclic load. To make comparisons between pre-existing and artificial tears, peak cyclic load was compared using an independent-samples Mann-Whitney U test, and stiffness at 300 N was compared using an independent-samples t-test. Significance was set at $p < 0.05$ for all statistical tests.

5.2.3 Results

Of the six shoulder specimens with pre-existing rotator cuff tears, four were medium/small, one was large, and one was massive (Table 5.3). The smallest tear was isolated to the supraspinatus tendon and measured only 0.5 cm in anterior-posterior width, and the largest tear was 6.7 cm in anterior-posterior width and included multiple tendons. The small and medium tears showed a typical crescent shape, whereas the large and massive tears exhibited a "U-shaped" configuration (19) (Figure 5.4 and Figure 5.5). For the large and medium tears, a significant portion of the surface area of the humeral head was visible, which often showed signs of severe osteoarthritis (Figure 5.4-C). Tendon retraction prior to mechanical testing ranged from 0.4 cm for the smallest tear up to 6.0 cm for the largest tear. Distances from the long head of the biceps tendon ranged from 12 mm for the smallest tear, to 1.5 mm for the large tear, while the massive tear extended past the long head of the biceps tendon. Measurements of anterior-posterior tear size and medial-lateral tendon retraction were generally larger at 90° compared to 0° of glenohumeral abduction.

Table 5.3. Summary of Pre-Existing Tear Specimen Testing Data

Specimen (Tear Size)	Age	AP Size (0 deg) (cm)	ML Size (0 deg) (cm)	AP Size (90 deg) (cm)	ML Size (90 deg) (cm)	Peak Cyclic Load (N)	Stiffness @ 300N (N/mm)	Peak # of Cycles	Ult. Load (N)
1 (medium)	49	1.9	1.5	1.0	0.6	500	128.9	1025	500
2 (large)	60	3.1	3.1	4.3	3.4	450	81.1	1000	965.8
3 (massive)	75	4.6	4.4	6.7	6.0	300	53.0	700	612.6
4 (medium)	68	1.1	1.1	2.1	1.9	450	78.7	934	450
5 (medium)	68	1.5	1.8	2.7	2.1	300	57.3	618	300
6 (small)	57	0.4	0.5	0.5	0.4	450	74.1	815	450

Of the six specimens, only the tendons with a large or massive tear reached critical amounts of tendon retraction without the tendon failing mid-substance. Among all tendons with pre-existing tears, the peak cyclic load was 408 ± 86 N, the stiffness at 300 N was 79 ± 27 N/mm, and the ultimate load at failure was 546 ± 229 N. Of the Pearson correlations performed, the only statistically significant correlations were between anterior-posterior tear size and medial-lateral tendon retraction ($r = 0.93$, $p = 0.007$), and between age and stiffness at 300N ($r = -0.86$, $p = 0.026$). For comparisons with peak cyclic load, statistically significant correlations were found with age ($\tau = -0.81$, $p = 0.037$), stiffness at 300 N ($\tau = 0.86$, $p = 0.024$), and with peak number of cycles ($\tau = 0.86$, $p = 0.024$). No other correlations were statistically significant. For the tendons with surgically-created tears, the peak cyclic load was 580 ± 181 N and the stiffness at 300 N was 129 ± 38 N/mm. A statistically significant difference was found between artificial and pre-existing tear specimens for stiffness at 300 N ($p = 0.013$), but there was no difference between peak cyclic load ($p > 0.05$).

5.2.4 Discussion

This study examined differences in tear propagation between artificial and pre-existing supraspinatus tendons tears through use of a uniaxial cyclic loading protocol. The results of this study show that the peak cyclic load required to reach critical amounts of tendon retraction in tendons with pre-existing rotator cuff tears was over 400 N, much greater than the typical loads expected for activities of daily living and exercise therapy (41, 214, 215). The strong negative correlations found between age and peak cyclic load/stiffness at 300N suggest that there is a relationship between increased age and decreased mechanical properties of tendon tissue, consistent with the effects of age-related degeneration. Additionally, the load required to cause critical amounts of tendon retraction did not differ significantly from tendons with surgically-created tears, contrary to the study hypothesis.

Interestingly, there were no clear relationships between tear size and tissue structural properties. This does not support the hypothesis that tendons with larger tears have greater amounts of degeneration, and therefore have worse mechanical properties. The main statistically significant correlations observed were between tendon age and peak load/stiffness, and between anterior-posterior and medial-lateral tear size. Additionally, strong positive correlations for peak cyclic load with stiffness and number of cycles were found, indicating that the tendons that failed at higher loads also tended to be stiffer and more resilient.

Though it was expected that tendons with larger tears would show inferior structural properties, this was not supported by the data from this study. However, the stiffness of the pre-existing tear specimens at 300 N was significantly less than the stiffness of the artificial tear specimens by a factor of approximately 1.6. This difference in stiffness may be partly due to a smaller amount of tissue being connected to the tendon insertion in specimens with larger tears,

and therefore there is less tissue taking up load in those specimens. Nevertheless, since there was no correlation between tear size and stiffness, the lower stiffness in specimens with pre-existing tears may also be due to greater tissue degeneration associated with the presence of a tear.

The most surprising result of this study was the mechanical resilience of tendons with pre-existing rotator cuff tears, despite the tear spanning two to three tendons for the larger tears. It was expected that due to increased degeneration in the tissue associated with the presence of a degenerative tendon tear, these tears would propagate at significantly lower loads compared to artificial tears. However, not only was there no statistical difference in peak cyclic load between pre-existing and artificial tears, the average peak cyclic load to reach critical tendon retraction in tendons with pre-existing tears was over 400 N. Additionally, the ultimate load required to cause total tissue failure was greater than 500 N for the tendons with pre-existing tears. This may indicate that degeneration associated with degenerative rotator cuff tears does not have a significant global effect on tissue properties. Furthermore, it is possible that significant tissue remodeling occurs at the anterior-posterior tear edges due to increased local strain (135, 142, 216), which may result in the tendon being able to better resist tear propagation by "blunting" the edges of the tear (i.e. less sharp angle between tear surfaces at the tear tips) to minimize stress concentrations, such as in certain hyper-elastic solids (267).

A limitation of this study is the number of samples with pre-existing rotator cuff tears that were tested. However, despite this, the peak cyclic load that resulted in critical amounts of tendon retraction was found to be much greater than loads expected during activities of daily living, and provided information on the ability of tendons with degenerative rotator cuff tears to resist tear propagation. Additionally, the chronicity of the torn tendons used for this study was unknown, since information was not available on the medical history of the cadavers used. It is

likely that, since the tears were never treated, they were asymptomatic, degenerative tears, rather than tears resulting from trauma. Similarly, the degeneration in the tendons could not be quantified to investigate specific relationships between tendon degeneration and tissue properties. Future directions for this study include performing correlations between the mechanical properties of degenerative rotator cuff tissue and measures of tendon degeneration using histology and quantitative ultrasound imaging. Ultimately, this work will provide information to surgeons to improve treatment of rotator cuff tears by better characterizing tissue quality in tendons with rotator cuff tears.

5.2.5 Conclusion

Despite the generally poor quality of tissue with degenerative rotator cuff tears, these tendons remain relatively resilient to tear propagation. Additionally, even though the tendon retraction increased for all tests, tears did not show any significant tear propagation in the anterior-posterior direction. Since cyclic uniaxial loading was insufficient to cause tear propagation in tendons with pre-existing rotator cuff tears, other extrinsic factors may be more important than tendon degeneration when considering tear propagation. These extrinsic mechanical factors could include abnormal firing of shoulder muscles that may result in different load and strain distributions, or sub-acromial impingement causing external wear on the tendon. By understanding the behavior of tendons with degenerative rotator cuff tears and the risk of tear propagation, treatments can be improved. The results of this study show that it may not be essential to immedately treat degenerative rotator cuff tears if these tear types are able to resist tear propagation at high magnitudes of load.

5.3 EFFECTS OF TENDON DEGENERATION ON PREDICTIONS OF SUPRASPINATUS TEAR PROPAGATION

5.3.1 Introduction

Over 30% of the general population suffers from degenerative rotator cuff tears, which have an incidence rate of over 50% in patients over the age of 70 (63, 66, 67). Although rotator cuff tears are a major clinical issue, it is not yet understood which tear characteristics lead to success or failure of operative and non-operative treatments for degenerative rotator cuff tears (138, 174). With respect to surgical management of degenerative rotator cuff tears, poor tendon quality due to severe tendon degeneration has been cited as a potentially significant factor related to poor patient outcomes (81, 137, 138). Additionally, various histological studies have found that chronic rotator cuff tears are associated with much greater amounts of tissue degeneration compared to intact tendons (163-166). The link between tissue quality (i.e. mechanical properties) and tissue degeneration has been shown previously in a study that found a strong correlation between decreases in mechanical properties and increased amounts of tissue degeneration at the supraspinatus tendon insertion (256). Therefore, there appears to be an important relationship between amount of tendon degeneration and the mechanical behavior of tendon tissue for degenerative tears of the rotator cuff tendons.

In addition to tissue degeneration, another factor that may affect the outcome of rotator cuff tear treatments is propagation of the tear over time. Various studies have shown that rotator cuff tears propagate in vivo following treatment by physical therapy (130-132), with up to 50%

of patients showing a clinically significant increase in tear size. Unfortunately, it is unclear which tear characteristics most affect propagation of a rotator cuff tear. Geometric factors such as tear shape (152, 153), size (135, 139), and location (150, 154, 155) have been shown to relate to propagation of rotator cuff tears, but the effect of tendon degeneration on tear propagation is unknown. Due to the difficulty of assessing tissue degeneration and procuring cadaveric shoulder specimens with existing degenerative rotator cuff tears for mechanical testing, the effects of rotator cuff tendon degeneration on tear propagation have been overlooked in the current body of literature.

In order to address issues related to complex experimental testing, computer models can be developed to assess the effects of different conditions on the behavior of biological tissues. Numerous studies have developed finite element models of the rotator cuff to assess the risk of tear initiation and propagation for various geometries of rotator cuff tears (152, 170, 216, 219, 239). Though these models provide valuable predictive tools to evaluate the mechanical behavior of torn rotator cuff tendons, these models can be limited by their simplifying assumptions made for the tendon material behavior and model geometry. Additionally, these models are unable to predict changes in tear size over time, and have not assessed how local stress and strain at the tips of rotator cuff tears change due to decreases in material properties (i.e. due to tissue degeneration).

Therefore, the objective of this study was to investigate the effects of tissue degeneration on propagation of rotator cuff tears by using an experimentally validated, subject-specific finite element model of supraspinatus tendon. This three-dimensional model incorporates subject-specific geometry and anisotropic material properties that allow for high-fidelity predictions of tear propagation using cohesive elements (241, 244). It was hypothesized that tears in tendons

with higher amounts of degeneration (represented as decreased modulus and failure properties) would propagate at lower loads.

5.3.2 Materials and Methods

The meshes used for this study were developed using the same process as in Section 4.4. Using the validated model geometry, 1 cm wide tears were introduced in either the anterior, middle, or posterior third of the supraspinatus tendon. All tears were located approximately 5 mm medial to the insertion of the tendon to the humerus on the articular side (Figure 4.25). The meshes consisted of approximately 35,000 nodes and 150,000 solid tetrahedral elements. The surfaces along which the tear was able to propagate consisted of approximately 2,500 2D cohesive elements that were roughly 0.5 mm in size (Table 5.4).

Table 5.4. Nodes and Elements for Each Degenerative Tear Model

Location	Nodes	Elements	Cohesive
Anterior	38165	177656	2618
Middle	31982	148306	2587
Posterior	33536	155985	2671

The subject-specific material properties obtained from mechanical testing of the intact tendon were varied for each tear location in order to investigate the effect of tissue degeneration (e.g. associated with a degenerative rotator cuff tear) on tear propagation. Material properties were varied based on the work of Sano et al, which showed a strong negative correlation between tissue degeneration (as determined by scoring degeneration on histological images) and material properties (in terms of ultimate stress calculated at the tendon insertion) for strips from

the middle third of intact supraspinatus tendons (256). A tendon with minimal degeneration (score of 2 or less) was assigned an ultimate stress of approximately 6 MPa. This value of ultimate stress for the middle third of the supraspinatus tendon was consistent with the failure properties measured for the shoulder specimen used to develop the present model (ultimate stress of 5.8 MPa), and also with another study investigating the material properties of the anterior, middle, and posterior thirds of the supraspinatus tendon that found the ultimate stress in the middle third of the tendon to be 6.0 ± 2.6 MPa (171). Based on the relationships between ultimate stress and degeneration scores determined by Sano et al, "moderate degeneration" (degeneration score of approximately 5) was estimated with an ultimate stress of 4 MPa, and "severe degeneration" (degeneration score of approximately 10) was estimated with an ultimate stress of 2 MPa.

In order to assign modified failure properties to the anterior and posterior tendon thirds, the ratios of failure stress with respect to the middle third were calculated (i.e. anterior ultimate stress with respect to middle ultimate stress and posterior ultimate stress with respect to middle posterior stress). This ratio was used as a scaling factor to estimate ultimate stress for the anterior and posterior tendon thirds for each level of degeneration to be modeled (Table 5.5). It was also assumed that the elastic modulus of the collagen fibers would scale with degeneration in the same manner as the ultimate stress. Therefore, the modulus for the middle third was divided by 1.5 (6 MPa divided 4 MPa) to estimate the modulus for moderate degeneration, and was divided by 3 (6 MPa divided by 2 MPa) to estimate the modulus for severe degeneration. Next, the ratios of the modulus for the middle third to the moduli of the anterior and posterior thirds were used to scale modulus based on amount of degeneration in a similar manner as for ultimate stress.

Table 5.5. Estimated Material Properties for Degenerative Tendon Tissue

	Ultimate Stress (MPa)			Collagen Fiber Modulus (MPa)		
	Minimal	**Moderate**	**Severe**	**Minimal**	**Moderate**	**Severe**
Anterior	5.8	4.0	2.0	9.9	6.6	3.3
Middle	5.8	4.0	2.0	14.4	9.6	4.8
Posterior	4.3	2.9	1.5	7.9	5.3	2.6

To model tear propagation, cohesive elements were created for all elements along the plane of the tear, as previously described (Section 4.4.2). The fracture toughness, like ultimate stress and elastic modulus, was also assumed to scale with degeneration. Material properties were assigned to the cohesive elements using the same method as for the Neo-Hookean model parameters. Specifically, the ultimate stress and estimated fracture toughness (defined by ultimate stress and maximum separation) were varied along the anterior-posterior width of the tendon, with the anterior third having the highest ultimate stress and fracture toughness and the posterior third having the lowest ultimate stress and fracture toughness. The medial edge of the supraspinatus tendon was loaded with a displacement condition to a total 5 mm (~15% bone-to-clamp strain) at a 70° angle (representing 70° of glenohumeral abduction) over 100 load steps. Stress and strain values were averaged for elements within a 2mm-diameter sphere at the anterior and posterior tear tips for the time step in which the maximum load was reached, indicating the point of critical failure. Model outputs included critical load and displacement required to propagate the tear, and principal stress magnitude and maximum principal strain at the critical load for the anterior and posterior tear tips. Correlations were performed to investigate the relationship between these parameters and tendon degeneration (ultimate stress and modulus). Statistical significance was set at $p < 0.05$.

5.3.3 Results

The simulations of tear propagation showed that propagation initiated at approximately 3.1 mm, 2.9 mm, and 2.5 mm of displacement to the clamped end of the tendon for minimal, moderate, and severe degeneration cases (Table 5.6, Figure 5.7). This ranged from 4-7% strain measured from bone to clamp for the tendon. For all locations, tendons with the highest amount of degeneration required the lowest magnitude of load to initiate tear propagation (Figure 5.6). Critical load was largest in the posterior third of the tendon, with loads ranging from 207 N for the most degenerative tendon to 488 N for the least degenerative. Both anterior and middle tears showed similar loads required to propagate the tendon, ranging from approximately 120 N for the most degenerative to 280 N for the least degenerative. The drop in critical load magnitude between degeneration states was consistent between the three tear locations. From minimal to moderate degeneration, the load for moderate was approximately 60% of the load for minimal. From moderate to severe degeneration, the load for severe was approximately 75% of the load for moderate.

On average, stresses at the tear edges at the critical load decreased with greater amounts of degeneration (Table 5.6). At the anterior tear tip, stresses ranged from 3.0 to 7.7 MPa for minimal degeneration, 2.2 to 5.4 MPa for moderate degeneration, and 1.1 to 2.9 MPa for severe degeneration. For the posterior tear tip, stresses ranged from 1.3 to 8.5 MPa for minimal degeneration, 1.0 to 6.1 MPa for moderate, and 0.6 to 3.1 MPa for severe. Strains at the tear tips showed a similar decrease in magnitude with greater amounts of degeneration. At the anterior tear tip, strains ranged from 14.7 to 32.6 % strain for minimal degeneration, 11.9 to 24.8 % strain for moderate degeneration, and 7.1 to 16.2 % strain for severe degeneration. For the posterior

tear tip, strains ranged from 8.9 to 24.1 % strain for minimal degeneration, 7.3 to 19.3 % strain for moderate, and 4.5 to 12.9 % strain for severe.

When comparing simulations of degeneration at the same time point, the anterior-posterior width of the tear was largest for tendons with severe degeneration (Figure 5.7). Using the time point at which the tendon with minimal degeneration reached its critical load, the tear was only slightly larger for moderate degeneration than for the case of minimal degeneration. However, for the same amount of displacement to the medial tendon edge, the tear for the severe degeneration case nearly reached the anterior edge of the supraspinatus tendon. Despite reaching different tear sizes for the same amount of displacement, the pattern of tear propagation was similar for all cases, with tears propagating first on the anterior side of the tendon before propagating on the bursal side. When comparing the tear shape to typical degenerative tears, the simulated tears in tendons with greater degeneration did not show large amounts of medial tendon retraction, and therefore did not look like the classic “crescent” or “U-shaped” tears observed clinically.

Of the correlations performed, the critical load was only correlated with stress at the anterior tear tip on the articular side ($r = 0.845$, $p = 0.004$). The critical load was not correlated with either ultimate stress or modulus. Ultimate stress showed strong positive correlations for stress and strain at the tear tips for all conditions except for the anterior tip on the articular side of the tendon (Table 5.7). Similarly, collagen fiber modulus was correlated with stress and strain for all conditions except for stress at the posterior tear tip on both sides of the tendon.

Table 5.6. Critical Failure Values at Tear Propagation by Amount of Degeneration

Location	Degeneration	Crit Load	Crit Disp	Stress at Critical Load (MPa)				Strain at Critical Load (% Strain)			
				Bursal		Articular		Bursal		Articular	
		(N)	(mm)	Ant Tip	Post Tip	Ant Tip	Post Tip	Ant Tip	Post Tip	Ant Tip	Post Tip
Anterior	Minimal	284	2.9	4.5	4.6	4.0	8.5	23.0	19.6	22.7	24.1
	Moderate	211	2.6	3.5	3.7	3.3	6.1	19.1	14.8	18.3	19.3
	Severe	122	2.1	2.6	2.1	2.3	3.1	15.0	10.1	14.8	12.1
Middle	Minimal	280	3.1	5.7	3.4	6.7	5.2	24.9	18.4	32.6	22.1
	Moderate	215	3.0	4.7	3.0	5.3	4.2	23.2	17.1	24.8	18.7
	Severe	132	2.5	2.9	1.8	2.9	2.4	16.2	11.5	15.6	12.9
Posterior	Minimal	488	3.4	3.0	1.3	7.7	2.2	14.7	8.9	18.9	12.1
	Moderate	357	3.1	2.2	1.0	5.4	1.7	11.9	7.3	17.2	10.2
	Severe	207	2.7	1.1	0.6	2.6	1.0	7.1	4.5	10.4	7.0

Table 5.7. Correlation for Ultimate Stress and Modulus versus Load, Stress, and Strain

		Load	Anterior Bursal Stress	Posterior Bursal Stress	Anterior Articular Stress	Posterior Articular Stress	Anterior Bursal Strain	Posterior Bursal Strain	Anterior Articular Strain	Posterior Articular Strain
Ultimate Stress	*r*	.469	**.857**	**.761**	.623	**.778**	**.815**	**.810**	**.861**	**.870**
	p	.203	**.003**	**.017**	.073	**.014**	**.007**	**.008**	**.003**	**.002**
Modulus	*r*	.349	**.936**	.655	**.680**	.612	**.858**	**.808**	**.980**	**.817**
	p	.357	**.000**	.055	**.044**	.080	**.003**	**.008**	**.000**	**.007**
Bolded values are statistically significant										

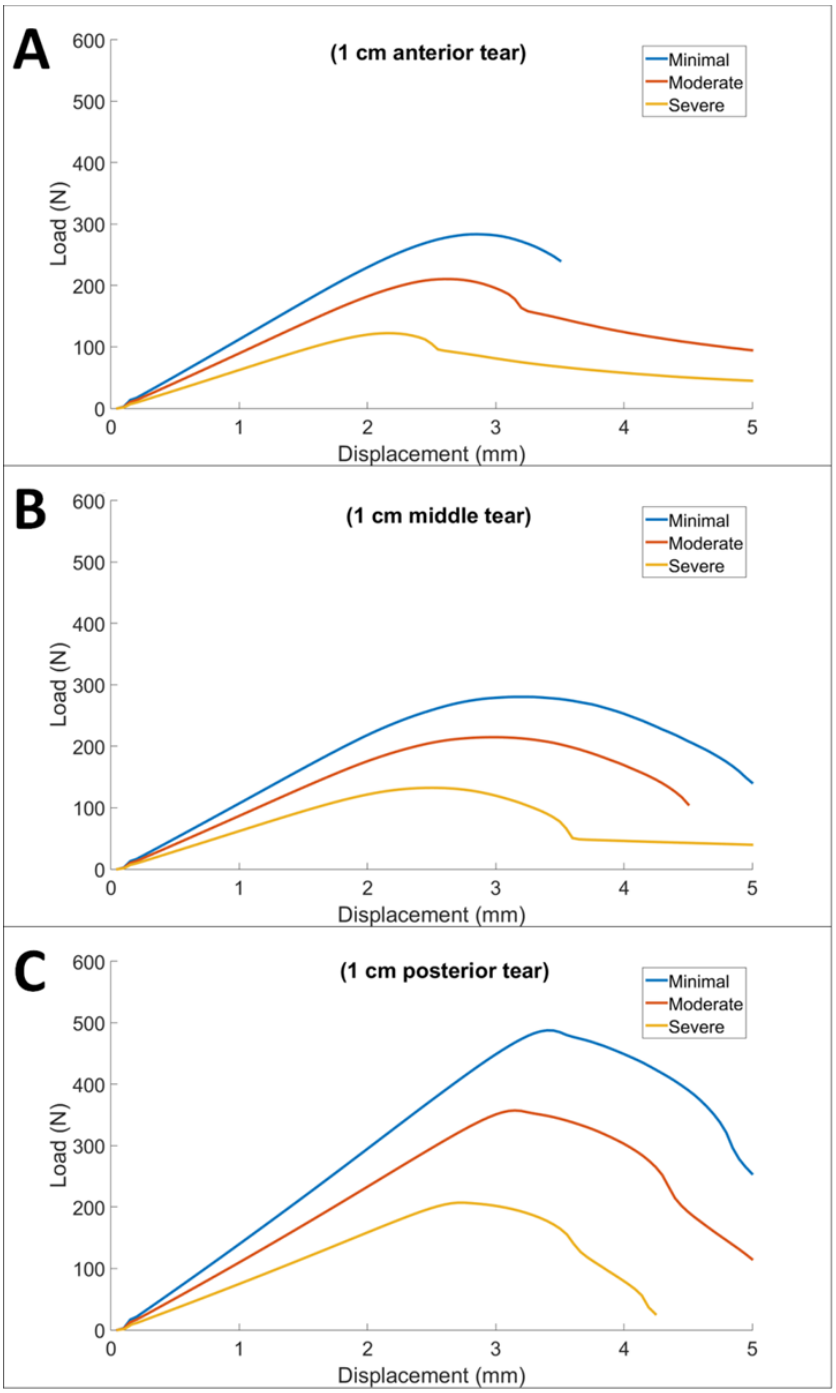

Figure 5.6. Load-displacement curves for tear propagation simulations of degenerative tears. A) Anterior tears 1 cm wide. B) Middle tears 1 cm wide. C) Posterior tears 1 cm wide. Load required to propagate the tear decreased with increased amounts of tendon degeneration.

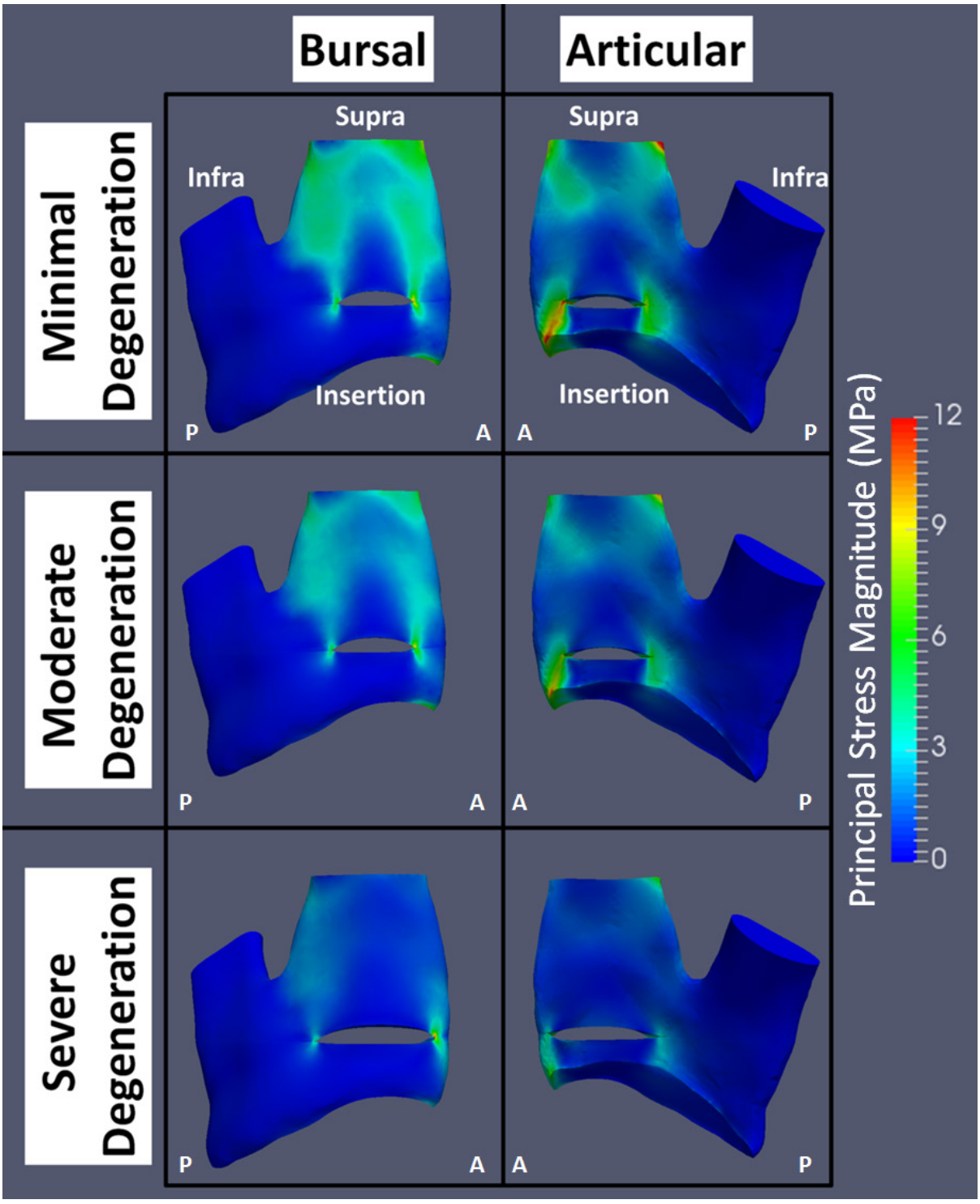

Figure 5.7. Images of the tear propagation simulations for varying degrees of tendon degeneration at the same time point. The time point chosen was for when the model with minimal degeneration reached its critical load. The pattern of tear propagation did not differ significantly between cases, showing early propagation on the articular side before propagating through the bursal side.

5.3.4 Discussion

This study investigated the effects of tendon degeneration on the risk of supraspinatus tendon tear propagation. Finite element models of rotator cuff tendon with 1 cm wide tears were developed using subject-specific geometry and material properties for a single specimen, and material properties were varied to simulate the effects of tissue degeneration. The primary finding for the tendon geometry and material properties tested was that tendons at more severe stages of degeneration are at higher risk for propagation, confirming the hypothesis under study. This finding confirms the importance of diagnosing and treating rotator cuff tears early, before the tendon can degenerate further and tears can propagate. For tendons with moderate and severe amounts of degeneration, the load required to propagate the tear ranged from 100 N to 200 N. This range of loads is within the normal range of supraspinatus activity (41, 214, 215) experienced during activities of daily living, indicating that propagation of tears is much more likely in patients with severe tendon degeneration.

The percent change in critical load for minimal degeneration with respect to moderate degeneration, and the percent change between load for moderate and severe degeneration, was consistent across the three tear locations tested. The change in material properties from minimal to moderate degeneration was ~30%, resulting in a 25% decrease in the critical load for all tear locations. The change in properties from moderate to severe was ~50%, resulting in a 40% decrease in critical load. Although the differences between ultimate stress for “minimal” and “moderate” cases and between “moderate” and “severe” were only ~2 MPa each, the larger change in properties from “moderate” and “severe” resulted in substantially more propagation. This is supported by the observation that while the tears in tendons with minimal and moderate degeneration were approximately the same size for the same amount of displacement, the tear in

the tendon with severe degeneration was much larger at that same time point. This observation provides further support for earlier diagnosis and treatment of degenerative rotator cuff tears, before the magnitude of change in material properties associated with degeneration reaches a "critical" point that will result in considerable tear propagation.

Large decreases in stress and strain at the tear tips were found between levels of degeneration, with the lowest values observed for the case of severe degeneration. Furthermore, significant positive correlations were found between ultimate load and modulus (representative of amount of tendon degeneration) and stress and strain at the tips of the tear. Therefore, greater amounts of degeneration (lower ultimate stress and modulus) result in lower stresses and strains at the anterior and posterior tear tips. However, these lower magnitudes of stress and strain are still sufficient to propagate the tear.

Although the model successfully predicted tear propagation at lower loading magnitudes for increased amounts of degeneration, it was unable to mimic the classic tear shapes observed for degenerative rotator cuff tears. Due to retraction of the medial edge of the tear over time, the most common tear geometries observed clinically are "crescent" or "U-shaped" tears (19, 153). However, the simulations predicted only small amounts of tendon retraction for all cases. Insufficient retraction to mimic "crescent" or "U-shaped" tears may be due to only allowing the tear to propagate along a single plane, or because remodeling at the edges of the tear over time was not modeled. Active remodeling at the edges of the rotator cuff tear in tendons due to changes in stress may contribute to "blunting" of the tear tips (i.e. less sharp angle between tear surfaces at the tear tips), changing the shape of the tear. The inability of the model to account for tendon remodeling and the tear blunting observed for degenerative tears clinically (19, 153) and experimentally (135, 228) may account for the differences observed in load required to propagate

the tear compared to experiments (Section 5.2). By allowing the tear to propagate in multiple directions and not along a single plane, it is possible that the model may exhibit greater amounts of tendon retraction and tear blunting or propagate at different loading magnitudes.

Other limitations for this study include that the results of the finite element simulations are specific to the subject-specific geometry, material properties, and loading conditions used. Loading the tendon at different glenohumeral joint positions or investigating tears of different size, shape, and location likely result in changes to the magnitudes of load and associated stress and strain during tear propagation. However, since the changes in load, stress, and strain were consistent with decreases in material properties regardless of tear location, this study provides a useful estimate of the behavior of degenerative rotator cuff tears. Additionally, the study used to estimate tendon material properties for different amounts of degeneration measured ultimate stress at the insertion site, and only from the middle third of the supraspinatus tendon. These material properties were extrapolated to the rest of the tendon and used to represent the behavior of the tendon mid-substance. Changes to the collagen fiber structure due to degeneration (i.e. loss of organization) were also not considered in this model. Additional subject-specific models are necessary to provide a library of different tendon geometries and material properties to make more generalizable predictions of rotator cuff tear propagation. Future simulations of tear propagation due to tendon degeneration should take into account changes in mechanical properties and fiber orientation throughout the whole tendon due to degeneration.

5.3.5 Conclusion

This study identifies the effects of tendon degeneration on the likelihood of rotator cuff tear propagation, and supports the early detection and treatment of rotator cuff tears. Additional studies are required to better identify rotator cuff tendon degeneration associated with degenerative tears and associate histological changes in the tendon due to degeneration with tendon material properties. It is also important to incorporate morphological changes to the tear due to tendon degenerative changes that can affect propagation of a tear. By better understanding the relationship between rotator cuff tears, tendon degeneration, and tear propagation, more useful information can be provided to clinicians to improve treatments of degenerative rotator cuff tears.

6.0 DISCUSSION

6.1 IMPLICATIONS OF FINDINGS

The three specific aims undertaken by this study provide valuable information about the effects of exercise therapy for the treatment of rotator cuff tears on glenohumeral joint kinematics. Additionally, the results elucidate the effects of tear geometry and tendon degeneration on tear propagation through the use of novel cadaveric testing and computational modeling.

The primary finding of the in vivo study was that current standards of exercise therapy for treating rotator cuff tears improve glenohumeral joint stability when considering coronal plane abduction. However, it was also determined that sub-acromial space did not increase for these patients after completion of therapy. Since exercise therapy is often used in the treatment of sub-acromial impingement of the rotator cuff (86, 89), this research has clinical implications with respect to improving exercise therapy protocols to better "target" different muscle groups that will lead to the desired kinematic outcomes. However, although the only statistically significant change in joint kinematics was observed for the joint contact path, all patients successfully completed exercise therapy with improved outcomes, especially in terms of range of motion, shoulder strength, pain, and other patient-reported outcomes. Therefore, current exercise therapy protocols for the treatment of rotator cuff tears appear to improve patient outcomes without having a substantial effect on glenohumeral joint kinematics. It remains to be seen if

kinematics or tear propagation changes for different types of exercises or joint motions, or if failure to improve joint kinematics leads to a loss of joint function and increased pain at time points long after therapy is completed.

The experiments used to address specific aims 2 and 3 use novel testing protocols to assess the risk of tear propagation in human cadavers. The combination of cyclic loading and increased loading magnitude provides information on both the long-term behavior of a propagating rotator cuff tear and the amount of load required to cause catastrophic propagation of a rotator cuff tear. This protocol can be further used in biomechanical testing of rotator cuff and other tendons prone to tearing in order to characterize tear propagation for a variety of tear configurations, including partial versus full-thickness tears, different tear shapes, and multi-tendon rotator cuff tears. Furthermore, this study used an optical tracking system to measure three-dimensional strains on both the articular and bursal sides of the tendon simultaneously. Though most studies tracking strain optically only measure strains on one side of the tendon at a time, this work supports previous studies that have shown a considerable strain gradient that differs through the full thickness of the rotator cuff tendons (141, 151). Therefore, in order to more accurately assess the mechanical behavior of rotator cuff tendon, it is important to measure strains simultaneously on both sides. This technique can be translated to additional tissues to investigate non-uniform strains across the tissue surface.

In addition to the experimental testing performed, this work developed and experimentally validated finite element models of rotator cuff tendon to characterize tear propagation for different tear sizes, locations, and tendon degeneration. An important conclusion derived from model development and validation was the vital need to explicitly report the reference configuration used for experiments and models. In order to make direct comparisons

between research studies and improve communication between researchers, it is important to be able to put tissue strains calculated and predicted in the context of the tissue's starting position. As demonstrated by this work, different joint positions and preloaded states can drastically alter the calculated strains, leading to problems with model validation. Apart from definitions of reference configuration, the developed models were able to predict propagation of rotator cuff tears, rather than only calculate stress and strain at the tips of an existing tear. The cohesive elements used to model propagation have previously been used to model aortic tissue (241), and the present work demonstrates their use as a powerful tool for modeling and predicting damage in commonly injured musculoskeletal tissues. However, it is important to note that the results gleaned from these models were specific to the tendon geometry and material properties used. Care must be taken to avoid making generalizations about the behavior of rotator cuff tears from one representative model.

The combined results of the cadaveric testing and computational modeling begin to clarify the effects of tear size, location, and tendon degeneration on the risk of tear propagation. With respect to tear size and location, experimental data showed a higher risk of propagation for anteriorly located supraspinatus tears as compared to tears in the middle third of the supraspinatus tendon, and also showed larger amounts of strain on the articular side of the tendon. Computational modeling demonstrated the same results, where anteriorly located tears required the least amount of load to propagate, and also showed that larger tears are at higher risk for propagation. These findings indicate that tears that adversely affect the ability of the tendon to redistribute load, i.e. disrupt the rotator cable structure or are associated with severe tissue degeneration, are most at risk for tear propagation. Therefore, since patients with these types of tears are unlikely to be successful with non-operative management, clinicians should consider

more aggressive treatment (such as surgical repair) for anteriorly located rotator cuff tears that interrupt the rotator cable, especially those that have already progressed to a larger size. However, since tears that leave the rotator cable intact require much higher loads to propagate, patients with small tears located in the middle third of the tendon may be more successful with non-operative management.

Histological analysis of cadaveric rotator cuff tendons from elderly individuals with and without degenerative tears showed that degeneration is not uniform throughout tendons, and that tendon lipoid degeneration is increased at the myotendinous junction. This data can be used to inform surgeons of regions of poor tissue quality that may not be visible to the naked eye, helping to inform decisions for suture placement during surgical repair to avoid tendon-suture interface failure. Additionally, histology showed that there was no statistical difference in degeneration between intact tendons and those with a degenerative tear. This finding supports the theory that age-related degeneration in rotator cuff tendons progresses to a point at which normal activities of daily living can initiate a tear, rather than the creation of a tear leading to degeneration. However, it is unknown if the presence of a tear accelerates degeneration further.

The effects of tendon degeneration were further investigated using cadaveric experiments and computational modeling. Interestingly, cadaveric tendons with pre-existing rotator cuff tears did not propagate at lower loads than tendons with artificial tears, and in fact only showed lower stiffness compared to tendons with artificial tears. It is possible that significant tissue remodeling occurs at the edges of degenerative rotator cuff tears over time, “blunting” the edges of the tear to reduce the risk of propagation. However, finite element model predictions of tear propagation for varying levels of tissue degeneration demonstrated an increased risk of tear propagation at loading magnitudes representative of activities of daily living. Taken together, it is important for

surgeons to consider the risks of increased degeneration of tendon tissue on tear propagation and tear shape, though further research is needed to understand the changes that occur to degenerative rotator cuff tears over time that can affect propagation.

The information gleaned from characterization of tears of different geometry and tendons of different tissue quality can provide important information to clinicians considering which treatment is best for their patients. Tears that are at high risk for propagation, such as tears larger than 1 cm, tears in the anterior supraspinatus, or tears in tendons with severe amounts of tissue degeneration, may be optimally treated by early surgical repair before propagation can occur. However, degenerative tears of small size that are at lower risk for propagation may show successful results with non-operative management, provided the exercises performed to strengthen the shoulder muscles do not result in further propagation of the tear.

6.2 FUTURE DIRECTIONS

This work provides valuable information on the effects of non-operative treatment on rotator cuff tears and the mechanics of rotator cuff tear propagation that can be used to improve current protocols for both non-operative and operative treatments. However, a variety of limitations associated with the three specific aims can be improved upon in future studies.

The in vivo testing to investigate the effects of exercise therapy on glenohumeral joint kinematics was performed for a single motion: coronal plane abduction. Additionally, the study followed a small cohort of patients that were all showed successful outcomes after exercise therapy. Future work will include testing different joint positions that are more representative of activities of daily living, such as reaching behind the back or raising the arm to reach an object

on a high shelf. Additionally, more subjects with rotator cuff tears need to be tested that fail exercise therapy in order to determine which factors are associated with success versus failure of non-operative management. It is also currently unknown if the positive changes subjects saw due to therapy were persistent over time, or if the patients eventually suffered from increased joint pain and loss of function long after completion of therapy. Therefore, future studies will include plans for long-term follow-up to assess if positive changes after therapy are consistent over long periods of time, or if patients eventually opt to receive surgical repair of their torn rotator cuff.

Another important factor that must be considered in future investigations of the success and failure of physical therapy is the propagation of rotator cuff tears during therapy. Future studies can use ultrasound to measure rotator cuff tear size at multiple time points during and after therapy to assess propagation over time. It is possible that propagation of the tear, as determined by the cadaveric experiments and computational models used in the present work, can contribute to poor outcomes of exercise therapy when treating rotator cuff tears. Ultimately, it is hoped that the data collected for specific aims 2 and 3 can contribute to the understanding of rotator cuff tear propagation during non-operative management to assist in treatment decisions.

The cadaveric testing performed for this work demonstrated the effects of tear location and tendon degeneration on tear propagation, but was unable to directly quantify the amount of degeneration in the tendon tissue. Future work will use mechanical testing combined with histology and quantitative ultrasound analysis to determine relationships between rotator cuff tendon material properties and amount of tendon degeneration. Additional histology using different stains specific to collagen, lipoid, and mucoid degeneration can be performed along with quantitative image analysis to provide more detailed information on the state of degeneration for a given rotator cuff tendon. A future goal stemming from this dissertation is to

use ultrasound imaging to predict tendon tissue quality based on the amount of degeneration measured by ultrasound analysis and histology and the associated material properties of the tendon.

Though the finite element modeling of rotator cuff tendon performed in this study has incorporated many improvements over previous models, additional improvements can be made. First, the models developed for this dissertation do not account for contact between the articular surface of the rotator cuff tendon and the head of the humerus, and therefore only glenohumeral joint positions greater than 60° of glenohumeral abduction were modeled. An important next step is to incorporate contact into the subsequent model iterations, such that tendon strains and tear propagation at different joint angles can be studied.

Other factors to be investigated include tear shape and fatigue failure. This work only created tears mimicking an anterior-posterior cut through the tendon, and did not account for different tear shapes that are observed clinically. “Crescent” tears lateral to the rotator cable may propagate differently than “U-shaped” tears with extensive retraction. Furthermore, both of these tears likely behave much differently than “L-shaped” tears at the anterior edge of the supraspinatus tendon. By testing cadaveric shoulders with pre-existing degenerative rotator cuff tears, subject-specific geometry can also be obtained for a variety of rotator cuff tear shapes. The models in this work also did not investigate the effects of long-term cyclic loading, as was done experimentally. Future models can incorporate cyclic loading and fatigue failure to study tear propagation over long-term shoulder use.

Additional cadaveric specimens should be used to create a library of subject-specific models that will represent a wider range of biological variability for modeling tear propagation. Although the results of the developed models provide insight into the factors affecting rotator

cuff tear propagation, further modeling is required to make generalizations about the behavior of rotator cuff tears. In addition to providing for variability in subject-specific geometry, additional testing will result in a greater range of tendon material properties. The validated finite element models of tendon in this work incorporated anisotropic, inhomogeneous material properties that are more representative of the actual mechanical behavior of rotator cuff tendon, but did not account for differences in fiber orientation between the supraspinatus and infraspinatus tendons, which have overlapping fibers near their insertions to the humerus. Furthermore, the material properties obtained from mechanical testing were specific to the mid-substance of the tendon, and are not necessarily representative of the properties of the rotator cable or tendon enthesis. By obtaining subject-specific information for tendon fiber organization, or changes in fiber organization due to degeneration, and for material properties throughout the whole tendon, more accurate simulations of tear propagation can be achieved.

Ultimately, the collected library of subject-specific tendon geometries, material properties, and loading conditions (i.e. determined from in vivo measurements of glenohumeral kinematics) can be used to develop a predictive simulator computational tool, for which patient-specific inputs can be used to output an appropriate treatment based on risk of tear propagation. These simulations can also be used to examine the effect of different exercise therapy protocols, such as use of internal/external rotation versus abduction, on the risk of tear propagation. Expanding the functionality of the model in this way can allow for modification of existing exercise therapy protocols to avoid exercises that are at risk for exacerbating tear propagation.

6.3 SUMMARY

The high occurrence rate and significant impact of degenerative rotator cuff tears places a heavy burden on the healthcare system. Although both non-operative and operative treatments of rotator cuff tears have been extensively studied, there is still considerable disagreement on the best course of action for treatment. By improving understanding of which types of rotator cuff tears (in terms of geometry and tendon degeneration) are associated with failure of treatment, improved treatment protocols can be developed to more effectively make clinical care decisions on a patient-by-patient basis.

Due to the high failure rate of up to 50% for non-operative management of rotator cuff tears, there is a clear need to identify which factors most contribute to failure of exercise therapy. One of the goals of exercise therapy is to strengthen the undamaged rotator cuff muscles to compensate for the loss of function of the torn muscle, but it is not clear how these exercises alter glenohumeral joint kinematics. Failure of exercise therapy to restore glenohumeral joint stability may ultimately contribute to poor patient outcomes after therapy. In order to investigate the effect of therapy on glenohumeral joint kinematics, subjects with rotator cuff tears had their joint kinematics measured before and after a 12 week-long program of exercise therapy to treat their injury. All subjects successfully completed therapy with reduced pain and improved range of motion. Additionally, it was found that the joint contact path length was significantly reduced after completion of exercise therapy. Therefore, for coronal plane abduction, exercise therapy can contribute to greater glenohumeral joint stability for patients with rotator cuff tears.

Another factor that may affect the outcome of treatments for rotator cuff tears is propagation of the tear over time. However, is it unclear which types of rotator cuff tears are at the highest risk for tear propagation, and would therefore benefit from earlier, more aggressive

treatment (such as surgical repair). Cadaveric experimentation and computational modeling of the rotator cuff were performed in order to investigate the effects of tear size, location, and tendon tissue degeneration on propagation of rotator cuff tears. Both experiments and models indicated that tears larger than 1 cm in anterior-posterior width and those located in the anterior third of the supraspinatus tendon are most at risk for tear propagation at loads experienced during activities of daily living or exercise therapy. Histological analysis of rotator cuff tendon degeneration demonstrated that age-related degeneration is a wide-spread phenomenon in both intact and torn rotator cuff tendons, and that degeneration throughout the tendon is not uniform. Simulation of tendon degeneration by altering model material parameters resulted in model predictions that determined even moderate amounts of tendon degeneration can result in propagation of rotator cuff tears at loads of less than 200 N.

Overall, the results of this study provide important information to clinicians for improving treatments of rotator cuff tears. Through modification of exercise therapy protocols, there is potential to better target kinematic changes in the joint that will lead to better patient outcomes. Furthermore, thorough characterization of rotator cuff tear geometry and tendon degeneration at diagnosis can assist in optimizing patient-specific treatment decisions by determining which types of tears will benefit from earlier intervention. The results of this work indicate that tears in the anterior third of the supraspinatus tendon, especially those that damage the rotator cable, are most at risk for tear propagation, and therefore patients with these types of tears are not ideal for non-operative management. Patients with small tears in the posterior or middle thirds of the tendon, i.e. tears that do not affect the function of the rotator cable to redistribute load, are likely to be successful with non-operative management in terms of tear propagation and pain management.

Future directions for this research include analysis of in vivo tear propagation throughout the course of exercise therapy, determining direct relationships between tendon material properties and amount of degeneration, and improving models to provide better predictions of tear propagation. Ultimately, the goal of this and future work is to develop a "rotator cuff tear index" to assist clinicians by providing a set of guidelines for more timely and efficient treatment of rotator cuff tears.

APPENDIX A

IN VIVO TESTING

This appendix includes additional information on testing protocol, data processing, and raw data.

A.1.1 Testing Protocol

1. Prior to DSX, subject is recruited from Center for Sports Medicine, gives informed consent, receives clinical MRI and research CT
2. If subject is female and pregnancy test was not administered during CT, must be given prior to DSX testing
3. **PRIOR TO SUBJECT ARRIVAL – DSX and Vicon Set-up**
    a. The distance between x-ray generator/collimator and collector/intensifier should be 1.8 m, with an angle of approximately 50 degrees between inline and offset beams (Figure A)
        i. Use control buttons on each arm to adjust distance between generator and intensifier
            1. Check distance with built-in measuring tape
        ii. Adjust angle by physically rotating arms to reach 50 degree angle between inline and offset, pushing at the base of the arm (generator or intensifier). **DO NOT PUSH ON THE GREY METAL COLUMNS.**
            1. Check angle with goniometer lined up with lasers
    b. The generator and intensifier must be angled to form a 10 degree angle with the floor in order to put sufficient soft tissue between the x-ray beam and scapula to prevent wash-out of the image without having the image blocked by lead aprons (Figure B)
        i. Inline must be at a positive 10 degree angle (as in figure B), offset must be at a negative 10 degree angle (reverse of figure B, beam source pointing downward)
        ii. Loosen the position locks on the sides of each x-ray collimator/intensifier
        iii. Keeping one hand on the bottom of the collimator/intensifier to provide support and slightly unweight it, pull out the pin that is not already sticking out and tilt the

collimator up 5 degrees or the intensifier down 5 degrees, depending on what is being adjusted. After the pin clicks, pull out the other pin and move another 5 degrees, until an angle of 10 degrees is reached.

iv. Retighten the locks

c. Place a low-backed chair at the intersection of the beams such that the chair (and the person's joint) would be both centered under the pivot point for the two arms of the DSX assembly AND centered on the treadmill, arranging the assembly arms based on a left-shoulder configuration (Figure C) or right-shoulder configuration (Figure D). If necessary, adjust the positioning of the collimators and intensifiers such that the chair is located more closely to the intensifiers while maintaining the position of the pivot point and the 1.8 m distance.

d. Set up the 8 Vicon cameras for left arm (Figure C) or right arm (Figure D), depending on which limb is being tested

i. Clear old masks and create new masks on Vicon program

e. Set up laser board on the left or right side of the room, depending on which limb is being tested

i. **BE CAREFUL TO NOT HIT ANY CAMERAS OR OTHER EQUIPMENT WHEN SETTING UP**

ii. Secure the upper beam to the lower beam to make sure it doesn't become detached

iii. Attach poster board to upper and lower beams to Velcro attachment points, keeping edges of upper and lower boards as flush as reasonable, lining up tape marks between boards

iv. Position board initially to be approximately perpendicular to the plane of subject abduction, adjust as necessary after subject is in room

v. Using painter's tape, make lines on the floor that extend from the board to the subject so that arm position can be maintained for lower elevation angles

vi. Make sure no cameras are blocked by the board

f. After setting up cameras and board, calibrate the Vicon system with the calibration wand

i. Prior to calibration, have subject sit in chair and wave arm to ensure all markers are picked up by cameras.

ii. Wave wand slowly around area of expected arm movement until flashing lights on all cameras stop flashing

iii. Lights will flash faster and faster until there is a constant light indicating calibration is complete

iv. Define GCS by setting calibration wand on the subject's chair such that the coronal plane is perpendicular to the surface of the laser board (Y axis is coronal plane, X axis points toward subject's back), set volume origin on program

v. Click camera icon and name trial prior to collecting any Vicon data.

g. Check default parameters for DSX to ensure system is set up for collecting data for the shoulder

4. Subject goes to study prep room to have Vicon markers attached, have measurements taken, and be informed of procedures.

a. The subject will be provided with a tank top if needed in order to allow for placement of reflective markers

b. The following 16 Vicon reflective markers are attached to the subject (see Plug-in-Gait Marker Placement):
    i. C7 (C7 vertebrae)
    ii. CLAV (clavicle)
    iii. LSHO and RSHO (shoulders)
    iv. LUPA and RUPA (upper arm)
    v. LELB and RELB (elbows)
    vi. LWRA and RWRA (wrist marker, thumb side)
    vii. LWRB and RWRB (wrist marker, pinkie side)

c. Fill out first page of Biodynamics Laboratory subject intake form:
    i. Study ID number
    ii. Date of testing
    iii. Subject date of birth
    iv. Height, weight, and BMI
    v. Affected extremity
    vi. Problems since study enrollment that would affect performance of arm abduction or internal/external rotation
    vii. Pregnancy test documentation

d. The following 10 measurements must be taken (see Required Subject Measurement page of Subject Intake form):
    i. Weight (kg)
    ii. Height (cm)
    iii. Shoulder offset for left and right shoulders (cm)
    iv. Elbow width for left and right arms (cm)
    v. Wrist width for left and right wrists (cm)
    vi. Hand thickness for left and right hands (cm)

e. Prior to being positioned in the DSX, subjects will be reminded of what is expected of them for this portion of the study, having been previously informed from the informed consent form

When we've finished applying the markers for tracking arm motion and taking the needed measurements, we'll be taking the x-ray images for the study. When collecting the images, you will be asked to sit in a chair with your back straight and complete a series of motions, including lifting and rotating your arms in different directions. We'll have you do two different motions of three times each, which will be demonstrated to you prior to doing the motions. So that you can make the motions be almost the same each time, we'll be attaching a laser pointer to your hand for the arm-lifting task. While you lift your arm, you'll be asked to follow a line on a board with the laser pointer to make sure your arm is following a straight path. You'll be able to rest between each motion and practice before the x-ray machine is activated to collect the images.

5. After initial DSX setup and subject has had measurements taken and markers attached, final adjustments must be done on the DSX apparatus to center the field of view on the subject's glenohumeral joint

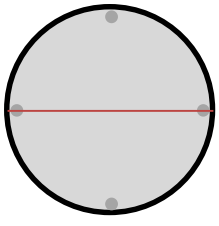

a. Help the subject to be seated in the chair between the x-ray beams, making sure that the chair is centered on the treadmill so that it is far enough from the edges that there is no risk of the legs falling into the treadmill pits
b. Turn on alignment lasers on x-ray collimators in order to focus beams
    i. Move columns of collimators and intensifiers up and down until lasers are crossed at center of glenohumeral joint
    ii. Horizontal laser lines should line up with middle pins on collectors/intensifiers (figure)
    iii. Translate/rotate DSX rig as necessary to center glenohumeral joint under DSX apparatus pivot point
    iv. Rotate subject and chair as needed to have glenohumeral joint centered at laser crosshair
c. **LOCK** DSX rig to prevent from moving
    i. If DSX is moved, need to recalibrate Vicon

6. Attach laser guide to hand of subject's affected arm
    a. Put battery into laser pointer, being careful to keep the laser end pointed down to avoid shining the laser in anyone's eyes
    b. Secure laser pointer to subject's hand as shown in Figure E, again being careful about where the laser is pointing
    c. Inform subject of purpose of laser pointer, to take care in where they point

This laser pointer is just to help you with raising your arm up in a straight line. If you look at the board with the vertical lines on it, when we ask you to raise your arm, just try to keep the laser pointer following whichever line is easiest to follow from the floor to the top of the board. It's ok if the laser pointer goes above the board when you lift your arm up as high as it can go. Please remember that the laser is on at all times, so please try not to shine it at any of the Vicon cameras or in anyone's eyes.

    d. After each data collection trial, be sure to ask patient if he or she is comfortable to continue, that his or her hand is not falling asleep

7. Prior to collecting dynamic trials, collect one static snapshot with DSX to determine appropriate x-ray dosage for best images for tracking, collect static Vicon trial during DSX snapshot
    a. Starting parameters:

Frame Rate	50 Hz
Pulse Width	2 ms
kV	70
mA	1

	25

b. Record final parameters on study data collection sheet
c. Note that frame rate may need to be adjusted based on speed at which subject is able to complete motions
d. Ensure that the frequency for Vicon is set to the same frequency of the DSX
    i. Under "system" tap on left side of screen, click on "local Vicon system" and set to the proper frequency
    ii. Right click, "synchronize"

8. Collect dynamic trials
    a. Arm abduction
        i. Subject will be asked to elevate his/her arm in the coronal plane (Figure F) for 3 trials
        ii. Starting from a resting position at the side with the thumb pointing outward, the subject elevates his/her arm to its maximum amount of elevation over a period of 2 seconds
            1. A metronome will be used to assist with timing with timing of 1 beat per second
            2. If the subject is in too much pain to perform the motion in the 2 second period, the time increment can be increased and the frequency of data collection can be decreased to obtain the same number of frames without increasing x-ray dosage (e.g. 4 seconds at 25 Hz).
        iii. The subject will follow a selected vertical line on the laser guide board as close as comfortably possible with the laser pointer to improve repeatability of the motion
        iv. Prior to collecting data, the subject will be allowed to practice the motion
            1. If in too much pain, can practice BREIFLY at a reduced range of motion to properly understand the motion.
            2. If pain is not an issue, should continuously ab/adduct his/her arm from resting position to maximum elevation over the chosen period of time to practice the motion
            3. In both cases, the practice motion should not be repeated more than 5 times to minimize fatigue and excessive pain.
        v. **ENSURE THAT SUBJECT KEEPS ELBOW STRAIGHT AND DOES FULL RANGE OF ELEVATION, BRINGING ARM BACK TO SIDE AT THE END OF EACH MOTION**
        vi. Data collection
            1. If subject is in pain, they will perform a single motion on a countdown from "3…2…1…go," beginning the motion on "go"
            2. If pain is not an issue, the subject will do continuous repetitions of the motion, with data collected for one complete period in the middle of the set.
            3. Take pictures between trials for records
                a. Video difficult to take during trial due to x-rays, would need to take through window
        vii. After each trial, the subject rests for 3 minutes to minimize fatigue

viii. Write down trial data (frequency, number of frames) on data sheets for each trial

Now we're going to ask you to elevate your arm straight out from your body, following one of the lines of your choice on the board with the laser pointer (demonstrate motion). Just be sure to use the same line on the board every time. We have the metronome going every 2 seconds, so you should try to complete the motion, either from side to fully lifted or fully lifted to side, each time the metronome sounds. Try to raise it as far as you can before you start to feel any shoulder pain. Please make sure you keep your elbow straight throughout the motion, and bring your arm back to your side at the end of each motion. Once you're comfortable making the motion after some practice, we'll have you continuously raise and lower your arm and then collect 2 seconds of data with the x-ray. Once the data is collected you can stop raising your arm, and we'll have you rest for 3 minutes, after which we'll do 2 more trials.

b. Internal/External Rotation
    i. Remove laser pointer from subject hand
    ii. Subject will be asked to perform a motion of full internal rotation in a resting position to full external rotation (Figure G) for 3 trials
    iii. Starting from a resting position of full IR with the arm bent at the elbow, the subject rotates his/her arm to full ER over 2 seconds
        1. A metronome will be used to assist with timing
    iv. Prior to collecting data, the subject will continuously move from full IR to full ER over the 2 second period to practice the motion, with 2 seconds of x-ray/Vicon data being collected for a single period of the motion
        1. If in too much pain, will follow same procedure as for coronal plane abduction, i.e. opportunity to practice the motion, "3…2…1…go" to collect data
    v. After each trial, the subject rests for 3 min to minimize fatigue
    vi. Take pictures between trials for records.
    vii. Write down trial data (frequency, number of frames) on data sheets for each trial

Now we're going to ask you to start with your arm fully internally rotated with your elbow bent at about 90 degrees, and then rotate your arm out to a position of full external rotation (demonstrate motion). Again, we have the metronome going every 2 seconds, so you should try to complete the motion each time the metronome sounds. Once you're comfortable making the motion after some practice, we'll have you continuously rotate your arm back and forth and then collect 2 seconds of data with the x-ray. Once the data is collected you can stop moving your arm, and we'll have you rest for 3 minutes, after which we'll do 2 more trials.

9. After testing and while subject is having markers removed:
    a. Perform post-test calibration of DSX
        i. Record parameters and DSX orientation on data sheet
        ii. Draw schematic of camera/calibration cube configuration
    b. Perform distortion correction
10. Disassemble and store laser guidance board

DATA MANAGEMENT:

- Proper Directory Organization for x-ray and Vicon data:
    - RCT_GH_Kinematics (study name)
        - RC-## (subject name)
            - Pre (separate folders for “before” and “after” visits)
            - Post
                - Cor1 (saved trials for each visit)
                - Rot1
                - Etc.
- All DSX data is burned to a Blu-ray disc at the end of data collection
    - Save to disc as subject name (e.g. RC-01 Pre)
    - 2 folders for data sets
        - Vicon
        - X-ray
- Copies of data are kept on X:\ drive in Biodynamics lab
- Data can be transferred to personal laptop using personal folder on Y:\ drive
- DSX video files labeled as “cor” for coronal plane abduction and “rot” for internal/external rotation
    - Number next to prefix (e.g. 1, 2, 3) indicates which trial the file corresponds to
    - No number indicates static trial
- All subject IDs labeled as RC-##, starting with “01”
    - No name identification on data sheets
- Each subject will have 28 associated DSX files per visit
    - 14 total for each motion (coronal plane abduction + IR/ER)
        - 8 for recorded trials: (static + trial 1 + trial 2 + trial 3) X 2 cameras
        - 6 for calibration: (calibration cube + distortion grid + white) X 2 cameras

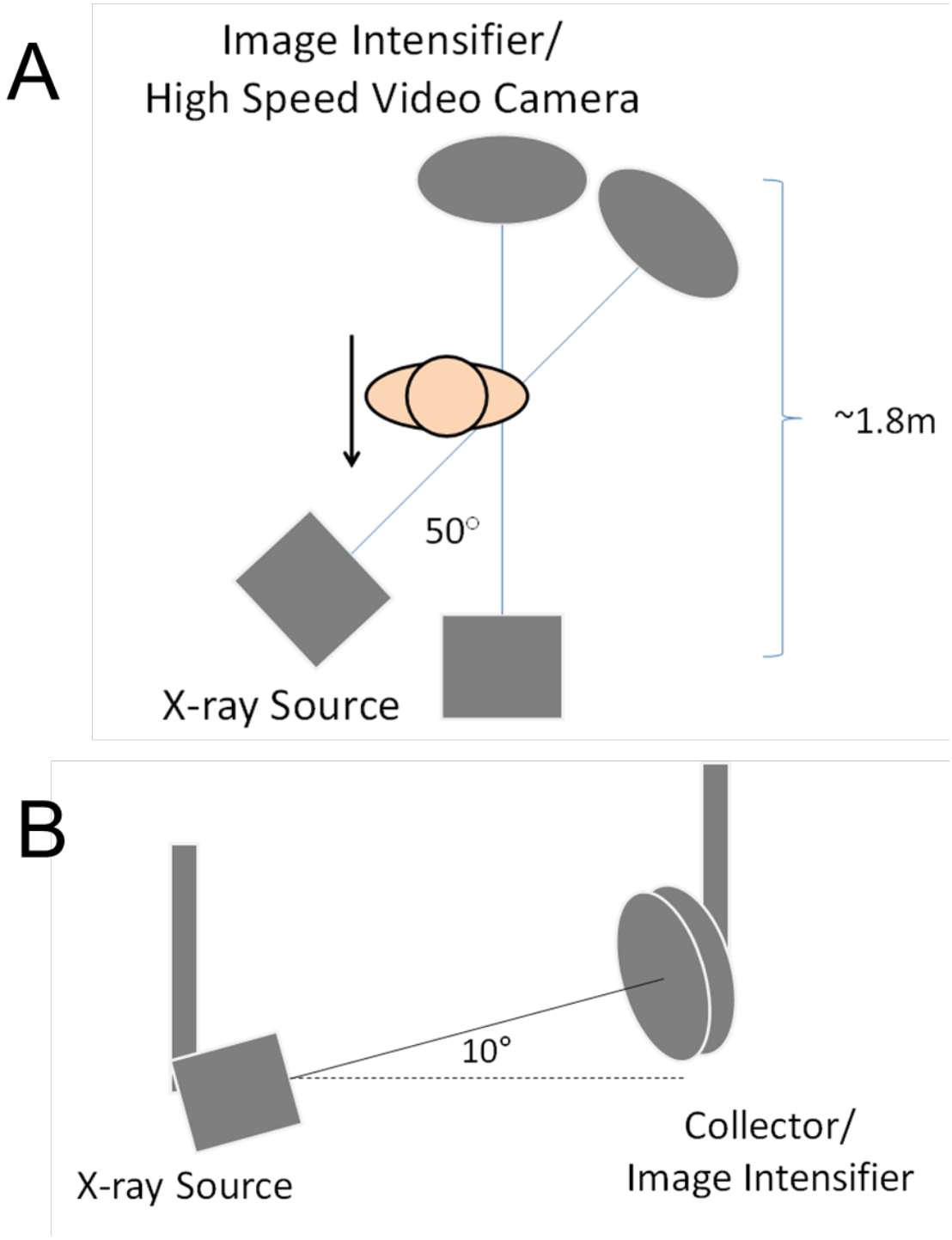
A
Image Intensifier/
High Speed Video Camera
~1.8m
50°
X-ray Source
B
10°
X-ray Source
Collector/
Image Intensifier

Vicon Camera Setup

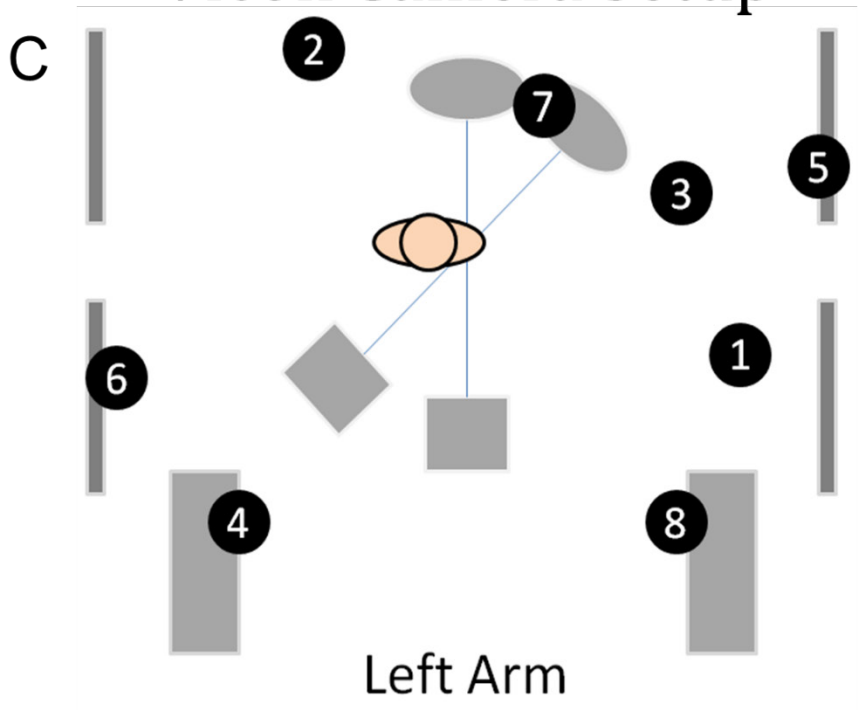

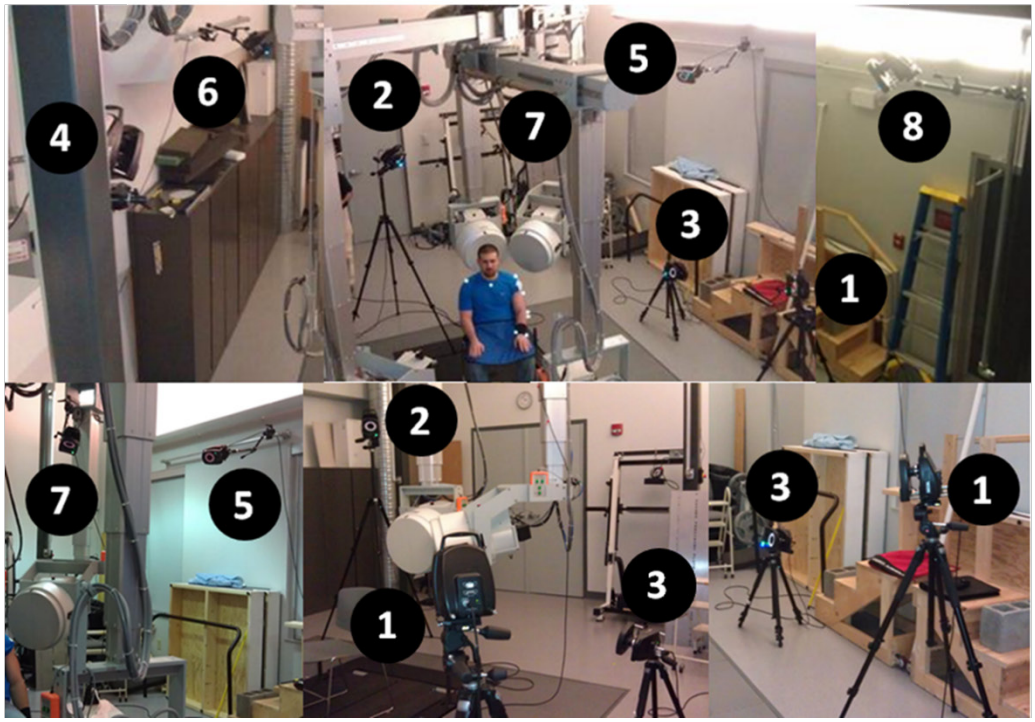

Vicon Camera Setup

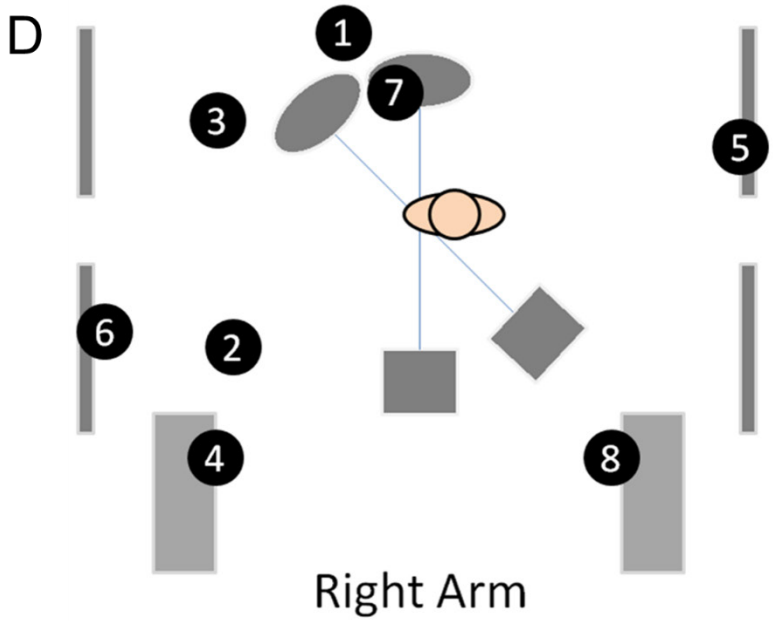

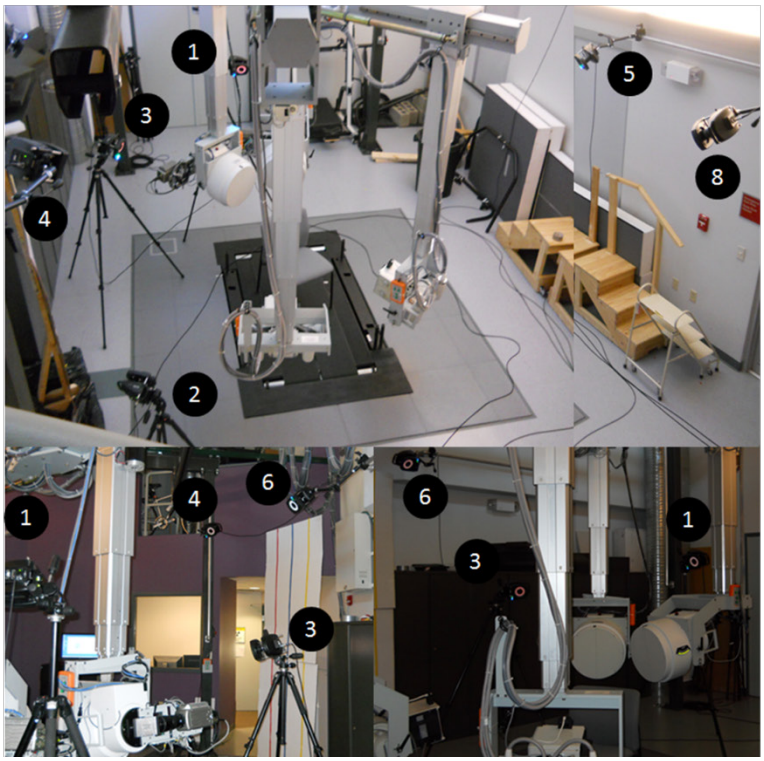

E

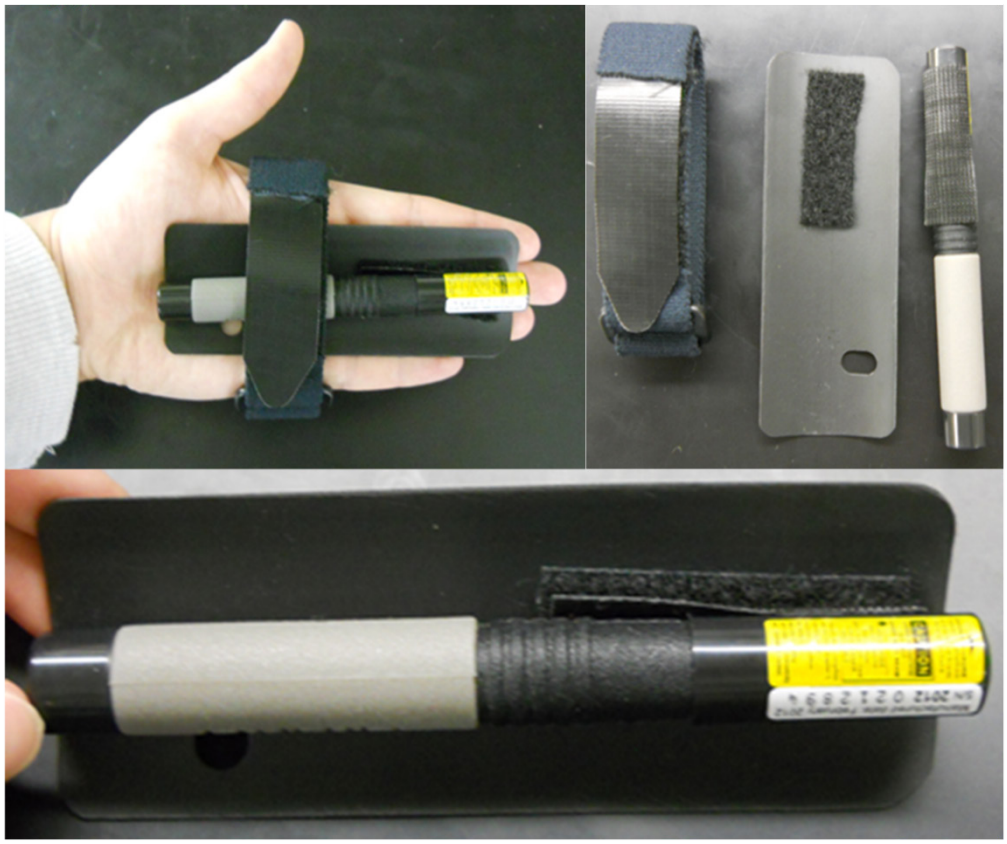

F

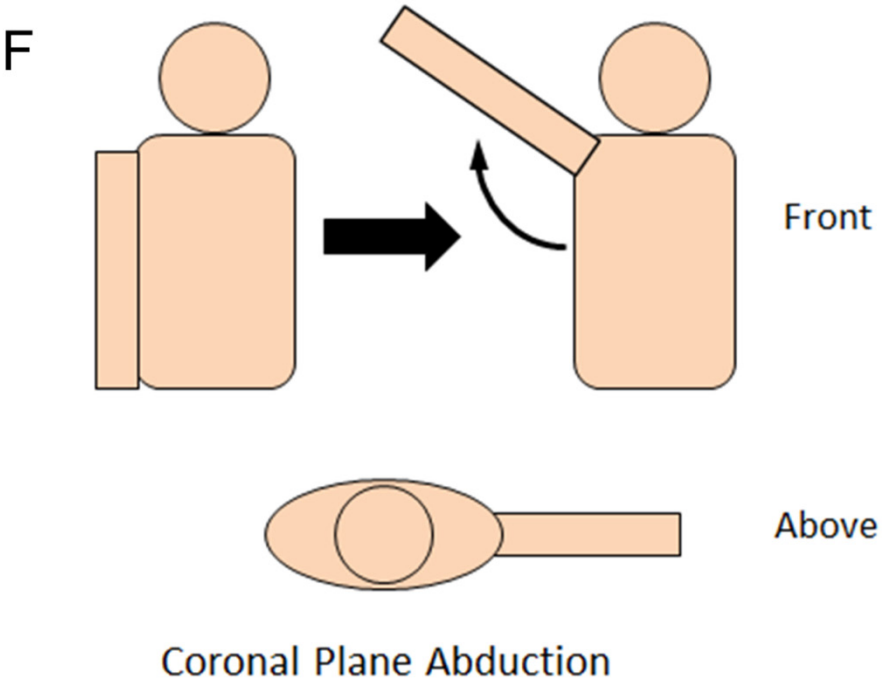

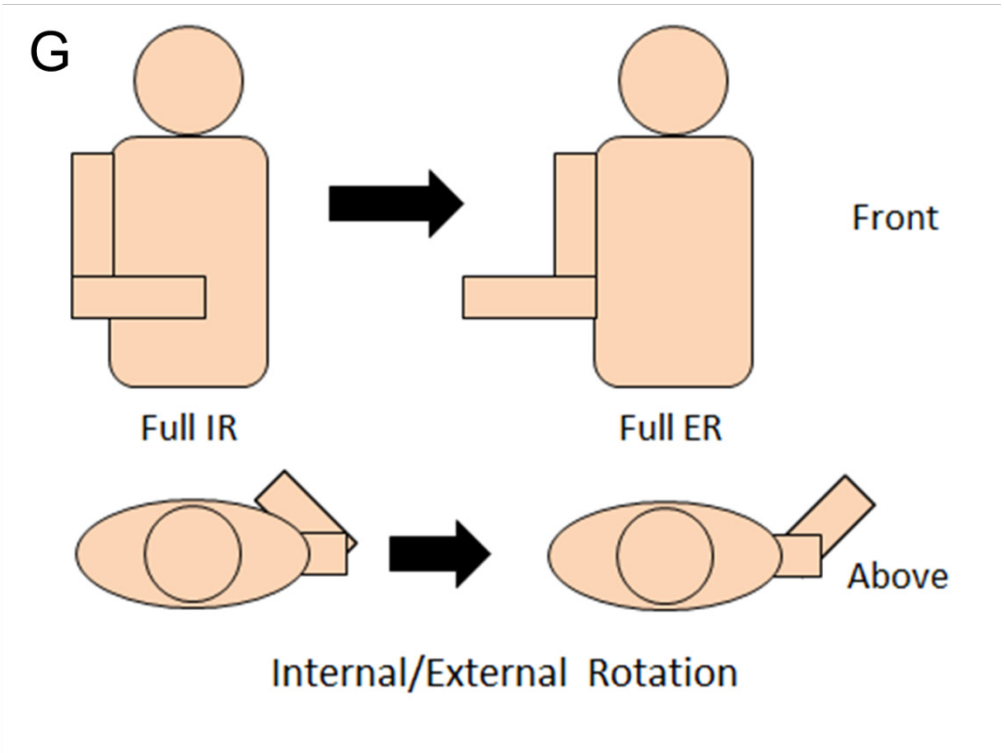
G
Front
Full IR
Full ER
Above
Internal/External Rotation

A.1.2 MATLAB Code for Data Processing

```
%Import kinematic data
workbookFile = 'C:\Users\R Matthew.LilBobbyPC\Documents\Lab Stuff\Research
Studies\In vivo RC kinematics study\Data\RCT_Kinematics\RC-05\RC-
05_data.xlsx';
data = importData(workbookFile,'Pre1','A2:F93');
Elevation = data(:,1);
SI = data(:,2);
AP = data(:,3);
SIContact = data(:,4);
APContact = data(:,5);
MinWidthStoH = data(:,6);

elev = 29:1:79;
SI_i=interp1(Elevation,SI,elev);
AP_i=interp1(Elevation,AP,elev);
SIContact_i=interp1(Elevation,SIContact,elev);
APContact_i=interp1(Elevation,APContact,elev);
AHD_i=interp1(Elevation,MinWidthStoH,elev);

interpdata = zeros(length(elev),6);
interpdata(:,1) = elev.';
interpdata(:,2) = SI_i.';
interpdata(:,3) = AP_i.';
interpdata(:,4) = SIContact_i.';
interpdata(:,5) = APContact_i.';
interpdata(:,6) = AHD_i.';
xlswrite('Interpolated.xls',interpdata,'Pre1','A2:F52')
heading=[{'Elevation'},{'SI Translation'},{'AP Translation'},{'SI Contact
Path'},{'AP Contact Path'},{'Minimum AHD'}];
xlswrite('Interpolated.xls',heading,'Pre1','A1:F1')

%%
%Import kinematic data
workbookFile = 'C:\Users\R Matthew.LilBobbyPC\Documents\Lab Stuff\Research
Studies\In vivo RC kinematics study\Data\RCT_Kinematics\RC-05\RC-
05_data.xlsx';
data = importData(workbookFile,'Pre2','A2:F72');
Elevation = data(:,1);
SI = data(:,2);
AP = data(:,3);
SIContact = data(:,4);
APContact = data(:,5);
MinWidthStoH = data(:,6);

elev = 29:1:77;
SI_i=interp1(Elevation,SI,elev);
AP_i=interp1(Elevation,AP,elev);
SIContact_i=interp1(Elevation,SIContact,elev);
APContact_i=interp1(Elevation,APContact,elev);
AHD_i=interp1(Elevation,MinWidthStoH,elev);
```

```
interpdata = zeros(length(elev),6);
interpdata(:,1) = elev.';
interpdata(:,2) = SI_i.';
interpdata(:,3) = AP_i.';
interpdata(:,4) = SIContact_i.';
interpdata(:,5) = APContact_i.';
interpdata(:,6) = AHD_i.';
xlswrite('Interpolated.xls',interpdata,'Pre2','A2:F50')
heading=[{'Elevation'},{'SI Translation'},{'AP Translation'},{'SI Contact
Path'},{'AP Contact Path'},{'Minimum AHD'}];
xlswrite('Interpolated.xls',heading,'Pre2','A1:F1')

%%
%Import kinematic data
workbookFile = 'C:\Users\R Matthew.LilBobbyPC\Documents\Lab Stuff\Research
Studies\In vivo RC kinematics study\Data\RCT_Kinematics\RC-05\RC-
05_data.xlsx';
data = importData(workbookFile,'Pre3','A2:F63');
Elevation = data(:,1);
SI = data(:,2);
AP = data(:,3);
SIContact = data(:,4);
APContact = data(:,5);
MinWidthStoH = data(:,6);

elev = 28:1:80;
SI_i=interp1(Elevation,SI,elev);
AP_i=interp1(Elevation,AP,elev);
SIContact_i=interp1(Elevation,SIContact,elev);
APContact_i=interp1(Elevation,APContact,elev);
AHD_i=interp1(Elevation,MinWidthStoH,elev);

interpdata = zeros(length(elev),6);
interpdata(:,1) = elev.';
interpdata(:,2) = SI_i.';
interpdata(:,3) = AP_i.';
interpdata(:,4) = SIContact_i.';
interpdata(:,5) = APContact_i.';
interpdata(:,6) = AHD_i.';
xlswrite('Interpolated.xls',interpdata,'Pre3','A2:F54')
heading=[{'Elevation'},{'SI Translation'},{'AP Translation'},{'SI Contact
Path'},{'AP Contact Path'},{'Minimum AHD'}];
xlswrite('Interpolated.xls',heading,'Pre3','A1:F1')

%%
%Import kinematic data
workbookFile = 'C:\Users\R Matthew.LilBobbyPC\Documents\Lab Stuff\Research
Studies\In vivo RC kinematics study\Data\RCT_Kinematics\RC-05\RC-
05_data.xlsx';
data = importData(workbookFile,'Post1','A2:F101');
Elevation = data(:,1);
SI = data(:,2);
AP = data(:,3);
SIContact = data(:,4);
APContact = data(:,5);
MinWidthStoH = data(:,6);
```

```
elev = 52:1:102;
SI_i=interp1(Elevation,SI,elev);
AP_i=interp1(Elevation,AP,elev);
SIContact_i=interp1(Elevation,SIContact,elev);
APContact_i=interp1(Elevation,APContact,elev);
AHD_i=interp1(Elevation,MinWidthStoH,elev);

interpdata = zeros(length(elev),6);
interpdata(:,1) = elev.';
interpdata(:,2) = SI_i.';
interpdata(:,3) = AP_i.';
interpdata(:,4) = SIContact_i.';
interpdata(:,5) = APContact_i.';
interpdata(:,6) = AHD_i.';
xlswrite('Interpolated.xls',interpdata,'Post1','A2:F52')
heading=[{'Elevation'},{'SI Translation'},{'AP Translation'},{'SI Contact
Path'},{'AP Contact Path'},{'Minimum AHD'}];
xlswrite('Interpolated.xls',heading,'Post1','A1:F1')

%%
%Import kinematic data
workbookFile = 'C:\Users\R Matthew.LilBobbyPC\Documents\Lab Stuff\Research
Studies\In vivo RC kinematics study\Data\RCT_Kinematics\RC-05\RC-
05_data.xlsx';
data = importData(workbookFile,'Post2','A2:F98');
Elevation = data(:,1);
SI = data(:,2);
AP = data(:,3);
SIContact = data(:,4);
APContact = data(:,5);
MinWidthStoH = data(:,6);

elev = 35:1:85;
SI_i=interp1(Elevation,SI,elev);
AP_i=interp1(Elevation,AP,elev);
SIContact_i=interp1(Elevation,SIContact,elev);
APContact_i=interp1(Elevation,APContact,elev);
AHD_i=interp1(Elevation,MinWidthStoH,elev);

interpdata = zeros(length(elev),6);
interpdata(:,1) = elev.';
interpdata(:,2) = SI_i.';
interpdata(:,3) = AP_i.';
interpdata(:,4) = SIContact_i.';
interpdata(:,5) = APContact_i.';
interpdata(:,6) = AHD_i.';
xlswrite('Interpolated.xls',interpdata,'Post2','A2:F52')
heading=[{'Elevation'},{'SI Translation'},{'AP Translation'},{'SI Contact
Path'},{'AP Contact Path'},{'Minimum AHD'}];
xlswrite('Interpolated.xls',heading,'Post2','A1:F1')

%%
%Import kinematic data
```

```
workbookFile = 'C:\Users\R Matthew.LilBobbyPC\Documents\Lab Stuff\Research
Studies\In vivo RC kinematics study\Data\RCT_Kinematics\RC-05\RC-
05_data.xlsx';
data = importData(workbookFile,'Post3','A2:F101');
Elevation = data(:,1);
SI = data(:,2);
AP = data(:,3);
SIContact = data(:,4);
APContact = data(:,5);
MinWidthStoH = data(:,6);

elev = 40:1:104;
SI_i=interp1(Elevation,SI,elev);
AP_i=interp1(Elevation,AP,elev);
SIContact_i=interp1(Elevation,SIContact,elev);
APContact_i=interp1(Elevation,APContact,elev);
AHD_i=interp1(Elevation,MinWidthStoH,elev);

interpdata = zeros(length(elev),6);
interpdata(:,1) = elev.';
interpdata(:,2) = SI_i.';
interpdata(:,3) = AP_i.';
interpdata(:,4) = SIContact_i.';
interpdata(:,5) = APContact_i.';
interpdata(:,6) = AHD_i.';
xlswrite('Interpolated.xls',interpdata,'Post3','A2:F66')
heading=[{'Elevation'},{'SI Translation'},{'AP Translation'},{'SI Contact
Path'},{'AP Contact Path'},{'Minimum AHD'}];
xlswrite('Interpolated.xls',heading,'Post3','A1:F1')
```

A.1.3 Individual Subject Raw Data

RC-01

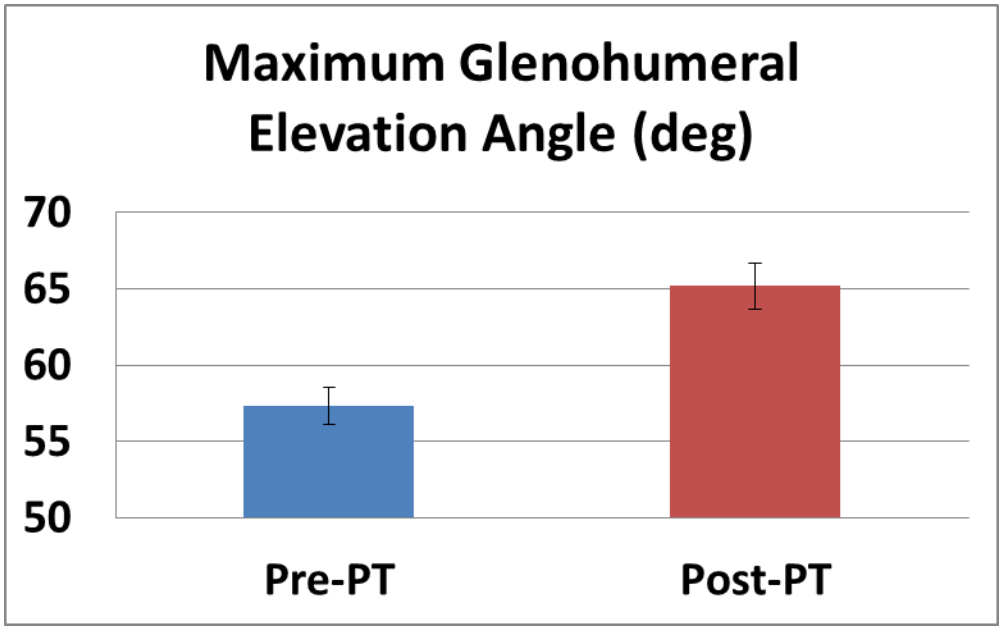

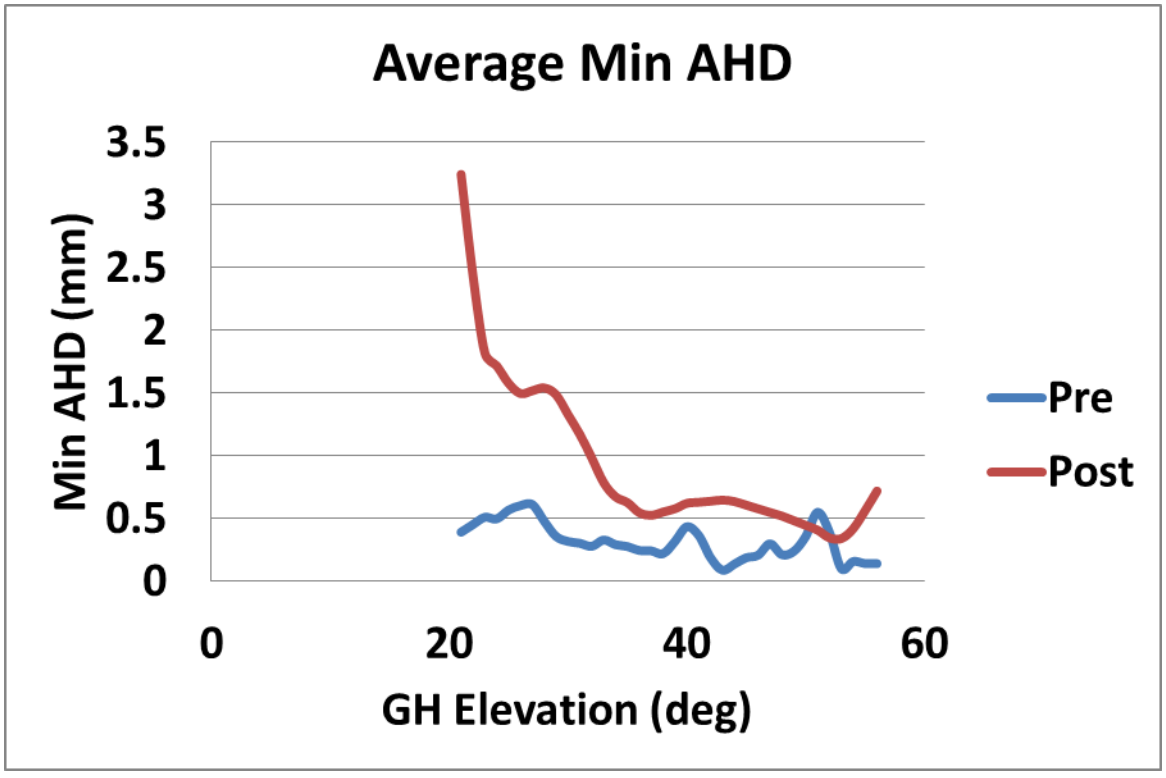

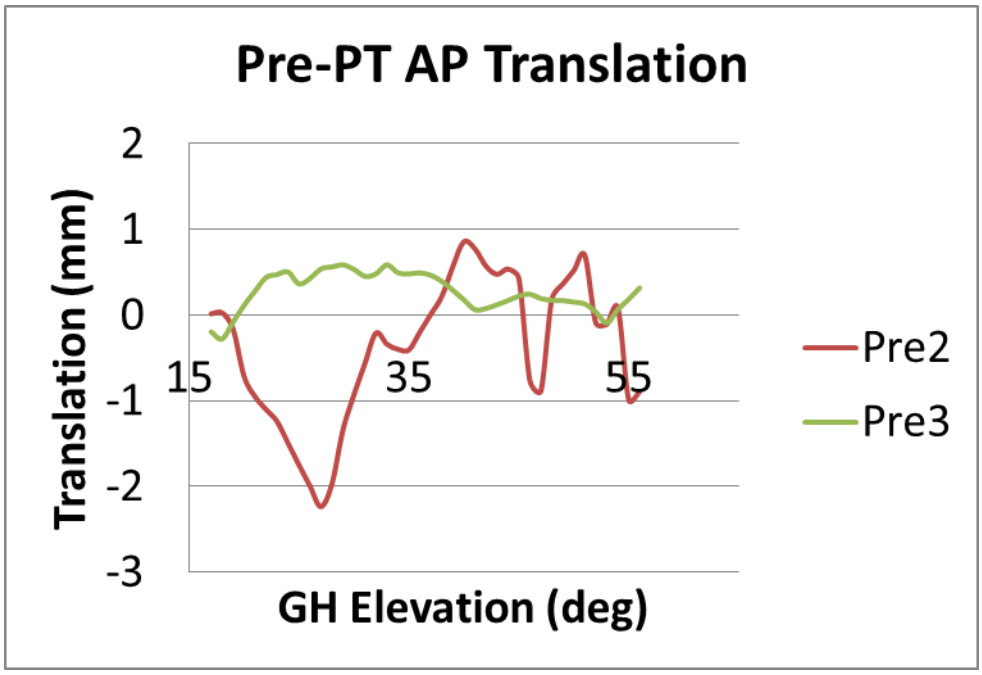
Pre-PT AP Translation
Translation (mm)
2
1
0
-1
-2
-3
15
35
55
GH Elevation (deg)
Pre2
Pre3

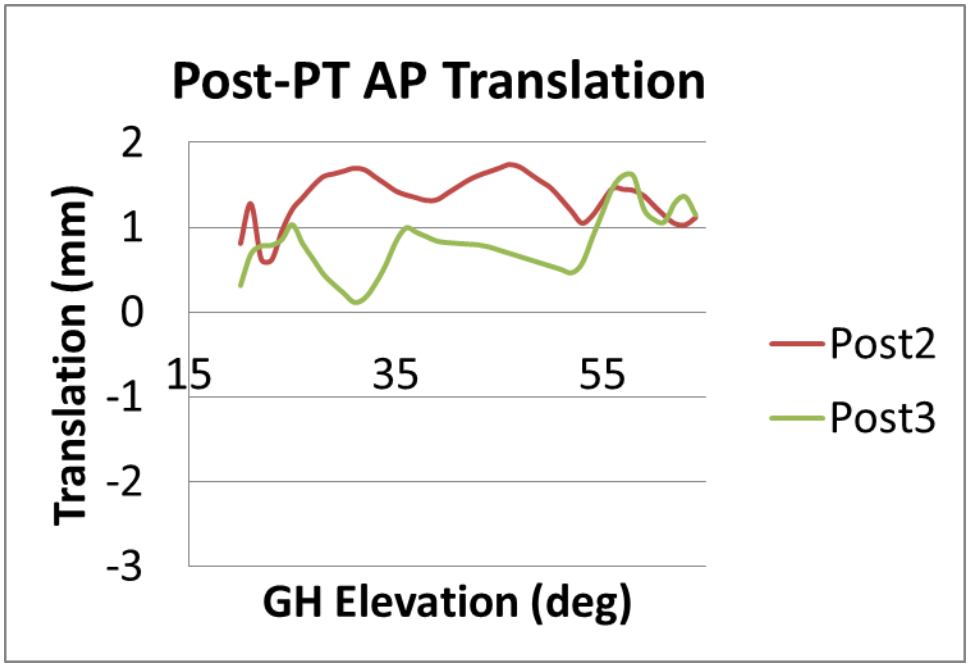
Post-PT AP Translation
Translation (mm)
2
1
0
-1
-2
-3
15
35
55
GH Elevation (deg)
Post2
Post3

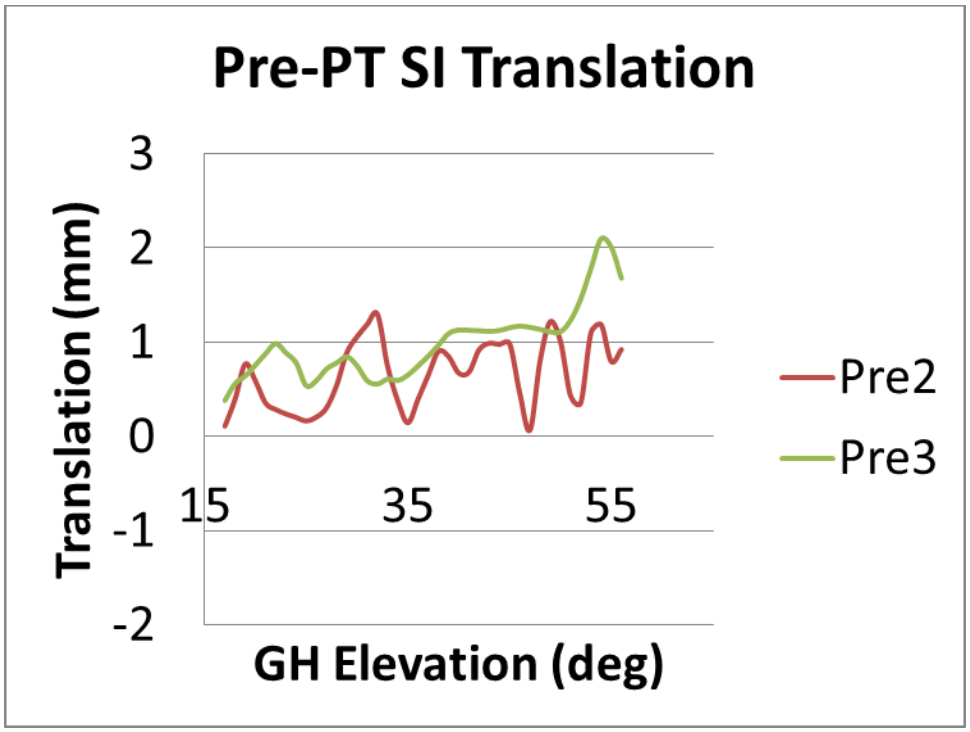
Pre-PT SI Translation
Translation (mm)
3
2
1
0
-1
-2
15
35
55
GH Elevation (deg)
Pre2
Pre3

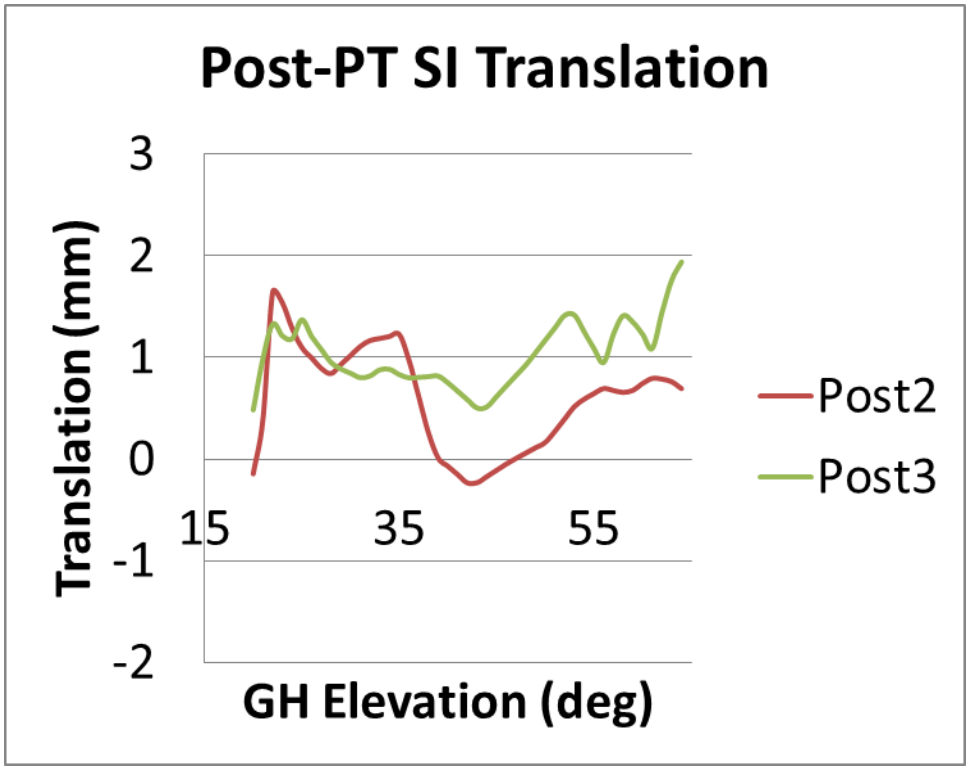
Post-PT SI Translation
Translation (mm)
3
2
1
0
-1
-2
15
35
55
GH Elevation (deg)
Post2
Post3

RC-02

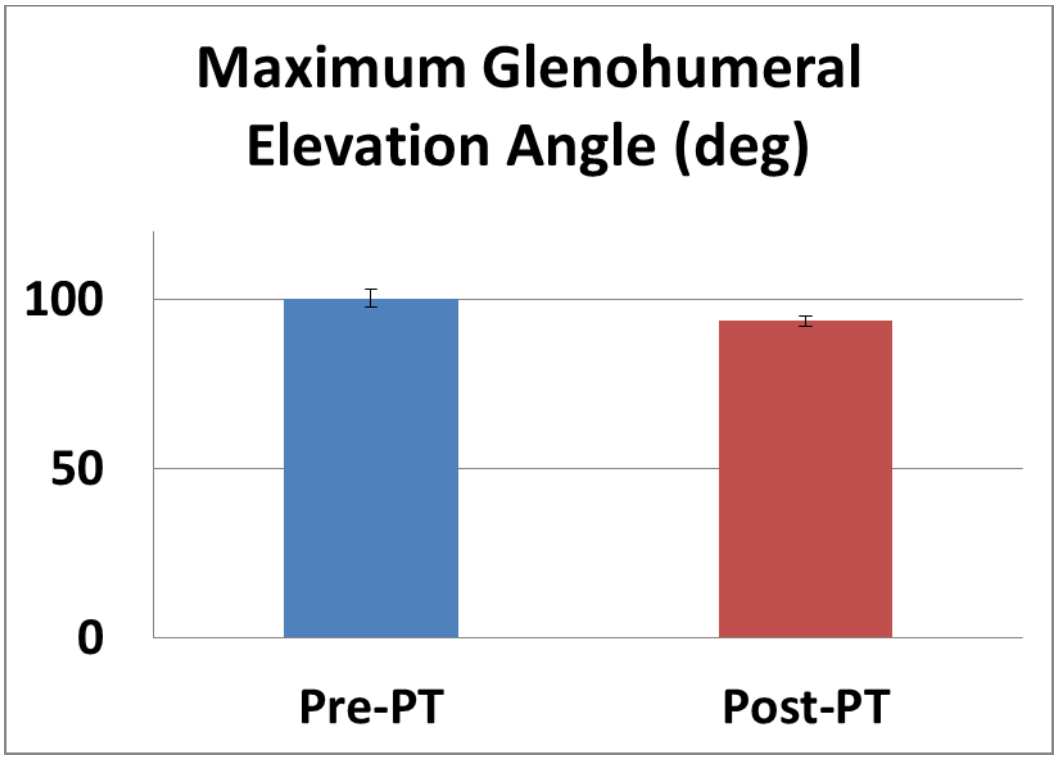
Maximum Glenohumeral Elevation Angle (deg)
100
50
0
Pre-PT
Post-PT

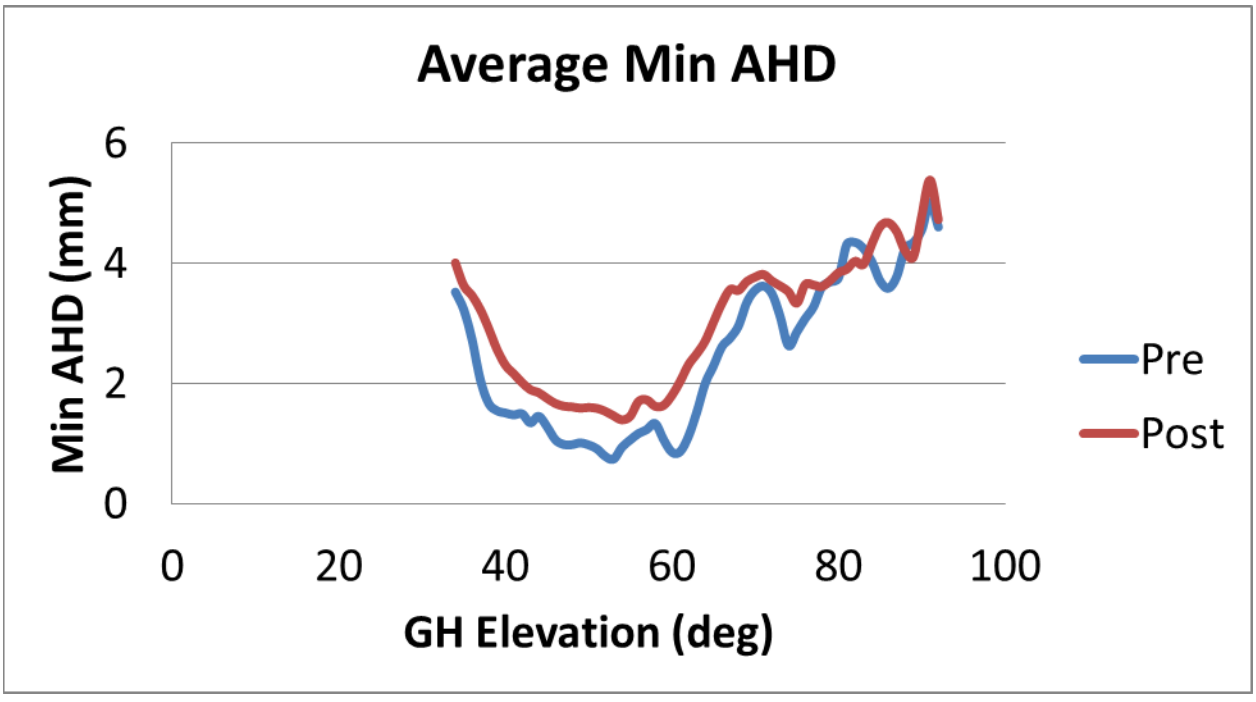
Average Min AHD
Min AHD (mm)
6
4
2
0
0
20
40
60
80
100
GH Elevation (deg)
Pre
Post

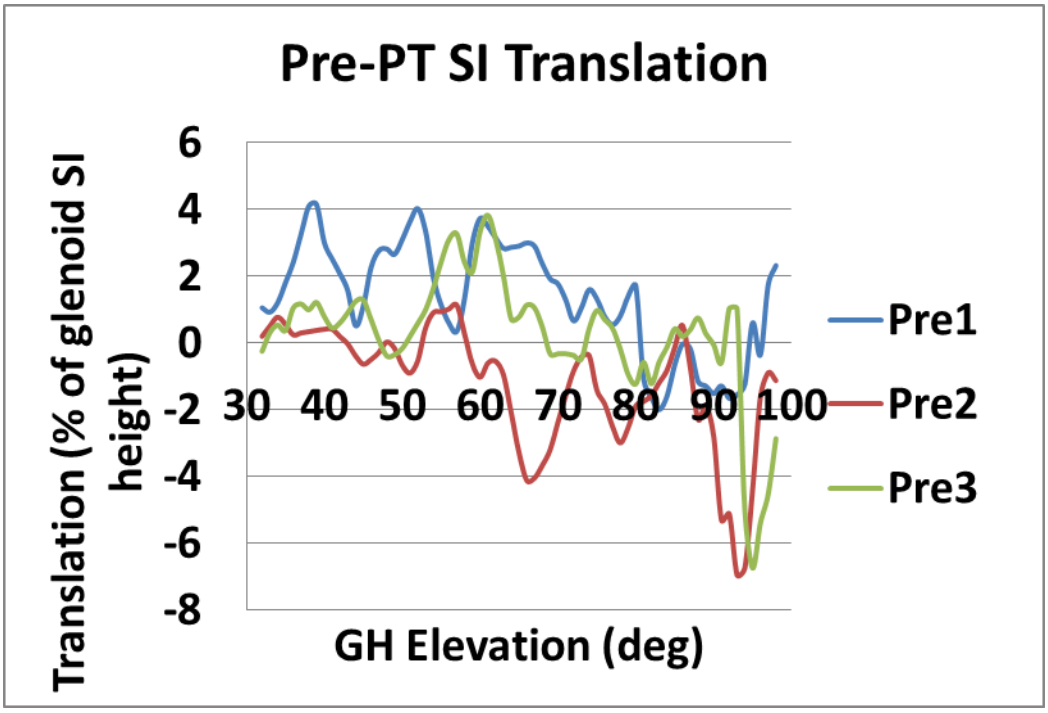
Pre-PT SI Translation
Translation (% of glenoid SI height)
6
4
2
0
-2
-4
-6
-8
30 40 50 60 70 80 90 100
GH Elevation (deg)
Pre1
Pre2
Pre3

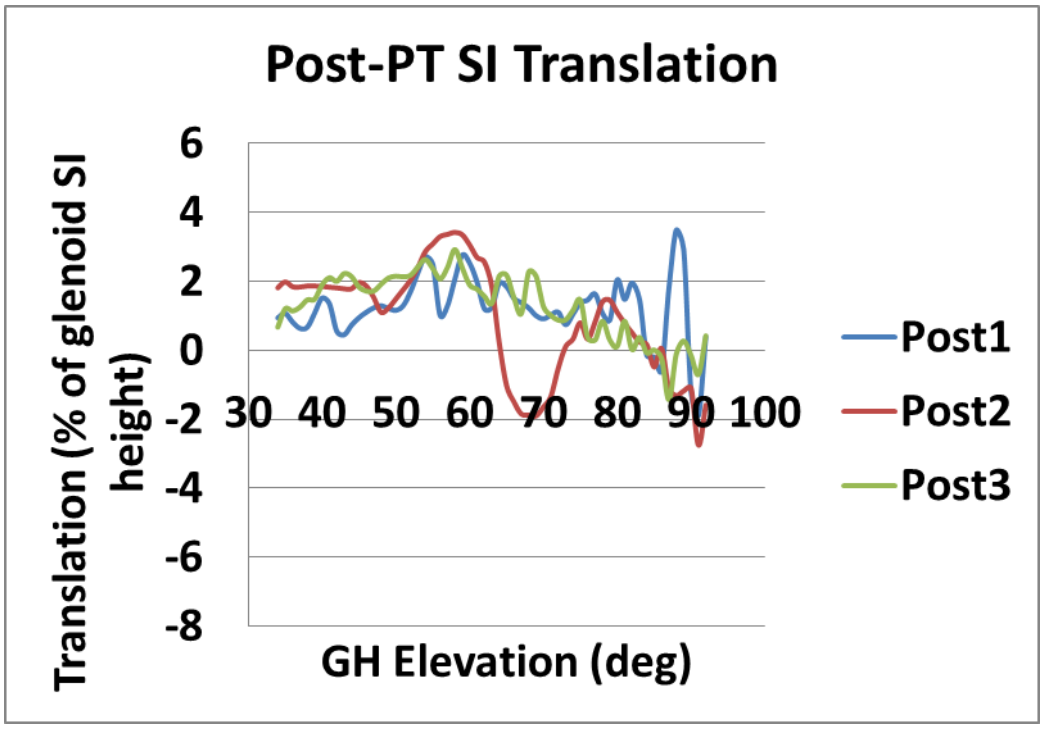
Post-PT SI Translation
Translation (% of glenoid SI height)
6
4
2
0
-2
-4
-6
-8
30 40 50 60 70 80 90 100
GH Elevation (deg)
Post1
Post2
Post3

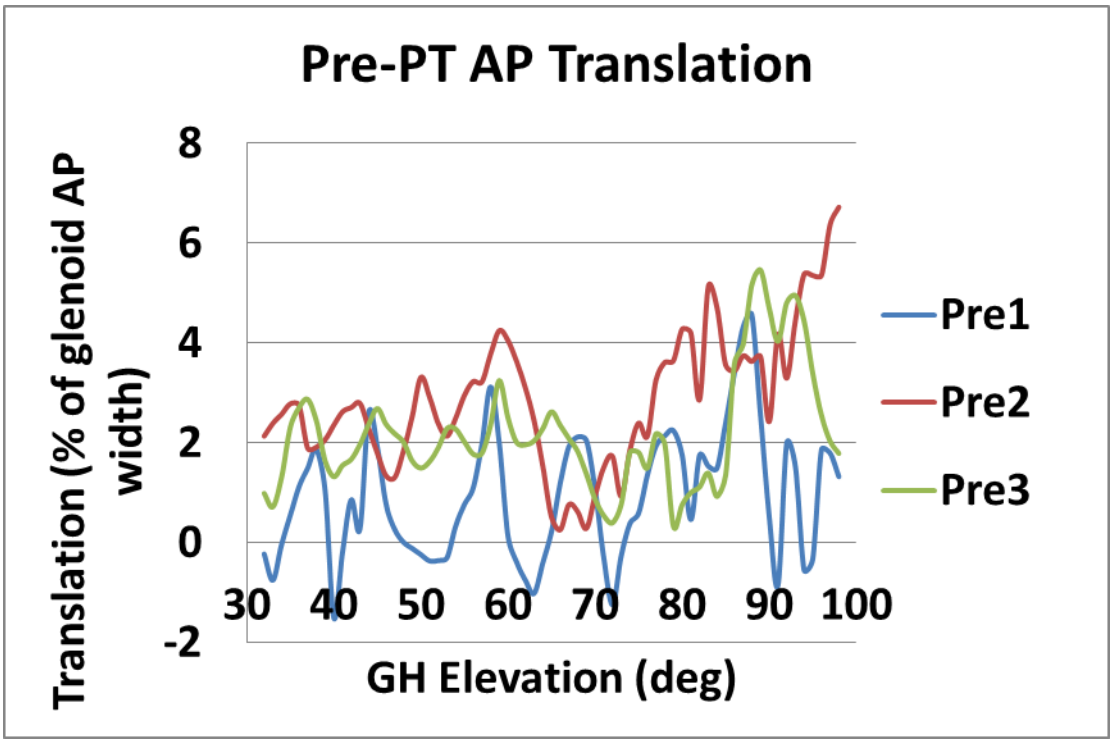
Pre-PT AP Translation
Translation (% of glenoid AP width)
8
6
4
2
0
-2
30 40 50 60 70 80 90 100
GH Elevation (deg)
Pre1
Pre2
Pre3

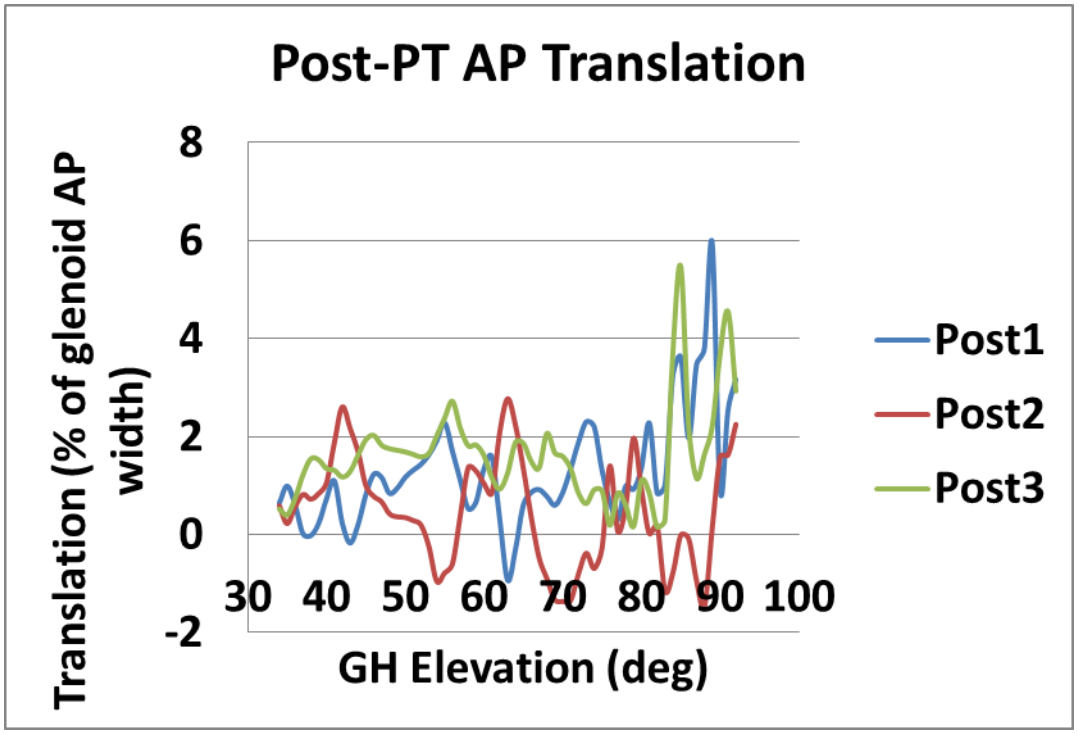
Post-PT AP Translation
Translation (% of glenoid AP width)
8
6
4
2
0
-2
30 40 50 60 70 80 90 100
GH Elevation (deg)
Post1
Post2
Post3

RC-03

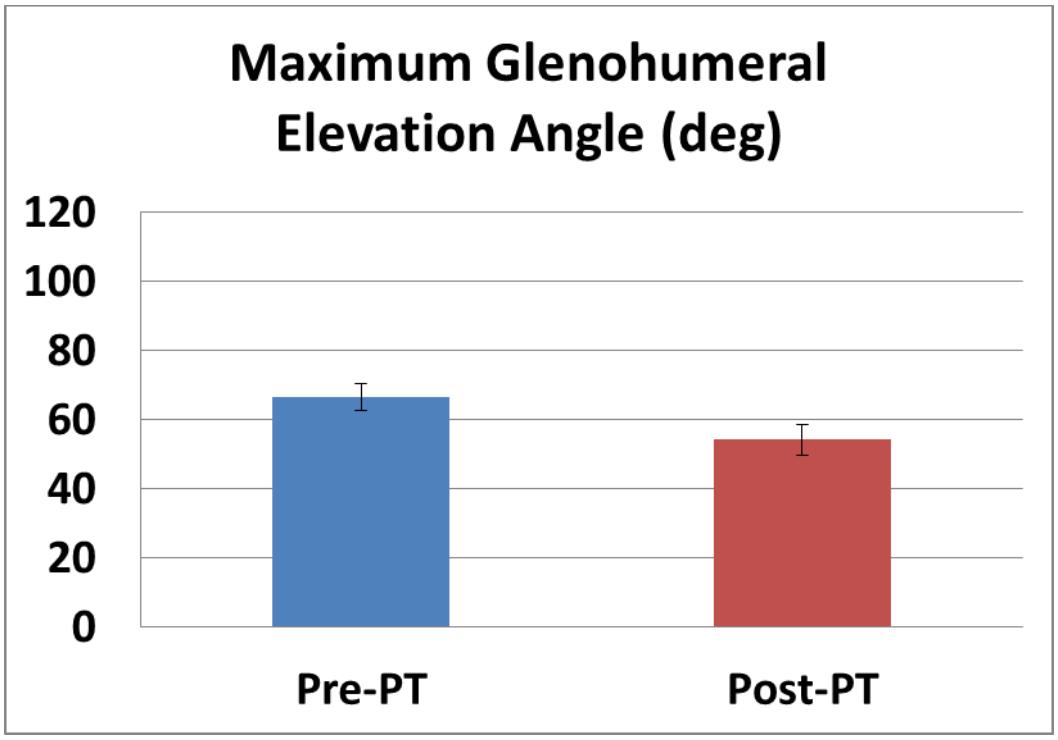
Maximum Glenohumeral Elevation Angle (deg)
120
100
80
60
40
20
0
Pre-PT
Post-PT

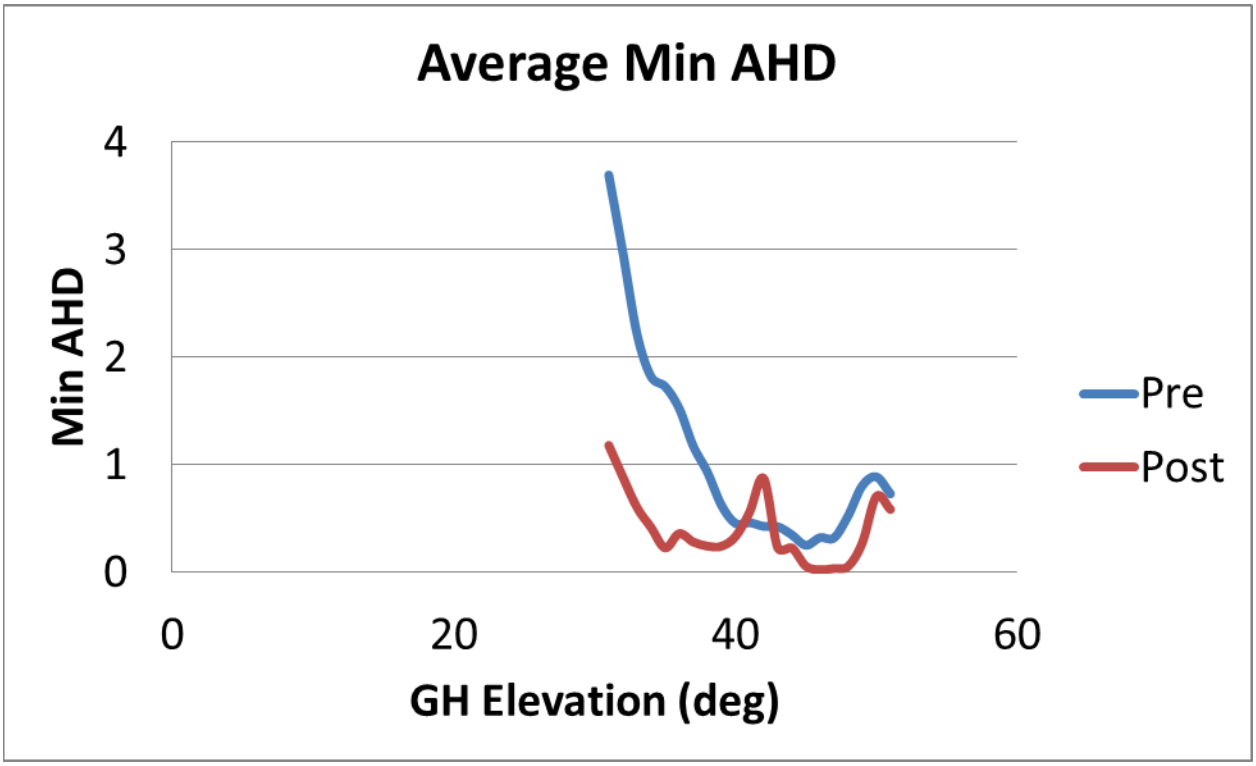
Average Min AHD
Min AHD
4
3
2
1
0
0
20
40
60
GH Elevation (deg)
Pre
Post

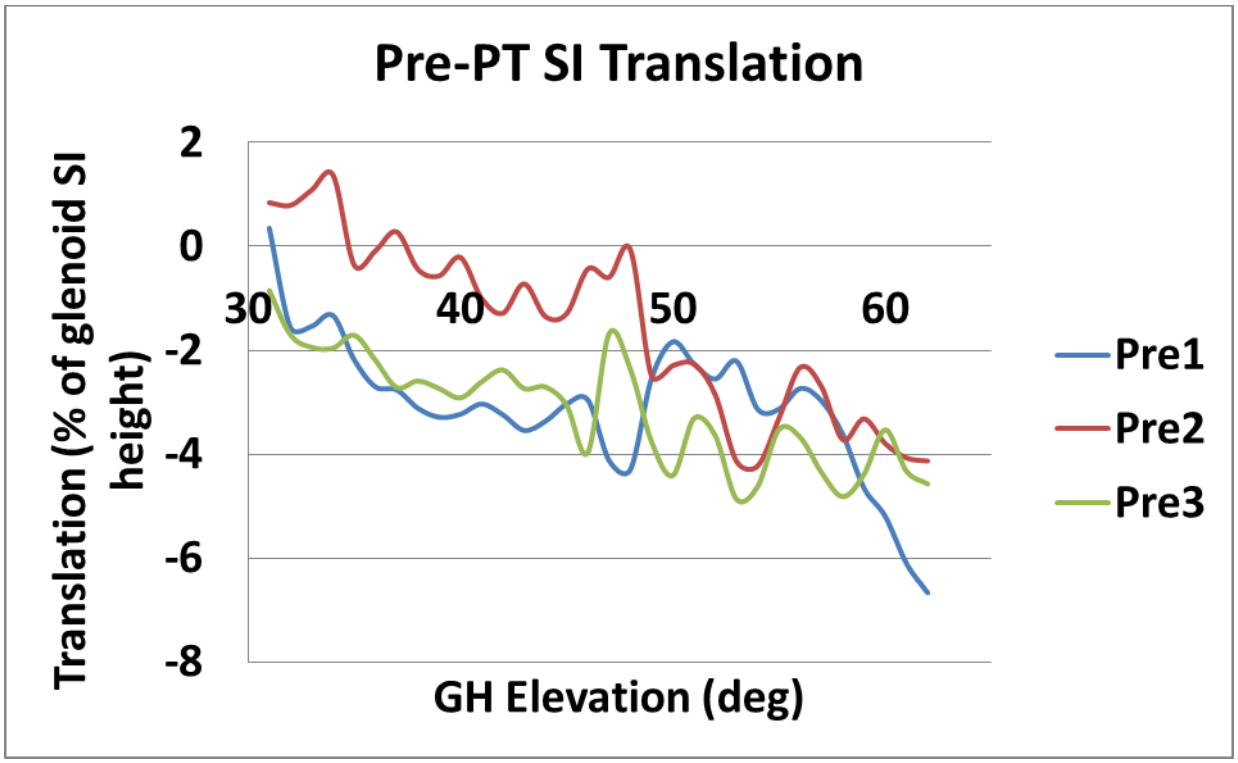
Pre-PT SI Translation
Translation (% of glenoid SI height)
2
0
-2
-4
-6
-8
30
40
50
60
GH Elevation (deg)
Pre1
Pre2
Pre3

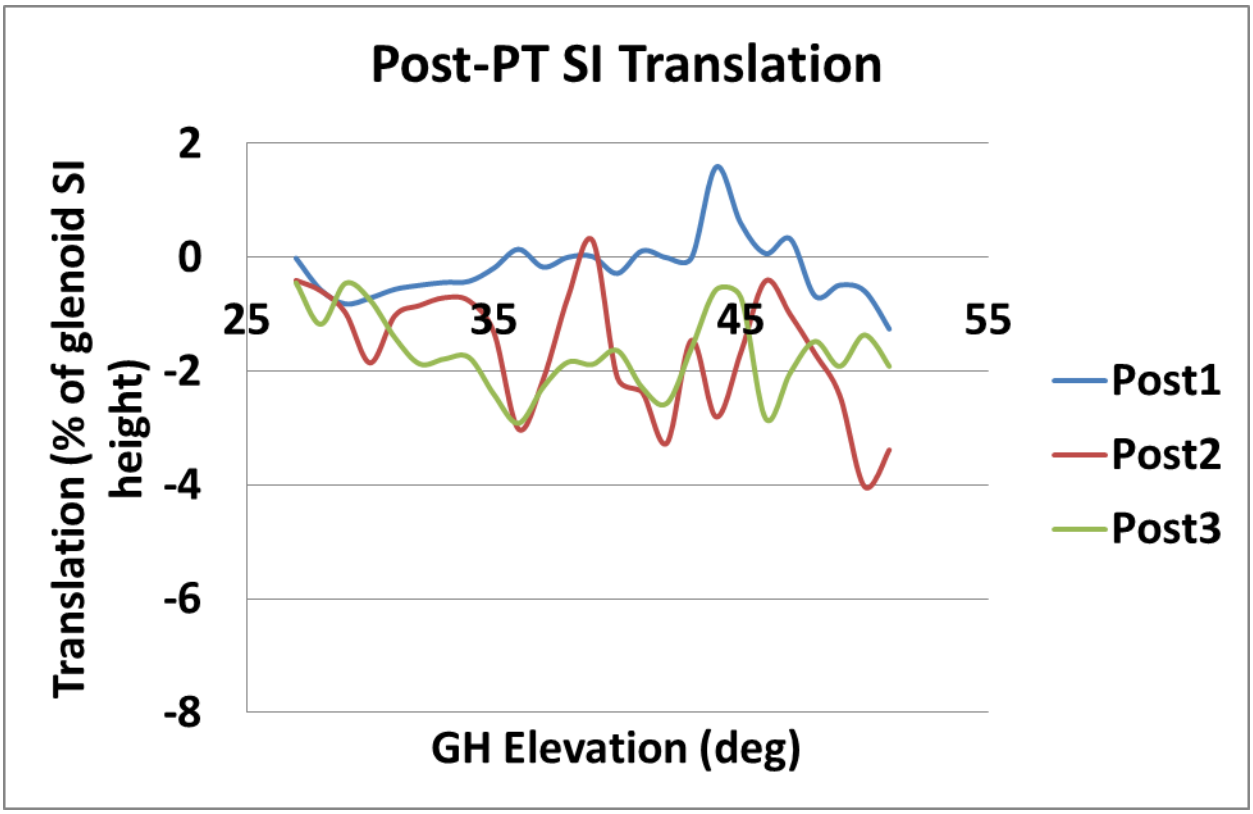
Post-PT SI Translation
Translation (% of glenoid SI height)
2
0
-2
-4
-6
-8
25
35
45
55
GH Elevation (deg)
Post1
Post2
Post3

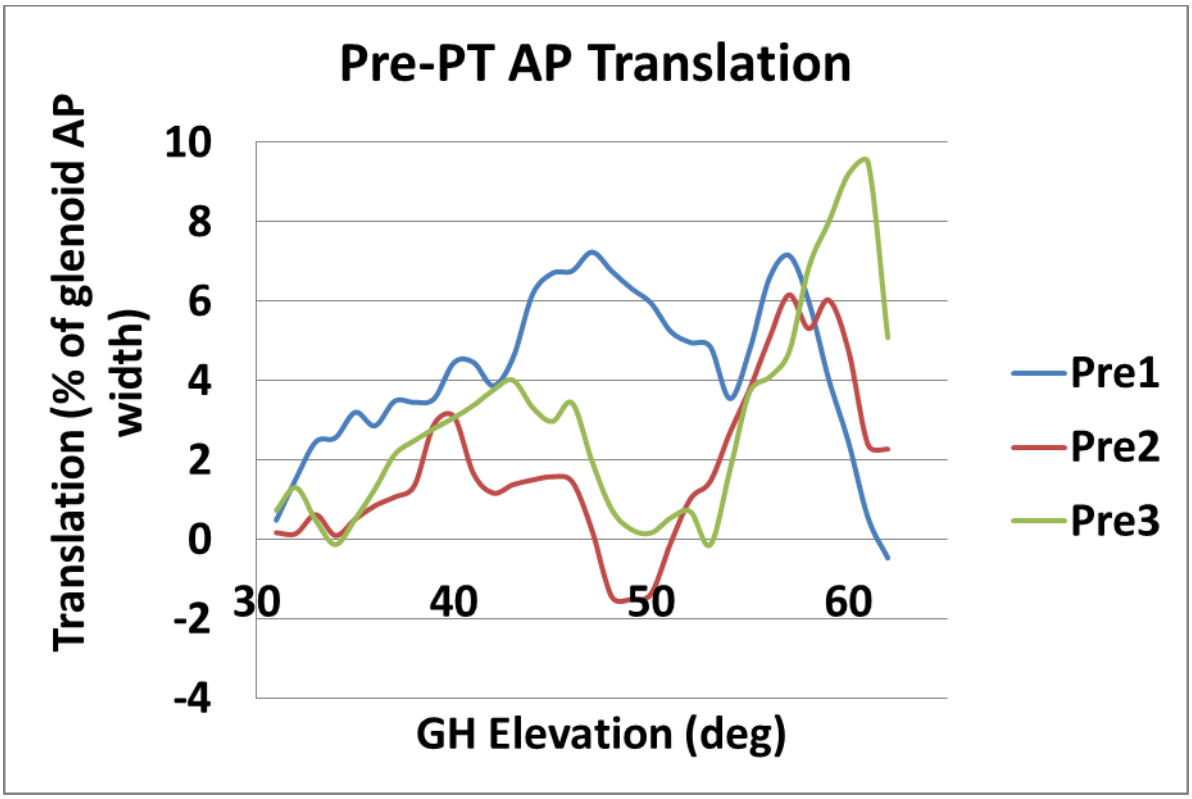
Pre-PT AP Translation
Translation (% of glenoid AP width)
10
8
6
4
2
0
-2
-4
30
40
50
60
GH Elevation (deg)
Pre1
Pre2
Pre3

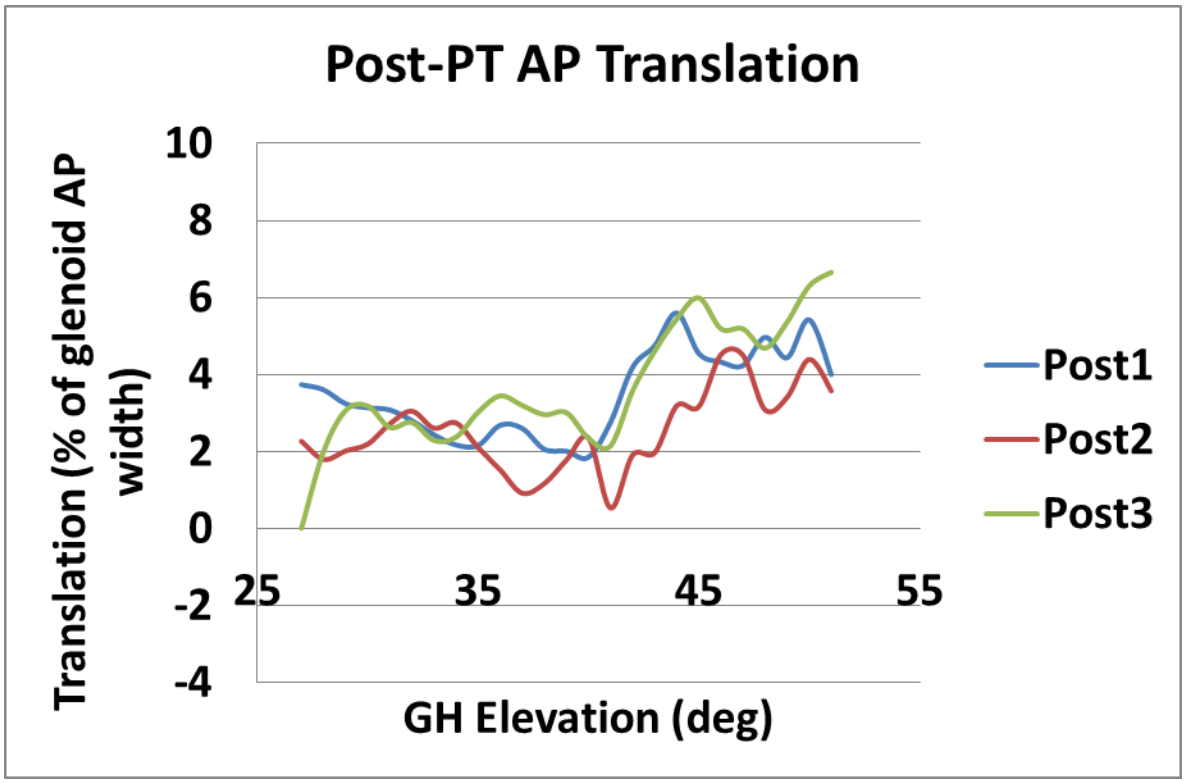
Post-PT AP Translation
Translation (% of glenoid AP width)
10
8
6
4
2
0
-2
-4
25
35
45
55
GH Elevation (deg)
Post1
Post2
Post3

RC-04

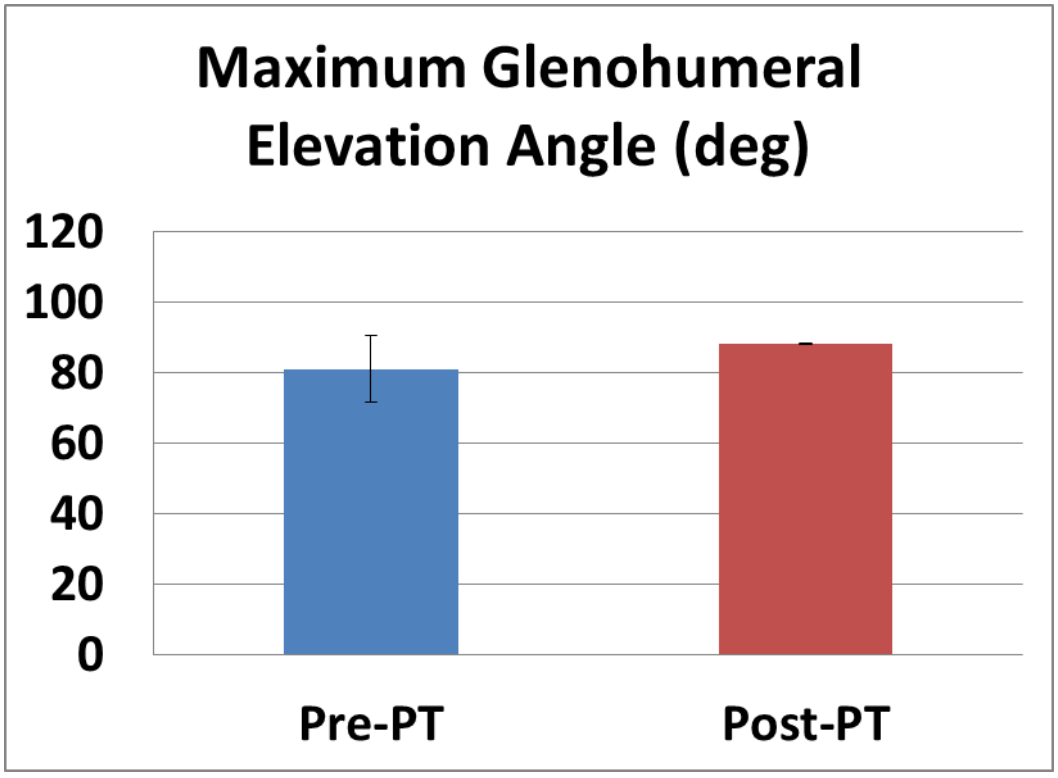
Maximum Glenohumeral Elevation Angle (deg)
120
100
80
60
40
20
0
Pre-PT
Post-PT

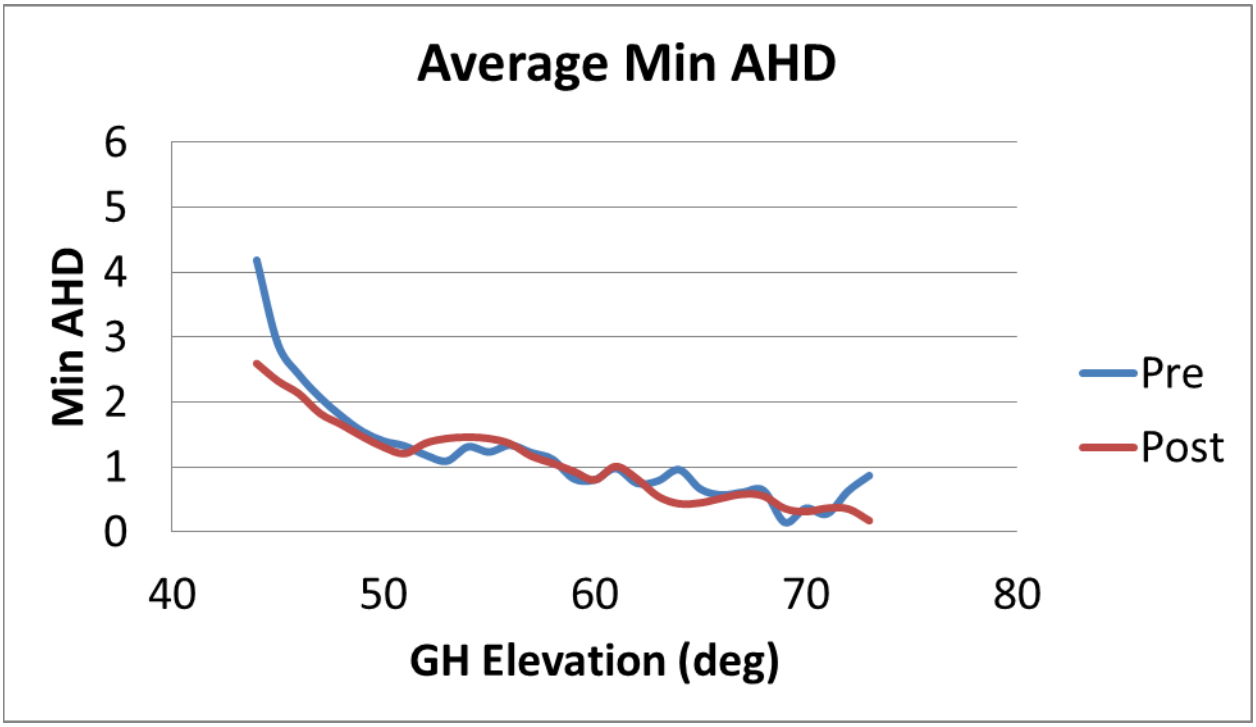
Average Min AHD
Min AHD
6
5
4
3
2
1
0
40
50
60
70
80
GH Elevation (deg)
Pre
Post

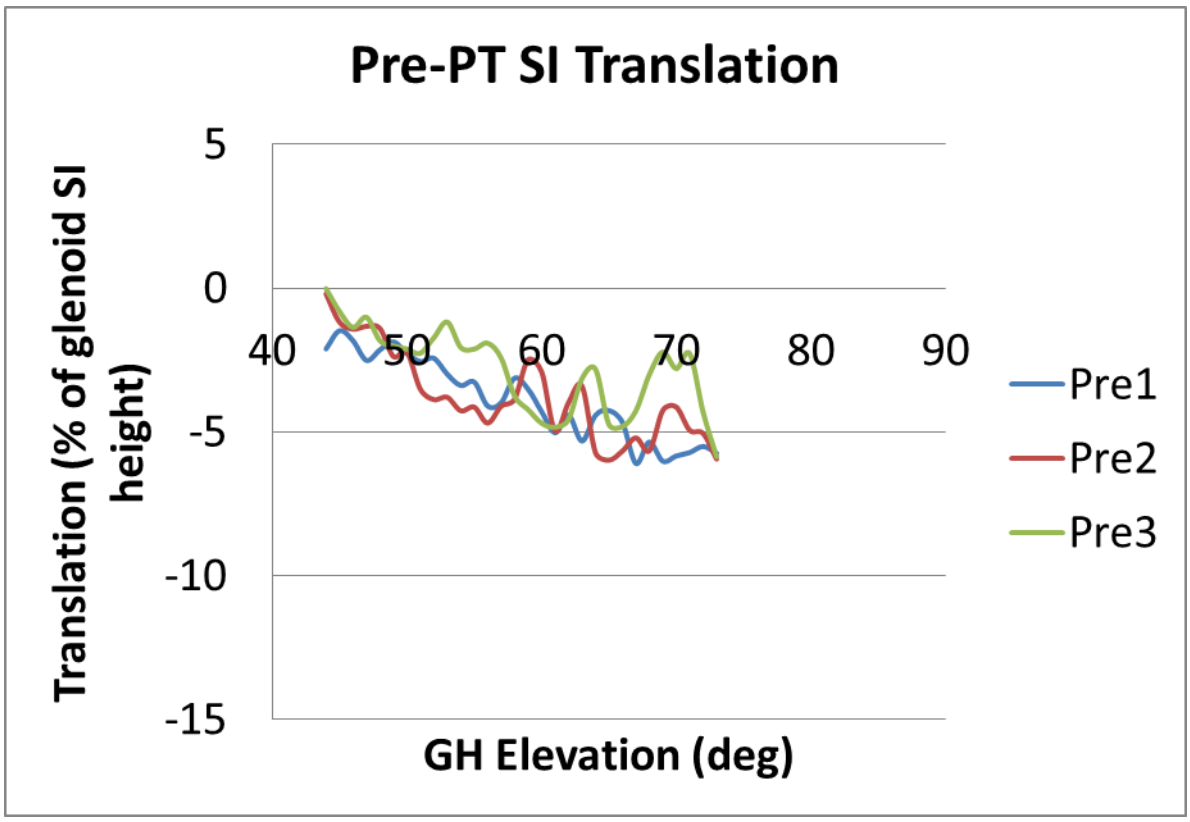
Pre-PT SI Translation
Translation (% of glenoid SI height)
5
0
-5
-10
-15
40
50
60
70
80
90
GH Elevation (deg)
Pre1
Pre2
Pre3

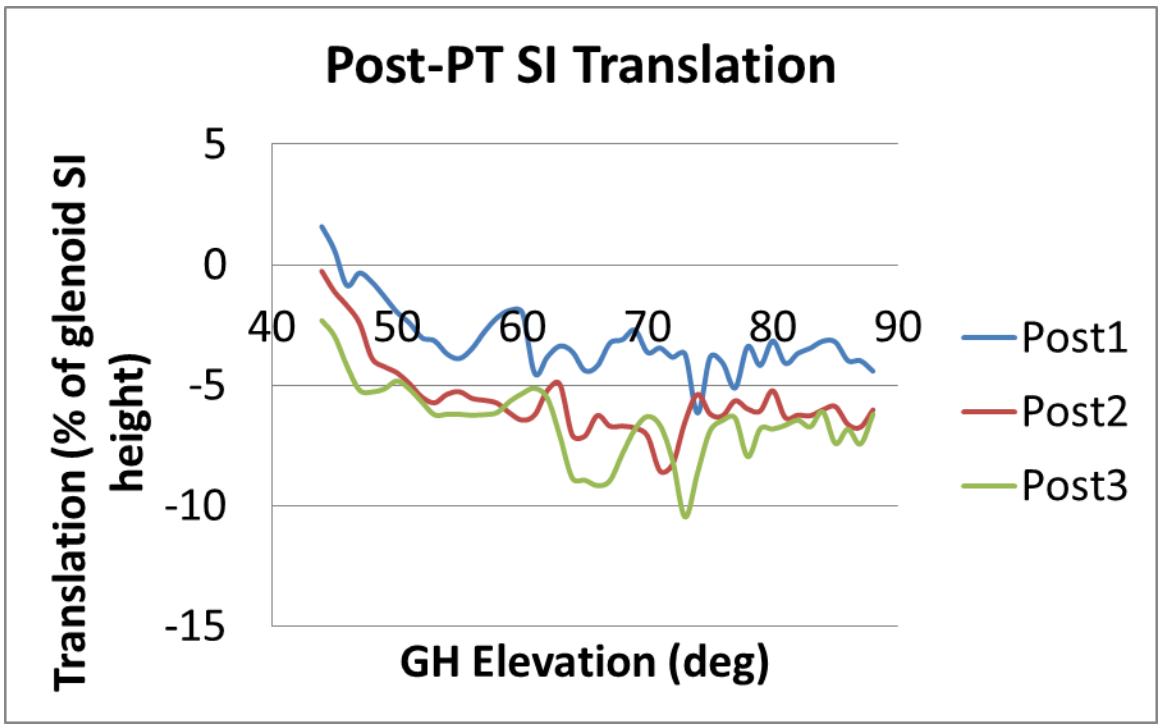
Post-PT SI Translation
Translation (% of glenoid SI height)
5
0
-5
-10
-15
40
50
60
70
80
90
GH Elevation (deg)
Post1
Post2
Post3

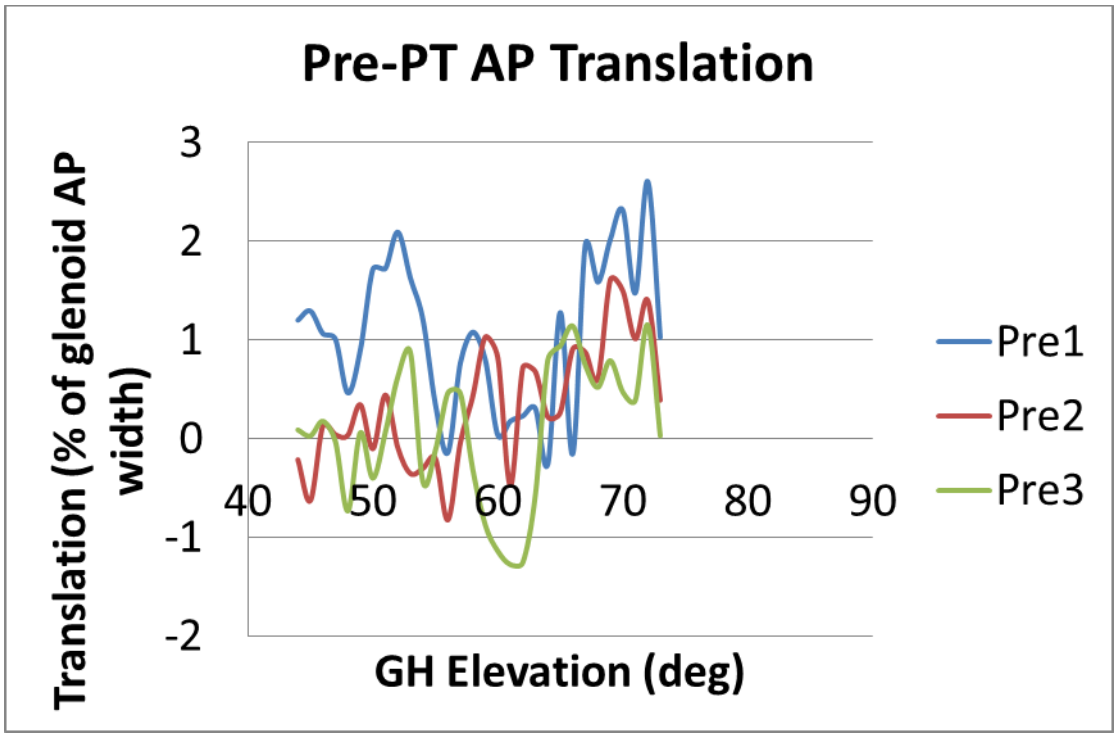
Pre-PT AP Translation
Translation (% of glenoid AP width)
3
2
1
0
-1
-2
40
50
60
70
80
90
GH Elevation (deg)
Pre1
Pre2
Pre3

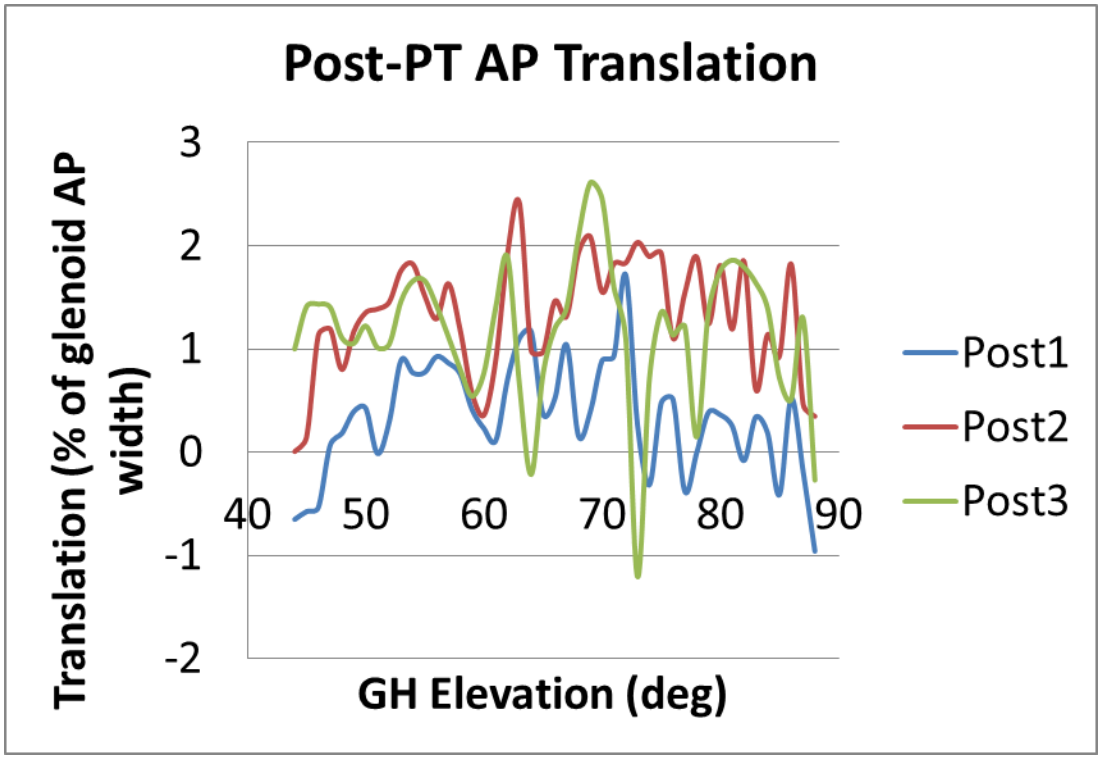
Post-PT AP Translation
Translation (% of glenoid AP width)
3
2
1
0
-1
-2
40
50
60
70
80
90
GH Elevation (deg)
Post1
Post2
Post3

RC-05

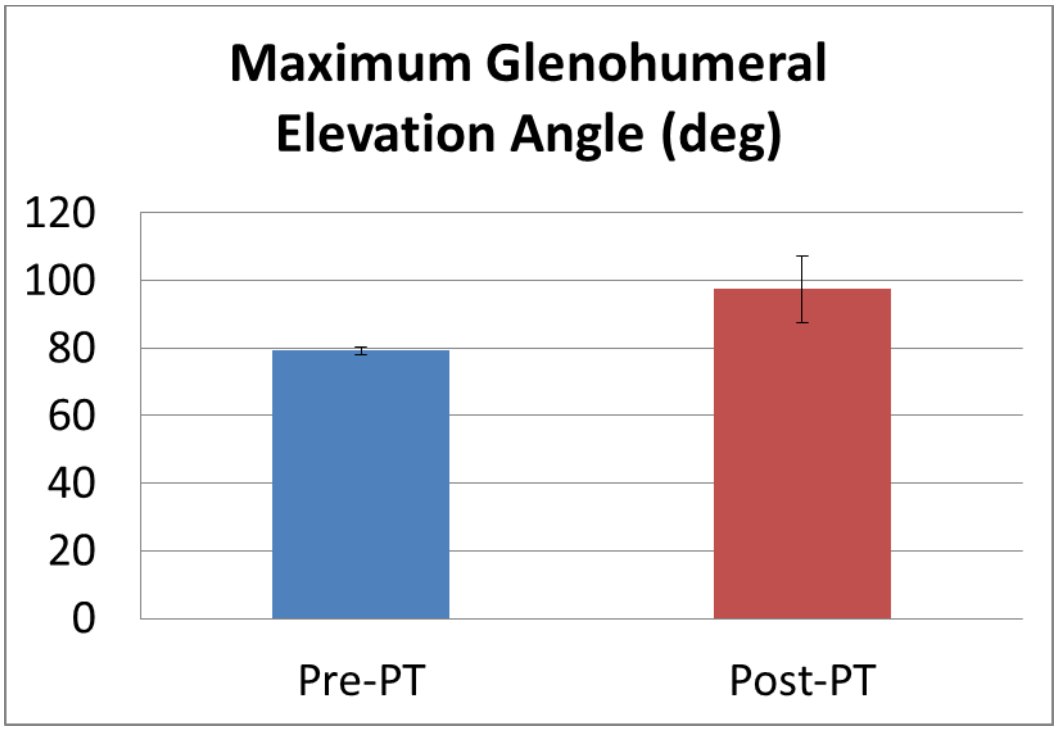
Maximum Glenohumeral Elevation Angle (deg)
120
100
80
60
40
20
0
Pre-PT
Post-PT

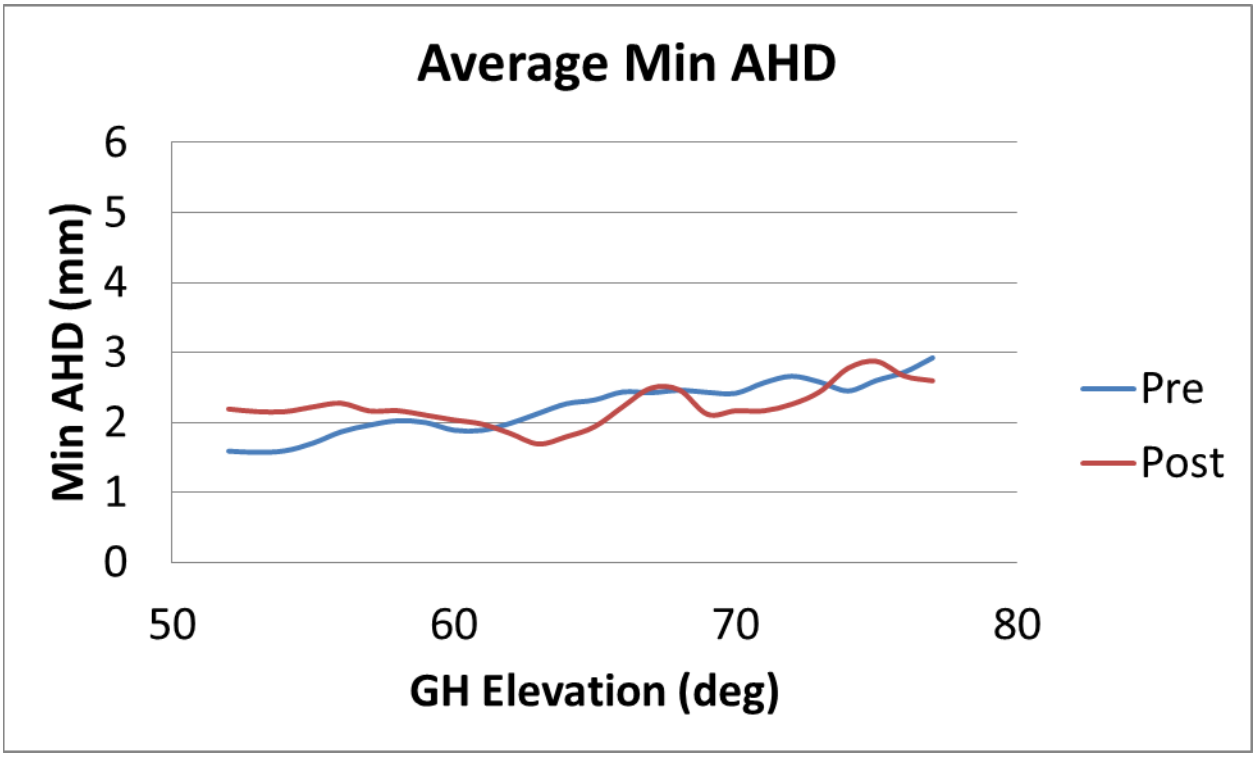
Average Min AHD
Min AHD (mm)
6
5
4
3
2
1
0
50
60
70
80
GH Elevation (deg)
Pre
Post

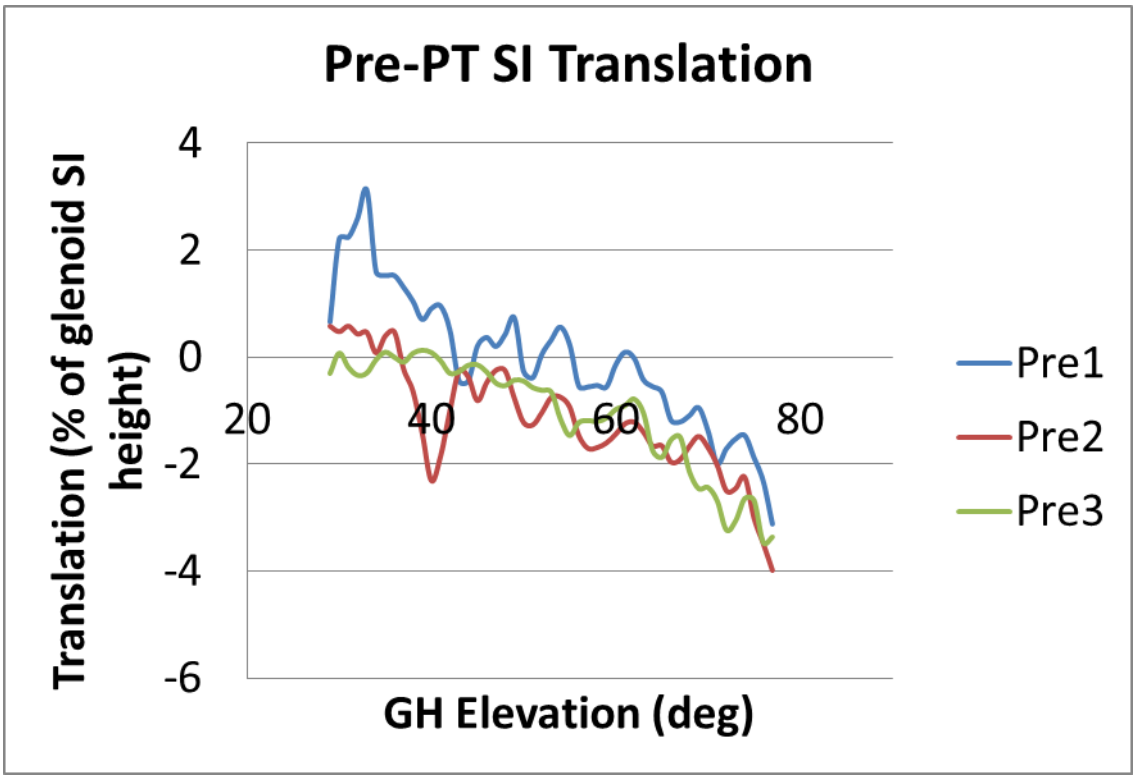
Pre-PT SI Translation
Translation (% of glenoid SI height)
4
2
0
-2
-4
-6
20
40
60
80
GH Elevation (deg)
Pre1
Pre2
Pre3

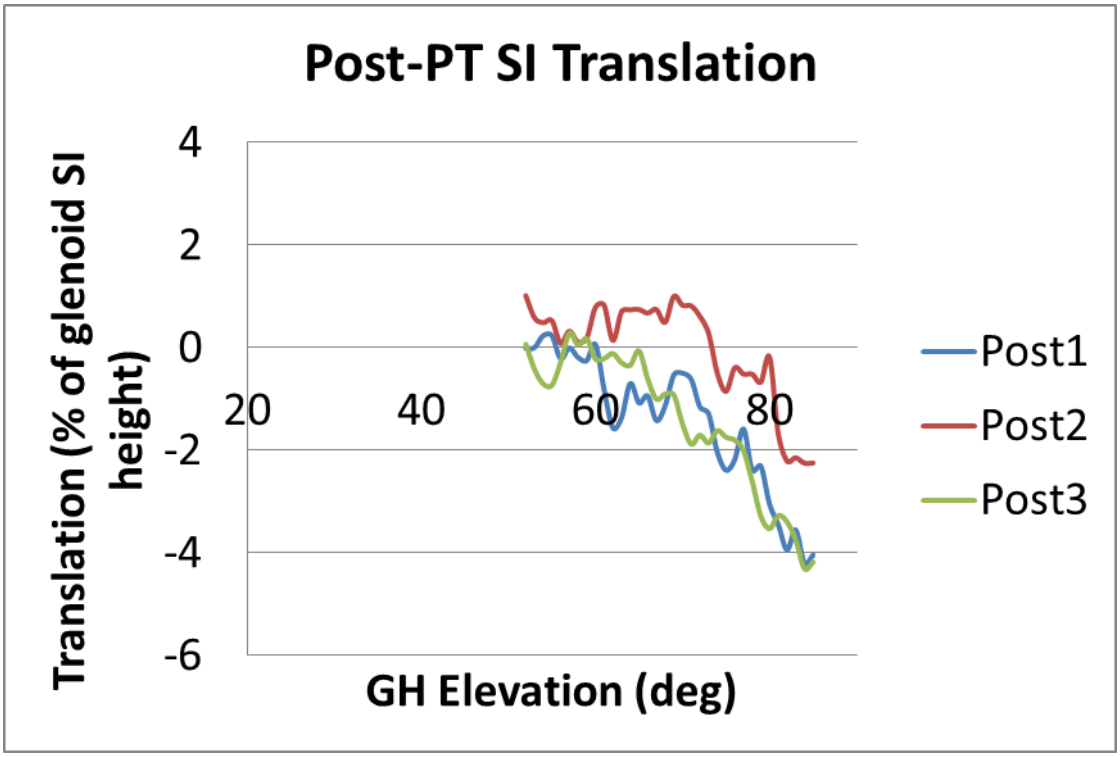
Post-PT SI Translation
Translation (% of glenoid SI height)
4
2
0
-2
-4
-6
20
40
60
80
GH Elevation (deg)
Post1
Post2
Post3

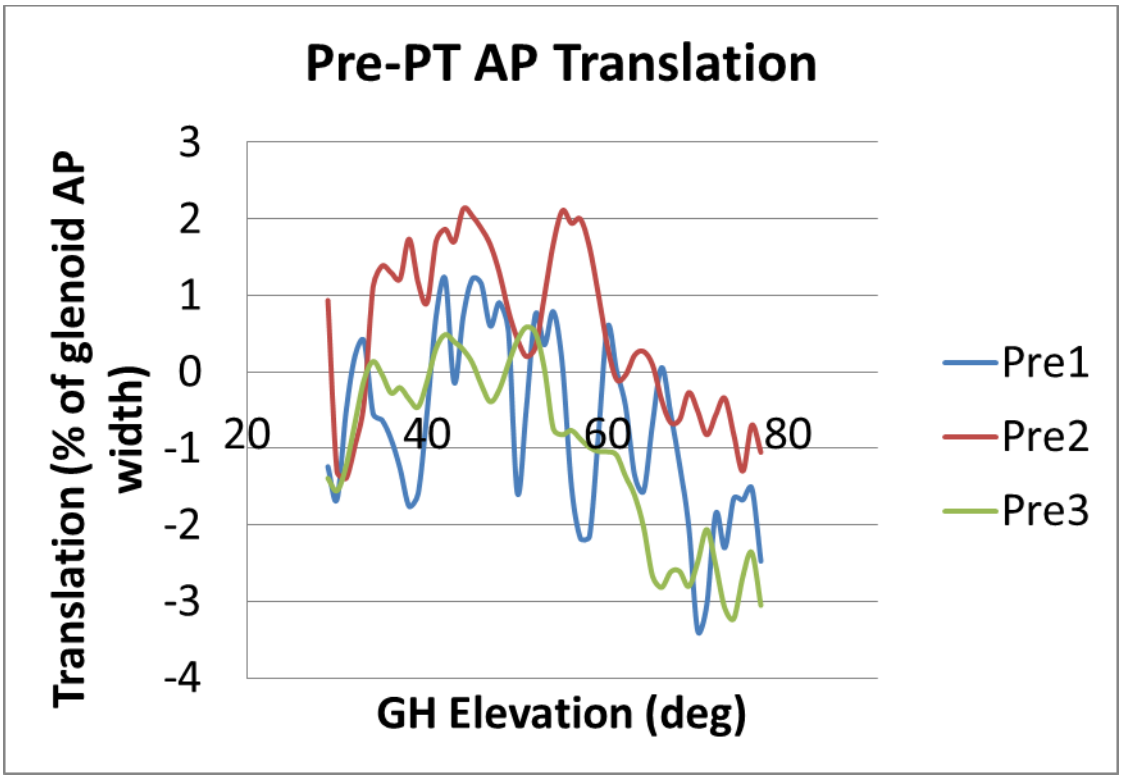
Pre-PT AP Translation
Translation (% of glenoid AP width)
3
2
1
0
-1
-2
-3
-4
20
40
60
80
GH Elevation (deg)
Pre1
Pre2
Pre3

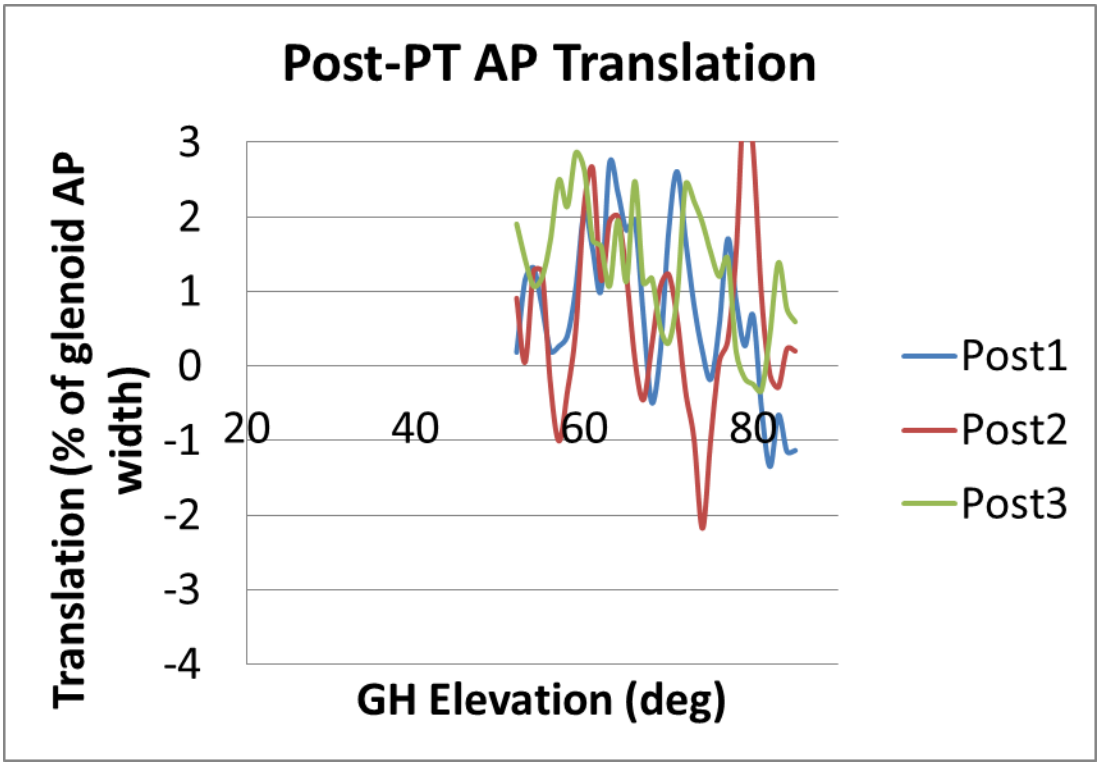
Post-PT AP Translation
Translation (% of glenoid AP width)
3
2
1
0
-1
-2
-3
-4
20
40
60
80
GH Elevation (deg)
Post1
Post2
Post3

APPENDIX B

EXPERIMENTAL STRAIN CALCULATIONS

This appendix contains ABAQUS input files for strain calculations and fringe plots of strain from experiments of anteriorly located rotator cuff tears.

B.1.1 Example Input File for 2D Strain Calculations

```
*Heading
*Preprint,echo=NO,model=NO,history=NO,contact=NO
*Part, name=BurAntTear
*End Part
*Assembly, name=Assembly
*Instance, name= BurAntTear, part= BurAntTear
*Node
1       ,       -14.53313       ,       28.50044
2       ,       -10.1841        ,       27.8379
3       ,       -5.21508        ,       27.41697
4       ,       0.74636         ,       27.19281
5       ,       5.89655         ,       26.05737
6       ,       -13.25906       ,       32.2193
7       ,       -8.9009         ,       32.15996
8       ,       -5.07836        ,       31.96864
9       ,       0.40841         ,       30.76445
10      ,       5.13285         ,       30.04547
11      ,       -11.70849       ,       36.10368
12      ,       -7.8865         ,       36.2636
13      ,       -4.6055         ,       36.62672
14      ,       0.09931         ,       35.17944
```

15 , 4.34327 , 33.61769
16 , -9.52859 , 40.93072
17 , -6.17399 , 42.79921
18 , -2.92249 , 41.54364
19 , 0.44082 , 40.68103
20 , 3.87057 , 38.65548

*Element, type=M3D4
1,1,2,7,6
2,2,3,8,7
3,3,4,9,8
4,4,5,10,9
5,6,7,12,11
6,7,8,13,12
7,8,9,14,13
8,9,10,15,14
9,11,12,17,16
10,12,13,18,17
11,13,14,19,18
12,14,15,20,19

*Elset, elset=_PickedSet2, internal, generate
1, 1500, 1
*Membrane Section, elset=_PickedSet2, material=Material-1
0.02,
*End Instance
*NSET, nset=node1, internal, instance=CapsuleInstance
1
*NSET, nset=node2, internal, instance=CapsuleInstance
2
*NSET, nset=node3, internal, instance=CapsuleInstance
3
*NSET, nset=node4, internal, instance=CapsuleInstance
4
*NSET, nset=node5, internal, instance=CapsuleInstance
5
*NSET, nset=node6, internal, instance=CapsuleInstance
6
*NSET, nset=node7, internal, instance=CapsuleInstance
7
*NSET, nset=node8, internal, instance=CapsuleInstance
8
*NSET, nset=node9, internal, instance=CapsuleInstance
9
*NSET, nset=node10, internal, instance=CapsuleInstance

```
10
*NSET, nset=node11, internal, instance=CapsuleInstance
11
*NSET, nset=node12, internal, instance=CapsuleInstance
12
*NSET, nset=node13, internal, instance=CapsuleInstance
13
*NSET, nset=node14, internal, instance=CapsuleInstance
14
*NSET, nset=node15, internal, instance=CapsuleInstance
15
*NSET, nset=node16, internal, instance=CapsuleInstance
16
*NSET, nset=node17, internal, instance=CapsuleInstance
17
*NSET, nset=node18, internal, instance=CapsuleInstance
18
*NSET, nset=node19, internal, instance=CapsuleInstance
19
*NSET, nset=node20, internal, instance=CapsuleInstance
20
*End Assembly
*Material, name=Material-1
*Hyperelastic, mooney-rivlin
0.02, 0.02,   0.
**-----------------------------------------------------------
*Step, name=scan2C,nlgeom=YES
*Static
0.05, 1., 1e-05, 1.
*Boundary
node1  ,       1       ,       1       ,       2.69057
node1  ,       2       ,       2       ,       0.52196
node2  ,       1       ,       1       ,       2.591
node2  ,       2       ,       2       ,       -0.02721
node3  ,       1       ,       1       ,       2.50869
node3  ,       2       ,       2       ,       0.30923
node4  ,       1       ,       1       ,       2.31594
node4  ,       2       ,       2       ,       0.49086
node5  ,       1       ,       1       ,       2.31495
node5  ,       2       ,       2       ,       0.31248
node6  ,       1       ,       1       ,       2.59193
node6  ,       2       ,       2       ,       0.86584
node7  ,       1       ,       1       ,       2.60537
node7  ,       2       ,       2       ,       1.01879
node8  ,       1       ,       1       ,       2.1667
node8  ,       2       ,       2       ,       1.44444
```

```
node9  ,      1      ,      1      ,      2.40324
node9  ,      2      ,      2      ,      1.21047
node10,       1      ,      1      ,      2.44908
node10,       2      ,      2      ,      0.88671
node11,       1      ,      1      ,      2.58859
node11,       2      ,      2      ,      1.1344
node12,       1      ,      1      ,      2.54278
node12,       2      ,      2      ,      1.22837
node13,       1      ,      1      ,      2.61931
node13,       2      ,      2      ,      1.4858
node14,       1      ,      1      ,      2.56889
node14,       2      ,      2      ,      1.08131
node15,       1      ,      1      ,      2.54588
node15,       2      ,      2      ,      1.05792
node16,       1      ,      1      ,      2.56063
node16,       2      ,      2      ,      1.62757
node17,       1      ,      1      ,      2.77715
node17,       2      ,      2      ,      1.40117
node18,       1      ,      1      ,      2.75554
node18,       2      ,      2      ,      1.31802
node19,       1      ,      1      ,      2.76959
node19,       2      ,      2      ,      1.2693
node20,       1      ,      1      ,      2.72365
node20,       2      ,      2      ,      1.0815


*Restart, write, frequency=1
*Output, field
*Node Output
COORD, U
*Element Output
3
EE,S
*Output, history, variable=PRESELECT
*El Print, freq=999999
*Node Print, freq=999999
*End Step
```

B.1.2 Example Input File for 3D Strain Calculations

```
*Heading
*Preprint,echo=NO,model=NO,history=NO,contact=NO
*Part, name=90degArticular
*End Part
```

*Assembly, name=Assembly
*Instance, name=90degArticular, part=90degArticular
*Node
1 , 49.276714 , -81.677063 , 37.882072
2 , 48.260014 , -78.371086 , 38.340618
3 , 49.001202 , -74.835304 , 38.570724
4 , 49.25095 , -71.018303 , 38.17482
5 , 49.943153 , -67.502098 , 37.364765
6 , 51.799294 , -65.110573 , 36.481583
7 , 49.9044 , -81.912834 , 43.739582
8 , 49.319096 , -79.31855 , 43.217808
9 , 48.849483 , -75.861855 , 43.625656
10 , 49.080101 , -70.959122 , 42.180443
11 , 50.430359 , -67.57267 , 41.48175
12 , 51.288937 , -63.885929 , 41.129707
13 , 49.380054 , -82.121742 , 48.257473
14 , 48.005566 , -78.561775 , 48.293266
15 , 47.823639 , -74.695511 , 46.794605
16 , 47.698669 , -71.397606 , 46.738861
17 , 48.779877 , -66.868294 , 45.880447
18 , 49.546879 , -63.475834 , 45.701839
19 , 48.100739 , -83.381027 , 52.35725
20 , 47.456776 , -79.123863 , 53.510632
21 , 46.735703 , -74.52388 , 52.770046
22 , 46.779003 , -71.369286 , 53.077457
23 , 46.745972 , -68.143311 , 53.154922
24 , 47.871883 , -63.755169 , 50.453362

*Element, type=M3D4
1,1,2,8,7
2,2,3,9,8
3,3,4,10,9
4,4,5,11,10
5,5,6,12,11
6,7,8,14,13
7,8,9,15,14
8,9,10,16,15
9,10,11,17,16
10,11,12,18,17
11,13,14,20,19
12,14,15,21,20
13,15,16,22,21
14,16,17,23,22
15,17,18,24,23

*Elset, elset=_PickedSet2, internal, generate

1, 1500,   1
*Membrane Section, elset=_PickedSet2, material=Material-1
0.02,
*End Instance
*NSET, nset=node1, internal, instance=CapsuleInstance
1
*NSET, nset=node2, internal, instance=CapsuleInstance
2
*NSET, nset=node3, internal, instance=CapsuleInstance
3
*NSET, nset=node4, internal, instance=CapsuleInstance
4
*NSET, nset=node5, internal, instance=CapsuleInstance
5
*NSET, nset=node6, internal, instance=CapsuleInstance
6
*NSET, nset=node7, internal, instance=CapsuleInstance
7
*NSET, nset=node8, internal, instance=CapsuleInstance
8
*NSET, nset=node9, internal, instance=CapsuleInstance
9
*NSET, nset=node10, internal, instance=CapsuleInstance
10
*NSET, nset=node11, internal, instance=CapsuleInstance
11
*NSET, nset=node12, internal, instance=CapsuleInstance
12
*NSET, nset=node13, internal, instance=CapsuleInstance
13
*NSET, nset=node14, internal, instance=CapsuleInstance
14
*NSET, nset=node15, internal, instance=CapsuleInstance
15
*NSET, nset=node16, internal, instance=CapsuleInstance
16
*NSET, nset=node17, internal, instance=CapsuleInstance
17
*NSET, nset=node18, internal, instance=CapsuleInstance
18
*NSET, nset=node19, internal, instance=CapsuleInstance
19
*NSET, nset=node20, internal, instance=CapsuleInstance
20
*NSET, nset=node21, internal, instance=CapsuleInstance
21

*NSET, nset=node22, internal, instance=CapsuleInstance
22
*NSET, nset=node23, internal, instance=CapsuleInstance
23
*NSET, nset=node24, internal, instance=CapsuleInstance
24
*NSET, nset=node25, internal, instance=CapsuleInstance
25
*NSET, nset=node26, internal, instance=CapsuleInstance
26
*NSET, nset=node27, internal, instance=CapsuleInstance
27
*NSET, nset=node28, internal, instance=CapsuleInstance
28
*NSET, nset=node29, internal, instance=CapsuleInstance
29
*NSET, nset=node30, internal, instance=CapsuleInstance
30
*NSET, nset=node31, internal, instance=CapsuleInstance
31
*NSET, nset=node32, internal, instance=CapsuleInstance
32
*NSET, nset=node33, internal, instance=CapsuleInstance
33
*NSET, nset=node34, internal, instance=CapsuleInstance
34
*NSET, nset=node35, internal, instance=CapsuleInstance
35
*NSET, nset=node36, internal, instance=CapsuleInstance
36
*NSET, nset=node37, internal, instance=CapsuleInstance
37
*NSET, nset=node38, internal, instance=CapsuleInstance
38
*NSET, nset=node39, internal, instance=CapsuleInstance
39
*NSET, nset=node40, internal, instance=CapsuleInstance
40

*End Assembly
*Material, name=Material-1
*Hyperelastic, mooney-rivlin
0.02, 0.02,   0.
**---
*Step, name=scan2C,nlgeom=YES

*Static
0.05, 1., 1e-05, 1.

*Boundary
node1 , 1 , 1 , -2.994735
node1 , 2 , 2 , -0.858009
node1 , 3 , 3 , 16.762825
node2 , 1 , 1 , -2.703793
node2 , 2 , 2 , -0.899269
node2 , 3 , 3 , 17.07922
node3 , 1 , 1 , -2.779137
node3 , 2 , 2 , -0.927216
node3 , 3 , 3 , 16.964833
node4 , 1 , 1 , -3.106312
node4 , 2 , 2 , -1.211838
node4 , 3 , 3 , 16.748486
node5 , 1 , 1 , -3.913459
node5 , 2 , 2 , -1.34391
node5 , 3 , 3 , 16.351402
node6 , 1 , 1 , -4.917473
node6 , 2 , 2 , -1.103493
node6 , 3 , 3 , 16.029041
node7 , 1 , 1 , -2.385998
node7 , 2 , 2 , -0.608811
node7 , 3 , 3 , 17.33012
node8 , 1 , 1 , -3.00911
node8 , 2 , 2 , -0.609833
node8 , 3 , 3 , 17.126926
node9 , 1 , 1 , -2.700054
node9 , 2 , 2 , -0.834899
node9 , 3 , 3 , 17.012497
node10, 1 , 1 , -3.048935
node10, 2 , 2 , -1.039703
node10, 3 , 3 , 16.830498
node11, 1 , 1 , -3.736099
node11, 2 , 2 , -1.342712
node11, 3 , 3 , 16.545708
node12, 1 , 1 , -4.558537
node12, 2 , 2 , -2.250492
node12, 3 , 3 , 16.582676
node13, 1 , 1 , -1.953495
node13, 2 , 2 , -0.426033
node13, 3 , 3 , 17.53059
node14, 1 , 1 , -2.219723
node14, 2 , 2 , -1.163513
node14, 3 , 3 , 17.431603

```
node15,      1      ,      1      ,      -2.413071
node15,      2      ,      2      ,      -1.189026
node15,      3      ,      3      ,      18.025631
node16,      1      ,      1      ,      -2.460754
node16,      2      ,      2      ,      -1.647468
node16,      3      ,      3      ,      16.807816
node17,      1      ,      1      ,      -3.476281
node17,      2      ,      2      ,      -1.949737
node17,      3      ,      3      ,      16.963112
node18,      1      ,      1      ,      -3.23061
node18,      2      ,      2      ,      -2.387417
node18,      3      ,      3      ,      17.182621
node19,      1      ,      1      ,      -1.575726
node19,      2      ,      2      ,      -0.495438
node19,      3      ,      3      ,      18.299481
node20,      1      ,      1      ,      -2.115269
node20,      2      ,      2      ,      -1.33384
node20,      3      ,      3      ,      18.027477
node21,      1      ,      1      ,      -1.854073
node21,      2      ,      2      ,      -1.44738
node21,      3      ,      3      ,      17.90839
node22,      1      ,      1      ,      -2.421081
node22,      2      ,      2      ,      -1.992446
node22,      3      ,      3      ,      16.66898
node23,      1      ,      1      ,      -1.792126
node23,      2      ,      2      ,      -1.524406
node23,      3      ,      3      ,      15.852845
node24,      1      ,      1      ,      -2.681987
node24,      2      ,      2      ,      -1.978146
node24,      3      ,      3      ,      17.484962

*Restart, write, frequency=1
*Output, field
*Node Output
COORD, U
*Element Output
3
EE,S
*Output, history, variable=PRESELECT
*El Print, freq=999999
*Node Print, freq=999999
*End Step
```

B.1.3 Load-Elongation Curves for Cadaveric Anterior Tear Propagation Specimens

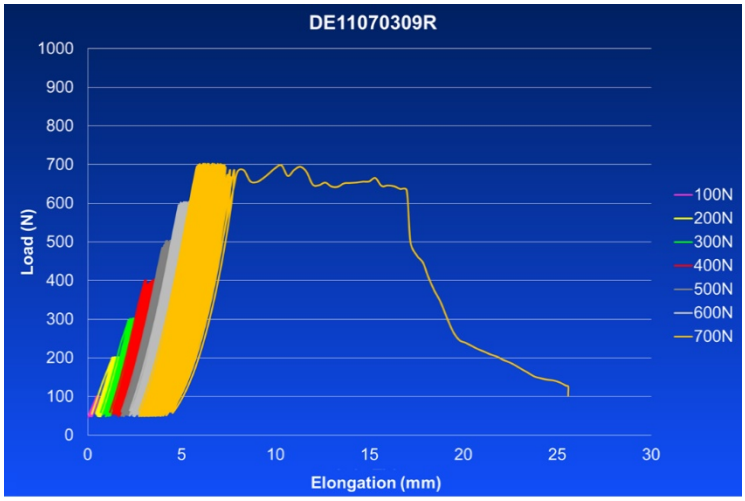

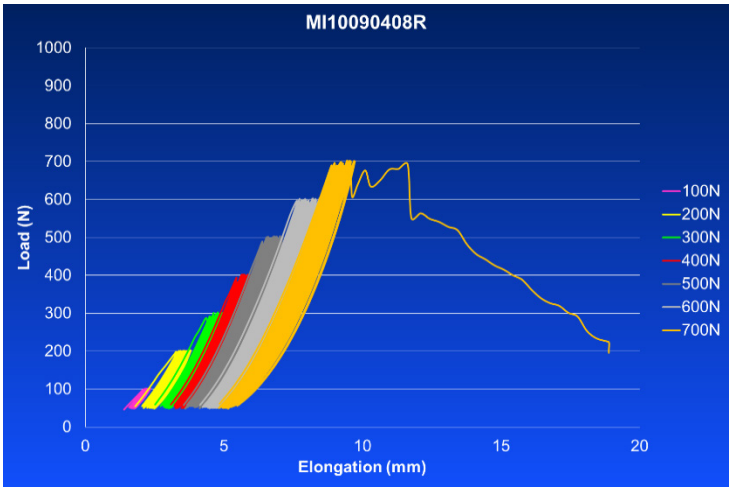

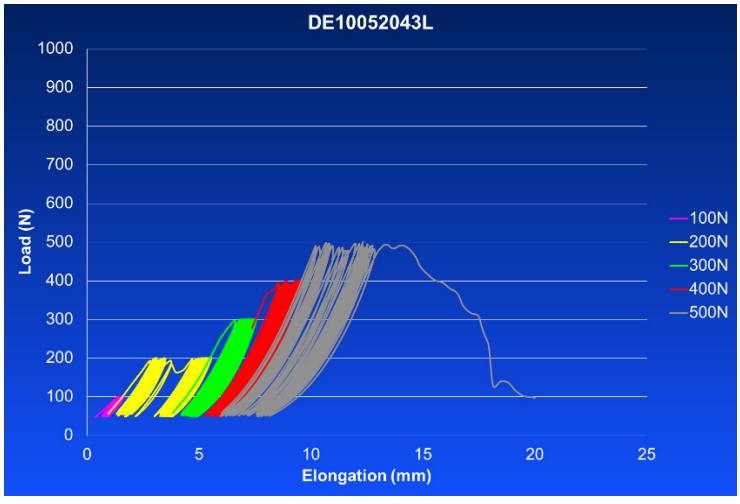

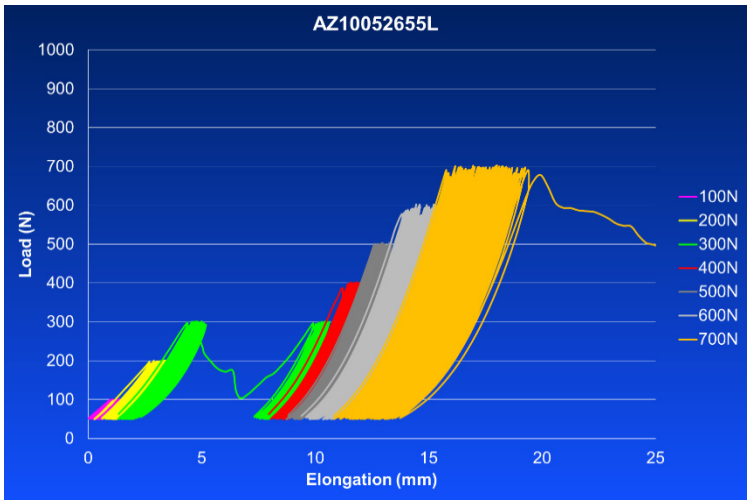
AZ10052655L
Load (N)
1000
900
800
700
600
500
400
300
200
100
0
0
5
10
15
20
25
Elongation (mm)
100N
200N
300N
400N
500N
600N
700N

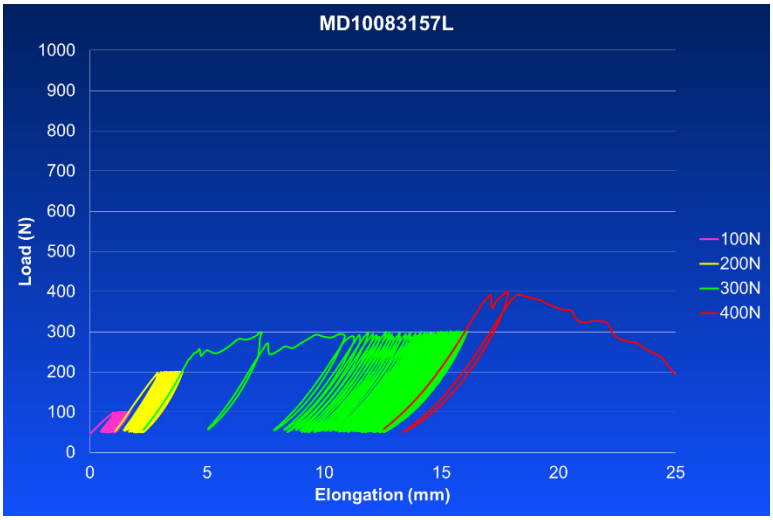
MD10083157L
Load (N)
1000
900
800
700
600
500
400
300
200
100
0
0
5
10
15
20
25
Elongation (mm)
100N
200N
300N
400N

B.1.4 Strain Fringe Plots for Cadaveric Anterior Tear Propagation Specimens

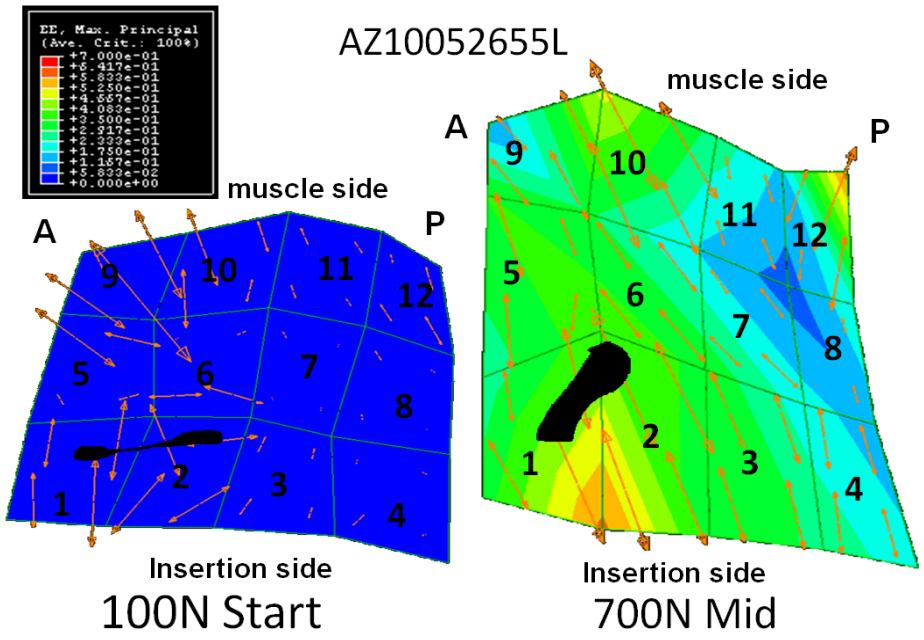

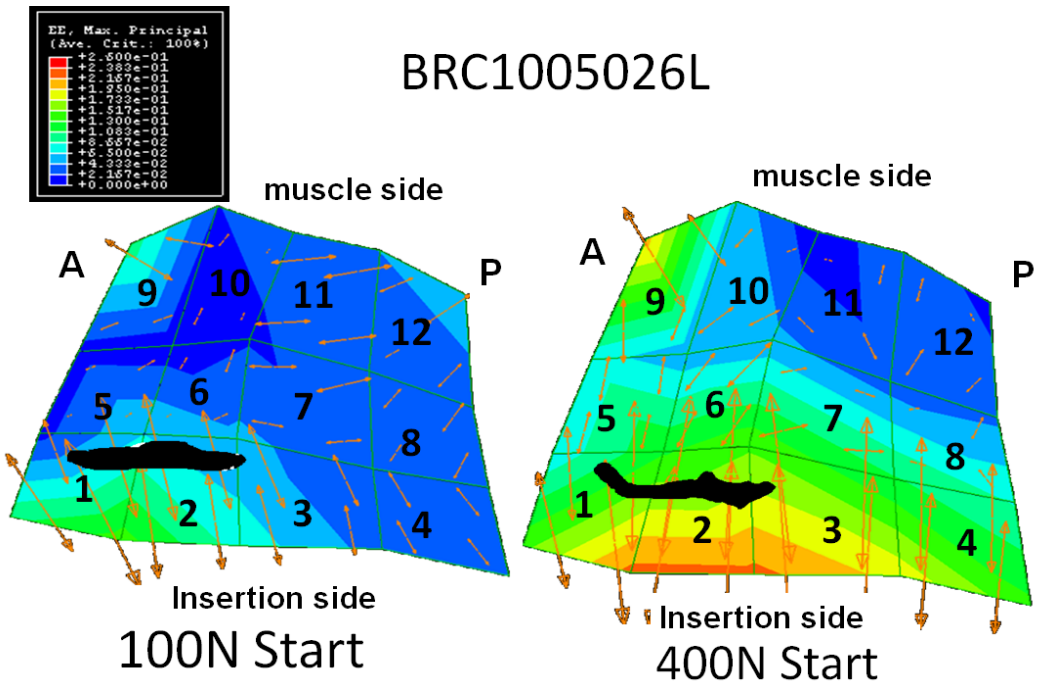

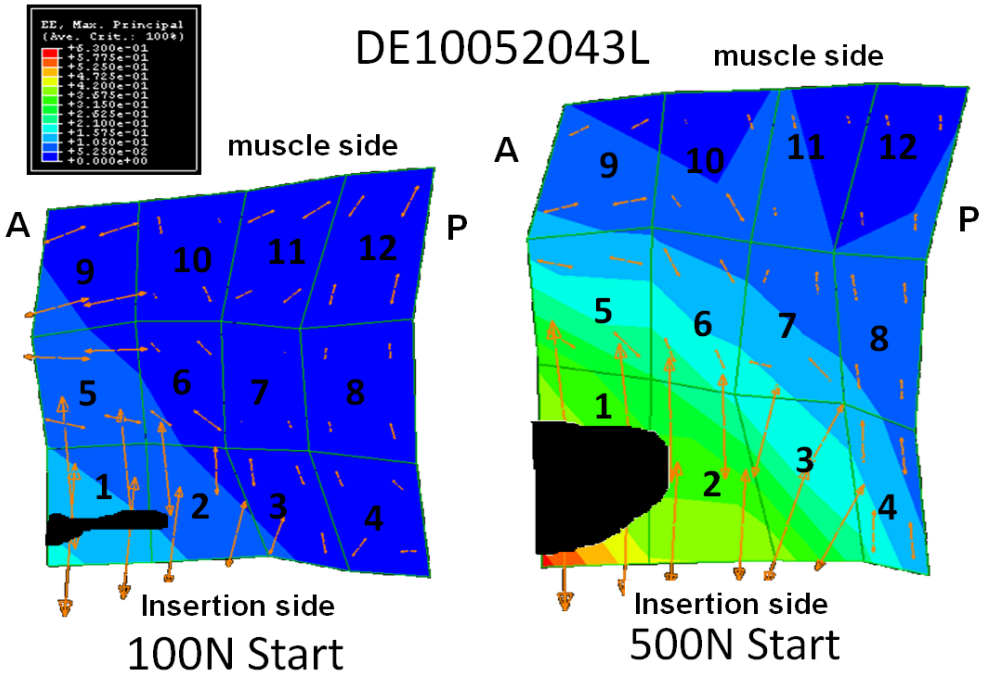
DE10052043L
muscle side
A
P
9
10
11
12
5
6
7
8
1
2
3
4
Insertion side
100N Start
muscle side
A
P
9
10
11
12
5
6
7
8
1
2
3
4
Insertion side
500N Start

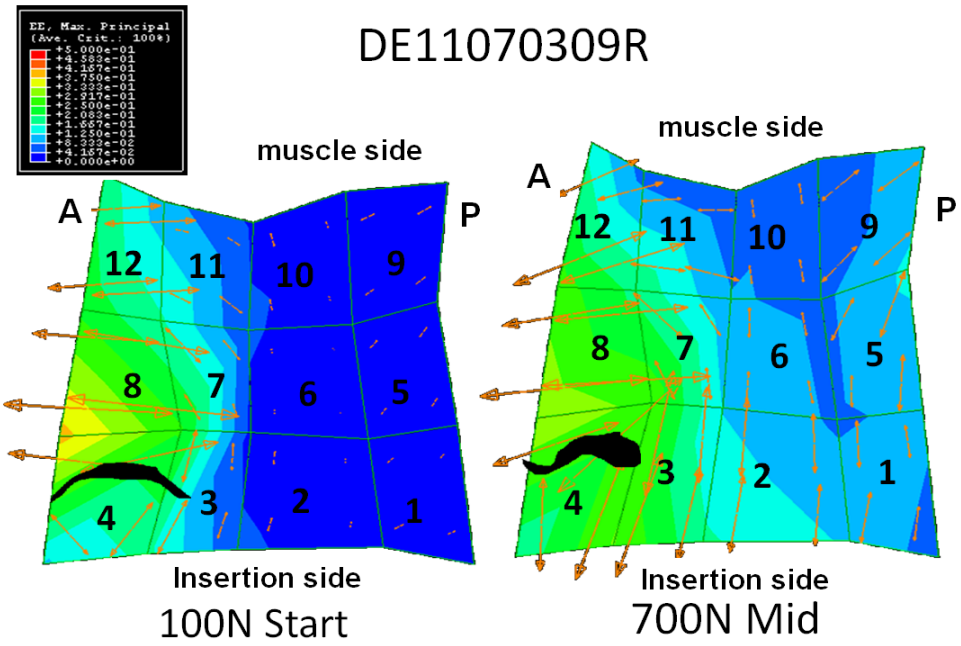
DE11070309R
muscle side
A
P
12
11
10
9
8
7
6
5
4
3
2
1
Insertion side
100N Start
muscle side
A
P
12
11
10
9
8
7
6
5
4
3
2
1
Insertion side
700N Mid

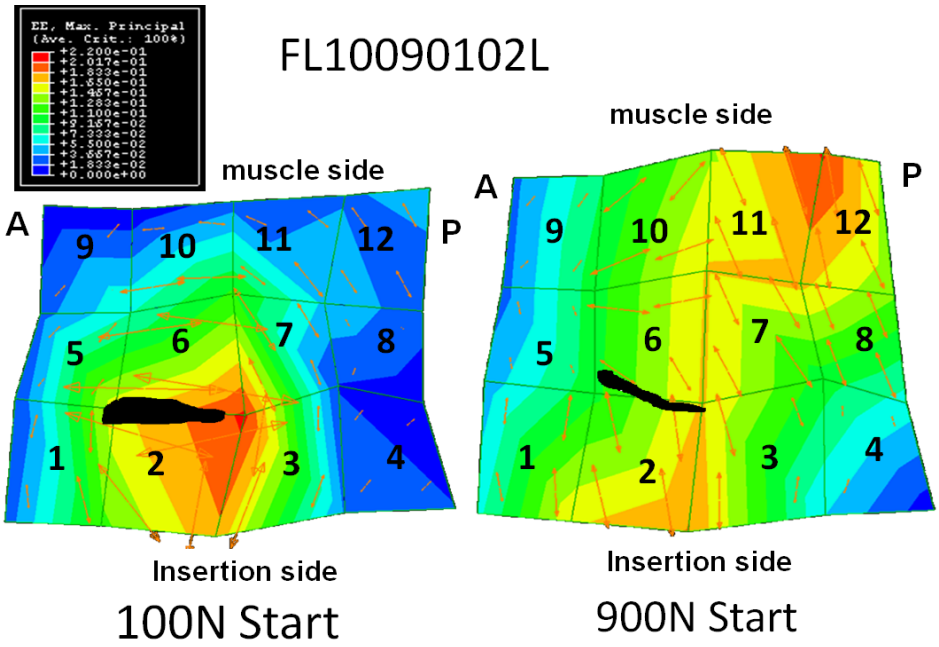
FL10090102L
muscle side
A
P
9
10
11
12
5
6
7
8
1
2
3
4
Insertion side
100N Start
muscle side
A
P
9
10
11
12
5
6
7
8
1
2
3
4
Insertion side
900N Start

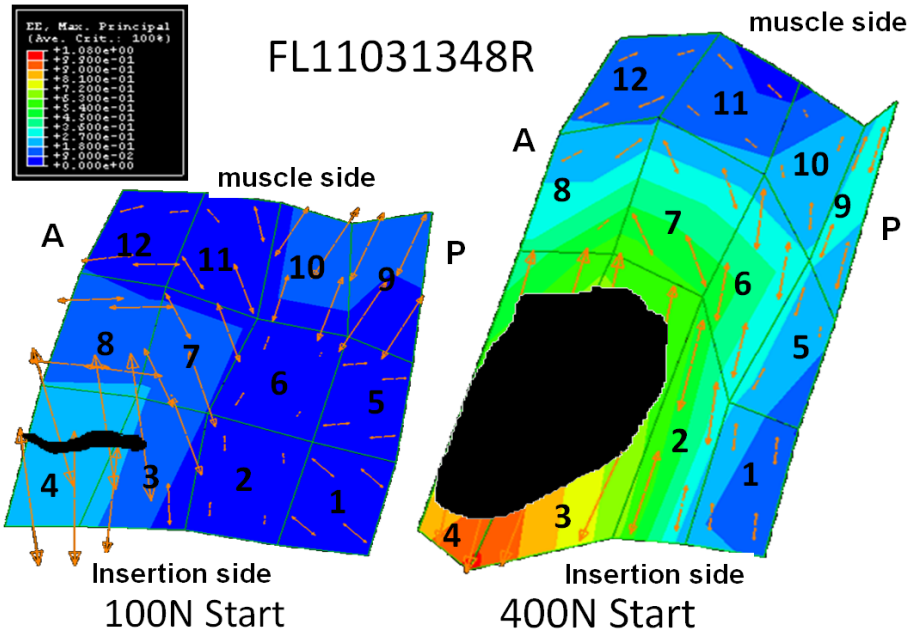
FL11031348R
muscle side
A
P
12
11
10
9
8
7
6
5
4
3
2
1
Insertion side
100N Start
muscle side
A
P
12
11
10
9
8
7
6
5
4
3
2
1
Insertion side
400N Start

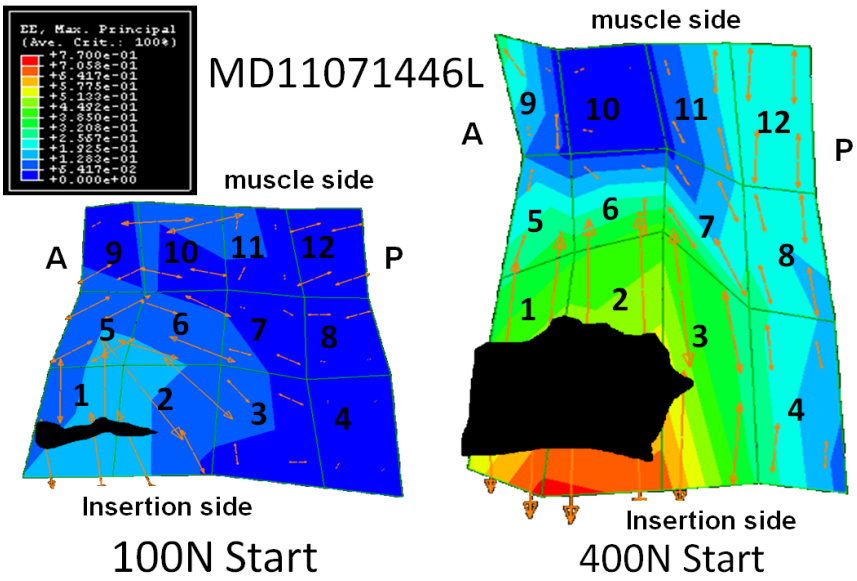
EE, Max. Principal
(Ave. Crit.: 100%)
+7.700e-01
+7.058e-01
+6.417e-01
+5.775e-01
+5.133e-01
+4.492e-01
+3.850e-01
+3.208e-01
+2.567e-01
+1.925e-01
+1.283e-01
+6.417e-02
+0.000e+00
MD11071446L
muscle side
A
P
9
10
11
12
5
6
7
8
1
2
3
4
Insertion side
100N Start
muscle side
A
P
9
10
11
12
5
6
7
8
1
2
3
4
Insertion side
400N Start

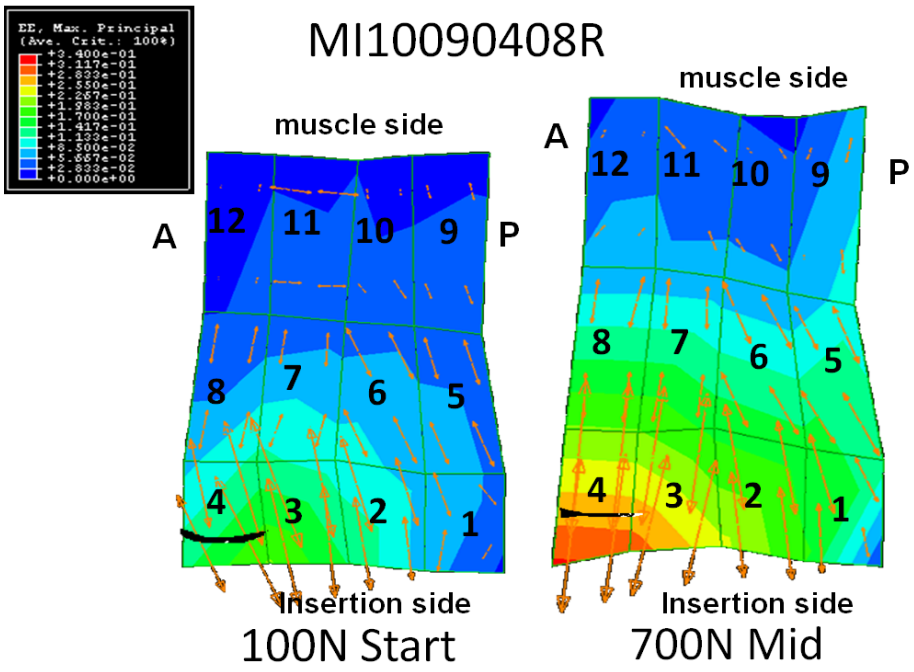
EE, Max. Principal
(Ave. Crit.: 100%)
+3.400e-01
+3.117e-01
+2.833e-01
+2.550e-01
+2.267e-01
+1.983e-01
+1.700e-01
+1.417e-01
+1.133e-01
+8.500e-02
+5.667e-02
+2.833e-02
+0.000e+00
MI10090408R
muscle side
A
P
12
11
10
9
8
7
6
5
4
3
2
1
Insertion side
100N Start
muscle side
A
P
12
11
10
9
8
7
6
5
4
3
2
1
Insertion side
700N Mid

B.1.5 Images of Bursal and Articular Tendon Surfaces During Tear Propagation

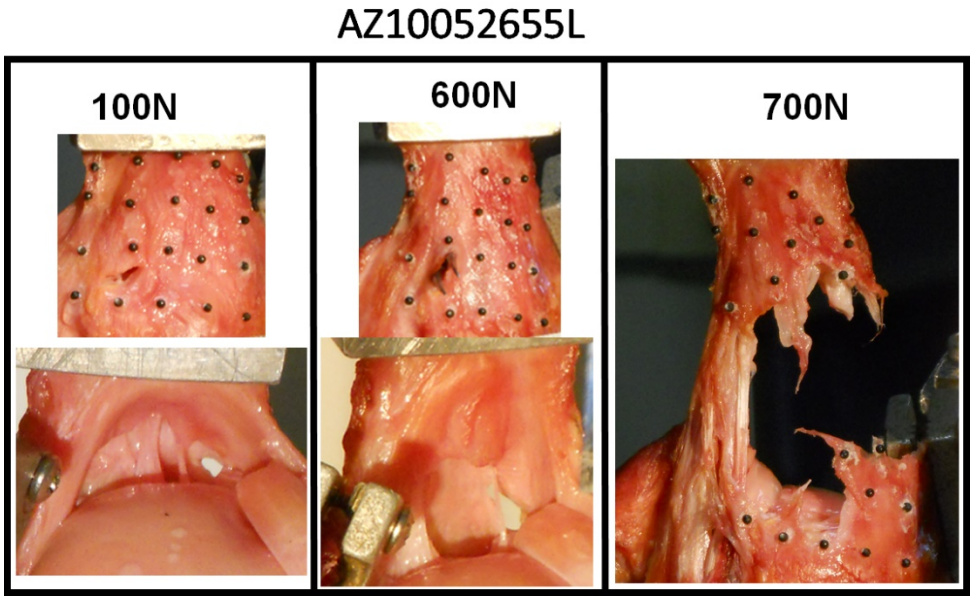

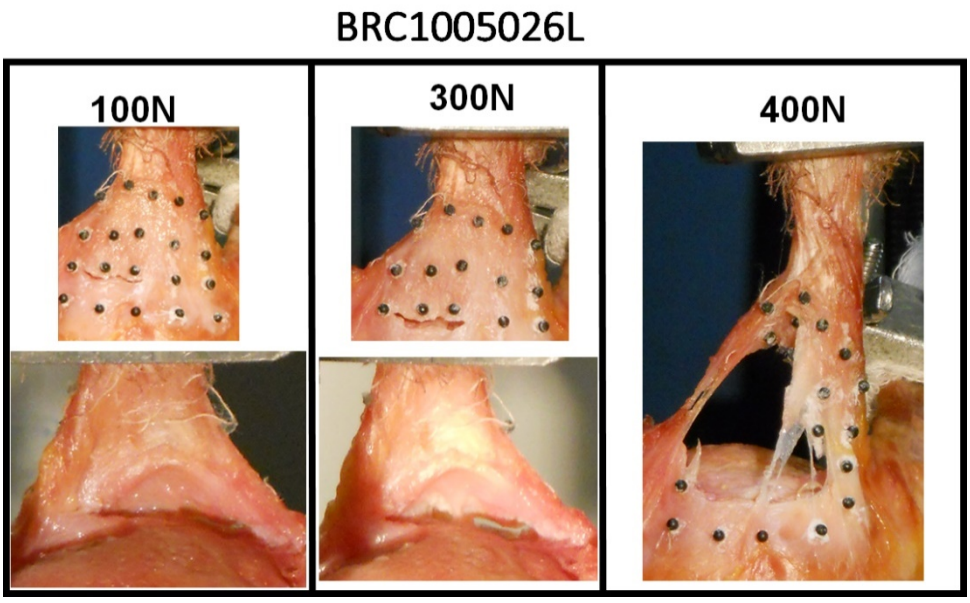

DE10052043L

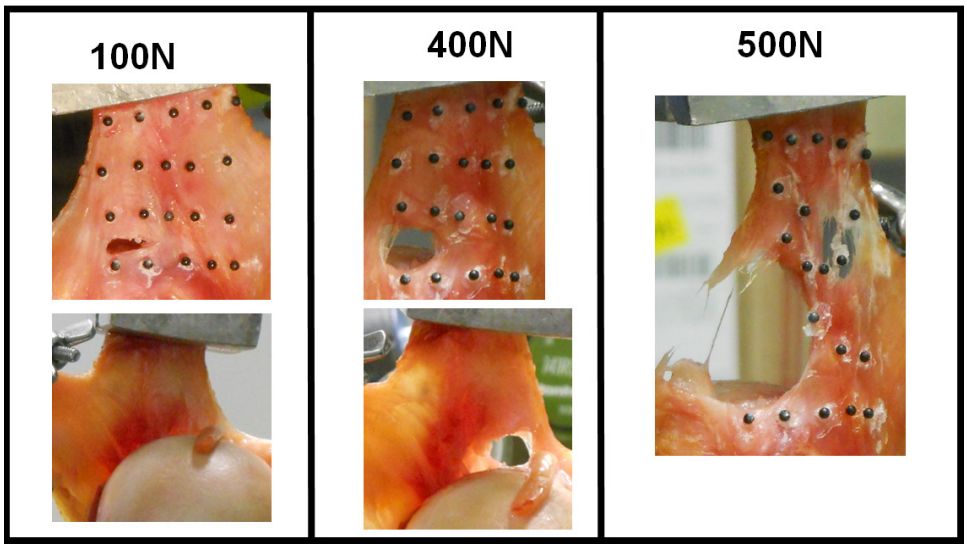

DE11070309R

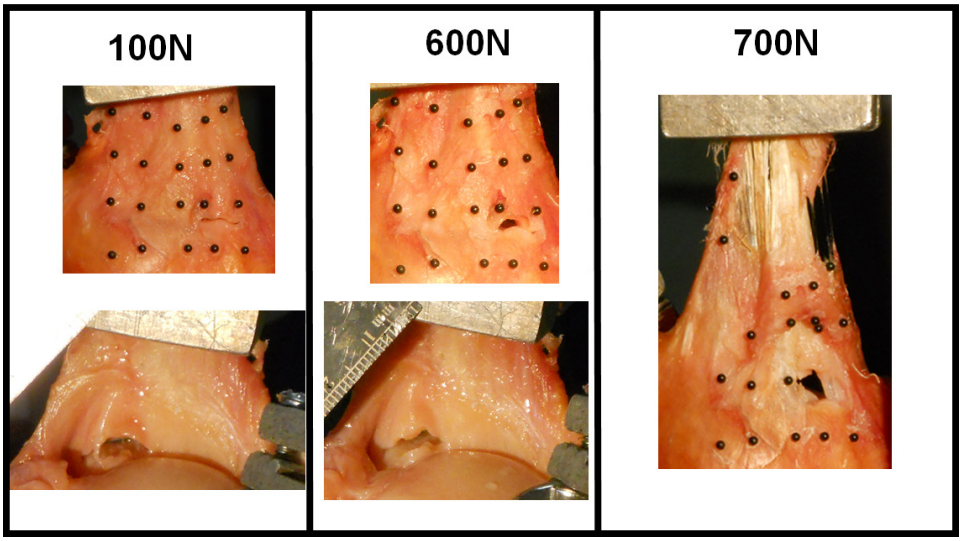

FL10090102L

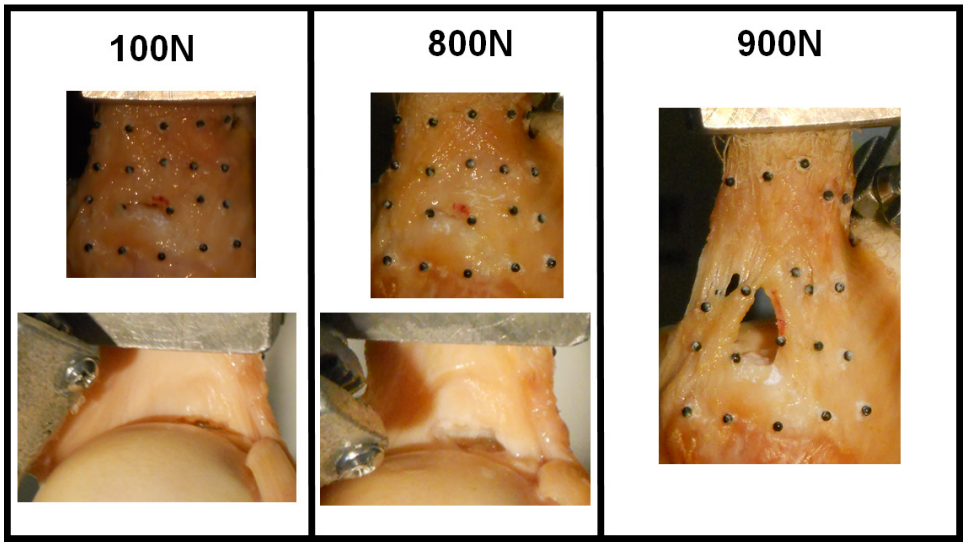

FL11031348R

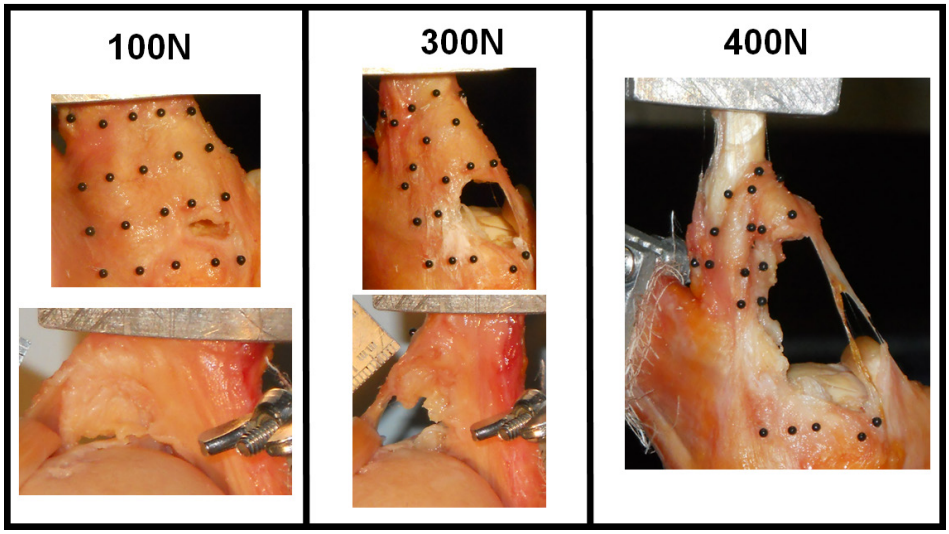

MD11071446L

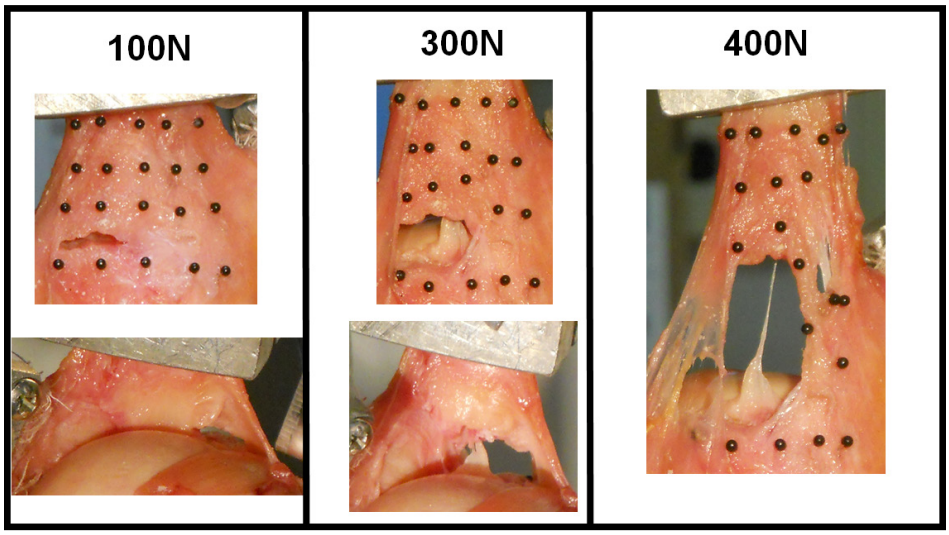

MI10090408R

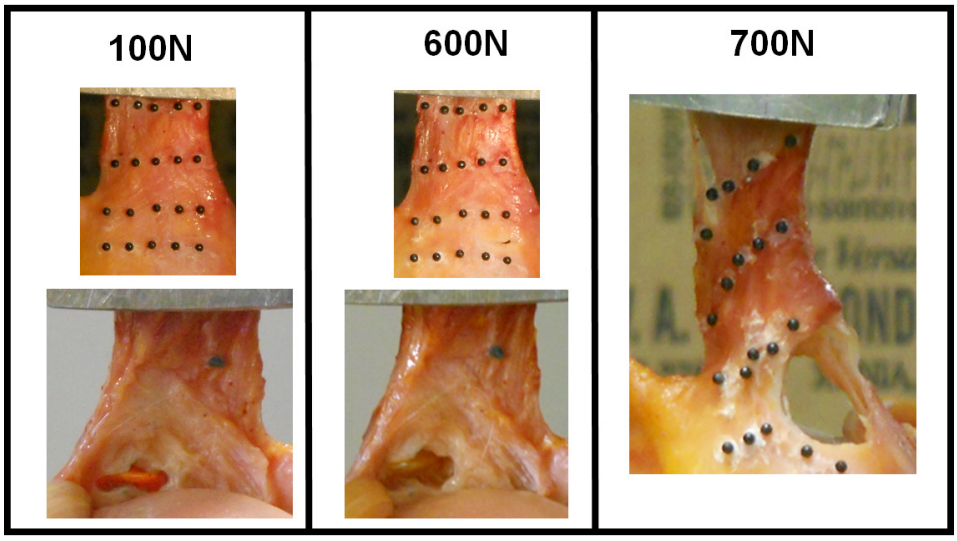

APPENDIX C

FINITE ELEMENT MODEL PRE-PROCESSING

This appendix contains calculations and MATLAB code used in the development of the finite element models of intact and torn supraspinatus tendon.

C.1.1 Derivation of Fiber Reinforced Neo-Hookean Material Model

Ψ: strain energy density

Ψ_{matrix}: strain energy density for the soft matrix component

Ψ_{fiber}: strain energy density for the collagen fibers

$\bar{I}_1, \bar{I}_4$: first and fourth strain invariants

C: Cauchy-Green deformation tensor

F: Deformation gradient

λ_1, λ_2, λ_3: x, y, and z components of stretch

c_1, k_1, k_2: material parameters

a_0: fiber orientation

σ: Cauchy stress tensor

$$\Psi = \Psi_{matrix} + \Psi_{fiber}$$

$$\Psi_{matrix} = c_1(\bar{I}_1 - 3)$$

$$\Psi_{fiber} = \frac{k_1}{2k_2}\left(e^{k_2(\bar{I}_4-1)^2} - 1\right)$$

Assuming the case of uniaxial tension and an incompressible material:

$$\lambda_1 = \lambda$$

$$\lambda_2 = \lambda_3 = \frac{1}{\sqrt{\lambda}}$$

Therefore:

$$\mathbf{C} = \mathbf{F}^T\mathbf{F}\begin{bmatrix} {\lambda_1}^2 & 0 & 0 \\ 0 & {\lambda_2}^2 & 0 \\ 0 & 0 & {\lambda_3}^2 \end{bmatrix} = \begin{bmatrix} \lambda^2 & 0 & 0 \\ 0 & \frac{1}{\lambda} & 0 \\ 0 & 0 & \frac{1}{\lambda} \end{bmatrix}$$

$$\bar{I}_1 = {\lambda_1}^2 + {\lambda_2}^2 + {\lambda_3}^2 = \lambda^2 + \frac{2}{\lambda}$$

$$\bar{I}_4 = a_0\mathbf{C}{a_0}^T = \lambda^2$$

$$\Psi_{matrix} = c_1\left(\lambda^2 + \frac{2}{\lambda} - 3\right)$$

$$\Psi_{fiber} = \frac{k_1}{2k_2}\left(e^{k_2\left(\lambda^2-1\right)^2} - 1\right)$$

Stress is described by:

$$\sigma_i = \frac{\lambda_i}{\lambda_1\lambda_2\lambda_3}\frac{\partial\Psi}{\partial\lambda_i}$$

For uniaxial tension:

$$\sigma_1 = \frac{\lambda_1}{\lambda_1\lambda_2\lambda_3}\frac{\partial\Psi}{\partial\lambda_1} = \frac{1}{\lambda_2\lambda_3}\frac{\partial\Psi}{\partial\lambda_1} = \frac{1}{\lambda}\frac{\partial\Psi}{\partial\lambda}$$

$$\sigma_1 = 2c_1\left(1-\frac{1}{\lambda^3}\right)+2k_1(\lambda^2-1)e^{k_2(\lambda^2-1)^2}$$

C.1.2 Material Model Fitting

```
function S = NeoHookeanFiber(x,lambda)
% c1 = x(1);
% k1 = x(2);
% k2 = x(3);

E = 10e6;
v = 0.45;
lam = E*v/((1+v)*(1-2*v));
mu = E/(2*(1+v));
K = E/(3*(1-2*v));

k1 = x(1);
k2 = x(2);
c1 = mu/2;

S = 2*c1*(lambda-1./lambda.^2)+2*(k1*(lambda.^2-1).*exp(k2*(lambda.^2-
1).^2));

end


%% Fitting for experimental data
% Use theoretical stress strain function for the material model and the
% lsqcurvefit function (least square fitting) to determine the material
% parameters for the experimental data.
clf,clear,clc

%% Read data
% read the experimental data

Ant = load('ant.csv');
Mid = load('mid.csv');
Post = load('post.csv');

%% Data fitting
% Use lsqcurvefit to fit the theoretical stress strain curves to the
% experimental data.

% iterate over all data sets

problemA = createOptimProblem('lsqcurvefit','x0',[1.2e5,.5],...
    'objective',@NeoHookeanFiber,...
    'xdata',Ant(:,1),'ydata',Ant(:,2),'lb',[0,0]);
```

```
%  problemA = createOptimProblem('lsqcurvefit','x0',[1e4,1e6,.5],...
%      'objective',@MooneyRivlinFiber,...
%      'xdata',Ant(:,1),'ydata',Ant(:,2),'lb',[0,0,0]);

ms = MultiStart;
xA = run(ms,problemA,10); %run lsqcurvefit 10 times

fitAnt = NeoHookeanFiber(xA,1:.01:1.2);
% fitAnt = MooneyRivlinFiber(xA,1:.01:1.2);

figure(1)
clf
plot(Ant(:,1),Ant(:,2))
hold
plot(1:.01:1.2,fitAnt,'g')
axis([1 1.2 0 max(fitAnt)])
title('Ant')
xlabel('stretch')
ylabel('stress')

% muA = 2*xA(1);
% v = 0.45;
% lamA = 2*muA*v/(1-2*v);

%%
problemM = createOptimProblem('lsqcurvefit','x0',[1.2e5,.5],...
    'objective',@NeoHookeanFiber,...
    'xdata',Mid(:,1),'ydata',Mid(:,2),'lb',[0,0]);

%  problemM = createOptimProblem('lsqcurvefit','x0',[1e4,1e6,.5],...
%      'objective',@MooneyRivlinFiber,...
%      'xdata',Mid(:,1),'ydata',Mid(:,2),'lb',[0,0,0]);

ms = MultiStart;
xM = run(ms,problemM,10); %run lsqcurvefit 10 times

fitMid = NeoHookeanFiber(xM,1:.01:1.2);
% fitMid = MooneyRivlinFiber(xM,1:.01:1.2);

figure(2)
clf
plot(Mid(:,1),Mid(:,2))
hold
plot(1:.01:1.2,fitMid,'g')
axis([1 1.2 0 max(fitMid)])
title('Mid')
xlabel('stretch')
ylabel('stress')


%%
problemP = createOptimProblem('lsqcurvefit','x0',[1.2e5,.5],...
    'objective',@NeoHookeanFiber,...
    'xdata',Post(:,1),'ydata',Post(:,2),'lb',[0,0]);
```

```
%  problemP = createOptimProblem('lsqcurvefit','x0',[1e4,1e6,.5],...
%      'objective',@MooneyRivlinFiber,...
%      'xdata',Post(:,1),'ydata',Post(:,2),'lb',[0,0,0]);

ms = MultiStart;
xP = run(ms,problemP,10); %run lsqcurvefit 10 times

fitPost = NeoHookeanFiber(xP,1:.01:1.2);
% fitPost = MooneyRivlinFiber(xP,1:.01:1.2);

figure(3)
clf
plot(Post(:,1),Post(:,2))
hold
plot(1:.01:1.2,fitPost,'g')
title('Post')
xlabel('stretch')
ylabel('stress')
axis([1 1.2 0 max(fitPost)])
```

C.1.3 Experimental Data Fit to Material Model

Experimental data is in blue, and experimental fit is in green.

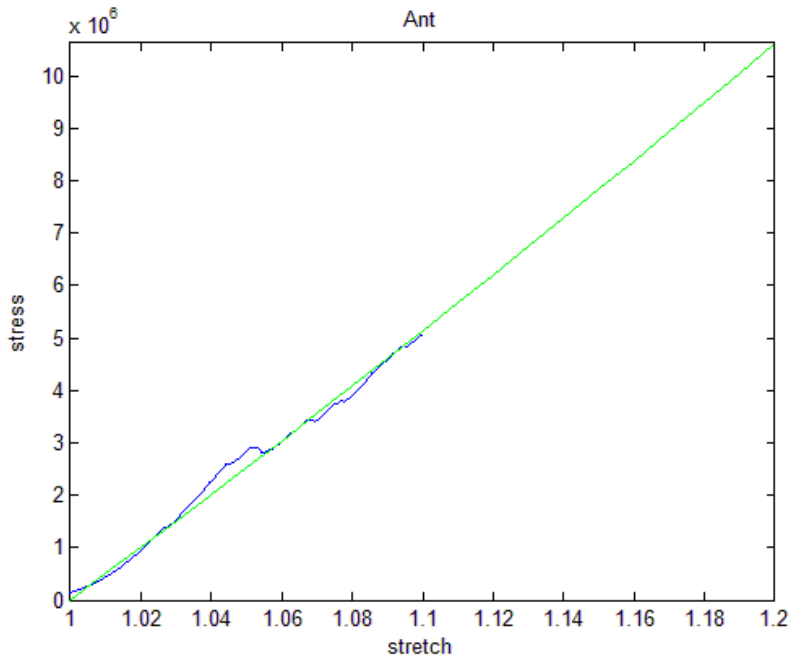
Ant
x 10^6
stress
stretch
0
1
2
3
4
5
6
7
8
9
10
1
1.02
1.04
1.06
1.08
1.1
1.12
1.14
1.16
1.18
1.2

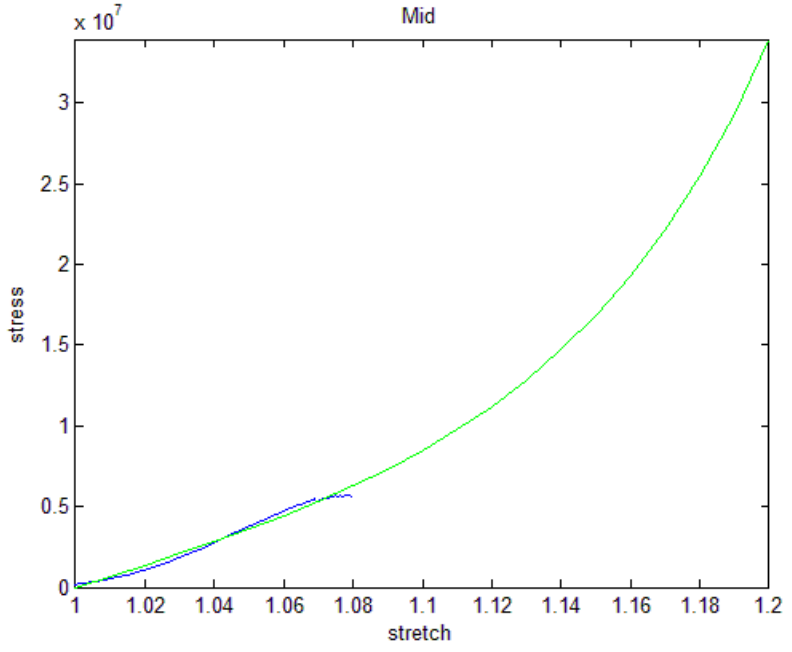
Mid
x 10^7
stress
stretch
0
0.5
1
1.5
2
2.5
3
1
1.02
1.04
1.06
1.08
1.1
1.12
1.14
1.16
1.18
1.2

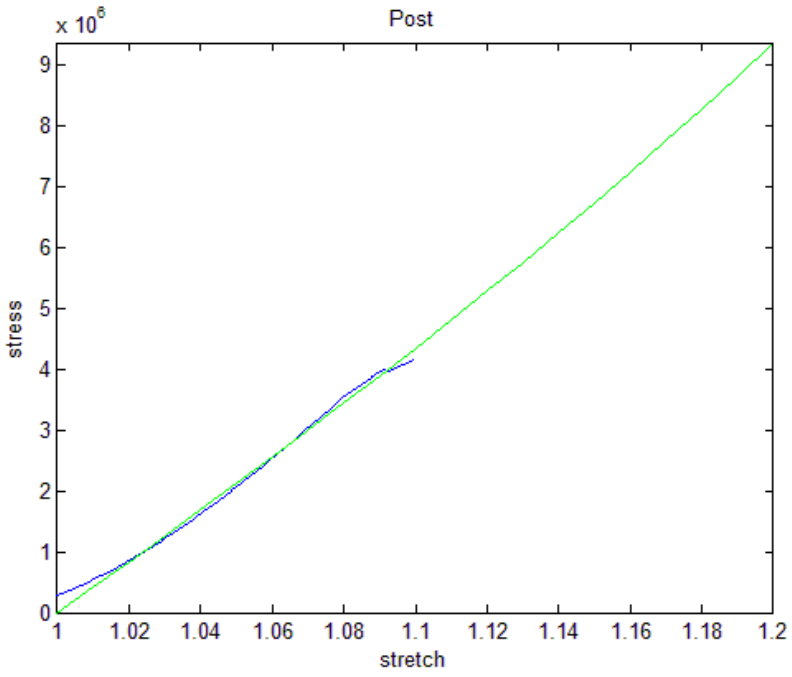

C.1.4 Infraspinatus Load

```
j = [4.2092999999999998E-002  -2.3987999999999999E-002  -7.1793999999999997E-
002]; %point on infraspinatus myotendinous junction
i = [3.6943999999999998E-002  -4.8374000000000000E-002  -3.8167000000000000E-
002]; %point on infraspinatus insertion
infra = j - i; %vector representing infraspinatus orientation
uinfra = infra./norm(infra); %infra unit vector

%CSA = 230.105; %infraspinatus CSA in mm^2
CSA=87.022;
P = 22/(CSA/1e6); %22N load on infra

load = P*uinfra %22N load on infra

quiver3(0,0,0,uinfra(1),uinfra(2),uinfra(3))
xlabel('x')
ylabel('y')
zlabel('z')
```

C.1.5 Preloaded Configuration

```
clear
clc

%load node reference coordinates
dat = load('t30deg_preload.dat');

%load displaced node coordinates
vtk = load('t30deg_disp.vtk');

%displace nodes into preloaded configuration
node = dat;
node(:,2:4) = dat(:,2:4)+vtk;

%write coordinates to file to copy into new .dat
dlmwrite('t30node',node,' ')
```

C.1.6 Assign Inhomogeneous Material Properties

```
clear all
clc

node = load('atear_node.txt');
elem = load('atear_elem.txt');

%normalize nodes to minimum values
node(:,2) = node(:,2) - min(node(:,2)); %x
node(:,3) = node(:,3) - min(node(:,3)); %y
node(:,4) = node(:,4) - min(node(:,4)); %z

%calculate centroid for each element
centroid = zeros(length(elem),3);
for n = 1:length(elem)
    centroid(n,1) = (node(elem(n,5),2)+ node(elem(n,6),2)+ node(elem(n,7),2)+
node(elem(n,8),2))/4;
    centroid(n,2) = (node(elem(n,5),3)+ node(elem(n,6),3)+ node(elem(n,7),3)+
node(elem(n,8),3))/4;
    centroid(n,3) = (node(elem(n,5),4)+ node(elem(n,6),4)+ node(elem(n,7),4)+
node(elem(n,8),4))/4;
end


%determine geometric width of model
%ensure correct axis is used
infra = 0.0198; %width of infra
```

```
width = max(node(:,3)) - min(node(:,3)) - infra;


%divide model into regions for material property assignment
%from image measurements, total width of SSP ~38mm
%anterior ~16mm
%middle ~8 mm
%posterior ~13mm

% xc1 = width/5;
% xc2 = width*2/5;
% xc3 = width*3/5;
% xc4 = width*4/5;

xc1 = width*20/100;
xc2 = xc1+width*15/100;
xc3 = xc2+width*20/100;
xc4 = xc3+width*15/100;
xc5 = xc4+width*10/100;

v1 = xc1:.0001:xc2;
v2 = xc3:.0001:xc4;

%assign elements to material blocks
block = zeros(length(centroid),8);
block(:,1) = 1:length(centroid);
block(:,2) = 3;
block(:,3) = 4;
block(:,5) = elem(:,5);
block(:,6) = elem(:,6);
block(:,7) = elem(:,7);
block(:,8) = elem(:,8);

mat=5;
m=1;
k=1;
for i = 1:length(centroid);
    if centroid(i,2) <= xc1
        block(i,4) = 1;
    elseif centroid(i,2) > xc1 && centroid(i,2) <= xc2
        for m = 1:length(v1)
            if centroid(i,2) > (xc1+(m-1)*((xc2-xc1)/length(v1))) &&
centroid(i,2) <= (xc1+m*((xc2-xc1)/length(v1)))
                block(i,4) = m+mat;
            end
        end
    elseif centroid(i,2) > xc2 && centroid(i,2) <= xc3
        block(i,4) = 2;
    elseif centroid(i,2) > xc3 && centroid(i,2) <= xc4
        for k = 1:length(v2)
            if centroid(i,2) > (xc3+(k-1)*((xc4-xc3)/length(v2))) &&
centroid(i,2) <= (xc3+k*((xc4-xc3)/length(v2)))
                block(i,4) = mat+k+m;
            end
        end
```

```
    elseif centroid(i,2) > xc4 && centroid(i,2) <= xc5
        block(i,4) = 3;
    elseif centroid(i,2) > xc5 && centroid(i,2) <= width
        block(i,4) = 4;
    elseif centroid(i,2) > width
        block(i,4) = 5;
    end
end

%write materials by block to file
dlmwrite('block',block,'delimiter',' ','precision',8)

%anterior
k1A = 9.95e6; %k1
k2A = 1.09e-7; %k2
% c1A = 1e6;
% c2A = 1e6;

%middle
k1M = 1.444e7; %k1
k2M = 5.02; %k2
% c1M = 1e5;
% c2M = 7.15e-10;

%posterior
k1P = 7.87e6; %k1
k2P = 0.63; %k2
% c1P = 1e5;
% c2P = 2.22e-14;

%anterior to middle
k1AM = interp1([xc1,xc2],[k1A,k1M],v1);
k2AM = interp1([xc1,xc2],[k2A,k2M],v1);
% c1AM = interp1([xc1,xc2],[c1A,c1M],v1);
% c2AM = interp1([xc1,xc2],[c2A,c2M],v1);

%middle to posterior
k1MP = interp1([xc3,xc4],[k1M,k1P],v2);
k2MP = interp1([xc3,xc4],[k2M,k2P],v2);
% c1MP = interp1([xc3,xc4],[c1M,c1P],v2);
% c2MP = interp1([xc3,xc4],[c2M,c2P],v2);

NH = zeros(mat+m+k,9);
NH(:,1) = 1:mat+m+k;
NH(:,2) = 3161;
NH(:,3) = 3.10e7;
NH(:,4) = 3.45e6;
NH(:,5) = 2e15;
NH(:,6) = 0.0;
NH(:,7) = 0.0;

bulk = zeros(mat+m+k,5);
bulk(:,1) = 1:mat+m+k;
bulk(:,2) = 0;
bulk(:,3) = .001e-4;
```

```
bulk(:,4) = .2;
bulk(:,5) = 1;

for i = 1:length(NH(:,1));
    if NH(i,1) == 1
%         NH(i,3) = c1A;
%         NH(i,4) = c2A;
        NH(i,8) = k1A;
        NH(i,9) = k2A;
    elseif NH(i,1) == 2
%         NH(i,3) = c1M;
%         NH(i,4) = c2M;
        NH(i,8) = k1M;
        NH(i,9) = k2M;
    elseif NH(i,1) >= 3 && NH(i,1) <= 5
%         NH(i,3) = c1P;
%         NH(i,4) = c2P;
        NH(i,8) = k1P;
        NH(i,9) = k2P;
    elseif NH(i,1) >= mat+1 && NH(i,1) <= mat+m
        for q = 1:length(v1)
            if NH(i,1) == mat+q
%                 NH(i,3) = c1AM(q);
%                 NH(i,4) = c2AM(q);
                NH(i,8) = k1AM(q);
                NH(i,9) = k2AM(q);
            end
        end
    elseif NH(i,1) >= mat+m+1 && NH(i,1) <= mat+m+k
        for p = 1:length(v2)
            if NH(i,1) == mat+q+p
%                 NH(i,3) = c1MP(p);
%                 NH(i,4) = c2MP(p);
                NH(i,8) = k1MP(p);
                NH(i,9) = k2MP(p);
            end
        end
    end
end

dlmwrite('NH',NH,' ')
dlmwrite('bulk',bulk,' ')

%%
%cohesive element failure data
%anterior
%max stress
ac = 5.78e6;
%ac = 8.2e6;
%ac = 3.36e6;

%max disp
ad = 0.799;
%ad = 8.2e6;
%ad = 3.36e6;
```

```
%middle
%max stress
mc = 5.81e6;
%mc = 8.24e6;
%mc = 3.38e6;

%max disp
md = 0.795;
%md = 8.24e6;
%md = 3.38e6;

%posterior
%max stress
pc = 4.25e6;
%pc = 6.03e6;
%pc = 2.47e6;

%max disp
pd = 1.087;
%pd = 6.03e6;
%pd = 2.47e6;

%anterior to middle
amc = interp1([xc1,xc2],[ac,mc],v1);

%middle to posterior
mpc = interp1([xc3,xc4],[mc,pc],v2);

cohelem = load('atear_coh.txt');

%calculate centroid for each coh elem
cohcent = zeros(length(cohelem),3);
for n = 1:length(cohelem)
    cohcent(n,1) = (node(cohelem(n,5),2)+ node(cohelem(n,6),2)+
node(cohelem(n,7),2))/3;
    cohcent(n,2) = (node(cohelem(n,5),3)+ node(cohelem(n,6),3)+
node(cohelem(n,7),3))/3;
    cohcent(n,3) = (node(cohelem(n,5),4)+ node(cohelem(n,6),4)+
node(cohelem(n,7),4))/3;
end

%define coh elem material assignment
coh = zeros(length(cohcent),10);
coh(:,1) = 1:length(cohcent);
coh(:,2) = 7;
coh(:,3) = 3;
coh(:,5) = cohelem(:,5);
coh(:,6) = cohelem(:,6);
coh(:,7) = cohelem(:,7);
coh(:,8) = cohelem(:,8);
coh(:,9) = cohelem(:,9);
coh(:,10) = cohelem(:,10);

xc1 = width/3;
xc2 = xc1+width*2/3;
```

```
for i = 1:length(cohcent);
    if cohcent(i,2) <= xc1
        coh(i,4) = 1;
    elseif cohcent(i,2) > xc1 && cohcent(i,2) <= xc2
        coh(i,4) = 2;
    elseif cohcent(i,2) > xc2
        coh(i,4) = 3;
    end
end

%define coh elem material properties
cohmat = zeros(3,5);
cohmat(:,5) = 0.98;
cohmat(:,6) = 0;

cohmat(1,1) = ac;
cohmat(1,3) = ac;
cohmat(2,1) = mc;
cohmat(2,3) = mc;
cohmat(3,1) = pc;
cohmat(3,3) = pc;
cohmat(1,2) = ad;
cohmat(1,4) = ad;
cohmat(2,2) = md;
cohmat(2,4) = md;
cohmat(3,2) = pd;
cohmat(3,4) = pd;

dlmwrite('cohmat',cohmat,' ')
dlmwrite('coh',coh,' ')
```

BIBLIOGRAPHY

1. Perry J. Anatomy and biomechanics of the shoulder in throwing, swimming, gymnastics, and tennis. *Clin Sports Med.* 1983;2(2):247-270.

2. Emery RJ, Mullaji AB. Glenohumeral joint instability in normal adolescents. Incidence and significance. *J Bone Joint Surg Br.* 1991;73(3):406-408.

3. Bigliani LU, Kelkar R, Flatow EL, Pollock RG, Mow VC. Glenohumeral stability. Biomechanical properties of passive and active stabilizers. *Clin Orthop Relat Res.* 1996(330):13-30.

4. Soslowsky LJ, Malicky DM, Blasier RB. Active and passive factors in inferior glenohumeral stabilization: a biomechanical model. *J Shoulder Elbow Surg.* 1997;6(4):371-379.

5. Wuelker N, Brewe F, Sperveslage C. Passive glenohumeral joint stabilization: A biomechanical study. *J Shoulder Elbow Surg.* 1994;3(3):129-134.

6. Debski RE, Sakone M, Woo SL, Wong EK, Fu FH, Warner JJ. Contribution of the passive properties of the rotator cuff to glenohumeral stability during anterior-posterior loading. *J Shoulder Elbow Surg.* 1999;8(4):324-329.

7. Labriola JE, Jolly JT, McMahon PJ, Debski RE. Active stability of the glenohumeral joint decreases in the apprehension position. *Clin Biomech (Bristol, Avon).* 2004;19(8):801-809.

8. Labriola JE, Lee TQ, Debski RE, McMahon PJ. Stability and instability of the glenohumeral joint: the role of shoulder muscles. *J Shoulder Elbow Surg.* 2005;14(1 Suppl S):32S-38S.

9. Thompson WO, Debski RE, Boardman ND, 3rd, et al. A biomechanical analysis of rotator cuff deficiency in a cadaveric model. *Am J Sports Med.* 1996;24(3):286-292.

10. Halder AM, Halder CG, Zhao KD, O'Driscoll SW, Morrey BF, An KN. Dynamic inferior stabilizers of the shoulder joint. *Clin Biomech (Bristol, Avon).* 2001;16(2):138-143.

11. Halder AM, Zhao KD, Odriscoll SW, Morrey BF, An KN. Dynamic contributions to superior shoulder stability. *J Orthop Res.* 2001;19(2):206-212.

12. Burkhart SS. Arthroscopic treatment of massive rotator cuff tears. Clinical results and biomechanical rationale. *Clin Orthop Relat Res.* 1991(267):45-56.

13. Lippitt S, Matsen F. Mechanisms of glenohumeral joint stability. *Clin Orthop Relat Res.* 1993(291):20-28.

14. Lippitt SB, Vanderhooft JE, Harris SL, Sidles JA, Harryman DT, 2nd, Matsen FA, 3rd. Glenohumeral stability from concavity-compression: A quantitative analysis. *J Shoulder Elbow Surg.* 1993;2(1):27-35.

15. Piepers I, Boudt P, Van Tongel A, De Wilde L. Evaluation of the muscle volumes of the transverse rotator cuff force couple in nonpathologic shoulders. *J Shoulder Elbow Surg.* 2014;23(7):e158-162.

16. Reuther KE, Thomas SJ, Tucker JJ, et al. Disruption of the anterior-posterior rotator cuff force balance alters joint function and leads to joint damage in a rat model. *J Orthop Res.* 2014;32(5):638-644.

17. Warner JJ, Micheli LJ, Arslanian LE, Kennedy J, Kennedy R. Patterns of flexibility, laxity, and strength in normal shoulders and shoulders with instability and impingement. *Am J Sports Med.* 1990;18(4):366-375.

18. Matsen FA, 3rd. Clinical practice. Rotator-cuff failure. *N Engl J Med.* 2008;358(20):2138-2147.

19. Lo IK, Burkhart SS. Current concepts in arthroscopic rotator cuff repair. *Am J Sports Med.* 2003;31(2):308-324.

20. Bedi A, Dines J, Warren RF, Dines DM. Massive tears of the rotator cuff. *J Bone Joint Surg Am.* 2010;92(9):1894-1908.

21. Hsu HC, Luo ZP, Cofield RH, An KN. Influence of rotator cuff tearing on glenohumeral stability. *J Shoulder Elbow Surg.* 1997;6(5):413-422.

22. Kirschenbaum D, Coyle MP, Jr., Leddy JP, Katsaros P, Tan F, Jr., Cody RP. Shoulder strength with rotator cuff tears. Pre- and postoperative analysis. *Clin Orthop Relat Res.* 1993(288):174-178.

23. Yamaguchi K, Sher JS, Andersen WK, et al. Glenohumeral motion in patients with rotator cuff tears: a comparison of asymptomatic and symptomatic shoulders. *J Shoulder Elbow Surg.* 2000;9(1):6-11.

24. Morrey BF, Itoi E, An KN. Biomechanics of the Shoulder. In: Rockwood CA, Matsen FA, Wirth MA, Harryman DT, eds. *The shoulder*. 2nd ed. Philadelphia: Saunders; 1998:233-272.

25. Inman VT, Saunders JB, Abbott LC. Observations of the function of the shoulder joint. 1944. *Clin Orthop Relat Res.* 1996(330):3-12.

26. McClure PW, Michener LA, Sennett BJ, Karduna AR. Direct 3-dimensional measurement of scapular kinematics during dynamic movements in vivo. *J Shoulder Elbow Surg.* 2001;10(3):269-277.

27. Murray MP, Gore DR, Gardner GM, Mollinger LA. Shoulder motion and muscle strength of normal men and women in two age groups. *Clin Orthop Relat Res.* 1985(192):268-273.

28. Poppen NK, Walker PS. Normal and abnormal motion of the shoulder. *J Bone Joint Surg Am.* 1976;58(2):195-201.

29. Soslowsky LJ, Flatow EL, Bigliani LU, Pawluk RJ, Ateshian GA, Mow VC. Quantitation of in situ contact areas at the glenohumeral joint: a biomechanical study. *J Orthop Res.* 1992;10(4):524-534.

30. Warner JJ, Bowen MK, Deng XH, Hannafin JA, Arnoczky SP, Warren RF. Articular contact patterns of the normal glenohumeral joint. *J Shoulder Elbow Surg.* 1998;7(4):381-388.

31. Itoi E, Newman SR, Kuechle DK, Morrey BF, An KN. Dynamic anterior stabilisers of the shoulder with the arm in abduction. *J Bone Joint Surg Br.* 1994;76(5):834-836.

32. Wuelker N, Korell M, Thren K. Dynamic glenohumeral joint stability. *J Shoulder Elbow Surg.* 1998;7(1):43-52.

33. Lee SB, Kim KJ, O'Driscoll SW, Morrey BF, An KN. Dynamic glenohumeral stability provided by the rotator cuff muscles in the mid-range and end-range of motion. A study in cadavera. *J Bone Joint Surg Am.* 2000;82(6):849-857.

34. Cain PR, Mutschler TA, Fu FH, Lee SK. Anterior stability of the glenohumeral joint. A dynamic model. *Am J Sports Med.* 1987;15(2):144-148.

35. Clark JM, Harryman DT, 2nd. Tendons, ligaments, and capsule of the rotator cuff. Gross and microscopic anatomy. *J Bone Joint Surg Am.* 1992;74(5):713-725.

36. Ogata S, Uhthoff HK. Acromial enthesopathy and rotator cuff tear. A radiologic and histologic postmortem investigation of the coracoacromial arch. *Clin Orthop Relat Res.* 1990(254):39-48.

37. Flatow EL, Soslowsky LJ, Ticker JB, et al. Excursion of the rotator cuff under the acromion. Patterns of subacromial contact. *Am J Sports Med.* 1994;22(6):779-788.

38. Yamamoto N, Muraki T, Sperling JW, et al. Contact between the coracoacromial arch and the rotator cuff tendons in nonpathologic situations: a cadaveric study. *J Shoulder Elbow Surg.* 2010;19(5):681-687.

39. Karduna AR, Williams GR, Williams JL, Iannotti JP. Kinematics of the glenohumeral joint: influences of muscle forces, ligamentous constraints, and articular geometry. *J Orthop Res.* 1996;14(6):986-993.

40. Dugas JR, Campbell DA, Warren RF, Robie BH, Millett PJ. Anatomy and dimensions of rotator cuff insertions. *J Shoulder Elbow Surg.* 2002;11(5):498-503.

41. Hughes RE, An KN. Force analysis of rotator cuff muscles. *Clin Orthop Relat Res.* 1996(330):75-83.

42. Mochizuki T, Sugaya H, Uomizu M, et al. Humeral insertion of the supraspinatus and infraspinatus. New anatomical findings regarding the footprint of the rotator cuff. *J Bone Joint Surg Am.* 2008;90(5):962-969.

43. Sharkey NA, Marder RA. The rotator cuff opposes superior translation of the humeral head. *Am J Sports Med.* 1995;23(3):270-275.

44. Parsons IM, Apreleva M, Fu FH, Woo SL. The effect of rotator cuff tears on reaction forces at the glenohumeral joint. *J Orthop Res.* 2002;20(3):439-446.

45. Oh JH, Jun BJ, McGarry MH, Lee TQ. Does a critical rotator cuff tear stage exist?: a biomechanical study of rotator cuff tear progression in human cadaver shoulders. *J Bone Joint Surg Am.* 2011;93(22):2100-2109.

46. Hansen ML, Otis JC, Johnson JS, Cordasco FA, Craig EV, Warren RF. Biomechanics of massive rotator cuff tears: implications for treatment. *J Bone Joint Surg Am.* 2008;90(2):316-325.

47. Hsu JE, Reuther KE, Sarver JJ, et al. Restoration of anterior-posterior rotator cuff force balance improves shoulder function in a rat model of chronic massive tears. *J Orthop Res.* 2011;29(7):1028-1033.

48. Liu J, Hughes RE, Smutz WP, Niebur G, Nan-An K. Roles of deltoid and rotator cuff muscles in shoulder elevation. *Clin Biomech (Bristol, Avon).* 1997;12(1):32-38.

49. Minagawa H, Itoi E, Konno N, et al. Humeral attachment of the supraspinatus and infraspinatus tendons: an anatomic study. *Arthroscopy.* 1998;14(3):302-306.

50. Andarawis-Puri N, Kuntz AF, Kim SY, Soslowsky LJ. Effect of anterior supraspinatus tendon partial-thickness tears on infraspinatus tendon strain through a range of joint rotation angles. *J Shoulder Elbow Surg.* 2010;19(4):617-623.

51. Andarawis-Puri N, Ricchetti ET, Soslowsky LJ. Interaction between the supraspinatus and infraspinatus tendons: effect of anterior supraspinatus tendon full-thickness tears on infraspinatus tendon strain. *Am J Sports Med.* 2009;37(9):1831-1839.

52. Burkhart SS, Esch JC, Jolson RS. The rotator crescent and rotator cable: an anatomic description of the shoulder's "suspension bridge". *Arthroscopy.* 1993;9(6):611-616.

53. Oh LS, Wolf BR, Hall MP, Levy BA, Marx RG. Indications for rotator cuff repair: a systematic review. *Clin Orthop Relat Res.* 2007;455:52-63.

54. Cofield RH. Tears of rotator cuff. *Instr Course Lect.* 1981;30:258-273.

55. Post M, Silver R, Singh M. Rotator cuff tear. Diagnosis and treatment. *Clin Orthop Relat Res.* 1983(173):78-91.

56. Cofield RH. Rotator cuff disease of the shoulder. *J Bone Joint Surg Am.* 1985;67(6):974-979.

57. Neviaser RJ. Ruptures of the rotator cuff. *Orthop Clin North Am.* 1987;18(3):387-394.

58. Neviaser RJ. Tears of the rotator cuff. *Orthop Clin North Am.* 1980;11(2):295-306.

59. Mather RC, 3rd, Koenig L, Acevedo D, et al. The societal and economic value of rotator cuff repair. *J Bone Joint Surg Am.* 2013;95(22):1993-2000.

60. Zhang AL, Montgomery SR, Ngo SS, Hame SL, Wang JC, Gamradt SC. Analysis of rotator cuff repair trends in a large private insurance population. *Arthroscopy.* 2013;29(4):623-629.

61. Yamaguchi K. New guideline on rotator cuff problems: board approves "optimizing the management of rotator cuff problems". *AAOS Now.* 2011:1.

62. Aurora A, McCarron JA, van den Bogert AJ, Gatica JE, Iannotti JP, Derwin KA. The biomechanical role of scaffolds in augmented rotator cuff tendon repairs. *J Shoulder Elbow Surg.* 2012;21(8):1064-1071.

63. Yamamoto A, Takagishi K, Osawa T, et al. Prevalence and risk factors of a rotator cuff tear in the general population. *J Shoulder Elbow Surg.* 2010;19(1):116-120.

64. Tempelhof S, Rupp S, Seil R. Age-related prevalence of rotator cuff tears in asymptomatic shoulders. *J Shoulder Elbow Surg.* 1999;8(4):296-299.

65. Sher JS, Uribe JW, Posada A, Murphy BJ, Zlatkin MB. Abnormal findings on magnetic resonance images of asymptomatic shoulders. *J Bone Joint Surg Am.* 1995;77(1):10-15.

66. Milgrom C, Schaffler M, Gilbert S, van Holsbeeck M. Rotator-cuff changes in asymptomatic adults. The effect of age, hand dominance and gender. *J Bone Joint Surg Br.* 1995;77(2):296-298.

67. Yamaguchi K, Ditsios K, Middleton WD, Hildebolt CF, Galatz LM, Teefey SA. The demographic and morphological features of rotator cuff disease. A comparison of asymptomatic and symptomatic shoulders. *J Bone Joint Surg Am.* 2006;88(8):1699-1704.

68. Carbone S, Gumina S, Arceri V, Campagna V, Fagnani C, Postacchini F. The impact of preoperative smoking habit on rotator cuff tear: cigarette smoking influences rotator cuff tear sizes. *J Shoulder Elbow Surg.* 2012;21(1):56-60.

69. Baumgarten KM, Gerlach D, Galatz LM, et al. Cigarette smoking increases the risk for rotator cuff tears. *Clin Orthop Relat Res.* 2010;468(6):1534-1541.

70. Tashjian RZ. Epidemiology, natural history, and indications for treatment of rotator cuff tears. *Clin Sports Med.* 2012;31(4):589-604.

71. Djerbi I, Chammas M, Mirous MP, et al. Impact of cardiovascular risk factor on the prevalence and severity of symptomatic full-thickness rotator cuff tears. *Orthop Traumatol Surg Res.* 2015;101(6 Suppl):S269-273.

72. Abboud JA, Kim JS. The effect of hypercholesterolemia on rotator cuff disease. *Clin Orthop Relat Res.* 2010;468(6):1493-1497.

73. Tashjian RZ, Granger EK, Farnham JM, Cannon-Albright LA, Teerlink CC. Genome-wide association study for rotator cuff tears identifies two significant single-nucleotide polymorphisms. *J Shoulder Elbow Surg.* 2015.

74. Longo UG, Berton A, Papapietro N, Maffulli N, Denaro V. Epidemiology, genetics and biological factors of rotator cuff tears. *Med Sport Sci.* 2012;57:1-9.

75. Yamamoto A, Takagishi K, Kobayashi T, et al. The impact of faulty posture on rotator cuff tears with and without symptoms. *J Shoulder Elbow Surg.* 2015;24(3):446-452.

76. Yamaguchi K, Tetro AM, Blam O, Evanoff BA, Teefey SA, Middleton WD. Natural history of asymptomatic rotator cuff tears: a longitudinal analysis of asymptomatic tears detected sonographically. *J Shoulder Elbow Surg.* 2001;10(3):199-203.

77. Liem D, Buschmann VE, Schmidt C, et al. The prevalence of rotator cuff tears: is the contralateral shoulder at risk? *Am J Sports Med.* 2014;42(4):826-830.

78. McCarron J. DK, Iannotti J., . Biologic augmentation of rotator cuff healing. In: L G, ed. *Orthopedic knowledge update: Shoulder and elbow*. Rosemont, IL: American Academy of Orthopedic Surgeons; 2008:pp. 211-219.

79. Miller BS, Downie BK, Kohen RB, et al. When do rotator cuff repairs fail? Serial ultrasound examination after arthroscopic repair of large and massive rotator cuff tears. *Am J Sports Med.* 2011;39(10):2064-2070.

80. Galatz LM, Ball CM, Teefey SA, Middleton WD, Yamaguchi K. The outcome and repair integrity of completely arthroscopically repaired large and massive rotator cuff tears. *J Bone Joint Surg Am.* 2004;86-A(2):219-224.

81. Gerber C, Fuchs B, Hodler J. The results of repair of massive tears of the rotator cuff. *J Bone Joint Surg Am.* 2000;82(4):505-515.

82. Kukkonen J, Joukainen A, Lehtinen J, et al. Treatment of Nontraumatic Rotator Cuff Tears: A Randomized Controlled Trial with Two Years of Clinical and Imaging Follow-up. *J Bone Joint Surg Am.* 2015;97(21):1729-1737.

83. Itoi E, Tabata S. Conservative treatment of rotator cuff tears. *Clin Orthop Relat Res.* 1992(275):165-173.

84. Itoi E. Rotator cuff tear: physical examination and conservative treatment. *J Orthop Sci.* 2013;18(2):197-204.

85. Kuhn JE, Dunn WR, Sanders R, et al. Effectiveness of physical therapy in treating atraumatic full-thickness rotator cuff tears: a multicenter prospective cohort study. *J Shoulder Elbow Surg.* 2013;22(10):1371-1379.

86. Kuhn JE. Exercise in the treatment of rotator cuff impingement: a systematic review and a synthesized evidence-based rehabilitation protocol. *J Shoulder Elbow Surg.* 2009;18(1):138-160.

87. Moosmayer S, Lund G, Seljom US, et al. Tendon repair compared with physiotherapy in the treatment of rotator cuff tears: a randomized controlled study in 103 cases with a five-year follow-up. *J Bone Joint Surg Am.* 2014;96(18):1504-1514.

88. Pappou IP, Schmidt CC, Jarrett CD, Steen BM, Frankle MA. AAOS appropriate use criteria: optimizing the management of full-thickness rotator cuff tears. *J Am Acad Orthop Surg.* 2013;21(12):772-775.

89. Escamilla RF, Yamashiro K, Paulos L, Andrews JR. Shoulder muscle activity and function in common shoulder rehabilitation exercises. *Sports Med.* 2009;39(8):663-685.

90. Apreleva M, Ozbaydar M, Fitzgibbons PG, Warner JJ. Rotator cuff tears: the effect of the reconstruction method on three-dimensional repair site area. *Arthroscopy.* 2002;18(5):519-526.

91. Nelson CO, Sileo MJ, Grossman MG, Serra-Hsu F. Single-row modified mason-allen versus double-row arthroscopic rotator cuff repair: a biomechanical and surface area comparison. *Arthroscopy.* 2008;24(8):941-948.

92. Boileau P, Brassart N, Watkinson DJ, Carles M, Hatzidakis AM, Krishnan SG. Arthroscopic repair of full-thickness tears of the supraspinatus: does the tendon really heal? *J Bone Joint Surg Am.* 2005;87(6):1229-1240.

93. Lo IK, Burkhart SS. Double-row arthroscopic rotator cuff repair: re-establishing the footprint of the rotator cuff. *Arthroscopy.* 2003;19(9):1035-1042.

94. Park MC, ElAttrache NS, Tibone JE, Ahmad CS, Jun BJ, Lee TQ. Part I: Footprint contact characteristics for a transosseous-equivalent rotator cuff repair technique compared with a double-row repair technique. *J Shoulder Elbow Surg.* 2007;16(4):461-468.

95. Park MC, Tibone JE, ElAttrache NS, Ahmad CS, Jun BJ, Lee TQ. Part II: Biomechanical assessment for a footprint-restoring transosseous-equivalent rotator cuff repair technique compared with a double-row repair technique. *J Shoulder Elbow Surg.* 2007;16(4):469-476.

96. Franceschi F, Ruzzini L, Longo UG, et al. Equivalent clinical results of arthroscopic single-row and double-row suture anchor repair for rotator cuff tears: a randomized controlled trial. *Am J Sports Med.* 2007;35(8):1254-1260.

97. Lafosse L, Brozska R, Toussaint B, Gobezie R. The outcome and structural integrity of arthroscopic rotator cuff repair with use of the double-row suture anchor technique. *J Bone Joint Surg Am.* 2007;89(7):1533-1541.

98. Kim DH, Elattrache NS, Tibone JE, et al. Biomechanical comparison of a single-row versus double-row suture anchor technique for rotator cuff repair. *Am J Sports Med.* 2006;34(3):407-414.

99. Mazzocca AD, Millett PJ, Guanche CA, Santangelo SA, Arciero RA. Arthroscopic single-row versus double-row suture anchor rotator cuff repair. *Am J Sports Med.* 2005;33(12):1861-1868.

100. Park MC, Elattrache NS, Ahmad CS, Tibone JE. "Transosseous-equivalent" rotator cuff repair technique. *Arthroscopy.* 2006;22(12):1360 e1361-1365.

101. Baydar M, Akalin E, El O, et al. The efficacy of conservative treatment in patients with full-thickness rotator cuff tears. *Rheumatol Int.* 2009;29(6):623-628.

102. Moosmayer S, Lund G, Seljom U, et al. Comparison between surgery and physiotherapy in the treatment of small and medium-sized tears of the rotator cuff: A randomised controlled study of 103 patients with one-year follow-up. *J Bone Joint Surg Br.* 2010;92(1):83-91.

103. Goldberg BA, Nowinski RJ, Matsen FA, 3rd. Outcome of nonoperative management of full-thickness rotator cuff tears. *Clin Orthop Relat Res.* 2001(382):99-107.

104. Koubaa S, Ben Salah FZ, Lebib S, Miri I, Ghorbel S, Dziri C. [Conservative management of full-thickness rotator cuff tears. A prospective study of 24 patients]. *Ann Readapt Med Phys.* 2006;49(2):62-67.

105. Duquin TR, Buyea C, Bisson LJ. Which method of rotator cuff repair leads to the highest rate of structural healing? A systematic review. *Am J Sports Med.* 2010;38(4):835-841.

106. Chung SW, Kim JY, Yoon JP, Lyu SH, Rhee SM, Oh SB. Arthroscopic repair of partial-thickness and small full-thickness rotator cuff tears: tendon quality as a prognostic factor for repair integrity. *Am J Sports Med.* 2015;43(3):588-596.

107. Castagna A, Conti M, Markopoulos N, et al. Arthroscopic repair of rotator cuff tear with a modified Mason-Allen stitch: mid-term clinical and ultrasound outcomes. *Knee Surg Sports Traumatol Arthrosc.* 2008;16(5):497-503.

108. Cole BJ, McCarty LP, 3rd, Kang RW, Alford W, Lewis PB, Hayden JK. Arthroscopic rotator cuff repair: prospective functional outcome and repair integrity at minimum 2-year follow-up. *J Shoulder Elbow Surg.* 2007;16(5):579-585.

109. Deutsch A, Kroll DG, Hasapes J, Staewen RS, Pham C, Tait C. Repair integrity and clinical outcome after arthroscopic rotator cuff repair using single-row anchor fixation: a prospective study of single-tendon and two-tendon tears. *J Shoulder Elbow Surg.* 2008;17(6):845-852.

110. Gazielly DF, Gleyze P, Montagnon C. Functional and anatomical results after rotator cuff repair. *Clin Orthop Relat Res.* 1994(304):43-53.

111. Frank JB, ElAttrache NS, Dines JS, Blackburn A, Crues J, Tibone JE. Repair site integrity after arthroscopic transosseous-equivalent suture-bridge rotator cuff repair. *Am J Sports Med.* 2008;36(8):1496-1503.

112. Fuchs B, Gilbart MK, Hodler J, Gerber C. Clinical and structural results of open repair of an isolated one-tendon tear of the rotator cuff. *J Bone Joint Surg Am.* 2006;88(2):309-316.

113. McElvany MD, McGoldrick E, Gee AO, Neradilek MB, Matsen FA, 3rd. Rotator cuff repair: published evidence on factors associated with repair integrity and clinical outcome. *Am J Sports Med.* 2015;43(2):491-500.

114. Bishop J, Klepps S, Lo IK, Bird J, Gladstone JN, Flatow EL. Cuff integrity after arthroscopic versus open rotator cuff repair: a prospective study. *J Shoulder Elbow Surg.* 2006;15(3):290-299.

115. Huijsmans PE, Pritchard MP, Berghs BM, van Rooyen KS, Wallace AL, de Beer JF. Arthroscopic rotator cuff repair with double-row fixation. *J Bone Joint Surg Am.* 2007;89(6):1248-1257.

116. Sugaya H, Maeda K, Matsuki K, Moriishi J. Repair integrity and functional outcome after arthroscopic double-row rotator cuff repair. A prospective outcome study. *J Bone Joint Surg Am.* 2007;89(5):953-960.

117. Kukkonen J, Kauko T, Virolainen P, Aarimaa V. The effect of tear size on the treatment outcome of operatively treated rotator cuff tears. *Knee Surg Sports Traumatol Arthrosc.* 2015;23(2):567-572.

118. Millar NL, Wu X, Tantau R, Silverstone E, Murrell GA. Open versus two forms of arthroscopic rotator cuff repair. *Clin Orthop Relat Res.* 2009;467(4):966-978.

119. Saccomanno MF, Sircana G, Cazzato G, Donati F, Randelli P, Milano G. Prognostic factors influencing the outcome of rotator cuff repair: a systematic review. *Knee Surg Sports Traumatol Arthrosc.* 2015.

120. Ponce BA, Hosemann CD, Raghava P, Tate JP, Sheppard ED, Eberhardt AW. A biomechanical analysis of controllable intraoperative variables affecting the strength of rotator cuff repairs at the suture-tendon interface. *Am J Sports Med.* 2013;41(10):2256-2261.

121. Thomazeau H, Boukobza E, Morcet N, Chaperon J, Langlais F. Prediction of rotator cuff repair results by magnetic resonance imaging. *Clin Orthop Relat Res.* 1997(344):275-283.

122. Schneeberger AG, von Roll A, Kalberer F, Jacob HA, Gerber C. Mechanical strength of arthroscopic rotator cuff repair techniques: an in vitro study. *J Bone Joint Surg Am.* 2002;84-A(12):2152-2160.

123. Gerber C, Schneeberger AG, Beck M, Schlegel U. Mechanical strength of repairs of the rotator cuff. *J Bone Joint Surg Br.* 1994;76(3):371-380.

124. Gimbel JA, Van Kleunen JP, Lake SP, Williams GR, Soslowsky LJ. The role of repair tension on tendon to bone healing in an animal model of chronic rotator cuff tears. *J Biomech.* 2007;40(3):561-568.

125. Burkhart SS, Diaz Pagan JL, Wirth MA, Athanasiou KA. Cyclic loading of anchor-based rotator cuff repairs: confirmation of the tension overload phenomenon and comparison of suture anchor fixation with transosseous fixation. *Arthroscopy.* 1997;13(6):720-724.

126. Denard PJ, Burkhart SS. Techniques for managing poor quality tissue and bone during arthroscopic rotator cuff repair. *Arthroscopy.* 2011;27(10):1409-1421.

127. Burkhart SS, Fischer SP, Nottage WM, et al. Tissue fixation security in transosseous rotator cuff repairs: a mechanical comparison of simple versus mattress sutures. *Arthroscopy.* 1996;12(6):704-708.

128. Cummins CA, Murrell GA. Mode of failure for rotator cuff repair with suture anchors identified at revision surgery. *J Shoulder Elbow Surg.* 2003;12(2):128-133.

129. Bisson LJ, Manohar LM. A biomechanical comparison of the pullout strength of No. 2 FiberWire suture and 2-mm FiberWire tape in bovine rotator cuff tendons. *Arthroscopy.* 2010;26(11):1463-1468.

130. Safran O, Schroeder J, Bloom R, Weil Y, Milgrom C. Natural history of nonoperatively treated symptomatic rotator cuff tears in patients 60 years old or younger. *Am J Sports Med.* 2011;39(4):710-714.

131. Guo W, Zingg JM, Meydani M, Azzi A. Alpha-Tocopherol counteracts ritonavir-induced proinflammatory cytokines expression in differentiated THP-1 cells. *Biofactors.* 2007;31(3-4):171-179.

132. Maman E, Harris C, White L, Tomlinson G, Shashank M, Boynton E. Outcome of nonoperative treatment of symptomatic rotator cuff tears monitored by magnetic resonance imaging. *J Bone Joint Surg Am.* 2009;91(8):1898-1906.

133. Fucentese SF, von Roll AL, Pfirrmann CW, Gerber C, Jost B. Evolution of nonoperatively treated symptomatic isolated full-thickness supraspinatus tears. *J Bone Joint Surg Am.* 2012;94(9):801-808.

134. Moosmayer S, Tariq R, Stiris M, Smith HJ. The natural history of asymptomatic rotator cuff tears: a three-year follow-up of fifty cases. *J Bone Joint Surg Am.* 2013;95(14):1249-1255.

135. Andarawis-Puri N, Ricchetti ET, Soslowsky LJ. Rotator cuff tendon strain correlates with tear propagation. *J Biomech.* 2009;42(2):158-163.

136. Reilly P, Amis AA, Wallace AL, Emery RJ. Mechanical factors in the initiation and propagation of tears of the rotator cuff. Quantification of strains of the supraspinatus tendon in vitro. *J Bone Joint Surg Br.* 2003;85(4):594-599.

137. Barry JJ, Lansdown DA, Cheung S, Feeley BT, Ma CB. The relationship between tear severity, fatty infiltration, and muscle atrophy in the supraspinatus. *J Shoulder Elbow Surg.* 2012.

138. Tanaka M, Itoi E, Sato K, et al. Factors related to successful outcome of conservative treatment for rotator cuff tears. *Ups J Med Sci.* 2010;115(3):193-200.

139. Bey MJ, Ramsey ML, Soslowsky LJ. Intratendinous strain fields of the supraspinatus tendon: effect of a surgically created articular-surface rotator cuff tear. *J Shoulder Elbow Surg.* 2002;11(6):562-569.

140. Kim YS, Kim JM, Bigliani LU, Kim HJ, Jung HW. In vivo strain analysis of the intact supraspinatus tendon by ultrasound speckles tracking imaging. *J Orthop Res.* 2011;29(12):1931-1937.

141. Huang CY, Wang VM, Pawluk RJ, et al. Inhomogeneous mechanical behavior of the human supraspinatus tendon under uniaxial loading. *J Orthop Res.* 2005;23(4):924-930.

142. Miller RM, Fujimaki Y, Araki D, Musahl V, Debski RE. Strain distribution due to propagation of tears in the anterior supraspinatus tendon. *J Orthop Res.* 2014;32(10):1283-1289.

143. Peltz CD, Haladik JA, Hoffman SE, et al. Associations among shoulder strength, glenohumeral joint motion, and clinical outcome after rotator cuff repair. *Am J Orthop (Belle Mead NJ).* 2014;43(5):220-226.

144. Bey MJ, Peltz CD, Ciarelli K, et al. In vivo shoulder function after surgical repair of a torn rotator cuff: glenohumeral joint mechanics, shoulder strength, clinical outcomes, and their interaction. *Am J Sports Med.* 2011;39(10):2117-2129.

145. Lee YS, Lee TQ. Specimen-specific method for quantifying glenohumeral joint kinematics. *Ann Biomed Eng.* 2010;38(10):3226-3236.

146. Massimini DF, Boyer PJ, Papannagari R, Gill TJ, Warner JP, Li G. In-vivo glenohumeral translation and ligament elongation during abduction and abduction with internal and external rotation. *J Orthop Surg Res.* 2012;7:29.

147. Su WR, Budoff JE, Luo ZP. The effect of anterosuperior rotator cuff tears on glenohumeral translation. *Arthroscopy.* 2009;25(3):282-289.

148. Reilly P, Amis AA, Wallace AL, Emery RJ. Supraspinatus tears: propagation and strain alteration. *J Shoulder Elbow Surg.* 2003;12(2):134-138.

149. Carpenter JE, Thomopoulos S, Flanagan CL, DeBano CM, Soslowsky LJ. Rotator cuff defect healing: a biomechanical and histologic analysis in an animal model. *J Shoulder Elbow Surg.* 1998;7(6):599-605.

150. Mall NA, Kim HM, Keener JD, et al. Symptomatic progression of asymptomatic rotator cuff tears: a prospective study of clinical and sonographic variables. *J Bone Joint Surg Am.* 2010;92(16):2623-2633.

151. Bey MJ, Song HK, Wehrli FW, Soslowsky LJ. Intratendinous strain fields of the intact supraspinatus tendon: the effect of glenohumeral joint position and tendon region. *J Orthop Res.* 2002;20(4):869-874.

152. Sano H, Hatta T, Yamamoto N, Itoi E. Stress distribution within rotator cuff tendons with a crescent-shaped and an L-shaped tear. *Am J Sports Med.* 2013;41(10):2262-2269.

153. Kandemir U, Allaire RB, Debski RE, Lee TQ, McMahon PJ. Quantification of rotator cuff tear geometry: the repair ratio as a guide for surgical repair in crescent and U-shaped tears. *Arch Orthop Trauma Surg.* 2010;130(3):369-373.

154. Mesiha MM, Derwin KA, Sibole SC, Erdemir A, McCarron JA. The biomechanical relevance of anterior rotator cuff cable tears in a cadaveric shoulder model. *J Bone Joint Surg Am.* 2013;95(20):1817-1824.

155. Keener JD, Hsu JE, Steger-May K, Teefey SA, Chamberlain AM, Yamaguchi K. Patterns of tear progression for asymptomatic degenerative rotator cuff tears. *J Shoulder Elbow Surg.* 2015;24(12):1845-1851.

156. Killian ML, Cavinatto LM, Ward SR, Havlioglu N, Thomopoulos S, Galatz LM. Chronic Degeneration Leads to Poor Healing of Repaired Massive Rotator Cuff Tears in Rats. *Am J Sports Med.* 2015;43(10):2401-2410.

157. Bigliani LU, Cordasco FA, McIlveen SJ, Musso ES. Operative treatment of failed repairs of the rotator cuff. *J Bone Joint Surg Am.* 1992;74(10):1505-1515.

158. Karthikeyan S, Griffin DR, Parsons N, et al. Microvascular blood flow in normal and pathologic rotator cuffs. *J Shoulder Elbow Surg.* 2015;24(12):1954-1960.

159. Lohr JF, Uhthoff HK. The microvascular pattern of the supraspinatus tendon. *Clin Orthop Relat Res.* 1990(254):35-38.

160. Wlk MV, Abdelkafy A, Hexel M, et al. Biomechanical evaluation of suture-tendon interface and tissue holding of three suture configurations in torn and degenerated versus intact human rotator cuffs. *Knee Surg Sports Traumatol Arthrosc.* 2015;23(2):386-392.

161. Hashimoto T, Nobuhara K, Hamada T. Pathologic evidence of degeneration as a primary cause of rotator cuff tear. *Clin Orthop Relat Res.* 2003(415):111-120.

162. Riley GP, Goddard MJ, Hazleman BL. Histopathological assessment and pathological significance of matrix degeneration in supraspinatus tendons. *Rheumatology (Oxford).* 2001;40(2):229-230.

163. Longo UG, Franceschi F, Ruzzini L, et al. Histopathology of the supraspinatus tendon in rotator cuff tears. *Am J Sports Med.* 2008;36(3):533-538.

164. Matthews TJ, Hand GC, Rees JL, Athanasou NA, Carr AJ. Pathology of the torn rotator cuff tendon. Reduction in potential for repair as tear size increases. *J Bone Joint Surg Br.* 2006;88(4):489-495.

165. Sano H, Ishii H, Trudel G, Uhthoff HK. Histologic evidence of degeneration at the insertion of 3 rotator cuff tendons: a comparative study with human cadaveric shoulders. *J Shoulder Elbow Surg.* 1999;8(6):574-579.

166. Gimbel JA, Van Kleunen JP, Mehta S, Perry SM, Williams GR, Soslowsky LJ. Supraspinatus tendon organizational and mechanical properties in a chronic rotator cuff tear animal model. *J Biomech.* 2004;37(5):739-749.

167. Giphart JE, van der Meijden OA, Millett PJ. The effects of arm elevation on the 3-dimensional acromiohumeral distance: a biplane fluoroscopy study with normative data. *J Shoulder Elbow Surg.* 2012;21(11):1593-1600.

168. Bey MJ, Kline SK, Zauel R, Lock TR, Kolowich PA. Measuring dynamic in-vivo glenohumeral joint kinematics: technique and preliminary results. *J Biomech.* 2008;41(3):711-714.

169. Millett PJ, Giphart JE, Wilson KJ, Kagnes K, Greenspoon JA. Alterations in Glenohumeral Kinematics in Patients With Rotator Cuff Tears Measured With Biplane Fluoroscopy. *Arthroscopy.* 2015.

170. Engelhardt C, Farron A, Becce F, Pioletti D, Terrier A. Impact of partial-thickness tears on supraspinatus tendon strain based on a finite element analysis. *Comput Methods Biomech Biomed Engin.* 2014;17 Suppl 1:118-119.

171. Itoi E, Berglund LJ, Grabowski JJ, et al. Tensile properties of the supraspinatus tendon. *J Orthop Res.* 1995;13(4):578-584.

172. Pedowitz RA, Yamaguchi K, Ahmad CS, et al. American Academy of Orthopaedic Surgeons Clinical Practice Guideline on: optimizing the management of rotator cuff problems. *J Bone Joint Surg Am.* 2012;94(2):163-167.

173. Seida JC, LeBlanc C, Schouten JR, et al. Systematic review: nonoperative and operative treatments for rotator cuff tears. *Ann Intern Med.* 2010;153(4):246-255.

174. Boorman RS, More KD, Hollinshead RM, et al. The Rotator Cuff Quality-of-Life Index Predicts the Outcome of Nonoperative Treatment of Patients with a Chronic Rotator Cuff Tear. *J Bone Joint Surg Am.* 2014;96(22):1883-1888.

175. Knight KL. Knee rehabilitation by the daily adjustable progressive resistive exercise technique. *Am J Sports Med.* 1979;7(6):336-337.

176. McCann PD, Wootten ME, Kadaba MP, Bigliani LU. A kinematic and electromyographic study of shoulder rehabilitation exercises. *Clin Orthop Relat Res.* 1993(288):179-188.

177. Reinold MM, Wilk KE, Fleisig GS, et al. Electromyographic analysis of the rotator cuff and deltoid musculature during common shoulder external rotation exercises. *J Orthop Sports Phys Ther.* 2004;34(7):385-394.

178. Reinold MM, Escamilla RF, Wilk KE. Current concepts in the scientific and clinical rationale behind exercises for glenohumeral and scapulothoracic musculature. *J Orthop Sports Phys Ther.* 2009;39(2):105-117.

179. Hudak PL, Amadio PC, Bombardier C. Development of an upper extremity outcome measure: the DASH (disabilities of the arm, shoulder and hand) [corrected]. The Upper Extremity Collaborative Group (UECG). *Am J Ind Med.* 1996;29(6):602-608.

180. King GJ, Richards RR, Zuckerman JD, et al. A standardized method for assessment of elbow function. Research Committee, American Shoulder and Elbow Surgeons. *J Shoulder Elbow Surg.* 1999;8(4):351-354.

181. Kirkley A, Alvarez C, Griffin S. The development and evaluation of a disease-specific quality-of-life questionnaire for disorders of the rotator cuff: The Western Ontario Rotator Cuff Index. *Clin J Sport Med.* 2003;13(2):84-92.

182. Beaton DE, Katz JN, Fossel AH, Wright JG, Tarasuk V, Bombardier C. Measuring the whole or the parts? Validity, reliability, and responsiveness of the Disabilities of the Arm,

Shoulder and Hand outcome measure in different regions of the upper extremity. *J Hand Ther.* 2001;14(2):128-146.

183. Michener LA, McClure PW, Sennett BJ. American Shoulder and Elbow Surgeons Standardized Shoulder Assessment Form, patient self-report section: reliability, validity, and responsiveness. *J Shoulder Elbow Surg.* 2002;11(6):587-594.

184. de Witte PB, Henseler JF, Nagels J, Vliet Vlieland TP, Nelissen RG. The Western Ontario rotator cuff index in rotator cuff disease patients: a comprehensive reliability and responsiveness validation study. *Am J Sports Med.* 2012;40(7):1611-1619.

185. Jaeschke R, Singer J, Guyatt GH. Measurement of health status. Ascertaining the minimal clinically important difference. *Control Clin Trials.* 1989;10(4):407-415.

186. Kirkley A, Griffin S, Dainty K. Scoring systems for the functional assessment of the shoulder. *Arthroscopy.* 2003;19(10):1109-1120.

187. Roy JS, MacDermid JC, Woodhouse LJ. Measuring shoulder function: a systematic review of four questionnaires. *Arthritis Rheum.* 2009;61(5):623-632.

188. Bey MJ, Zauel R, Brock SK, Tashman S. Validation of a new model-based tracking technique for measuring three-dimensional, in vivo glenohumeral joint kinematics. *J Biomech Eng.* 2006;128(4):604-609.

189. Wu G, van der Helm FC, Veeger HE, et al. ISB recommendation on definitions of joint coordinate systems of various joints for the reporting of human joint motion--Part II: shoulder, elbow, wrist and hand. *J Biomech.* 2005;38(5):981-992.

190. Bey MJ, Kline SK, Zauel R, Kolowich PA, Lock TR. In Vivo Measurement of Glenohumeral Joint Contact Patterns. *EURASIP J Adv Signal Process.* 2010;2010.

191. Anderst WJ, Tashman S. A method to estimate in vivo dynamic articular surface interaction. *J Biomech.* 2003;36(9):1291-1299.

192. Bey MJ, Brock SK, Beierwaltes WN, Zauel R, Kolowich PA, Lock TR. In vivo measurement of subacromial space width during shoulder elevation: technique and preliminary results in patients following unilateral rotator cuff repair. *Clin Biomech (Bristol, Avon).* 2007;22(7):767-773.

193. Massimini DF, Warner JJ, Li G. Glenohumeral joint cartilage contact in the healthy adult during scapular plane elevation depression with external humeral rotation. *J Biomech.* 2014;47(12):3100-3106.

194. Oh JH, Kim SH, Ji HM, Jo KH, Bin SW, Gong HS. Prognostic factors affecting anatomic outcome of rotator cuff repair and correlation with functional outcome. *Arthroscopy.* 2009;25(1):30-39.

195. Williams GR, Jr., Rockwood CA, Jr., Bigliani LU, Iannotti JP, Stanwood W. Rotator cuff tears: why do we repair them? *J Bone Joint Surg Am.* 2004;86-A(12):2764-2776.

196. Itoi E. Rotator cuff tear: physical examination and conservative treatment. *J Orthop Sci.* 2013.

197. Keener JD, Wei AS, Kim HM, Steger-May K, Yamaguchi K. Proximal humeral migration in shoulders with symptomatic and asymptomatic rotator cuff tears. *J Bone Joint Surg Am.* 2009;91(6):1405-1413.

198. Pouliart N, Gagey O. Concomitant rotator cuff and capsuloligamentous lesions of the shoulder: a cadaver study. *Arthroscopy.* 2006;22(7):728-735.

199. Burkhart SS. Fluoroscopic comparison of kinematic patterns in massive rotator cuff tears. A suspension bridge model. *Clin Orthop Relat Res.* 1992(284):144-152.

200. Krackow KA, Thomas SC, Jones LC. Ligament-tendon fixation: analysis of a new stitch and comparison with standard techniques. *Orthopedics.* 1988;11(6):909-917.

201. Fallon J, Blevins FT, Vogel K, Trotter J. Functional morphology of the supraspinatus tendon. *J Orthop Res.* 2002;20(5):920-926.

202. Burkhart SS, Danaceau SM, Pearce CE, Jr. Arthroscopic rotator cuff repair: Analysis of results by tear size and by repair technique-margin convergence versus direct tendon-to-bone repair. *Arthroscopy.* 2001;17(9):905-912.

203. Cohen J. A power primer. *Psychol Bull.* 1992;112(1):155-159.

204. Voycheck CA, Rainis EJ, McMahon PJ, Weiss JA, Debski RE. Effects of region and sex on the mechanical properties of the glenohumeral capsule during uniaxial extension. *J Appl Physiol (1985).* 2010;108(6):1711-1718.

205. O'Brien TD, Reeves ND, Baltzopoulos V, Jones DA, Maganaris CN. Mechanical properties of the patellar tendon in adults and children. *J Biomech.* 2010;43(6):1190-1195.

206. Lake SP, Miller KS, Elliott DM, Soslowsky LJ. Effect of fiber distribution and realignment on the nonlinear and inhomogeneous mechanical properties of human supraspinatus tendon under longitudinal tensile loading. *J Orthop Res.* 2009;27(12):1596-1602.

207. Schaffler MB, Choi K, Milgrom C. Aging and matrix microdamage accumulation in human compact bone. *Bone.* 1995;17(6):521-525.

208. Bassett RW, Cofield RH. Acute tears of the rotator cuff. The timing of surgical repair. *Clin Orthop Relat Res.* 1983(175):18-24.

209. Domb BG, Glousman RE, Brooks A, Hansen M, Lee TQ, ElAttrache NS. High-tension double-row footprint repair compared with reduced-tension single-row repair for massive rotator cuff tears. *J Bone Joint Surg Am.* 2008;90 Suppl 4:35-39.

210. Park MC, Bui C, Park CJ, Oh JH, Lee TQ. Rotator cuff tendon repair morphology comparing 2 single-anchor repair techniques. *Arthroscopy.* 2013;29(7):1149-1156.

211. Rainis CA, Brown AJ, McMahon PJ, Debski RE. Effects of simulated injury on the anteroinferior glenohumeral capsule. *Med Biol Eng Comput.* 2012.

212. Malicky DM, Soslowsky LJ, Kuhn JE, et al. Total strain fields of the antero-inferior shoulder capsule under subluxation: a stereoradiogrammetric study. *J Biomech Eng.* 2001;123(5):425-431.

213. Moore SM, Stehle JH, Rainis EJ, McMahon PJ, Debski RE. The current anatomical description of the inferior glenohumeral ligament does not correlate with its functional role in positions of external rotation. *J Orthop Res.* 2008;26(12):1598-1604.

214. van Drongelen S, van der Woude LH, Janssen TW, Angenot EL, Chadwick EK, Veeger DH. Glenohumeral contact forces and muscle forces evaluated in wheelchair-related activities of daily living in able-bodied subjects versus subjects with paraplegia and tetraplegia. *Arch Phys Med Rehabil.* 2005;86(7):1434-1440.

215. Favre P, Sheikh R, Fucentese SF, Jacob HA. An algorithm for estimation of shoulder muscle forces for clinical use. *Clin Biomech (Bristol, Avon).* 2005;20(8):822-833.

216. Thunes J, Matthew Miller R, Pal S, Damle S, Debski RE, Maiti S. The Effect of Size and Location of Tears in the Supraspinatus Tendon on Potential Tear Propagation. *J Biomech Eng.* 2015;137(8):081012.

217. Funakoshi T, Suenaga N, Sano H, Oizumi N, Minami A. In vitro and finite element analysis of a novel rotator cuff fixation technique. *J Shoulder Elbow Surg.* 2008;17(6):986-992.

218. Sano H, Imagawa K, Yamamoto N, Ozawa H, Yokobori AT, Itoi E. Predicting failures of suture anchors used for rotator cuff repair: a CT-based 3-dimensional finite element analysis. *Biomed Mater Eng.* 2015;25(4):371-380.

219. Sano H, Wakabayashi I, Itoi E. Stress distribution in the supraspinatus tendon with partial-thickness tears: an analysis using two-dimensional finite element model. *J Shoulder Elbow Surg.* 2006;15(1):100-105.

220. Sano H, Yamashita T, Wakabayashi I, Itoi E. Stress distribution in the supraspinatus tendon after tendon repair: suture anchors versus transosseous suture fixation. *Am J Sports Med.* 2007;35(4):542-546.

221. Seki N, Itoi E, Shibuya Y, et al. Mechanical environment of the supraspinatus tendon: three-dimensional finite element model analysis. *J Orthop Sci.* 2008;13(4):348-353.

222. Wakabayashi I, Itoi E, Sano H, et al. Mechanical environment of the supraspinatus tendon: a two-dimensional finite element model analysis. *J Shoulder Elbow Surg.* 2003;12(6):612-617.

223. Inoue A, Chosa E, Goto K, Tajima N. Nonlinear stress analysis of the supraspinatus tendon using three-dimensional finite element analysis. *Knee Surg Sports Traumatol Arthrosc.* 2013;21(5):1151-1157.

224. Mantovani M, Pellegrini A, Garofalo P, Baudi P. A 3D finite element model for geometrical and mechanical comparison of different supraspinatus repair techniques. *J Shoulder Elbow Surg.* 2015.

225. Drury NJ, Ellis BJ, Weiss JA, McMahon PJ, Debski RE. The impact of glenoid labrum thickness and modulus on labrum and glenohumeral capsule function. *J Biomech Eng.* 2010;132(12):121003.

226. Drury NJ, Ellis BJ, Weiss JA, McMahon PJ, Debski RE. Finding consistent strain distributions in the glenohumeral capsule between two subjects: implications for development of physical examinations. *J Biomech.* 2011;44(4):607-613.

227. Moore SM, Ellis B, Weiss JA, McMahon PJ, Debski RE. The glenohumeral capsule should be evaluated as a sheet of fibrous tissue: a validated finite element model. *Ann Biomed Eng.* 2010;38(1):66-76.

228. Araki D, Miller RM, Fujimaki Y, Hoshino Y, Musahl V, Debski RE. Effect of tear location on propagation of isolated supraspinatus tendon tears during increasing levels of cyclic loading. *J Bone Joint Surg Am.* 2015;97(4):273-278.

229. Rainis CA, Brown AJ, McMahon PJ, Debski RE. Effects of simulated injury on the anteroinferior glenohumeral capsule. *Med Biol Eng Comput.* 2012;50(12):1299-1307.

230. Debski RE, Weiss JA, Newman WJ, Moore SM, McMahon PJ. Stress and strain in the anterior band of the inferior glenohumeral ligament during a simulated clinical examination. *J Shoulder Elbow Surg.* 2005;14(1 Suppl S):24S-31S.

231. Ellis BJ, Lujan TJ, Dalton MS, Weiss JA. Medial collateral ligament insertion site and contact forces in the ACL-deficient knee. *J Orthop Res.* 2006;24(4):800-810.

232. Wagner DR, Lotz JC. Theoretical model and experimental results for the nonlinear elastic behavior of human annulus fibrosus. *J Orthop Res.* 2004;22(4):901-909.

233. Payne LZ, Altchek DW, Craig EV, Warren RF. Arthroscopic treatment of partial rotator cuff tears in young athletes. A preliminary report. *Am J Sports Med.* 1997;25(3):299-305.

234. Sakurai G, Ozaki J, Tomita Y, Kondo T, Tamai S. Incomplete tears of the subscapularis tendon associated with tears of the supraspinatus tendon: cadaveric and clinical studies. *J Shoulder Elbow Surg.* 1998;7(5):510-515.

235. Kim TK, Rauh PB, McFarland EG. Partial tears of the subscapularis tendon found during arthroscopic procedures on the shoulder: a statistical analysis of sixty cases. *Am J Sports Med.* 2003;31(5):744-750.

236. Gasser TC, Ogden RW, Holzapfel GA. Hyperelastic modelling of arterial layers with distributed collagen fibre orientations. *Journal of the Royal Society Interface.* 2006;3(6):15-35.

237. Weiss JA, Maker BN, Govindjee S. Finite element implementation of incompressible, transversely isotropic hyperelasticity. *Computer Methods in Applied Mechanics and Engineering.* 1996;135(1-2):107-128.

238. Ellis BJ, Drury NJ, Moore SM, McMahon PJ, Weiss JA, Debski RE. Finite element modelling of the glenohumeral capsule can help assess the tested region during a clinical exam. *Comput Methods Biomech Biomed Engin.* 2010;13(3):413-418.

239. Luo ZP, Hsu HC, Grabowski JJ, Morrey BF, An KN. Mechanical environment associated with rotator cuff tears. *J Shoulder Elbow Surg.* 1998;7(6):616-620.

240. DeOrio JK, Cofield RH. Results of a second attempt at surgical repair of a failed initial rotator-cuff repair. *J Bone Joint Surg Am.* 1984;66(4):563-567.

241. Pal S, Tsamis A, Pasta S, et al. A mechanistic model on the role of "radially-running" collagen fibers on dissection properties of human ascending thoracic aorta. *J Biomech.* 2014;47(5):981-988.

242. Vahdati A, Wagner DR. Implant size and mechanical properties influence the failure of the adhesive bond between cartilage implants and native tissue in a finite element analysis. *J Biomech.* 2013;46(9):1554-1560.

243. Dantuluri V, Maiti S, Geubelle PH, Patel R, Kilic H. Cohesive modeling of delamination in Z-pin reinforced composite laminates. *Composites science and technology.* 2007;67(3):616-631.

244. Maiti S, Geubelle PH. A cohesive model for fatigue failure of polymers. *Engineering Fracture Mechanics.* 2005;72(5):691-708.

245. Pereira BP, Lucas PW, Swee-Hin T. Ranking the fracture toughness of thin mammalian soft tissues using the scissors cutting test. *Journal of Biomechanics.* 1997;30(1):91-94.

246. Azar T, Hayward V. Estimation of the Fracture Toughness of Soft Tissue from Needle Insertion. In: Bello F, Edwards PJE, eds. *Biomedical Simulation: 4th International Symposium, ISBMS 2008, London, UK, July 7-8, 2008 Proceedings*. Berlin, Heidelberg: Springer Berlin Heidelberg; 2008:166-175.

247. Nho SJ, Yadav H, Shindle MK, Macgillivray JD. Rotator cuff degeneration: etiology and pathogenesis. *Am J Sports Med.* 2008;36(5):987-993.

248. Thomopoulos S, Parks WC, Rifkin DB, Derwin KA. Mechanisms of tendon injury and repair. *J Orthop Res.* 2015;33(6):832-839.

249. Yadav H, Nho S, Romeo A, MacGillivray JD. Rotator cuff tears: pathology and repair. *Knee Surg Sports Traumatol Arthrosc.* 2009;17(4):409-421.

250. Teunis T, Lubberts B, Reilly BT, Ring D. A systematic review and pooled analysis of the prevalence of rotator cuff disease with increasing age. *J Shoulder Elbow Surg.* 2014;23(12):1913-1921.

251. Oh JH, Kim SH, Kang JY, Oh CH, Gong HS. Effect of age on functional and structural outcome after rotator cuff repair. *Am J Sports Med.* 2010;38(4):672-678.

252. Hattrup SJ. Rotator cuff repair: relevance of patient age. *J Shoulder Elbow Surg.* 1995;4(2):95-100.

253. Bjornsson HC, Norlin R, Johansson K, Adolfsson LE. The influence of age, delay of repair, and tendon involvement in acute rotator cuff tears: structural and clinical outcomes after repair of 42 shoulders. *Acta Orthop.* 2011;82(2):187-192.

254. Park JS, Park HJ, Kim SH, Oh JH. Prognostic Factors Affecting Rotator Cuff Healing After Arthroscopic Repair in Small to Medium-sized Tears. *Am J Sports Med.* 2015;43(10):2386-2392.

255. Pauly S, Stahnke K, Klatte-Schulz F, Wildemann B, Scheibel M, Greiner S. Do patient age and sex influence tendon cell biology and clinical/radiographic outcomes after rotator cuff repair? *Am J Sports Med.* 2015;43(3):549-556.

256. Sano H, Ishii H, Yeadon A, Backman DS, Brunet JA, Uhthoff HK. Degeneration at the insertion weakens the tensile strength of the supraspinatus tendon: a comparative mechanical and histologic study of the bone-tendon complex. *J Orthop Res.* 1997;15(5):719-726.

257. Maffulli N, Longo UG, Franceschi F, Rabitti C, Denaro V. Movin and Bonar scores assess the same characteristics of tendon histology. *Clin Orthop Relat Res.* 2008;466(7):1605-1611.

258. Plate JF, Bates CM, Mannava S, et al. Age-related degenerative functional, radiographic, and histological changes of the shoulder in nonhuman primates. *J Shoulder Elbow Surg.* 2013;22(8):1019-1029.

259. Arnoczky SP, Lavagnino M, Egerbacher M. The mechanobiological aetiopathogenesis of tendinopathy: is it the over-stimulation or the under-stimulation of tendon cells? *Int J Exp Pathol.* 2007;88(4):217-226.

260. Arnoczky SP, Tian T, Lavagnino M, Gardner K, Schuler P, Morse P. Activation of stress-activated protein kinases (SAPK) in tendon cells following cyclic strain: the effects of

strain frequency, strain magnitude, and cytosolic calcium. *J Orthop Res.* 2002;20(5):947-952.

261. Screen HR, Lee DA, Bader DL, Shelton JC. An investigation into the effects of the hierarchical structure of tendon fascicles on micromechanical properties. *Proc Inst Mech Eng H.* 2004;218(2):109-119.

262. Maffulli N, Barrass V, Ewen SW. Light microscopic histology of achilles tendon ruptures. A comparison with unruptured tendons. *Am J Sports Med.* 2000;28(6):857-863.

263. Goutallier D, Postel JM, Bernageau J, Lavau L, Voisin MC. Fatty muscle degeneration in cuff ruptures. Pre- and postoperative evaluation by CT scan. *Clin Orthop Relat Res.* 1994(304):78-83.

264. Melis B, Wall B, Walch G. Natural history of infraspinatus fatty infiltration in rotator cuff tears. *J Shoulder Elbow Surg.* 2010;19(5):757-763.

265. Hantes ME, Karidakis GK, Vlychou M, Varitimidis S, Dailiana Z, Malizos KN. A comparison of early versus delayed repair of traumatic rotator cuff tears. *Knee Surg Sports Traumatol Arthrosc.* 2011;19(10):1766-1770.

266. MacKechnie MA, Chahal J, Wasserstein D, Theodoropoulos JS, Henry P, Dwyer T. Repair of full-thickness rotator cuff tears in patients aged younger than 55 years. *Arthroscopy.* 2014;30(10):1366-1371.

267. Hui CY, A J, Bennison SJ, Londono JD. Crack blunting and the strength of soft elastic solids. *Proceedings of the Royal Society of London. Series A: Mathematical, Physical and Engineering Sciences.* 2003;459(2034):1489-1516.